


2023

Artificial Light at Night Disrupts Pain Behavior and Cerebrovascular Structure in Mice

Jacob Raymond Bumgarner

West Virginia University, jrbumgarner@mix.wvu.edu

Follow this and additional works at: <https://researchrepository.wvu.edu/etd>

 Part of the [Behavioral Neurobiology Commons](#), [Bioinformatics Commons](#), [Computational Neuroscience Commons](#), and the [Laboratory and Basic Science Research Commons](#)

Recommended Citation

Bumgarner, Jacob Raymond, "Artificial Light at Night Disrupts Pain Behavior and Cerebrovascular Structure in Mice" (2023). *Graduate Theses, Dissertations, and Problem Reports*. 12037.
<https://researchrepository.wvu.edu/etd/12037>

This Dissertation is protected by copyright and/or related rights. It has been brought to you by the The Research Repository @ WVU with permission from the rights-holder(s). You are free to use this Dissertation in any way that is permitted by the copyright and related rights legislation that applies to your use. For other uses you must obtain permission from the rights-holder(s) directly, unless additional rights are indicated by a Creative Commons license in the record and/ or on the work itself. This Dissertation has been accepted for inclusion in WVU Graduate Theses, Dissertations, and Problem Reports collection by an authorized administrator of The Research Repository @ WVU. For more information, please contact researchrepository@mail.wvu.edu.

**Artificial Light at Night Disrupts Pain Behavior
and Cerebrovascular Structure in Mice**

Jacob R. Bumgarner

Dissertation submitted to the School of Medicine
at West Virginia University
in partial fulfillment of the requirements for the degree of

Doctor of Philosophy
in Neuroscience

Committee Members:

Randy J. Nelson, Ph.D., Advisor
A. Courtney DeVries, Ph.D., Chair
Zachary M. Weil, Ph.D.
Gordon P. Meares, Ph.D.
Vincent S. Setola, Ph.D.

Department of Neuroscience
Morgantown, WV
2023

Copyright 2023 Jacob Bumgarner

Abstract

Artificial Light at Night Disrupts Pain Behavior and Cerebrovascular Structure in Mice

Jacob R. Bumgarner

Circadian rhythms are intrinsic biological processes that fluctuate in function with a period of approximately 24 hours. These rhythms are precisely synchronized to the 24-hour day of the Earth by external rhythmic signaling cues. Solar light-dark cycles are the most potent environmental signaling cue for terrestrial organisms to align internal rhythms with the external day. Proper alignment and synchrony of internal circadian rhythms with external environmental rhythms are essential for health and optimal biological function.

The modern human environment on Earth is no longer conducive to properly aligned circadian rhythms. Following the industrial revolution, artificial lighting and an ever-growing 24-hour global economy have shifted humans away from natural environments suited for rhythmic behavior and physiology. Humans, and much of the natural environment, are routinely exposed to circadian rhythm disruptors. The most pervasive disruptor of circadian rhythms is artificial light at night (ALAN).

A growing 80% of humans on Earth are exposed to ALAN beyond natural nighttime environmental lighting levels. ALAN exposure is associated with numerous negative consequences on behavior and physiology, including neuroinflammation, cardiovascular disease, and altered immune function. This dissertation examines two previously uninvestigated effects of ALAN exposure on physiology and behavior in mice.

In **Part 1**, I investigated the effects of ALAN exposure on pain behavior in mice. I observed that ALAN exposure had detrimental effects on rodent pain behavior in contexts of both health and models of human disease. ALAN exposure heightened responsiveness to noxious cold stimuli and innocuous mechanical touch. Differences in these effects were noted based on sex and disease state. I conclude this section with a report on the mechanisms by which ALAN exposure altered pain behavior.

In **Part 2**, I investigated the effects of ALAN exposure on cerebrovascular structure in mice. To conduct these investigations, I first developed VesselVio, an open-source application for the analysis and visualization of vasculature datasets. Using this application and additional analytical frameworks, I examined the effects of short-term ALAN exposure on hippocampal vasculature in mice. ALAN exposure reduced hippocampal vascular density in mice, with notable regional sex differences. I also observed that ALAN exposure altered hippocampal vascular network connectivity and structure, with persistent regional sex differences.

The data in this dissertation contribute to the ever-growing field of circadian rhythm biology focused on studying circadian rhythm disruption. These data highlight the continuing need to mitigate the pervasiveness of ALAN in human and natural environments. Most importantly, the results presented in this dissertation emphasize the need to consider ALAN as a mitigating factor for the treatment of both cardiovascular disease and pain.

Dedication

To my wife, Madelyn, for her unconditional love and support.

Acknowledgments

Pursuing a Ph.D. is a journey of the individual and their village. My tenure as a graduate student was transformational on an academic, scientific, professional, and personal level. I could not have completed this degree without the outstanding individuals, scientists, and friends around me.

First, I thank my wife, Madelyn. You have been an unconditional source of support, laughter, reason, and love. Our lives in graduate school were sometimes quiet but generally hectic. You listened earnestly, humored, and participated in endless amounts of long, rambling conversations about hypotheses and algorithms (~800 hours of exercised patience, assuming *at least* four hours of research ramblings per week for four years). You were patient and encouraging throughout late nights and countless hours of work. My time in graduate school wouldn't have been nearly as successful if I didn't have you around, as you keep me grounded in the most meaningful aspects of life. You are a wonderful partner, and I am lucky to have you.

I thank my family for their support. To Jayme and Mike, thank you for your patient ears and unconditional support. Your advice, wisdom, and perspective are invaluable to me. You've watched me grow as an individual, a musician, and a scientist. I'm beyond lucky to have such supportive parents as you. To Justin and Ryan, thank you for our many years of friendship, advice, memes, and support. I'm lucky to have such wonderful brothers. To Gretchen and Steve, thank you for your excitement, encouragement, and guidance. I am lucky to have your support.

I thank the undergraduate students I was fortunate to mentor: Alex Richmond, Rhett White, and Jordan Brown. You each provided invaluable assistance, ideas, and advice throughout your many years of work and volunteered time. I hope that you each gained as much value from your experience working with me in the lab as I gained from being able to mentor you. I am delighted to see the success that you're each finding in your next stages of education and life.

To my peers, Jennifer Liu and Hecmarie Meléndez-Fernández, thank you for your many years of support both in and out of the lab. It was a pleasure to pursue my degree alongside the two of you. I am thankful for our many hours of conversation, and I

appreciate the time you spent helping me with my experiments, analyses, and tissue collections.

To my friends, Darius, Brandon, Schuyler, William, Richard, Ben, Felix, and Andras. You've each provided endless and earnest conversation, wisdom, advice, and memes. I'm not sure I could've gotten through this degree without your support. Life would be much less fulfilling without your friendship.

To the countless others I haven't named here: thank you. The list of individuals who have supported me at WVU and on various coding forums is too large to consider here, but I thank you, nonetheless. My development as a scientist is a product of the immeasurable institutional and professional support of those I can and cannot see.

I thank the current and previous Department of Neuroscience administrative staff, including Erica Stewart, Cassie George, Becca Rohn, and Morgan Prunty for your kindness, helpfulness, knowledge, and support. I thank the WVU Office of Graduate Education and Research and Dr. Julie Lockman, Joe Andria, Conner Ferguson, and Dr. Lisa Salati for their professional and academic support. I thank the WVU vivarium veterinarians, animal husbandry staff, and the Office of Lab Animal Resources for your diligence and excellent care for my animals throughout my years of research. I thank Terri Poling for her many years of kindness and support in the vivarium and lab. I thank my direct funding support, including the Arlen G. & Louise Stone Swiger Fellowship and the WVU ADRD T32, with funding guidance support from Dr. Jim Simpkins and Dr. Candice Brown. I also thank my indirect funding support from the lab, including the NCCIH and the NIGMS.

To William Walker, thank you for your endless support, advice, and guidance, both in and out of the lab. You helped shape my ability to reason as a scientist and individual. You have a careful eye and fantastic vision for science that I was lucky to learn from as an undergraduate and graduate student. I'm fortunate to call you both a mentor and a friend.

To James Walton, thank you for your questions, challenges, pedantry, and support. I mean it. You were an excellent scientific and intellectual figure to look up to throughout my degree. I appreciate how much you pushed me as a young scientist to

form a diligent and careful eye. You shaped my ability to think critically, so I am indebted to you for that. Thanks, as well for our many conversations about hiking and life.

To Courtney DeVries, thank you for being such a brilliant guiding figure of professionalism, curiosity, and vision. Your attitude towards science and research is contagious, and I am lucky to have you as a mentor. I look up to your penchant and skill for crafting pointed scientific questions and hypotheses. Thank you for your many years of support.

To my committee members, Zach Weil, Vincent Setola, and Gordon Meares, thank you for providing mentorship and guidance throughout my degree. I am fortunate to have had your support and advice, from designing my first experiment to preparing my defense. I appreciate your impact on my graduate training both from and beyond being on my committee.

Finally, to Randy Nelson, thank you for the many years of fulfilling and meaningful mentorship. I am grateful for your willingness to mentor and guide me from a young pianist into the scientist I am today. Your humor and wit brought many moments of laughter. Your pedantry and stubbornness yielded many moments of growth. Your editorial insights were invaluable. You pushed me carefully to expand and improve beyond myself. At times we were both difficult to manage, but I am glad that we have the artistic vision required to understand one another. Your wisdom and vision provided the clarity and guidance needed for the scientific and philosophical challenges that accompany the pursuit of a Ph.D. I hope you know how much I genuinely appreciate your support. Thanks for everything over the past four years. I am lucky to have you as a mentor.

Table of Contents

Part 1

Artificial Light at Night Disrupts Pain Behavior in Mice.....	1
Chapter 1 Circadian Rhythms and Pain.....	2
Chapter 2 Dim Light at Night Exposure Induces Cold Hyperalgesia and Mechanical Allodynia in Male Mice	54
Chapter 3 Artificial Light at Night Exacerbates Cold Neuropathy in a Mouse Model of Type II Diabetes Mellitus	76
Chapter 4 Artificial Light at Night Exposure Exacerbates Paclitaxel-Induced Mechanical Allodynia in Female Mice	92
Chapter 5 Investigating the Mechanisms of Disrupted Pain Behavior Induced by Exposure to Artificial Light at Night	105

Part 2

Artificial Light at Night Alters Cerebrovascular Structure in Mice.....	126
Chapter 6 Circadian Regulation of the Blood-Brain Barrier and Angiogenesis..	127
Chapter 7 Open-source analysis and visualization of segmented vasculature datasets with VesselVio	143
Chapter 8 Acute Exposure to Artificial Light at Night Alters Hippocampal Vascular Structure in Mice	179
Chapter 9 Conclusions.....	207

Part 1

Artificial Light at Night Disrupts Pain Behavior in Mice

Chapter 1

Circadian Rhythms and Pain

Published as:

Bumgarner, J. R., Walker II, W. H., & Nelson, R. J. (2021). Circadian rhythms and pain. *Neuroscience & Biobehavioral Reviews*, 129, 296-306.

1. Introduction

The vast majority of organisms on earth have evolved with internal manifestations of the external daily light-dark cycles. These circadian (*circa* = about; *dies* = day) rhythms are self-sustained, endogenous oscillations generated by circadian clocks that persist with a period of around 24 hours under constant conditions (Golombek & Rosenstein, 2010). Exposure to the daily external light-dark cycle synchronizes (entrains) these rhythms to the 24-hour cycle of the external world via signaling to a so-called ‘master clock’. Among mammals, this master clock is located in the suprachiasmatic nuclei (SCN) of the hypothalamus (Stephan & Zucker, 1972). Together, the SCN and the circadian clocks throughout the body comprise what is known as the circadian system.

Circadian clocks are self-sustaining and self-regulated through what is known as the transcription-translation feedback loop (TTFL). The TTFL comprises a family of core canonical ‘clock’ genes, including *Clock*, *Bmal1*, *Per*, and *Cry*, among several others. In brief, circadian rhythms are generated within the nucleus of cells by the autoregulatory TTFL of the core circadian genes. At the beginning of the circadian day, BMAL1 and CLOCK interact in the cytosol to form a heterodimer that then is translocated into the nucleus. This heterodimer binds to E-box promoter sequences of the *Cry* and *Per* genes to activate their transcription. The gene products of *Per* and *Cry* accumulate in the cytoplasm, dimerize, and then form a complex that is translocated back into the nucleus to repress their own transcription by interacting with CLOCK and BMAL1. Notably, a complete cycle of this feedback loop takes ~24 hours to occur. There are additional feedback loops interlocked with the core CLOCK-BMAL1/PER-CRY loop. Further intricate details of the TTFL are beyond the scope of this review, but they have been

extensively characterized elsewhere (Partch et al., 2014). The daily oscillation in the expression of these proteins is responsible for the generation of circadian rhythms at molecular, cellular, physiological, and behavioral levels.

In mammals, the TTFL of the circadian clock is present in nearly every cell (Yoo et al., 2004; Ruben et al., 2018; Nagoshi et al., 2004). Individual circadian clocks within the body can run with different period lengths, so without a coordinating signal, the circadian rhythms of various tissues and cells become misaligned. Alignment of internal rhythms generally occurs via signaling from the hypothalamic SCN.

The SCN acts as a conductor to align internal circadian rhythms with the external daily light-dark cycle by interpreting photic signaling from the retina and communicating that information with the rest of the brain and body. In mammals, photosensitive retinal cells, specifically, intrinsically photosensitive retinal ganglion cells containing the photopigment melanopsin, communicate time-of-day cues to the SCN via photic signaling information. Photic information is relayed along the retinohypothalamic tract to the SCN to inform time-of-day by modifying cellular activity and the expression of specific clock proteins within neurons and glia. For example, light pulses alter the expression of *Per1/Per2* within the rat SCN, but only during the night (Miyake et al., 2000). After receiving and interpreting retinal photic information, the SCN aligns internal rhythms with the external solar day via neuronal projections and humoral signaling (Pevet & Challet, 2011).

Many behavioral, physiological, and biochemical processes display circadian rhythms. Sleep-wake cycles, locomotor activity rhythms, body temperature fluctuations, as well as immune and endocrine function, are examples of rhythmic processes regulated by the circadian system (Walker et al., 2020; Scheiermann et al., 2013; Gamble et al., 2014). Most importantly for the context of this review, pain is also regulated by the circadian system, although our current understanding of the interaction between the pain and circadian systems remains unspecified. Below, I have outlined our current understanding of the relationship between these two systems to inform potential hypotheses surrounding the nature of their function. I also highlight the importance of

proper circadian rhythm health and the consequences of circadian rhythm disruption on pain.

2. The Pain System - An Overview

The pain system encodes and relays noxious sensory information from the periphery into the central nervous system to produce protective behavioral outcomes. Noxious information is relayed by peripheral nociceptors to the spinal cord, brainstem, midbrain, and forebrain where withdrawal or wound-protection behaviors are elicited to prevent or minimize injury (Baliki & Apkarian, 2015). Nociceptive information delivered to the brain is processed into the sensory-discriminative and affective aspects of pain by a network of supraspinal structures that comprise what is commonly referred to as the pain matrix (Kulkarni et al., 2005; Garcia-Larrea & Peyron, 2013; Iannetti & Mouraux, 2010; Legrain et al., 2011; Auvray et al., 2010).

It is understood that none of the nuclei or structures considered to be part of the pain matrix are exclusively responsible for processing pain (Baliki & Apkarian, 2015). Instead, this matrix can be described as a 'distributed nociceptive system' because sensory-discriminative and affective components of pain can still be processed in the absence of one or more components of the system (Coghill, 2020). For the purpose of this review, I operationally classify supraspinal regions commonly implicated in the central processing of pain as part of the pain system while understanding that these regions do not exclusively process pain and may be equally involved in the processing of innocuous and noxious stimuli alike (Iannetti & Mouraux, 2010).

2.1 Functional Anatomy of the Pain System

Noxious stimuli are encoded and relayed centrally by peripheral pseudounipolar nociceptor neurons of two primary classes: A δ fibers and C fibers. A δ neurons are medium-sized myelinated fibers that rapidly transmit localized pain information, whereas C neurons are small unmyelinated fibers that transmit slow, low-resolution pain information. Upon exposure to a noxious stimulus, thermosensitive ion channels, mechanotransduction channels, or chemoreceptors on peripheral nociceptor terminals

will transduce the noxious stimuli into depolarization events that activate local voltage-gated ion channels (Basbaum et al., 2009). For example, exposure to noxious heat above 43 °C activates TRPV1 and other heat-sensitive ion channels, producing inward depolarizing currents at peripheral nociceptor terminals. Upon sufficient channel activation, action potentials will be generated and then propagated through the dorsal root ganglia (DRG) and into the dorsal horn of the spinal cord.

Nociceptor input into the dorsal horn of the spinal cord is processed and relayed rostrally to the brain. Action potentials from primary nociceptors produce excitatory postsynaptic potentials on secondary nociceptive specific neurons and wide dynamic range neurons located within the gray matter of the dorsal horn via glutamate and co-transmitter release (such as substance P). These excitatory potentials are gated by feedforward inhibition produced by A β -fibers that excite inhibitory local glycinergic and GABAergic interneurons that synapse with secondary nociceptive specific and wide dynamic range neurons (Lu et al., 2013; Todd, 2010; Guo & Hu, 2014). Upon depolarization, nociceptive specific and wide dynamic range neurons relay nociceptive information across the anterior white commissure and into the brain along five main ascending tracts: the spinothalamic, the spinoreticular, the spinomesencephalic (or parabrachial tract), the cervicothalamic, and the spinohypothalamic tracts.

Supraspinal structures process nociceptive information in a distributed manner to produce the sensory-discriminative and affective components of pain. Sensory-discriminative components of pain (e.g., location, temporal quality, and intensity) are mainly produced by the primary somatosensory cortex (Bushnell et al., 1999; Rainville et al., 1997). Sensory discriminative information is relayed to the primary somatosensory cortex via projections from the ventral posterolateral and ventral posteromedial nuclei of the thalamus (Ab Aziz & Ahmad, 2006; Hsu et al., 2014). The secondary somatosensory cortex (Maihöfner et al., 2006; Timmermann et al., 2001), prefrontal cortex (PFC) (Ong et al., 2019), and insular cortex (Ostrowsky et al., 2002; Lu et al., 2016; Starr et al., 2009), also are suggested to play a role in sensory-discriminative pain processing.

Affective-motivational components of pain (e.g., subjective unpleasantness, motivation to escape painful stimulus) arise from the processing of nociceptive

information within the PFC (including the anterior cingulate cortex (ACC)) (Ong et al., 2019; Xiao & Zhang, 2018; Porro et al., 2002; Metz et al., 2009), insula (Ostrowsky et al., 2002; Lu et al., 2016), amygdala (Neugebauer, 2015), and hypothalamus (Bernard, 2007). Nociceptive information is relayed to these regions from the intralaminar and ventromedial thalamic nuclei (Ab Aziz & Ahmad, 2006).

The ascending transmission of nociceptive information is regulated by the descending pain modulatory system. The descending pain modulatory system comprises primarily the periaqueductal gray (PAG), the locus coeruleus (LC), and the rostral ventromedial medulla (RVM) (Ossipov et al., 2014). Together, these three regions can both facilitate and inhibit the spinal transmission of nociceptive information. Descending regulation is achieved by direct descending projections from the LC and RVM to the dorsal horn of the spinal cord; these projections then either function to inhibit or facilitate nociceptive transmission. For example, pain “On” or “Off” neurons located in the RVM are thought to respectively facilitate or inhibit the transmission of nociceptive information within the spinal cord (Khasabov et al., 2015). The activity of the LC and RVM is regulated heavily by the PAG (Lau & Vaughan, 2014), which receives and processes pain signaling information from other supraspinal regions.

Other supraspinal regions in the pain system can also project directly to the PAG, LC, RVM, and dorsal horn of the spinal cord, forming an extended descending modulatory system. These regions include the PFC (Ong et al., 2019), nucleus submedius -> ventrolateral orbital cortex -> PAG circuit originating from the thalamus, (Tang et al., 2009), various regions of the hypothalamus (Bernard, 2007), and the amygdala (Pertovaara & Almeida, 2006). It is also notable that orexin/hypocretin neurons of the lateral hypothalamus appear to play a role in mediating analgesia via projections to the descending pain modulatory system, spinal cord, and other supraspinal components of the pain system (Colas et al., 2014; Ahmadi-Soleimani et al., 2020; Marcus & Elmquist, 2006).

The pain system adapts in response to painful stimuli. After acute pain stimulation, sites of original injury/stimulation can become hypersensitive to innocuous stimuli (allodynia) and noxious stimuli (hyperalgesia) in a process known as peripheral

sensitization (Gangadharan & Kuner, 2013). Central plastic changes can also occur in the form of central sensitization; these changes enhance the reactivity and activity of the central pain system (Latremoliere & Woolf, 2009). Acute sensitization is thought to be useful for promoting wound healing and wound-protection behavior. But, sensitivity alterations to the pain system are not always beneficial, as they can contribute to the development of chronic pain states that may be useful for wound protection and healing behaviors (de C Williams, 2016) yet are typically considered to be detrimental to the function and well-being of an individual (Mansour et al., 2014). Maladaptive pain states such as neuropathic or chronic pain (pain lasting for more than 6 months) can arise via sensitization when 'useful' pain information outlasts its acute protective function or when damage to the peripheral or central pain system occurs (Schaible, 2006).

3. Diurnal and Circadian Rhythms of the Pain System

In this section, I present direct and correlative evidence of the interaction between the circadian and pain systems. I first briefly highlight behavioral studies of circadian rhythms of pain and then examine the involvement of specific nodes of the pain system in the circadian regulation of pain thresholds.

3.1 Circadian Rhythms of Pain

The pain system exhibits circadian rhythms in function (Segal et al., 2018; Palada et al., 2020). Clinical and experimental evidence suggest that pain responsiveness varies across the day in both sexes of diurnal and nocturnal species, including humans (Bruguerolle & Labrecque, 2007; Chassard & Bruguerolle, 2004). Indeed, daily variations in pain responsiveness have been observed in rodents housed in constant conditions, suggesting that these variations reflect true circadian rhythms (Oliverio et al., 1982; Pickard, 1987). In a meta-analysis of daily rhythms of pain sensitivity in healthy humans, pain sensitivity was observed to be highest at the end of the active phase and during the night (Fig. 1) (Hagenauer et al., 2017). However, pain threshold rhythms in humans vary

dramatically in response to disease, with peaks and troughs of sensitivity varying inconsistently across different disease states (Kim et al., 2015).

If I assumed that pain threshold rhythms were phase-dependent (in common with locomotor activity rhythms), then I could reasonably predict that nocturnal species have rhythms that are antiphase to diurnal species. However, this is not always the case. Several rodent studies have reported highest pain responsiveness during the active phase (Oliverio et al., 1982; Martínez-Gómez et al., 1994; Frederickson et al., 1977), whereas others report the peak of sensitivity during the inactive phase (Kavaliers & Hirst, 1983). The phase of rhythms can even change based on whether rodents are entrained or free running (Pickard, 1987). One study also reported antiphase thresholds in two strains of nocturnal mice (Castellano et al., 1985). Thus, further research is needed to understand the relationship between chronotype and pain threshold rhythms to optimally translate preclinical pain research, regardless of whether the research is focused on circadian biology.

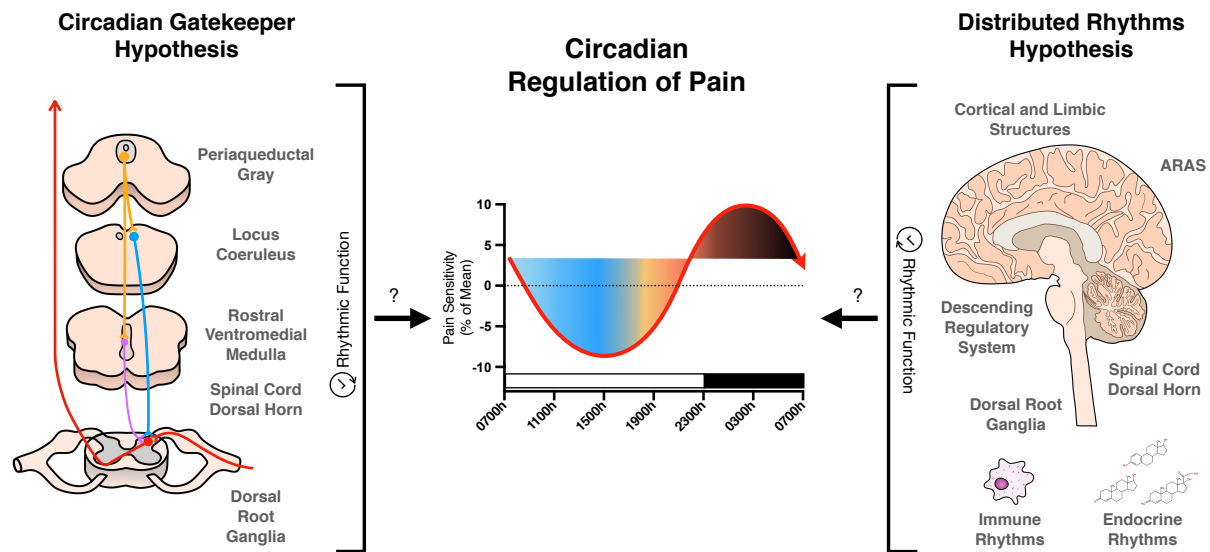


Figure 1. The circadian regulation of pain. Two hypotheses are proposed to explain the potential origins of circadian pain rhythms. On the left, the “Circadian Gatekeeper” hypothesis is shown. This hypothesis proposes that the descending pain modulatory system, dorsal horn, and DRG regulate the ascending transmission of nociceptive input in a time-specific manner to produce diurnal alterations in pain responsiveness. On the right, the “Distributed Rhythms” hypothesis is depicted. Similar to the description of the pain system as a “Distributed System” (Coghill, 2020), this hypothesis suggests that circadian rhythms present throughout the entire pain system and interacting systems function together to produce an integrated circadian rhythm of pain responsiveness. The center graph was adapted from Hagenauer et al. (Hagenauer et al., 2017). The white and black bars above the x-axis represent typical wake/sleep periods, respectively.

3.2 Dorsal Root Ganglia

Daily rhythmic activity is observed within the primary nociceptors of the DRG. In mice, DRG express clock genes that drive the rhythmic expression of substance P across the day, likely via *Tac1* transcriptional enhancer E-box sites (Zhang et al., 2012). Substance P is a pleiotropic neuropeptide that functions to transmit and modulate pain signaling within the pain system (Li et al., 2012). Synaptic release of glutamate and substance P by DRG in events of nociception results in the depolarization of spinal neurons (Zieglgänsberger, 2019). This circadian pattern of substance P expression is correlated with circadian patterns of responsiveness to inflammatory pain induced by formalin injections (Zhang et al., 2012). DRG also exhibit a circadian oscillation in expression of $\alpha 2\delta$ -1, a voltage-gated calcium channel subunit (Kusunose et al., 2010). The expression of other nociceptive proteins in DRG is likely regulated by clock genes, considering the presence of the clock output gene *Tef* or the presence of prokineticin receptors (Lee et al., 2017; Negri et al., 2002). Additionally, diurnal variations in TRPV1 expression in the human esophagus have been observed (Yang et al., 2015). Though the findings of the previous study were not directly linked to the DRG, a study using male rats observed a diurnal profile of *Trp* channel expression in the DRG across the day (Kim et al., 2020), indicating that there may be daily variations of channel expression at nociceptor terminals.

3.3 Dorsal Horn of the Spinal Cord

The spinal cord displays circadian rhythms in nociceptive function. The circadian clock gene *TTFL* is present in neurons and astrocytes of the dorsal horn of the spinal cord (Morioka et al., 2012; Morioka et al., 2016); additional studies confirmed the expression of *Rev- erba* and *Per1* in the dorsal horn, although expression was only examined at single timepoints (Onishi et al., 2002; Yamamoto et al., 2001). The dorsal horn of the spinal cord displays a circadian pattern in enzymatic activity of the Na^+ / K^+ ATPase (Eblen-Zajjur et al., 2015), which is essential for neuronal function and plays an integral role in pain processing (LaCroix-Fralish et al., 2009). Although not yet reported, the expression of Na^+ / K^+ ATPase may be directly or indirectly influenced by clock genes.

Another study reported that the TTFL present in spinal astrocytes drives the rhythmic expression of cyclooxygenase-1 and glutamine synthase, both of which play roles in pain processing (Morioka et al., 2016).

Several studies to date have explicitly examined the relationship between pain threshold rhythms and circadian rhythms in the spinal cord. In a rat model of chronic constriction injury, a diurnal oscillation was detected in the NR2B-CREB-CRTC1 signaling pathway within the dorsal horn of the spinal cord. Diurnal rhythms of protein and mRNA expression were observed in each component of the pathway, including the NR2B NMDA glutamate receptor subunit and two of its response elements: CREB, and CRTC1 (Xia et al., 2016). This pathway regulates synaptic plasticity and the development of pain hypersensitivity (Xia et al., 2017). An adenovirus-driven knockdown of CREB and CRTC1 expression increased mechanical withdrawal (von Frey filaments) thresholds and led to altered withdrawal threshold rhythms across the day (Xia et al., 2017). Next, rhythmic expression of substance P has been observed in the dorsal horn of the spinal cord (Zhang et al., 2012). Lastly, corticosterone-driven astrocytic ATP release in the spinal cord has been linked to diurnal rhythms of allodynia in a mouse model of nerve injury (Koyanagi et al., 2016). In this study, ablation of glucocorticoid secretion by adrenalectomy abolished diurnal astrocytic ATP release in the dorsal horn of the spinal cord and therefore diurnal allodynia rhythms (Koyanagi et al., 2016).

3.4 Periaqueductal Gray

The PAG exhibits circadian rhythms, but little is known about these rhythms in the context of pain modulation. The PAG receives direct input from ipRGCs (Kriegsfeld et al., 2004; Hattar et al., 2006), receives neuronal projections from the SCN (Zhang et al., 2009), and exhibits clock gene rhythms *in vitro* (Landgraf et al., 2016). One group reported daily differences in μ -opioid receptor mRNA expression in the PAG of mice with sham nerve ligation surgeries (Takada et al., 2013). In addition to its role in analgesia, the ventrolateral PAG acts in tandem with the ascending arousal system to gate rapid eye movement (REM) sleep. A population of 'REM sleep-on' and 'REM sleep-off' neurons are present throughout the vIPAG, providing additional evidence for diurnal variations in PAG

activity (Sapin et al., 2009). Further, the PAG's daily activity may be altered by fluctuations in levels of endogenous opioids (discussed below). Additional research is needed to understand how pain is modulated by daily molecular and physiological variations in the PAG.

3.5 Rostral Ventromedial Medulla

There is currently limited direct evidence on the role of the RVM in circadian rhythms of pain. The TTFL appears to be present in the caudal ventrolateral medulla (Monošíková et al., 2007), but has not yet been openly examined in the RVM or other regions of the medullary pain system. Additionally, diurnal variation in the activity of tryptophan-5-hydroxylase activity in the nucleus raphe magnus of the RVM has been reported, suggesting that there may be a temporal regulation of neuronal activity in the region (Hery et al., 1977). Importantly, the previously described pain On/Off neurons in the RVM appear to display circadian rhythmicity in activity that is intrinsically related to the sleep-wake cycle. In anesthetized animals, On-/Neutral cells fire spontaneously during waking and have little activity during sleep, whereas Off-cells fire sporadically during waking but have continuous activity during sleep (Leung & Mason, 1999). This observation is coincident with the hypothesis that circadian rhythms of pain are regulated at the level of the spinal cord via the differential activity of RVM On-/Off-neurons and their control over local serotonergic projections to the dorsal horn (Foo & Mason, 2003).

3.6 Locus Coeruleus

As a core member of the ascending reticular activating system (which is responsible for regulating arousal and the sleep-wake cycle), there is abundant correlative evidence for the role of the LC in circadian pain processing. Although one study reported no evidence of the clock gene TTFL in the LC (Warnecke et al., 2005), another reported that *Per1* is expressed in the LC and that expression levels vary across the day, suggesting that the LC does have its own clock gene loops (Mahoney et al., 2013). There is variation in LC tyrosine hydroxylase activity across the day (Natali et al., 1980). In rats, LC neurons are more active during the active period than in the inactive

period. But these rhythms are dependent on SCN signaling, as dorsal medial hypothalamic lesions abolished this circadian variation in LC neuronal activity (Aston-Jones et al., 2001). The LC plays a role in regulating the circadian rhythm of the sleep-wake cycle. Because of this, alteration of basal activity in the LC by chronic or even acute pain may modulate circadian rhythms (González & Aston-Jones, 2006). In relation to the varying activity of LC neurons across the day, NA α 2 receptors located in the mPFC seem to have an analgesic effect when activated by NA released by the LC (Kaushal et al., 2016). However, NA α 1 receptors, which have a lower affinity for NA, seem to generate allodynia and hyperalgesia in chronic pain conditions (Kaushal et al., 2016). This may also be relevant for prolonged periods of disrupted circadian rhythms where LC activity is heightened.

3.7 Thalamus

Diurnal changes in human thalamic activity (Ku et al., 2018) and rodent corticothalamic connectivity have been observed (Cardoso-Cruz et al., 2011). Additionally, the paraventricular thalamus expresses clock gene rhythms (Feillet et al., 2008). Nonetheless, there is limited evidence for circadian rhythms in thalamic function in relation to pain processing.

3.8 Hypothalamus

Few studies have examined the role of the hypothalamus in regulating diurnal variations in pain thresholds. However, there is correlative evidence of circadian rhythms in many nociceptive nuclei within the hypothalamus. Given that the SCN is located within the hypothalamus and projects to the hypothalamic preoptic area, paraventricular nucleus, dorsomedial hypothalamic nuclei, ventromedial hypothalamus (Kriegsfeld et al., 2004), it is not unexpected that the TTFL has been reported in each of these regions (Girotti et al., 2009; Kriegsfeld et al., 2003; Kalil et al., 2016; Orozco-Solis et al., 2016; Moriya et al., 2009). Beta-endorphin and met-enkephalin display rhythmic levels of protein expression in the hypothalamus of rat brains (Takahashi et al., 1986), and levels of endogenous opioids display diurnal fluctuations in the rat hypothalamus (Asai et al.,

2007), suggesting that the hypothalamic processing of nociceptive input may vary across the day. The hypothalamus has also been implicated to play a role in cluster headaches (Holland & Goadsby, 2007; Burish et al., 2019), which exhibit diurnal variations in occurrence (Pringsheim, 2002). The diurnal variation in the incidence of cluster headaches suggests a causative relationship to the rhythmic activity of the SCN and other hypothalamic regions, but this role has yet to be directly determined.

3.9 Lateral Hypothalamus (Orexin)

The orexin system has been implicated to play a role in pain regulation (Razavi & Hosseinzadeh, 2017), and its involvement in the circadian regulation of the sleep-wake cycle suggests a correlative relationship in the circadian regulation of pain. A diurnal variation of orexin-A is observed in the cerebrospinal fluid of humans, rats, and diurnal squirrel monkeys, although it is worth noting that the pattern of orexin-A levels in human CSF did not follow the predicted levels (Salomon et al., 2003; Fujiki et al., 2001; Zeitzer et al., 2003). Plasma orexin-A levels do not exhibit a circadian pattern of expression (Mäkelä et al., 2018). Importantly, orexin-A is observed to have anti-nociceptive activity (Razavi & Hosseinzadeh, 2017). Ablation of the SCN abolishes CSF orexin-A rhythms, suggesting that these rhythms are either directly or indirectly regulated by the SCN (Zhang et al., 2004).

Orexin neurons display circadian rhythms of firing activity, with peaks of activity observed during the active period as indicated by *c-fos* expression (Marston et al., 2008; Estabrooke et al., 2001). The rhythmic activity of the LC is directed in part by orexin neurons of the DMH (Gompf & Aston-Jones, 2008), consistent with the flip-flop switch model of arousal (Schwartz & Roth, 2008) and the demonstrated circadian rhythmicity of orexin-A levels in the pons and the lateral/medial hypothalamus (Taheri et al., 2000). It has also been proposed that projections from the DMH, mPOA, and SPVZ to orexin act as indirect projections from the SCN to help maintain entrainment (Deurveilher & Semba, 2005). Orexin neurons project to various components of the descending pain modulatory system and modulate their activity, providing further correlative evidence for the involvement of this region in pain rhythms (Ahmadi-Soleimani et al., 2020).

3.10 Cortical and Limbic Structures

Direct evidence for the involvement of cortical and limbic regions in the circadian regulation of pain is scarce. However, circadian variations are present in these regions, suggesting that they may play a role in the temporal variation of pain thresholds. Rhythmic clock gene expression is present in the human ACC, dorsolateral prefrontal cortex, nucleus accumbens, and amygdala (Li et al., 2013). The presence of clock gene expression has also been observed in rodent cortical and limbic regions, including the ACC, prelimbic and infralimbic cortices, ventral orbital cortex, insular cortex, amygdala, and nucleus accumbens (Woodruff et al., 2016; Chun et al., 2015; Christiansen et al., 2016; Lamont et al., 2005). The SCN do not directly innervate the prefrontal cortex; instead, entrainment of these regions is proposed to occur via a relay circuit from the SCN -> paraventricular thalamic nucleus -> PFC (Sylvester et al., 2002). One study reported a slight but significant variation in the expression of μ -opioid receptor expression across the day in the frontal cortex (Takada et al., 2013). There are also diurnal variations in cortical ACh release in rats, with higher release during the active phase (Mitsushima et al., 1996). Anterior insular lesions disrupt the sleep-wake cycle and disturb locomotor activity cycles, suggesting that the insula plays a role in the behavioral regulation of circadian rhythms (Chen et al., 2016a). Rhythmic expression of serotonin, its 5HIAA metabolite, and 3-methoxy-4-hydroxyphenylglycol, the main metabolites of norepinephrine are present in the amygdala (Moriya et al., 2015). Another group reported diurnal rhythms of serotonin and dopamine in the amygdala, though specific statistical analyses were not provided (Izumo et al., 2012). Lastly, there are diurnal variations in cortical synaptic activity and spine density (Hayashi et al., 2013a). Further research explicitly examining circadian rhythms in cortical and limbic pain processing seems warranted.

4. Interacting Systems

In this section, I discuss circadian rhythms of the endogenous opioid, immune, and endocrine systems to consider how their interaction with the pain system may influence circadian rhythms of pain.

4.1 Endogenous Opioid System

The endogenous opioid system functions to regulate pain, emotional, and stress responses (Ferdousi & Finn, 2018). Circadian variations in opioid levels and binding activity throughout the day suggest that the opioid system plays a role in the circadian regulation of pain, potentially via the modulation of the activity of the pain system. Leu-enkephalin and met-enkephalin display circadian fluctuations within various forebrain regions of the rat (Asai et al., 2007; Kurumaji et al., 1988). Melatonin can induce dose-dependent increases of met-enkephalin, but this effect is not entirely mediated by binding to melatonin receptors (Asai et al., 2007). Dynorphin, but not beta-endorphin, levels also fluctuate across the day in the rat hypothalamus and pituitary (Reid et al., 1982). Diurnal rhythms of plasma met-enkephalin and beta-endorphin have been reported in humans (Mozzanica et al., 1991; Mozzanica et al., 1992; Petraglia et al., 1983). Daily variation in whole brain met-enkephalin levels in rats was observed when tissue was collected immediately after prolonged exposure to a hot plate; higher levels of met-enkephalin during the dark phase were associated with increased withdrawal latencies (Wesche & Frederickson, 1981). Hypophysectomy did not abolish this daily variation but did blunt the levels of whole brain enkephalin (Wesche & Frederickson, 1981).

Pain responses induced by morphine and naloxone injections vary across the day, suggesting an endogenous fluctuation in the expression of opioid receptors or the expression of components of their downstream signaling pathway (Frederickson et al., 1977; Kavaliers & Hirst, 1983). Recent work examining the analgesic effects of green light exposure during the light phase determined that green light-induced analgesia is dependent on descending RVM signaling and opioid signaling in the spinal cord of male rats (Ibrahim et al., 2017; Martin et al., 2021). These data indicate a role of photic signaling and potentially circadian rhythm entrainment in the modulation of pain by the endogenous opioid system. Lastly, there is a diurnal variation in opioid receptor expression in the rodent PAG and frontal cortex that was correlated with circadian variations in hot plate withdrawal thresholds (Takada et al., 2013).

Further research will be needed to identify whether the circadian rhythms of the endogenous opioid system modulate the pain system, or if the rhythms of the opioid system are an output of rhythms within the pain system. Taken together, the evidence above correlates with diurnal variations in reported opioid analgesic efficacy and requests for opioid analgesics in the clinic (Junker & Wirz, 2010). Additional insights into the interactions between these systems can improve patient treatment and chronotherapeutic efforts for pain management.

4.2 Endocrine System

Many hormones that interact with the pain system exhibit circadian rhythms, including cortisol, gonadal hormones, and melatonin. Cortisol modulates acute pain responsiveness and is thought to play a role in the development of chronic pain (Benson et al., 2019). Rhythms of cortisol concentrations are phase-dependent and fluctuate across the day; levels rise in the hours before waking and peak just after the onset of activity (Weitzman et al., 1971; Albers et al., 1985). One report suggests that cortisol rhythms are not necessary for diurnal variations in pain thresholds (Heybach & Vernikos-Danellis, 1978). But, as described above, one study reported that circadian corticosterone rhythms are necessary for the development of diurnal patterns of neuropathic allodynia in mice (Koyanagi et al., 2016). The rhythmic release of ATP from astrocytes in the dorsal horn of the spinal cord is dependent on corticosterone rhythms, as demonstrated by abolished ATP rhythms in adrenalectomized mice; it was suggested that the rhythmic release of ATP induces a rhythmic activation of microglia via P2Y₁₂R signaling (Koyanagi et al., 2016). However, differences in microglial activation were not observed as determined by Iba-1 staining. Perhaps the cortisol-dependent allodynia rhythms observed are instead a result of diurnal differences in neuronal synaptic transmission driven by the diurnal activity of astrocytic ATP production. Regardless of mechanisms, this study contributes an important understanding of the role of glucocorticoids in daily changes in neuropathic pain thresholds.

Gonadal hormones can play both pro- and anti-nociceptive roles and likely contribute to sex differences in pain thresholds; as an oversimplification, androgens tend

to be anti-nociceptive whereas estrogens are pro-nociceptive (Craft et al., 2004; Aloisi & Bonifazi, 2006). Androgen levels have rhythmic expression (Bremner et al., 1983), and although ovarian estrogen and progesterone levels in females are altered throughout estrous cycles, evidence suggests that they do exhibit circadian rhythms in secretion during the luteal phase (Spies et al., 1974; Kriegsfeld et al., 2002).

Melatonin has a primarily analgesic effect, although the exact mechanism by which it produces analgesia is unknown (Wilhelmsen et al., 2011; Chen et al., 2016b). Melatonin concentrations fluctuate in a phase-independent manner; its concentrations peak and persist in the dark phase and are almost entirely absent in the light phase (Brown, 1994).

4.3 Immune System

The immune system is regulated by circadian rhythms and displays circadian variations in function. Briefly, the TTFL is present in immune and glial cells, driving rhythmic immune activity and the expression of various inflammatory mediators involved in both innate and adaptive immune function (Logan & Sarkar, 2012). For example, microglia may be involved in the circadian regulation of pain (Inoue & Tsuda, 2018). Via circadian expression of cathepsin S, microglia drive the previously mentioned diurnal variations in cortical synaptic activity and spine density (Hayashi et al., 2013a). P2Y₁₂, the purinergic receptor that regulates microglia activation and neuropathic pain transmission within the spinal cord (Yu et al., 2019) is regulated by circadian rhythms (Hayashi et al., 2013b). Numerous other examples of the circadian regulation of immune and glial function and their influence on pain have been extensively reviewed (Segal et al., 2018). As the pain system is modulated by the activity of the immune system, there are considerable implications for the effects of rhythmic immune activity on pain rhythms.

5. Disrupted Circadian Rhythms and Pain

Within the past two centuries, humans have adopted lifestyles and environmental modifications that routinely disrupt our circadian rhythms. As a result of environmental or behavioral disturbances, our internal circadian rhythms can become shifted from the external world, blunted, or abolished. Examples of environmental or behavioral factors

that disrupt circadian rhythms are numerous: between 15-25% of the world's working population is involved in shift work (Drake & Wright, 2011), 70% of the population regularly experiences shifted sleep-wake cycles on weekends and work days - a phenomenon known as social "jet lag" (Roenneberg et al., 2012), and 80% percent of the global population is exposed to light pollution at night (Falchi et al., 2016). Other examples of circadian disruption include mistimed eating and jet lag resulting from transmeridian travel (Thaiss et al., 2014; Gibson et al., 2010; Challet, 2019; Zheng et al., 2020).

5.1 Circadian Rhythm Disruption and Pain

Multiple clinical and foundational science studies report that circadian rhythm disruption can directly alter pain thresholds. Disrupted circadian rhythms are linked to inflammation and altered endocrine function, both of which have direct implications on pain. In addition to directly affecting pain, many other consequences of disrupted circadian rhythms may be linked to altered pain, including increased risks for obesity (McHill & Wright, 2017), cancer (Davis & Mirick, 2006; Reiter et al., 2007; Haus & Smolensky, 2013), cardiovascular dysfunction (Chellappa et al., 2019), depression (Tsuneki et al., 2018) and altered immune (Logan & Sarkar, 2012) and endocrine function (Russart & Nelson, 2018).

The effects of circadian rhythm disruption on pain in humans have been examined in the context of night shift work and sleep disruption. Night shift work is associated with an increased risk for incidence of lower back pain (Takahashi et al., 2015; Eriksen et al., 2004; Zhao et al., 2012). Night-shift work is also correlated with reduced pain thresholds. One cross-over study reported that night-shift workers have higher sensitivity to electrical and heat pain, but not cold or pressure pain (Matre et al., 2017). In another study, night shift workers had lower cold pain thresholds immediately after finishing a 12-hour shift in comparison to a normal sleep day before and after the shift (Pieh et al., 2018). Selective and total sleep deprivation also heightens pain sensitivity, although inconsistently in human studies (Onen et al., 2001). Total sleep deprivation reduces heat pain thresholds (Kundermann et al., 2004; Kundermann et al., 2008), as well as mechanical pain thresholds (Onen et al., 2001).

Basic research has examined the effects of dim light at night exposure, mistimed eating, simulated jet lag, and sleep deprivation on pain in rodents. Male Swiss Webster mice exposed to dim light at night (~5 lux of light) experienced mechanical allodynia and cold hyperalgesia (Bumgarner et al., 2020). Notably, cold hyperalgesia was observed in these mice after only four nights of exposure to dim light at night. These behavioral effects were correlated with upregulated expression of *Il-6* and *μ-opioid receptor* expression in the RVM and PAG, respectively. Another study examined the role of mistimed eating on allodynia in a rodent model of neuropathy. It was observed that food consumption restricted to the inactive phase exacerbated mechanical allodynia in male mice with chronic constriction injury (Xu et al., 2018). Another study reported that jet lag can induce mechanical allodynia and heat hyperalgesia in female mice (Das et al., 2018). At the conclusion of the experiment, mice that experienced 14 weeks of weekly alternating light-dark cycles had lower mechanical thresholds and shorter hot plate withdrawal latencies than mice that received 6 weeks of shifts and had 8 weeks of typical light-dark cycles afterward. Appropriate control groups were missing in additional experiments of this study. Finally, multiple rodent studies have indicated that sleep deprivation heightens pain responsiveness (Lautenbacher et al., 2006). Together, these studies demonstrate a link between circadian rhythm disruption and altered function of the pain system.

5.2 Disrupted Rhythms of Pain

Multiple chronic and maladaptive pain conditions are associated with altered circadian rhythms in pain thresholds (Junker & Wirz, 2010). Altered pain rhythms manifest inconsistently across various disease states. The peak of breakthrough pain episodes in cancer patients occurs in the late morning/early afternoon (Campagna et al., 2019; Saini et al., 2013). This is somewhat consistent with reported early morning peaks of pain in patients with fibromyalgia (Bellamy et al., 2004) and rheumatoid arthritis (Bellamy et al., 1991; Harkness et al., 1982), although one group reported no diurnal variation in rheumatoid arthritis pain (Dekkers et al., 2000). Morning peaks in reported pain for these diseases contrast sharply with the reported night peaks of pain associated with diabetic neuropathy and postherpetic neuralgia (Odrich et al., 2006), evening peaks of pain in

patients with varying forms of intractable pain (Folkard et al., 1976), and nocturnal painful spasms associated with multiple sclerosis patients who have pyramidal tract dysfunction (Solaro et al., 2000). Considering the heterogeneous physiological consequences of these various disease states, the observed differences in acrophases of pain thresholds across the day could be explained by varying disruptions of individual components of the pain system or other circadian regulatory systems.

Many chronic pain conditions are also associated with disrupted circadian rhythms, including endocrine and sleep-wake rhythms. Cervical spinal cord injury in humans disrupts daily serum melatonin and cortisol rhythms (Fatima et al., 2016). In more severe instances of chronic pain, such as fibromyalgia, sleep-wake rhythms are highly perturbed (Korszun, 2000). However, sleep-wake disturbances are also reported in chronic pain patients (McCracken & Iverson, 2002; Smith et al., 2000). Altered sleep rhythms and decreased sleep quality can in turn have numerous negative consequences on the function of the circadian system (Palada et al., 2020).

Lastly, disrupted circadian rhythms have been observed in several rodent models of neuropathy. For example, sciatic nerve ligation alters the rhythmic expression of the melatonin 1A and 1B receptor in male mice (Odo et al., 2014). Spinal cord injury in rats disrupted circadian rhythms of locomotor activity, glucocorticoid secretion, inflammatory gene expression, and clock gene expression (Gaudet et al., 2018).

5.3 Circadian Disruption and Maladaptive Pain: A Feedback Loop?

The evidence reviewed in sections 5.1 and 5.2 lay the groundwork for describing a feedback loop that arises between circadian rhythm disruption and chronic pain, particularly the chronic pain associated with disease conditions (Fig. 2). Chronic pain can alter sleep-wake cycles and clock gene rhythms, among other rhythms, and circadian rhythm disruption can alter pain thresholds as well as the circadian rhythms of other interacting systems. Once initiated, this feedback loop likely results in states of chronically lowered pain thresholds and could contribute to prolonged periods of chronic pain. A clinically relevant example of this loop may be observed in fibromyalgia patients in whom

sleep-wake cycles and other rhythmic processes are affected by intense chronic pain. This disruption of circadian rhythms will in turn likely reduce pain thresholds.

It is unlikely that this loop drives pain thresholds to absolute minima or even close, particularly in healthy individuals. Though circadian rhythm disruption may temporarily or even chronically reduce pain thresholds, it is also unlikely that minor injuries would be sufficient to initiate the loop. Instead, this loop is likely more prominent in chronic pain caused by serious injury or disease. As further research validates the relationship between the circadian and pain systems, it will be important to consider this feedback loop in the treatment and management of acute and chronic pain. Environmental manipulations that support circadian rhythms may help to ameliorate pain symptoms in chronic pain patients and others.

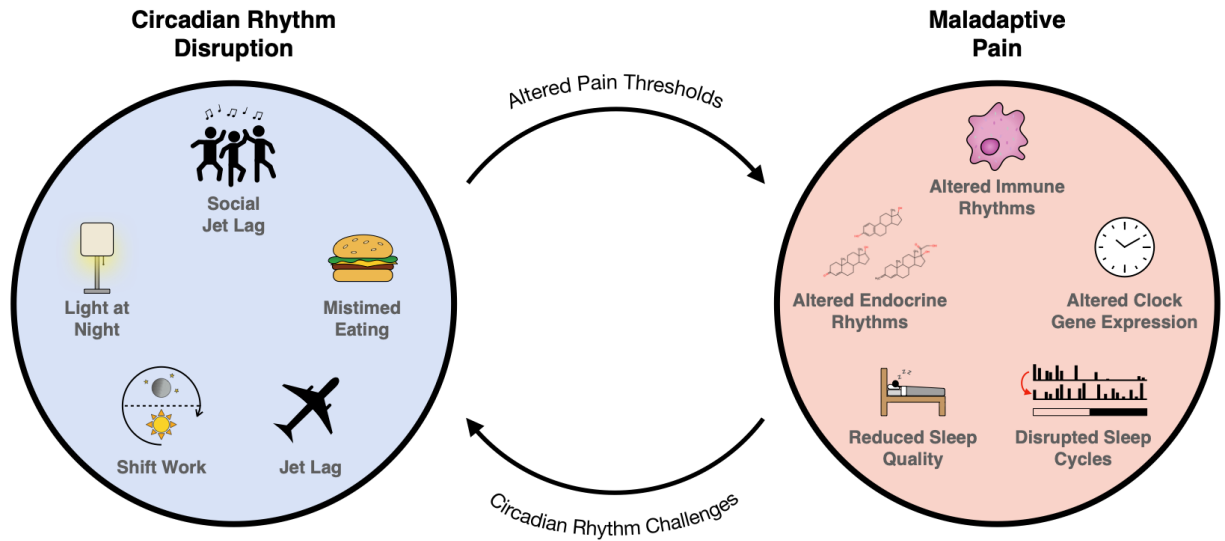


Figure 2. Disruption of circadian rhythms and maladaptive pain: A feedback loop. Maladaptive pain is negatively affected by common and seemingly innocuous forms of disrupted circadian rhythms, in addition to more severe forms of disruption. Many of the consequences of circadian rhythm disruption can negatively alter pain thresholds and affect maladaptive pain. The physiological consequences of maladaptive pain can induce various forms of disrupted circadian rhythms, thus generating a deleterious feedback loop. The consequences of this feedback loop should be considered in future clinical and preclinical research aiming to resolve and treat chronic and maladaptive pain.

6. Limitations

Several limitations arise from this review. First, much of the evidence regarding the regulation of pain behavior by circadian rhythms is correlative rather than causative. This is particularly apparent when examining higher-order components of the pain system, including cortical and limbic structures. As such, conclusions regarding the involvement of numerous supraspinal structures in the circadian regulation of pain behavior are limited. Second, several of the non-human studies described in Section 5.1 tested pain behavior during the light phase when nocturnal species are typically inactive, potentially hindering translational conclusions (Nelson et al., 2021). Lastly, there is a dramatic disparity in the sex of the animals in the reviewed literature. The vast majority of non-human studies only examined males (Supplemental Table 1). In the meta-analysis used to generate a model of human circadian rhythms in pain, only half of the 16 primary studies included females (Hagenauer et al., 2017). Because of known sex differences in circadian rhythms and pain behavior, this disparity leads to further potential limitations on the conclusions that can be drawn from the reviewed literature. Future human and non-human research should strive to examine circadian pain behaviors in both sexes.

7. Interpretations

The pain system exhibits circadian rhythms in function at all levels of hierarchical organization, but the origins of these rhythms are still not clear. Direct evidence has demonstrated that circadian regulation of pain occurs directly within DRG and the spinal cord, and abundant direct and correlative evidence have demonstrated that the supraspinal distributed pain system also processes pain differently across the day. Nonetheless, currently available evidence does not allow us to explicitly state that the circadian rhythmicity of pain thresholds exclusively arises from rhythms within the pain system alone. The variations in thresholds may instead be influenced or result from the integral relationships between the pain system and the circadian, endogenous opioid, immune, and endocrine systems as well as the ascending reticular activating system. Despite these uncertainties, the compiled evidence does outline several potential explanations of the origins of circadian rhythms of the pain system.

I propose that the circadian rhythms of the pain system may arise from a set of collective rhythms within the DRG, spinal cord, and descending pain modulatory system (Fig. 1). Collectively, these structures may act as circadian ‘gatekeepers’ that diurnally modulate the transmission of nociceptive information into supraspinal structures responsible for the salient processing of pain. The sleep/wake-dependent variation in the activity of neurons within numerous components of the descending pain modulatory system supports this theory. For example, the modulation of serotonergic input to the spinal cord from the RVM is regulated by On/Off neurons whose activity fluctuates based on sleep/wake states (Foo & Mason, 2003). The ‘circadian gatekeeper’ system could also be influenced by other circadian rhythms, leaving room to explain inconsistently altered pain rhythms among various disease states.

Alternatively, circadian rhythms of the pain system may not be a result of rhythms only within the ‘gatekeeper’ system. Instead, I alternatively propose that a distributed network of circadian rhythms within the pain system and those with which it interacts. Just as there is no single region of the pain system responsible for processing pain, there may be no single region responsible for the circadian rhythmicity of pain thresholds. The rhythmicity of the pain system likely arises from rhythms within three groups of organization: the DRG and spinal cord, cortical and limbic structures, and the descending pain modulatory system. These groups each have rhythmicity in function, but their collective activity and interaction may produce the pain threshold rhythms observed in constant conditions. The rhythmic function of the disturbed system is likely also influenced by interactions with the ascending reticular activating system, circadian system, endocrine system, and immune system. Disease-specific disruption of individual, but not all, of these modulatory systems, may explain the difference in circadian pain threshold variations across the day observed in different disease states. The concept of distributed circadian rhythms within the pain system will be difficult to elucidate, just as the examination of cerebral pain processing.

Importantly, *why* are there circadian rhythms in pain thresholds across the day? As of now, this trait has only been observed in mammals. But, considering the highly conserved characteristics of nociceptive signaling, it is not unreasonable to speculate that

these rhythms exist in other organisms; a discovery of rhythms in other organisms may point to an evolutionarily/adaptive beneficial function. Admittedly, it may be wrong to assume that these rhythms are functionally relevant. To a skeptical eye, the overlap between the ascending reticular activating system and the pain system could suggest that rhythms in pain thresholds might only be a behavioral byproduct that ultimately serves no adaptive benefit. Additional research will be needed to address these points. Conversely, variations in pain thresholds may allow for optimal behavioral function throughout the active hours by allowing animals to ignore small scrapes and wounds that may only distract from survival until activity slows down before rest. Or, as suggested by Foo (Foo & Mason, 2003), circadian variations in the rostral projection of nociceptive information may be crucial for sustained sleep. Regardless of the evolutionary origins of these rhythms, their nature must be considered. Further characterization of circadian rhythms of the pain system will allow us to adapt pain management and treatment strategies that optimize patient outcomes and well-being.

8. References

- Ab Aziz, C. B., & Ahmad, A. H. (2006). The role of the thalamus in modulating pain. *The Malaysian Journal of Medical Sciences (MJMS)*, 13(2), 11.
- Ahmadi-Soleimani, S. M., Mianbandi, V., Azizi, H., Zarmehri, H. A., Jandabi, M. G., Abbasi-Mazar, A., Mohajer, Y., & Darana, S. P. (2020). Coregulation of sleep-pain physiological interplay by orexin system: An unprecedented review. *Behavioural Brain Research*, 112650.
- Albers, H. E., Yogev, L. E. A. H., Todd, R. B., & Goldman, B. D. (1985). Adrenal corticoids in hamsters: role in circadian timing. *Journal of Psychiatry and Neuroscience*, 248(4), R434-R438.
- Aloisi, A. M., & Bonifazi, M. (2006). Sex hormones, central nervous system and pain. *Hormones and behavior*, 50(1), 1-7.
- Asai, M. A. M., Mayagoitia, L. M. L., García, D. G. D., Matamoros-Trejo, G. M.-T. G., Valdés-Tovar, M. V.-T. M., & Leff, P. L. P. (2007). Rat brain opioid peptides-circadian rhythm is under control of melatonin. *Neuropeptides*, 41(6), 389-397.

- Aston-Jones, G., Chen, S., Zhu, Y., & Oshinsky, M. L. (2001). A neural circuit for circadian regulation of arousal. *Nature Neuroscience*, 4(7), 732-738.
- Auvray, M., Myin, E., & Spence, C. (2010). The sensory-discriminative and affective-motivational aspects of pain. *Neuroscience & Biobehavioral Reviews*, 34(2), 214-223.
- Baliki, M. N., & Apkarian, A. V. (2015). Nociception, pain, negative moods, and behavior selection. *Neuron*, 87(3), 474-491.
- Basbaum, A. I., Bautista, D. M., Scherrer, G., & Julius, D. (2009). Cellular and Molecular Mechanisms of Pain. *Cell*, 139(2), 267-284.
- Bellamy, N., Sothorn, R. B., & Campbell, J. (2004). Aspects of diurnal rhythmicity in pain, stiffness, and fatigue in patients with fibromyalgia. *Annals of the Rheumatic Diseases*.
- Bellamy, N., Sothorn, R. B., Campbell, J., & Buchanan, W. W. (1991). Circadian rhythm in pain, stiffness, and manual dexterity in rheumatoid arthritis: relation between discomfort and disability. *Annals of the Rheumatic Diseases*, 50(4), 243-248.
- Benson, S., Siebert, C., Koenen, L. R., Engler, H., Kleine-Borgmann, J., Bingel, U., Icenhour, A., & Elsenbruch, S. (2019). Cortisol affects pain sensitivity and pain-related emotional learning in experimental visceral but not somatic pain: a randomized controlled study in healthy men and women. *Pain*, 160(8), 1719-1728.
- Bernard, J.-F. (2007). Hypothalamus and Nociceptive Pathways. In R. Schmidt, Willis, W. (Ed.), *Encyclopedia of Pain* (pp. 944-948). Springer Berlin Heidelberg.
- Bremner, W. J., Vitiello, M. V., & Prinz, P. N. (1983). Loss of circadian rhythmicity in blood testosterone levels with aging in normal men. *Journal of Psychiatry and Neuroscience*, 56(6), 1278-1281.
- Brown, G. M. (1994). Light, melatonin and the sleep-wake cycle. *Journal of Psychiatry and Neuroscience*, 19(5), 345.
- Bruguerolle, B., & Labrecque, G. (2007). Rhythmic pattern in pain and their chronotherapy. *Advanced Drug Delivery Reviews*, 59(9-10), 883-895.

- Bumgarner, J. R., Walker, W. H., Liu, J. A., Walton, J. C., & Nelson, R. J. (2020). Dim Light at Night Exposure Induces Cold Hyperalgesia and Mechanical Allodynia in Male Mice. *Neuroscience*, 434, 111-119.
- Burish, M. J., Chen, Z., & Yoo, S. (2019). Emerging relevance of circadian rhythms in headaches and neuropathic pain. *Acta Physiologica*, 225(1), e13161.
- Bushnell, M. C., Duncan, G. H., Hofbauer, R. K., Ha, B., Chen, J. I., & Carrier, B. (1999). Pain perception: is there a role for primary somatosensory cortex. *Proceedings of the National Academy of Sciences*, 96(14), 7705-7709.
- Campagna, S., Sperlinga, R., Milo, A., Sannuto, S., Acquafredda, F., Saini, A., Gonella, S., Berruti, A., Scagliotti, G. V., & Tampellini, M. (2019). The circadian rhythm of breakthrough pain episodes in terminally-ill cancer patients. *Cancers*, 11(1), 18.
- Cardoso-Cruz, H., Sameshima, K., Lima, D., & Galhardo, V. (2011). Dynamics of circadian thalamocortical flow of information during a peripheral neuropathic pain condition. *Frontiers in Integrative Neuroscience*, 5, 43.
- Castellano, C., Puglisi-Allegra, S., Renzi, P., & Oliverio, A. (1985). Genetic differences in daily rhythms of pain sensitivity in mice. *Pharmacology Biochemistry and Behavior*, 23(1), 91-92.
- Challet, E. (2019). The circadian regulation of food intake. *Nature Reviews Endocrinology*, 15(7), 393-405.
- Chassard, D., & Bruguerolle, B. (2004). Chronobiology and anesthesia. *Current Opinion in Neurobiology*, 100(2), 413-427.
- Chellappa, S. L., Vujovic, N., Williams, J. S., & Scheer, F. A. J. L. (2019). Impact of Circadian Disruption on Cardiovascular Function and Disease. *Trends in Endocrinology & Metabolism*, 30(10), 767-779.
- Chen, M. C., Chiang, W. Y., Yugay, T., Patxot, M., Özçivit, İ. B., Hu, K., & Lu, J. (2016a). Anterior Insula Regulates Multiscale Temporal Organization of Sleep and Wake Activity. *Journal of Biological Rhythms*, 31(2), 182-193.
- Chen, W., Zhang, X., & Huang, W. (2016b). Pain control by melatonin: Physiological and pharmacological effects. *Experimental and Therapeutic Medicine*, 12(4), 1963-1968.

- Christiansen, S. L., Bouzinova, E. V., Fahrenkrug, J., & Wiborg, O. (2016). Altered expression pattern of clock genes in a rat model of depression. *International Journal of Neuropsychopharmacology*, 19(11), pyw061.
- Chun, L. E., Woodruff, E. R., Morton, S., Hinds, L. R., & Spencer, R. L. (2015). Variations in Phase and Amplitude of Rhythmic Clock Gene Expression across Prefrontal Cortex, Hippocampus, Amygdala, and Hypothalamic Paraventricular and Suprachiasmatic Nuclei of Male and Female Rats. *Journal of Biological Rhythms*, 30(5), 417-436.
- Coghill, R. C. (2020). The Distributed Nociceptive System: A Framework for Understanding Pain. *Trends in Neurosciences*, 43(10), 780-794.
- Colas, D., Manca, A., & Mourrain, P. (2014). Orexin A and orexin receptor 1 axonal traffic in dorsal roots at the CNS/PNS interface. *Frontiers in Neuroscience*, 8, 20.
- Craft, R. M., Mogil, J. S., & Aloisi, A. M. (2004). Sex differences in pain and analgesia: the role of gonadal hormones. *Journal of Psychiatry and Neuroscience*, 8(5), 397-411.
- Das, V., Kc, R., Li, X., Varma, D., Qiu, S., Kroin, J. S., Forsyth, C. B., Keshavarzian, A., van Wijnen, A. J., Park, T. J., Stein, G. S., O-Sullivan, I., Burris, T. P., & Im, H. J. (2018). Pharmacological targeting of the mammalian clock reveals a novel analgesic for osteoarthritis-induced pain. *Gene*, 655, 1-12.
- Davis, S., & Mirick, D. K. (2006). Circadian disruption, shift work and the risk of cancer: a summary of the evidence and studies in Seattle. *Cancer Causes Control*, 17(4), 539-545.
- de C Williams, A. C. (2016). What can evolutionary theory tell us about chronic pain. *Pain*, 157(4), 788-790.
- Dekkers, J. C., Geenen, R., Godaert, G. L. R., Doornen, L. J. P., & Bijlsma, J. W. J. (2000). Diurnal courses of cortisol, pain, fatigue, negative mood, and stiffness in patients with recently diagnosed rheumatoid arthritis. *International Journal of Behavioral Medicine*, 7(4), 353-371.

- Deurveilher, S., & Semba, K. (2005). Indirect projections from the suprachiasmatic nucleus to major arousal-promoting cell groups in rat: implications for the circadian control of behavioural state. *Neuroscience*, 130(1), 165-183.
- Drake, C. L., & Wright, K. P. (2011). Shift Work, Shift-Work Disorder, and Jet Lag. In *Principles and Practice of Sleep Medicine* (pp. 784-798). Elsevier.
- Eblen-Zajjur, A., Marín, R., Vanegas, H., Proverbio, F., & Proverbio, T. (2015). Diurnal changes in ouabain-sensitive Na⁺,K⁺-ATPase activity in the rat spinal dorsal horn. *Neurochemical Journal*, 9(4), 266-270.
- Eriksen, W., Bruusgaard, D., & Knardahl, S. (2004). Work factors as predictors of intense or disabling low back pain; a prospective study of nurses' aides. *Occupational and Environmental Medicine*, 61(5), 398-404.
- Estabrooke, I. V., McCarthy, M. T., Ko, E., Chou, T. C., Chemelli, R. M., Yanagisawa, M., Saper, C. B., & Scammell, T. E. (2001). Fos expression in orexin neurons varies with behavioral state. *Journal of Neuroscience*, 21(5), 1656-1662.
- Falchi, F., Cinzano, P., Duriscoe, D., Kyba, C. C., Elvidge, C. D., Baugh, K., Portnov, B. A., Rybnikova, N. A., & Furgoni, R. (2016). The new world atlas of artificial night sky brightness. *Science Advances*, 2(6), e1600377.
- Fatima, G., Sharma, V. P., & Verma, N. S. (2016). Circadian variations in melatonin and cortisol in patients with cervical spinal cord injury. *Spinal Cord*, 54(5), 364-367.
- Feillet, C. A., Mendoza, J., Albrecht, U., Pévet, P., & Challet, E. (2008). Forebrain oscillators ticking with different clock hands. *Molecular and Cellular Neurosciences*, 37(2), 209-221.
- Ferdousi, M., & Finn, D. P. (2018). Stress-induced modulation of pain: role of the endogenous opioid system. In S. O'Mara (Ed.), *Progress in Brain Research* (pp. 121-177). Elsevier.
- Folkard, S., Glynn, C. J., & Lloyd, J. W. (1976). Diurnal variation and individual differences in the perception of intractable pain. *Journal of Psychosomatic Research*, 20(4), 289-301.
- Foo, H., & Mason, P. (2003). Brainstem modulation of pain during sleep and waking. *Sleep Medicine Reviews*, 7(2), 145-154.

- Frederickson, R. C., Burgis, V., & Edwards, J. D. (1977). Hyperalgesia induced by naloxone follows diurnal rhythm in responsivity to painful stimuli. *Science*, *198*(4318), 756-758.
- Fujiki, N., Yoshida, Y., Ripley, B., Honda, K., Mignot, E., & Nishino, S. (2001). Changes in CSF hypocretin-1 (orexin A) levels in rats across 24 hours and in response to food deprivation. *Neuroreport*, *12*(5), 993-997.
- Gamble, K. L., Berry, R., Frank, S. J., & Young, M. E. (2014). Circadian clock control of endocrine factors. *Nature Reviews Endocrinology*, *10*(8), 466-475.
- Gangadharan, V., & Kuner, R. (2013). Pain hypersensitivity mechanisms at a glance. *Disease Models & Mechanisms*, *6*(4), 889-895.
- Garcia-Larrea, L., & Peyron, R. (2013). Pain matrices and neuropathic pain matrices: a review. *PAIN®*, *154*, S29-S43.
- Gaudet, A. D., Fonken, L. K., Ayala, M. T., Bateman, E. M., Schleicher, W. E., Smith, E. J., D'Angelo, H. M., Maier, S. F., & Watkins, L. R. (2018). Spinal cord injury in rats disrupts the circadian system. *eNeuro*, *5*(6), ENEURO.0328-18.2018.
- Gibson, E. M., Wang, C., Tjho, S., Khattar, N., & Kriegsfeld, L. J. (2010). Experimental 'jet lag' inhibits adult neurogenesis and produces long-term cognitive deficits in female hamsters. *PLoS One*, *5*(12), e15267.
- Girotti, M., Weinberg, M. S., & Spencer, R. L. (2009). Diurnal expression of functional and clock-related genes throughout the rat HPA axis: system-wide shifts in response to a restricted feeding schedule. *American Journal of Physiology - Endocrinology and Metabolism*, *296*(4), E888-97.
- Golombek, D. A., & Rosenstein, R. E. (2010). Physiology of circadian entrainment. *Physiological Reviews*, *90*(3), 1063-1102.
- Gompf, H. S., & Aston-Jones, G. (2008). Role of orexin input in the diurnal rhythm of locus coeruleus impulse activity. *Brain Research*, *1224*, 43-52.
- González, M. M. C., & Aston-Jones, G. (2006). Circadian regulation of arousal: role of the noradrenergic locus coeruleus system and light exposure. *Sleep*, *29*(10), 1327-1336.

- Guo, D., & Hu, J. (2014). Spinal presynaptic inhibition in pain control. *Neuroscience*, 283, 95-106.
- Hagenauer, M. H., Crodelle, J. A., Piltz, S. H., Toporikova, N., Ferguson, P., & Booth, V. (2017). The modulation of pain by circadian and sleep-dependent processes: A review of the experimental evidence. In A. Layton & L. Miller (Eds.), *Women in Mathematical Biology* (pp. 1-21). Springer, Cham.
- Harkness, J. A., Richter, M. B., Panayi, G. S., Van de Pette, K., Unger, A., Pownall, R., & Geddawi, M. (1982). Circadian variation in disease activity in rheumatoid arthritis. *British Medical Journal (Clinical research ed.)*, 284(6315), 551-554.
- Hattar, S., Kumar, M., Park, A., Tong, P., Tung, J., Yau, K., & Berson, D. M. (2006). Central projections of melanopsin-expressing retinal ganglion cells in the mouse. *Journal of Comparative Neurology*, 497(3), 326-349.
- Haus, E. L., & Smolensky, M. H. (2013). Shift work and cancer risk: potential mechanistic roles of circadian disruption, light at night, and sleep deprivation. *Sleep Medicine Reviews*, 17(4), 273-284.
- Hayashi, Y., Koyanagi, S., Kusunose, N., Okada, R., Wu, Z., Tozaki-Saitoh, H., Ukai, K., Kohsaka, S., Inoue, K., Ohdo, S., & Nakanishi, H. (2013a). The intrinsic microglial molecular clock controls synaptic strength via the circadian expression of cathepsin S. *Scientific Reports*, 3, 2744.
- Hayashi, Y., Koyanagi, S., Kusunose, N., Takayama, F., Okada, R., Wu, Z., & Nakanishi, H. (2013b). Diurnal spatial rearrangement of microglial processes through the rhythmic expression of P2Y₁₂ receptors. *Journal of Neurological Disorders*, 1(120), 10.4172.
- Hery, F., Chouvet, G., Kan, J. P., Pujol, J. F., & Glowinski, J. (1977). Daily variations of various parameters of serotonin metabolism in the rat brain. II. Circadian variations in serum and cerebral tryptophan levels: lack of correlation with 5-HT turnover. *Brain Research*, 123(1), 137-145.
- Heybach, J. P., & Vernikos-Danellis, J. (1978). The effect of pituitary-adrenal function in the modulation of pain sensitivity in the rat. *Journal of Psychiatry and Neuroscience*, 283(1), 331-340.

- Holland, P., & Goadsby, P. J. (2007). The Hypothalamic Orexinergic System: Pain and Primary Headaches. *Headache: The Journal of Head and Face Pain*, 47(6), 951-962.
- Hsu, D. T., Kirouac, G. J., Zubieta, J. K., & Bhatnagar, S. (2014). Contributions of the paraventricular thalamic nucleus in the regulation of stress, motivation, and mood. *Frontiers in Behavioral Neuroscience*, 8, 73.
- Iannetti, G. D., & Mouraux, A. (2010). From the neuromatrix to the pain matrix (and back). *Experimental Brain Research*, 205(1), 1-12.
- Ibrahim, M. M., Patwardhan, A., Gilbraith, K. B., Moutal, A., Yang, X., Chew, L. A., Largent-Milnes^b, T., Malan, T. P., Vanderah, T. W., & Porreca, F. (2017). Long-lasting antinociceptive effects of green light in acute and chronic pain in rats. *Pain*, 158(2), 347.
- Inoue, K., & Tsuda, M. (2018). Microglia in neuropathic pain: cellular and molecular mechanisms and therapeutic potential. *Nature Reviews Neuroscience*, 19(3), 138-152.
- Izumo, N., Ishibashi, Y., Ohba, M., Morikawa, T., & Manabe, T. (2012). Decreased voluntary activity and amygdala levels of serotonin and dopamine in ovariectomized rats. *Behavioural Brain Research*, 227(1), 1-6.
- Junker, U., & Wirz, S. (2010). Chronobiology: influence of circadian rhythms on the therapy of severe pain. *Journal of Oncology Pharmacy Practice*, 16(2), 81-87.
- Kalil, B., Ribeiro, A. B., Leite, C. M., Uchôa, E. T., Carolino, R. O., Cardoso, T. S. R., Elias, L. L. K., Rodrigues, J. A., Plant, T. M., & Poletini, M. O. (2016). The increase in signaling by kisspeptin neurons in the preoptic area and associated changes in clock gene expression that trigger the LH surge in female rats are dependent on the facilitatory action of a noradrenaline input. *Endocrinology*, 157(1), 323-335.
- Kaushal, R., Taylor, B. K., Jamal, A. B., Zhang, L., Ma, F., Donahue, R., & Westlund, K. N. (2016). GABA-A receptor activity in the noradrenergic locus coeruleus drives trigeminal neuropathic pain in the rat; contribution of NAA1 receptors in the medial prefrontal cortex. *Neuroscience*, 334, 148-159.

- Kavaliers, M., & Hirst, M. (1983). Daily rhythms of analgesia in mice: effects of age and photoperiod. *Brain Research*, 279(1-2), 387-393.
- Khasabov, S. G., Malecha, P., Noack, J., Tabakov, J., Okamoto, K., Bereiter, D. A., & Simone, D. A. (2015). Activation of rostral ventromedial medulla neurons by noxious stimulation of cutaneous and deep craniofacial tissues. *Journal of Neurophysiology*, 113(1), 14-22.
- Kim, H. K., Lee, S.-Y., Koike, N., Kim, E., Wirianto, M., Burish, M. J., Yagita, K., Lee, H. K., Chen, Z., & Chung, J. M. (2020). Circadian regulation of chemotherapy-induced peripheral neuropathic pain and the underlying transcriptomic landscape. *Scientific Reports*, 10(1), 1-13.
- Kim, M. J., Chung, J. W., Kho, H.-S., & Park, J. W. (2015). The Circadian Rhythm Variation of Pain in the Orofacial Region. *Journal of Oral Medicine and Pain*, 40(3), 89-95.
- Korszun, A. (2000). Sleep and circadian rhythm disorders in fibromyalgia. *Current Rheumatology Reports*, 2, 124-130.
- Koyanagi, S., Kusunose, N., Taniguchi, M., Akamine, T., Kanado, Y., Ozono, Y., Masuda, T., Kohro, Y., Matsunaga, N., Tsuda, M., Salter, M. W., Inoue, K., & Ohdo, S. (2016). Glucocorticoid regulation of ATP release from spinal astrocytes underlies diurnal exacerbation of neuropathic mechanical allodynia. *Nature Communications*, 7, 13102.
- Kriegsfeld, L. J., LeSauter, J., Hamada, T., Pitts, S. M., & Silver, R. (2002). Circadian rhythms in the endocrine system. In Pfaff DW, Arnold AP, Fahrbach SE, Etgen AM, & R. RT (Eds.), *Hormones, Brain and Behavior* (pp. 33-91). Elsevier.
- Kriegsfeld, L. J., Korets, R., & Silver, R. (2003). Expression of the circadian clock gene Period 1 in neuroendocrine cells: an investigation using mice with a Per1::GFP transgene. *European Journal of Neuroscience*, 17(2), 212-220.
- Kriegsfeld, L. J., Leak, R. K., Yackulic, C. B., LeSauter, J., & Silver, R. (2004). Organization of suprachiasmatic nucleus projections in Syrian hamsters (*Mesocricetus auratus*): an anterograde and retrograde analysis. *Journal of Comparative Neurology*, 468(3), 361-379.

- Ku, J., Lee, Y. S., Chang, H. W., Earley, C. J., Allen, R. P., & Cho, Y. W. (2018). Diurnal variation of default mode network in patients with restless legs syndrome. *Sleep Medicine*, 41, 1-8.
- Kulkarni, B., Bentley, D. E., Elliott, R., Youell, P., Watson, A., Derbyshire, S. W., Frackowiak, R. S., Friston, K. J., & Jones, A. K. (2005). Attention to pain localization and unpleasantness discriminates the functions of the medial and lateral pain systems. *European Journal of Neuroscience*, 21(11), 3133-3142.
- Kundermann, B., Hemmeter-Spernal, J., Huber, M. T., Krieg, J. C., & Lautenbacher, S. (2008). Effects of total sleep deprivation in major depression: overnight improvement of mood is accompanied by increased pain sensitivity and augmented pain complaints. *Psychosomatic Medicine*, 70(1), 92-101.
- Kundermann, B., Spernal, J., Huber, M. T., Krieg, J. C., & Lautenbacher, S. (2004). Sleep deprivation affects thermal pain thresholds but not somatosensory thresholds in healthy volunteers. *Psychosomatic Medicine*, 66(6), 932-937.
- Kurumaji, A., Takashima, M., Ohi, K., & Takahashi, K. (1988). Circadian fluctuations in pain responsiveness and brain Met-enkephalin-like immunoreactivity in the rat. *Pharmacology, Biochemistry, and Behavior*, 29(3), 595-599.
- Kusunose, N., Koyanagi, S., Hamamura, K., Matsunaga, N., Yoshida, M., Uchida, T., Tsuda, M., Inoue, K., & Ohdo, S. (2010). Molecular basis for the dosing time-dependency of anti-allodynic effects of gabapentin in a mouse model of neuropathic pain. *Molecular Pain*, 6, 83.
- LaCroix-Fralish, M. L., Mo, G., Smith, S. B., Sotocinal, S. G., Ritchie, J., Austin, J.-S., Melmed, K., Schorscher-Petcu, A., Laferriere, A. C., & Lee, T. H. (2009). The $\beta 3$ subunit of the Na⁺, K⁺-ATPase mediates variable nociceptive sensitivity in the formalin test. *Neuroscience*, 144(3), 294-302.
- Lamont, E. W., Robinson, B., Stewart, J., & Amir, S. (2005). The central and basolateral nuclei of the amygdala exhibit opposite diurnal rhythms of expression of the clock protein Period2. *Proceedings of the National Academy of Sciences*, 102(11), 4180-4184.

- Landgraf, D., Long, J. E., & Welsh, D. K. (2016). Depression-like behaviour in mice is associated with disrupted circadian rhythms in nucleus accumbens and periaqueductal grey. *European Journal of Neuroscience*, 43(10), 1309-1320.
- Latremoliere, A., & Woolf, C. J. (2009). Central sensitization: a generator of pain hypersensitivity by central neural plasticity. *The Journal of Pain*, 10(9), 895-926.
- Lau, B. K., & Vaughan, C. W. (2014). Descending modulation of pain: the GABA disinhibition hypothesis of analgesia. *Current Opinion in Neurobiology*, 29, 159-164.
- Lautenbacher, S., Kundermann, B., & Krieg, J. C. (2006). Sleep deprivation and pain perception. *Sleep Medicine Reviews*, 10(5), 357-369.
- Lee, P. R., Cohen, J. E., Iacobas, D. A., Iacobas, S., & Fields, R. D. (2017). Gene networks activated by specific patterns of action potentials in dorsal root ganglia neurons. *Scientific Reports*, 7, 43765.
- Legrain, V., Iannetti, G. D., Plaghki, L., & Mouraux, A. (2011). The pain matrix reloaded: a salience detection system for the body. *Progress in Neurobiology*, 93(1), 111-124.
- Leung, C. G., & Mason, P. (1999). Physiological properties of raphe magnus neurons during sleep and waking. *Journal of Neurophysiology*, 81(2), 584-595.
- Li, J. Z., Bunney, B. G., Meng, F., Hagenauer, M. H., Walsh, D. M., Vawter, M. P., Evans, S. J., Choudary, P. V., Cartagena, P., Barchas, J. D., Schatzberg, A. F., Jones, E. G., Myers, R. M., Watson, S. J., Akil, H., & Bunney, W. E. (2013). Circadian patterns of gene expression in the human brain and disruption in major depressive disorder. *Proceedings of the National Academy of Sciences*, 110(24), 9950-9955.
- Li, W. W., Guo, T. Z., Liang, D. Y., Sun, Y., Kingery, W. S., & Clark, J. D. (2012). Substance P signaling controls mast cell activation, degranulation, and nociceptive sensitization in a rat fracture model of complex regional pain syndrome. *Anesthesiology*, 116(4), 882-895.
- Logan, R. W., & Sarkar, D. K. (2012). Circadian nature of immune function. *Molecular and Cellular Endocrinology*, 349(1), 82-90.
- Lu, C., Yang, T., Zhao, H., Zhang, M., Meng, F., Fu, H., Xie, Y., & Xu, H. (2016). Insular Cortex is Critical for the Perception, Modulation, and Chronification of Pain. *Neuroscience Bulletin*, 32(2), 191-201.

- Lu, Y., Dong, H., Gao, Y., Gong, Y., Ren, Y., Gu, N., Zhou, S., Xia, N., Sun, Y. Y., Ji, R. R., & Xiong, L. (2013). A feed-forward spinal cord glycinergic neural circuit gates mechanical allodynia. *Journal of Clinical Investigation*, 123(9), 4050-4062.
- Mahoney, C. E., Brewer, J. M., & Bittman, E. L. (2013). Central control of circadian phase in arousal-promoting neurons. *PLoS One*, 8(6), e67173.
- Maihöfner, C., Herzner, B., & Otto Handwerker, H. (2006). Secondary somatosensory cortex is important for the sensory-discriminative dimension of pain: a functional MRI study. *European Journal of Neuroscience*, 23(5), 1377-1383.
- Mäkelä, K. A., Karhu, T., Jurado Acosta, A., Vakkuri, O., Leppäluoto, J., & Herzig, K. H. (2018). Plasma Orexin-A Levels Do Not Undergo Circadian Rhythm in Young Healthy Male Subjects. *Frontiers in Endocrinology*, 9, 710.
- Mansour, A. R., Farmer, M. A., Baliki, M. N., & Apkarian, A. V. (2014). Chronic pain: the role of learning and brain plasticity. *Restorative Neurology and Neuroscience*, 32(1), 129-139.
- Marcus, J. N., & Elmquist, J. K. (2006). Orexin Projections and Localization of Orexin Receptors. In *The Orexin/Hypocretin System* (pp. 21-43). Humana Press.
- Marston, O. J., Williams, R. H., Canal, M. M., Samuels, R. E., Upton, N., & Piggins, H. D. (2008). Circadian and dark-pulse activation of orexin/hypocretin neurons. *Molecular Brain*, 1, 19.
- Martin, L. F., Moutal, A., Cheng, K., Washington, S. M., Calligaro, H., Goel, V., Kranz, T., Largent-Milnes, T. M., Khanna, R., & Patwardhan, A. (2021). Green light antinociceptive and reversal of thermal and mechanical hypersensitivity effects rely on endogenous opioid system stimulation. *The Journal of Pain*, 22(12), 1646-1656.
- Martínez-Gómez, M., Cruz, Y., Salas, M., Hudson, R., & Pacheco, P. (1994). Assessing pain threshold in the rat: changes with estrus and time of day. *Physiology & Behavior*, 55(4), 651-657.
- Matre, D., Knardahl, S., & Nilsen, K. B. (2017). Night-shift work is associated with increased pain perception. *Scandinavian Journal of Work, Environment & Health*, 43(3), 260-268.

- McCracken, L. M., & Iverson, G. L. (2002). Disrupted sleep patterns and daily functioning in patients with chronic pain. *Pain Research & Management*, 7(2), 75-79.
- McHill, A. W., & Wright, K. P. (2017). Role of sleep and circadian disruption on energy expenditure and in metabolic predisposition to human obesity and metabolic disease. *Obesity Reviews*, 18 Suppl 1, 15-24.
- Metz, A. E., Yau, H. J., Centeno, M. V., Apkarian, A. V., & Martina, M. (2009). Morphological and functional reorganization of rat medial prefrontal cortex in neuropathic pain. *Proceedings of the National Academy of Sciences*, 106(7), 2423-2428.
- Mitsushima, D., Mizuno, T., & Kimura, F. (1996). Age-related changes in diurnal acetylcholine release in the prefrontal cortex of male rats as measured by microdialysis. *Neuroscience*, 72(2), 429-434.
- Miyake, S., Sumi, Y., Yan, L., Takekida, S., Fukuyama, T., Ishida, Y., Yamaguchi, S., Yagita, K., & Okamura, H. (2000). Phase-dependent responses of Per1 and Per2 genes to a light-stimulus in the suprachiasmatic nucleus of the rat. *Neuroscience Letters*, 294(1), 41-44.
- Monošíková, J., Herichová, I., Mravec, B., Kiss, A., & Zeman, M. (2007). Effect of upregulated renin–angiotensin system on per2 and bmal1 gene expression in brain structures involved in blood pressure control in TGR(mREN-2)27 rats. *Brain Research*, 1180, 29-38.
- Morioka, N., Saeki, M., Sugimoto, T., Higuchi, T., Zhang, F. F., Nakamura, Y., Hisaoka-Nakashima, K., & Nakata, Y. (2016). Downregulation of the spinal dorsal horn clock gene Per1 expression leads to mechanical hypersensitivity via c-jun N-terminal kinase and CCL2 production in mice. *Molecular and Cellular Neurosciences*, 72, 72-83.
- Morioka, N., Sugimoto, T., Tokuhara, M., Nakamura, Y., Abe, H., Hisaoka, K., Dohi, T., & Nakata, Y. (2012). Spinal astrocytes contribute to the circadian oscillation of glutamine synthase, cyclooxygenase-1 and clock genes in the lumbar spinal cord of mice. *Neurochemistry International*, 60(8), 817-826.

- Moriya, S., Tahara, Y., Sasaki, H., Ishigooka, J., & Shibata, S. (2015). Phase-delay in the light-dark cycle impairs clock gene expression and levels of serotonin, norepinephrine, and their metabolites in the mouse hippocampus and amygdala. *Sleep Medicine*, 16(11), 1352-1359.
- Moriya, T., Aida, R., Kudo, T., Akiyama, M., Doi, M., Hayasaka, N., Nakahata, N., Mistlberger, R., Okamura, H., & Shibata, S. (2009). The dorsomedial hypothalamic nucleus is not necessary for food-anticipatory circadian rhythms of behavior, temperature or clock gene expression in mice. *European Journal of Neuroscience*, 29(7), 1447-1460.
- Mozzanica, N., Finzi, A. F., Foppa, S., Vignati, G., & Villa, M. L. (1991). Association between circadian rhythms of endogenous hypothalamic opioid peptides and of natural killer cell activity. *International Journal of Immunopharmacology*, 13(2-3), 317-321.
- Mozzanica, N., Villa, M. L., Foppa, S., Vignati, G., Cattaneo, A., Diotti, R., & Finzi, A. F. (1992). Plasma alpha-melanocyte-stimulating hormone, beta-endorphin, met-enkephalin, and natural killer cell activity in vitiligo. *Journal of the American Academy of Dermatology*, 26(5 Pt 1), 693-700.
- Nagoshi, E., Saini, C., Bauer, C., Laroche, T., Naef, F., & Schibler, U. (2004). Circadian gene expression in individual fibroblasts: cell-autonomous and self-sustained oscillators pass time to daughter cells. *Cell*, 119(5), 693-705.
- Natali, J.-P., McRae-Degueurce, A., Keane, P., Debilly, G., & Pujol, J.-F. (1980). Genetic studies of daily variations of first-step enzymes of monoamines metabolism in the brain of inbred strains of mice and hybrids. II. Daily variations of tyrosine hydroxylase activity in the locus coeruleus. *Brain Research*, 191(1), 205-213.
- Negri, L., Lattanzi, R., Giannini, E., Metere, A., Colucci, M., Barra, D., Kreil, G., & Melchiorri, P. (2002). Nociceptive sensitization by the secretory protein Bv8. *British Journal of Pharmacology*, 137(8), 1147-1154.
- Nelson, R. J., Bumgarner, J. R., Walker, W. H., & DeVries, A. C. (2021). Time-of-day as a critical biological variable. *Neuroscience & Biobehavioral Reviews*, 127, 740-746.

- Neugebauer, V. (2015). Amygdala pain mechanisms. *Handbook of Experimental Pharmacology*, 227, 261-284.
- Odo, M., Koh, K., Takada, T., Yamashita, A., Narita, M., Kuzumaki, N., Ikegami, D., Sakai, H., Iseki, M., Inada, E., & Narita, M. (2014). Changes in circadian rhythm for mRNA expression of melatonin 1A and 1B receptors in the hypothalamus under a neuropathic pain-like state. *Synapse*, 68(4), 153-158.
- Odrocich, M., Bailey, J. M., Cahill, C. M., & Gilron, I. (2006). Chronobiological characteristics of painful diabetic neuropathy and postherpetic neuralgia: diurnal pain variation and effects of analgesic therapy. *Pain*, 120(1-2), 207-212.
- Oliverio, A., Castellano, C., & Puglisi-Allegra, S. (1982). Opiate analgesia: evidence for circadian rhythms in mice. *Brain Research*, 249(2), 265-270.
- Onen, S. H., Alloui, A., Gross, A., Eschallier, A., & Dubray, C. (2001). The effects of total sleep deprivation, selective sleep interruption and sleep recovery on pain tolerance thresholds in healthy subjects. *Journal of Sleep Research*, 10(1), 35-42.
- Ong, W. Y., Stohler, C. S., & Herr, D. R. (2019). Role of the Prefrontal Cortex in Pain Processing. *Molecular Neurobiology*, 56(2), 1137-1166.
- Onishi, H., Yamaguchi, S., Yagita, K., Ishida, Y., Dong, X., Kimura, H., Jing, Z., Ohara, H., & Okamura, H. (2002). Rev-erb α gene expression in the mouse brain with special emphasis on its circadian profiles in the suprachiasmatic nucleus. *Journal of Neuroscience Research*, 68(5), 551-557.
- Orozco-Solis, R., Aguilar-Arnal, L., Murakami, M., Peruquetti, R., Ramadori, G., Coppari, R., & Sassone-Corsi, P. (2016). The Circadian Clock in the Ventromedial Hypothalamus Controls Cyclic Energy Expenditure. *Cell Metabolism*, 23(3), 467-478.
- Ossipov, M. H., Morimura, K., & Porreca, F. (2014). Descending pain modulation and chronification of pain. *Behavioural Brain Research*, 268, 143-151.
- Ostrowsky, K., Magnin, M., Ryvlin, P., Isnard, J., Guenot, M., & Mauguière, F. (2002). Representation of pain and somatic sensation in the human insula: a study of responses to direct electrical cortical stimulation. *Cerebral Cortex*, 12(4), 376-385.

- Palada, V., Gilron, I., Canlon, B., Svensson, C. I., & Kalso, E. (2020). The circadian clock at the intercept of sleep and pain. *Pain*, 161(5), 894-900.
- Partch, C. L., Green, C. B., & Takahashi, J. S. (2014). Molecular architecture of the mammalian circadian clock. *Trends in Cell Biology*, 24(2), 90-99.
- Pertovaara, A., & Almeida, A. (2006). Descending inhibitory systems. *Handbook of Clinical Neurology*, 81, 179-192.
- Petraglia, F., Facchinetti, F., Parrini, D., Micieli, G., De Luca, S., & Genazzani, A. R. (1983). Simultaneous circadian variations of plasma ACTH, beta-lipotropin, beta-endorphin and cortisol. *Hormone Research*, 17(3), 147-152.
- Pevet, P., & Challet, E. (2011). Melatonin: both master clock output and internal time-giver in the circadian clocks network. *Journal of Physiology-Paris*, 105(4-6), 170-182.
- Pickard, G. E. (1987). Circadian rhythm of nociception in the golden hamster. *Brain Research*, 425(2), 395-400.
- Pieh, C., Jank, R., Waiß, C., Pfeifer, C., Probst, T., Lahmann, C., & Oberndorfer, S. (2018). Night-shift work increases cold pain perception. *Sleep Medicine*, 45, 74-79.
- Porro, C. A., Baraldi, P., Pagnoni, G., Serafini, M., Facchin, P., Maieron, M., & Nichelli, P. (2002). Does Anticipation of Pain Affect Cortical Nociceptive Systems. *The Journal of Neuroscience*, 22(8), 3206-3214.
- Pringsheim, T. (2002). Cluster headache: evidence for a disorder of circadian rhythm and hypothalamic function. *Canadian Journal of Neurological Sciences*, 29(1), 33-40.
- Rainville, P., Duncan, G. H., Price, D. D., Carrier, B., & Bushnell, M. C. (1997). Pain affect encoded in human anterior cingulate but not somatosensory cortex. *Science*, 277(5328), 968-971.
- Razavi, B. M., & Hosseinzadeh, H. (2017). A review of the role of orexin system in pain modulation. *Biomedicine & Pharmacotherapy*, 90, 187-193.
- Reid, L. D., Konecka, A. M., Przewłocki, R., Millan, M. H., Millan, M. J., & Herz, A. (1982). Endogenous opioids, circadian rhythms, nutrient deprivation, eating and drinking. *Life Sciences*, 31(16-17), 1829-1832.

- Reiter, R. J., Tan, D. X., Korkmaz, A., Erren, T. C., Piekarski, C., Tamura, H., & Manchester, L. C. (2007). Light at night, chronodisruption, melatonin suppression, and cancer risk: a review. *Critical Reviews in Oncogenesis*, 13(4), 303-328.
- Roenneberg, T., Allebrandt, K. V., Merrow, M., & Vetter, C. (2012). Social jetlag and obesity. *Current Biology*, 22(10), 939-943.
- Ruben, M. D., Wu, G., Smith, D. F., Schmidt, R. E., Francey, L. J., Lee, Y. Y., Anafi, R. C., & Hogenesch, J. B. (2018). A database of tissue-specific rhythmically expressed human genes has potential applications in circadian medicine. *Science Translational Medicine*, 10(458), eaat8806.
- Russart, K. L. G., & Nelson, R. J. (2018). Artificial light at night alters behavior in laboratory and wild animals. *Proceedings of the National Academy of Sciences*, 329(8-9), 401-408.
- Saini, A., Tucci, M., Tampellini, M., Maina, D., Bouraouia, K., Giuliano, P. L., Termine, A., Castellano, M., Campagna, S., Laciura, P., & Berruti, A. (2013). Circadian variation of breakthrough pain in cancer patients. *European Journal of Pain*, 17(2), 264-270.
- Salomon, R. M., Ripley, B., Kennedy, J. S., Johnson, B., Schmidt, D., Zeitzer, J. M., Nishino, S., & Mignot, E. (2003). Diurnal variation of cerebrospinal fluid hypocretin-1 (Orexin-A) levels in control and depressed subjects. *Biological Psychiatry*, 54(2), 96-104.
- Sapin, E., Lapray, D., Bérød, A., Goutagny, R., Léger, L., Ravassard, P., Clément, O., Hanriot, L., Fort, P., & Luppi, P. H. (2009). Localization of the brainstem GABAergic neurons controlling paradoxical (REM) sleep. *PLoS One*, 4(1), e4272.
- Schaible, H.-G. (2006). Peripheral and central mechanisms of pain generation. In C. Stein (Ed.), *Analgesia* (pp. 3-28). Springer.
- Scheiermann, C., Kunisaki, Y., & Frenette, P. S. (2013). Circadian control of the immune system. *Nature Reviews Immunology*, 13(3), 190-198.
- Schwartz, J. R., & Roth, T. (2008). Neurophysiology of sleep and wakefulness: basic science and clinical implications. *Current Neuropharmacology*, 6(4), 367-378.

- Segal, J. P., Tresidder, K. A., Bhatt, C., Gilron, I., & Ghasemlou, N. (2018). Circadian control of pain and neuroinflammation. *Journal of Neuroscience Research*, 96(6), 1002-1020.
- Smith, M. T., Perlis, M. L., Smith, M. S., Giles, D. E., & Carmody, T. P. (2000). Sleep quality and presleep arousal in chronic pain. *Journal of Behavioral Medicine*, 23(1), 1-13.
- Solaro, C., Uccelli, M. M., Guglieri, P., Uccelli, A., & Mancardi, G. L. (2000). Gabapentin is effective in treating nocturnal painful spasms in multiple sclerosis. *Multiple Sclerosis*, 6(3), 192-193.
- Spies, H. G., Mahoney, C. J., Norman, R. L., Clifton, D. K., & Resko, J. A. (1974). Evidence for a diurnal rhythm in ovarian steroid secretion in the rhesus monkey. *Journal of Psychiatry and Neuroscience*, 39(2), 347-351.
- Starr, C. J., Sawaki, L., Wittenberg, G. F., Burdette, J. H., Oshiro, Y., Quevedo, A. S., & Coghill, R. C. (2009). Roles of the insular cortex in the modulation of pain: insights from brain lesions. *Journal of Neuroscience*, 29(9), 2684-2694.
- Stephan, F. K., & Zucker, I. (1972). Circadian rhythms in drinking behavior and locomotor activity of rats are eliminated by hypothalamic lesions. *Proceedings of the National Academy of Sciences*, 69(6), 1583-1586.
- Sylvester, C. M., Krout, K. E., & Loewy, A. D. (2002). Suprachiasmatic nucleus projection to the medial prefrontal cortex: a viral transneuronal tracing study. *Neuroscience*, 114(4), 1071-1080.
- Taheri, S., Sunter, D., Dakin, C., Moyes, S., Seal, L., Gardiner, J., Rossi, M., Ghatei, M., & Bloom, S. (2000). Diurnal variation in orexin A immunoreactivity and prepro-orexin mRNA in the rat central nervous system. *Neuroscience Letters*, 279(2), 109-112.
- Takada, T., Yamashita, A., Date, A., Yanase, M., Suhara, Y., Hamada, A., Sakai, H., Ikegami, D., Iseki, M., Inada, E., & Narita, M. (2013). Changes in the circadian rhythm of mRNA expression for μ -opioid receptors in the periaqueductal gray under a neuropathic pain-like state. *Synapse*, 67(5), 216-223.

- Takahashi, H., Motomatsu, T., Nawata, H., Kato, K., Ibayashi, H., & Nobunaga, M. (1986). Influences of feeding and drinking on circadian rhythms of opioid peptides in plasma, hypothalamus and pituitary gland in rats. *Physiology & Behavior*, 37(4), 609-614.
- Takahashi, M., Matsudaira, K., & Shimazu, A. (2015). Disabling low back pain associated with night shift duration: sleep problems as a potentiator. *American Journal of Industrial Medicine*, 58(12), 1300-1310.
- Tang, J. S., Qu, C. L., & Huo, F. Q. (2009). The thalamic nucleus submedialis and ventrolateral orbital cortex are involved in nociceptive modulation: a novel pain modulation pathway. *Progress in Neurobiology*, 89(4), 383-389.
- Thaiss, C. A., Zeevi, D., Levy, M., Zilberman-Schapira, G., Suez, J., Tengeler, A. C., Abramson, L., Katz, M. N., Korem, T., Zmora, N., Kuperman, Y., Biton, I., Gilad, S., Harmelin, A., Shapiro, H., Halpern, Z., Segal, E., & Elinav, E. (2014). Transkingdom control of microbiota diurnal oscillations promotes metabolic homeostasis. *Cell*, 159(3), 514-529.
- Timmermann, L., Ploner, M., Haucke, K., Schmitz, F., Baltissen, R., & Schnitzler, A. (2001). Differential coding of pain intensity in the human primary and secondary somatosensory cortex. *Journal of Neurophysiology*, 86(3), 1499-1503.
- Todd, A. J. (2010). Neuronal circuitry for pain processing in the dorsal horn. *Nature Reviews Neuroscience*, 11(12), 823-836.
- Tsuneki, H., Wada, T., & Sasaoka, T. (2018). Chronopathophysiological implications of orexin in sleep disturbances and lifestyle-related disorders. *Pharmacology and Therapeutics*, 186, 25-44.
- Walker, W. H., Walton, J. C., DeVries, A. C., & Nelson, R. J. (2020). Circadian rhythm disruption and mental health. *Translational Psychiatry*, 10(1), 28.
- Warnecke, M., Oster, H., Revelli, J. P., Alvarez-Bolado, G., & Eichele, G. (2005). Abnormal development of the locus coeruleus in Ear2(Nr2f6)-deficient mice impairs the functionality of the forebrain clock and affects nociception. *Genes and Development*, 19(5), 614-625.

- Weitzman, E. D., Fukushima, D., Nogeire, C., Roffwarg, H., Gallagher, T. F., & Hellman, L. (1971). Twenty-four hour pattern of the episodic secretion of cortisol in normal subjects. *Journal of Psychiatry and Neuroscience*, 33(1), 14-22.
- Wesche, D. L., & Frederickson, R. C. (1981). The role of the pituitary in the diurnal variation in tolerance to painful stimuli and brain enkephalin levels. *Life Sciences*, 29(21), 2199-2205.
- Wilhelmsen, M., Amirian, I., Reiter, R. J., Rosenberg, J., & Gögenur, I. (2011). Analgesic effects of melatonin: a review of current evidence from experimental and clinical studies. *Journal of Pineal Research*, 51(3), 270-277.
- Woodruff, E. R., Chun, L. E., Hinds, L. R., & Spencer, R. L. (2016). Diurnal Corticosterone Presence and Phase Modulate Clock Gene Expression in the Male Rat Prefrontal Cortex. *Endocrinology*, 157(4), 1522-1534.
- Xia, T., Chu, S., Cui, Y., Xu, F., Liu, Y., Song, J., Qian, Y., Shao, X., Li, X., Gu, X., & Ma, Z. (2017). The Role of NR2B-CREB-miR212/132-CRTC1-CREB Signal Network in Pain Regulation In Vitro and In Vivo. *Anesthesia & Analgesia*, 124(6), 2045-2053.
- Xia, T., Cui, Y., Qian, Y., Chu, S., Song, J., Gu, X., & Ma, Z. (2016). Regulation of the NR2B-CREB-CRTC1 signaling pathway contributes to circadian pain in murine model of chronic constriction injury. *Neuroscience*, 122(2), 542-552.
- Xiao, X., & Zhang, Y. Q. (2018). A new perspective on the anterior cingulate cortex and affective pain. *Neuroscience & Biobehavioral Reviews*, 90, 200-211.
- Xu, F., Zhao, X., Liu, H., Shao, X., Chu, S., Gong, X., Ma, Z., & Gu, X. (2018). Misaligned Feeding May Aggravate Pain by Disruption of Sleep-Awake Rhythm. *Molecular Pain*, 127(1), 255-262.
- Yamamoto, S., Shigeyoshi, Y., Ishida, Y., Fukuyama, T., Yamaguchi, S., Yagita, K., Moriya, T., Shibata, S., Takashima, N., & Okamura, H. (2001). Expression of the Per1 gene in the hamster: brain atlas and circadian characteristics in the suprachiasmatic nucleus. *Journal of Comparative Neurology*, 430(4), 518-532.
- Yang, S. C., Chen, C. L., Yi, C. H., Liu, T. T., & Shieh, K. R. (2015). Changes in Gene Expression Patterns of Circadian-Clock, Transient Receptor Potential Vanilloid-1

- and Nerve Growth Factor in Inflamed Human Esophagus. *Scientific Reports*, 5, 13602.
- Yoo, S. H., Yamazaki, S., Lowrey, P. L., Shimomura, K., Ko, C. H., Buhr, E. D., Siepka, S. M., Hong, H. K., Oh, W. J., Yoo, O. J., Menaker, M., & Takahashi, J. S. (2004). PERIOD2::LUCIFERASE real-time reporting of circadian dynamics reveals persistent circadian oscillations in mouse peripheral tissues. *Proceedings of the National Academy of Sciences*, 101(15), 5339-5346.
- Yu, T., Zhang, X., Shi, H., Tian, J., Sun, L., Hu, X., Cui, W., & Du, D. (2019). P2Y12 regulates microglia activation and excitatory synaptic transmission in spinal lamina II neurons during neuropathic pain in rodents. *Cell Death & Disease*, 10(3), 1-16.
- Zeitzer, J. M., Buckmaster, C. L., Parker, K. J., Hauck, C. M., Lyons, D. M., & Mignot, E. (2003). Circadian and Homeostatic Regulation of Hypocretin in a Primate Model: Implications for the Consolidation of Wakefulness. *The Journal of Neuroscience*, 23(8), 3555-3560.
- Zhang, C., Truong, K. K., & Zhou, Q. Y. (2009). Efferent projections of prokineticin 2 expressing neurons in the mouse suprachiasmatic nucleus. *PLoS One*, 4(9), e7151.
- Zhang, J., Li, H., Teng, H., Zhang, T., Luo, Y., Zhao, M., Li, Y. Q., & Sun, Z. S. (2012). Regulation of peripheral clock to oscillation of substance P contributes to circadian inflammatory pain. *Anesthesiology*, 117(1), 149-160.
- Zhang, S., Zeitzer, J. M., Yoshida, Y., Wisor, J. P., Nishino, S., Edgar, D. M., & Mignot, E. (2004). Lesions of the suprachiasmatic nucleus eliminate the daily rhythm of hypocretin-1 release. *Sleep*, 27(4), 619-627.
- Zhao, I., Bogossian, F., & Turner, C. (2012). The effects of shift work and interaction between shift work and overweight/obesity on low back pain in nurses: results from a longitudinal study. *Journal of Occupational and Environmental Medicine*, 54(7), 820-825.
- Zheng, D., Ratiner, K., & Elinav, E. (2020). Circadian Influences of Diet on the Microbiome and Immunity. *Trends in Immunology*, 41(6), 512-530.
- Zieglgänsberger, W. (2019). Substance P and pain chronicity. *Cell and Tissue Research*, 375(1), 227-241.

10. Supplemental Material

Supplemental Table 1 - Sex Reporting Bumgarner JR, Walker II WH, and Nelson RJ, 2021. Circadian Rhythms and Pain.				
Section	Citation	Species	Sex	Reported Rhythm/Result
Pain Behavior	Oliverio et al., 1982	Mouse	Not described	Circadian rhythms in pain behavior and morphine sensitivity
	Pickard, 1987	Hamster	Male	Circadian rhythms in pain behavior
	Hagenauer et al., 2017	Human	Female/Male	Model of diurnal rhythm of pain sensitivity in humans generated by field meta-analysis
	Martínez-Gómez et al., 1994	Rat	Female	Diurnal variations in pain behavior
	Frederickson et al., 1977	Mouse	Not described	Varying effect of morphine/naloxone on rhythmic pain behavior
	Kavaliers and Hirst, 1983	Mouse	Male	Rhythmic pain behavior, rhythmic morphine analgesia
	Castellano et al., 1985	Mouse	Not described	Varying diurnal rhythms in pain behavior between two strains of mice
DRG	Zhang et al., 2012	Mouse	Male	Rhythmic clock gene expression, substance P expression, pain behavior
	Kusunose et al., 2010	Mouse	Male	Rhythmic $\alpha 2\delta$ -1 expression
	Lee et al., 2017	Mouse	Not described	Pro-kineticin expression (single time-point)
	Negri et al., 2002	Rat	Male	<i>Tef</i> expression (single time-point)
	Yang et al., 2015	Human	Female/Male	Rhythmic esophageal TRPV1 protein expression
	Kim et al., 2020	Mouse	Male	Rhythmic TRP channel expression
Spinal Cord	Morioka et al., 2012	Mouse	Male	Rhythmic clock gene expression

	Morioka et al., 2016	Mouse	Male	Rhythmic clock gene expression
	Onishi et al., 2002	Mouse	Male	Rev-erba expression (single time-point)
	Yamamoto et al., 2001	Hamster	Male	<i>Per1</i> expression (single time-point)
	Eblen-Zajjur et al., 2015	Rat	Male	Rhythmic Na ⁺ /K ⁺ ATPase activity
	Xia et al., 2016	Mouse	Male	Rhythmic NR2B-CREB-CRTC1 signaling protein/gene expression, pain behavior
	Xia et al., 2017	Rat, Mouse	Male	Rhythmic pain behavior
	Zhang et al., 2012	Mouse	Male	Rhythmic substance P protein expression
	Koyanagi et al., 2016	Mouse	Male	Rhythmic ATP concentrations, SGK-1 protein/gene expression, pain behavior
PAG	Kriegsfeld et al., 2004	Hamster	Male	ipRGC projections to PAG
	Hattar et al., 2006	Mouse	Female/Male	ipRGC projections to PAG
	Zhang et al., 2009	Mouse	Male	SCN Prokineticin projections to PAG
	Landgraf et al., 2016	Mouse	Male	Rhythmic PER2 expression
	Takada et al., 2013	Mouse	Male	Rhythmic μ -Opioid Receptor gene expression
	Sapin et al., 2009	Rat	Male	Rhythmic REM 'on' & 'off' neuronal activity
RVM	Monošíková et al., 2007	Rat	Male	Rhythmic clock gene expression
	Hery et al., 1977	Rat	Male	Rhythmic tryptophan-5-hydroxylase activity
	Leung and Mason, 1999	Rat	Male	Rhythmic RVM On/Off neuronal activity

LC	Warnecke et al., 2005	Mouse	Not described	Lack of clock gene expression
	Mahoney et al., 2013	Hamsters	Male	Rhythmic <i>Per1</i> expression
	Natali et al., 1980	Mouse	Male	Rhythmic tyrosine hydroxylase activity
	Aston-Jones et al., 2001	Rat	Male	Lack of rhythmic LC activity following dorsomedial hypothalamic lesions
	González and Aston-Jones, 2006	Rat	Male	Altered sleep-wake rhythms following chemical LC lesion
Thalamus	Ku et al., 2018	Human	Female/Male	Rhythmic connectivity/activity
	Cardoso-Cruz et al., 2011	Rat	Male	Varying thalamocortical partial directed coherence across the day
	Feillet et al., 2008	Mouse	Male	Rhythmic clock gene expression
Hypothalamus	Kriegsfeld et al., 2004	Hamster	Male	ipRGC projections to PAG
	Girotti et al., 2009	Rat	Male	Rhythmic clock gene expression
	Kriegsfeld et al., 2003	Mouse	Female	Rhythmic <i>Per1</i> protein/gene expression
	Kalil et al., 2016	Rat	Female	Rhythmic clock gene expression
	Orozco-Solis et al., 2016	Mouse	Not described	Rhythmic clock gene expression
	Moriya et al., 2009	Mouse	Male	Rhythmic clock gene expression
	Takahashi et al., 1986	Rat	Male	Rhythmic met-enkephalin and β -endorphin concentrations
	Asai et al., 2007	Rat	Male	Rhythmic met-enkephalin and leu-enkephalin concentrations
Orexin	Salomon et al., 2003	Human	Female/Male	Rhythmic cerebrospinal fluid orexin-A concentration fluctuations

	Fujiki et al., 2001	Rat	Male	Rhythmic cerebrospinal fluid orexin-A concentration fluctuations
	Zeitzer et al., 2003	Squirrel Monkey	Female	Rhythmic cerebrospinal fluid orexin-A concentration fluctuations
	Mäkelä et al., 2018	Human	Male	Lack of plasma orexin-A fluctuation
	Zhang et al., 2004	Rat	Male	SCN lesions abolish cerebrospinal fluid orexin-A rhythms
	Marston et al., 2008	Mouse	Male	Rhythmic orexin-A neuron activity
	Estabrooke et al., 2001	Rat	Male	Rhythmic orexin-A neuron activity
	Gompf and Aston-Jones, 2008	Rat	Male	Rhythmic orexin-A neuron activity, projections to LC with correlated activity rhythms
	Taheri et al., 2000	Rat	Male	Rhythmic orexin-A protein expression in pons and hypothalamus
Cortical/Limbic	Li et al., 2013	Human	Female/Male	Rhythmic gene expression
	Woodruff et al., 2016	Rat	Male	Rhythmic clock gene expression
	Chun et al., 2015	Rat	Female/Male	Rhythmic clock gene expression
	Christiansen et al., 2016	Rat	Male	Rhythmic clock gene expression
	Lamont et al., 2005	Rat	Male	Rhythmic clock gene expression
	Sylvester et al., 2002	Rat	Female	SCN -> PVN -> PFC Projections
	Takada et al., 2013	Mouse	Male	Rhythmic frontal cortex μ -opioid receptor gene expression
	Mitsushima et al., 1996	Rat	Male	Rhythmic cortical ACh release

	Chen et al., 2016	Rat	Male	Disrupted circadian rhythms following insular lesions
	Moriya et al., 2015	Mouse	Male	Rhythmic serotonin and serotonin metabolite concentration fluctuations
	Izumo et al., 2012	Rat	Female	Rhythmic serotonin and dopamine expression
	Hayashi et al., 2013	Mouse	Male	Rhythmic cortical synaptic activity and spine density
Opioid System	Asai et al., 2007	Rat	Male	Rhythmic met-enkephalin and leu-enkephalin concentration fluctuations
	Kurumaji et al., 1988	Rat	Male	Rhythmic striatal and mesolimbic met-enkephalin expression
	Reid et al., 1982	Rat	Male	Rhythmic hypothalamic and pituitary dynorphin expression
	Mozzanica et al., 1991	Human	Not described	Rhythmic plasma Met-enkephalin and β -endorphin concentration fluctuations
	Mozzanica et al., 1992	Human	Female/Male	Rhythmic plasma Met-enkephalin and β -endorphin concentration fluctuations
	Petraglia et al., 1983	Human	Female/Male	Rhythmic plasma β -endorphin concentration fluctuations
	Wesche and Frederickson, 1981	Rat	Male	Rhythmic whole-brain met-enkephalin concentration fluctuations
	Frederickson et al., 1977	Mouse	Not described	Varying effect of morphine/naloxone on rhythmic pain behavior
	Kavaliers and Hirst, 1983	Mice	Male	Rhythmic pain behavior, rhythmic morphine analgesia
	Ibrahim et al., 2017	Rat	Male	Examines green-light induced analgesia and the role of RVM activity
	Martin et al., 2021	Rat	Male	Green light analgesia dependent on μ - and δ -opioid receptor signaling in the spinal cord

	Takada et al., 2013	Mouse	Male	Rhythmic PAG/Frontal cortex μ -opioid receptor gene expression
Endocrine System	Weitzman et al., 1971	Human	Female/Male	Diurnal plasma cortisol concentration fluctuations
	Albers et al., 1985	Hamsters	Male	Rhythmic serum cortisol/corticosterone concentration fluctuations
	Heybach and Vernikos-Danellis, 1978	Rat	Male	Adrenalectomy does not abolish diurnal variations in pain behavior
	Koyanagi et al., 2016	Mouse	Male	Rhythmic corticosterone secretion necessary for diurnal neuropathic pain behavior
	Bremner et al., 1983	Human	Male	Rhythmic androgen concentration fluctuations
	Spies et al., 1974	Rhesus Monkey	Female	Rhythmic serum progesterone and estradiol concentration fluctuations during luteal phase of estrous cycle
Immune System	Hayashi et al. 2013	Mouse	Male	Microglia-driven rhythmic cortical synaptic activity and spine density

Chapter 2

Dim Light at Night Exposure Induces Cold Hyperalgesia and Mechanical Allodynia in Male Mice

Published as:

Bumgarner, J. R., Walker, W. H., Liu, J. A., Walton, J. C., & Nelson, R. J. (2020). Dim Light at Night Exposure Induces Cold Hyperalgesia and Mechanical Allodynia in Male Mice. *Neuroscience*, 434, 111-119.

Introduction

Artificial lighting is an indispensable feature of the 21st century that provides abundant benefits for human society. Nonetheless, a growing body of evidence has elucidated the detrimental effects of exposure to artificial light at night (LAN), a nearly ubiquitous form of artificial lighting. Most organisms on Earth evolved with endogenous circadian systems that rely on light days and dark nights for circadian system coordination (Reppert & Weaver, 2002). As such, LAN can disrupt a range of behavioral and physiological processes that interact with the circadian system, including sleep-wake cycles, metabolism, and immune function (Russart & Nelson, 2018; Cho et al., 2015). Disruption of circadian rhythms is provoked by atypical light signaling from retinal photoreceptors to the suprachiasmatic nucleus (SCN) during the dark phase; the SCN is known as the ‘master clock’ of the mammalian circadian system, (Lucas et al., 2012).

LAN exposure has been linked to health issues in both biomedical and ecological contexts. In humans, LAN exposure is correlated with an increased risk of breast and prostate cancers, depression in the elderly population, and obesity (Kloog et al., 2009; Davis et al., 2001; Obayashi et al., 2013; McFadden et al., 2014). Animal studies have demonstrated that dim LAN (~5 lx; dLAN) exposure can result in increased body mass, altered metabolism, disrupted immune function, and disrupted inflammatory signaling in the brain (Hogan et al., 2015; Bedrosian et al., 2011b; Bedrosian et al., 2011a; Borniger et al., 2014; Fonken et al., 2013b). Notably, dLAN augments the central expression of //-

1 β in female mice and induces depressive-like behavior in both sexes in as few as four nights of exposure (Walker et al., 2020).

dLAN-induced inflammation may play a role in the induction of hyperalgesia or other similar chronic pain states, as pain sensitivity is influenced by the central and peripheral expression of cytokines. For example, pro-inflammatory cytokines heighten pain sensitivity through peripheral and central sensitization (Zhang et al., 2012). Peripherally, inflammation in the dorsal root ganglia (DRG) can lead to sensitization (Martin et al., 2019) and ultimately hyperalgesia (i.e., increased sensitivity of noxious stimuli) and allodynia (i.e., painful reactions to innocuous stimuli). Centrally, inflammation can lead to sensitization and reduced inhibitory signaling in the dorsal horn of the spinal cord (Kawasaki et al., 2008) and in regions of the midbrain or brainstem, such as the periaqueductal grey (PAG) or the rostral ventral medulla (RVM), respectively (Wei et al., 2008; Xu et al., 2018). Typically, the PAG-RVM axis plays a role in the regulation of descending facilitatory and inhibitory nociceptive signaling (Bodnar & Heinricher, 2013).

Additionally, dLAN exposure can be characterized as a disruptor of circadian rhythms. Other forms of circadian rhythm disruption, such as night-shift work or sleep disruption have been correlated with altered pain thresholds (Matre et al., 2017; Onen et al., 2001). Pain sensitivity follows circadian patterns in both humans and mice; pain sensitivity is often highest following the end of the active period, likely reflecting the rhythmic expression of inflammatory markers and/or opioid receptors in the brain (Kavaliers & Hirst, 1983; Takada et al., 2013). Disruption of these patterns could lead to altered pain sensitivity.

In the present study, I investigated the effects of acute (3-4 nights) dLAN exposure on pain responsiveness and the effects of chronic dLAN exposure (27-28 nights) of dLAN exposure on pain responsiveness and expression of pronociceptive transcripts in male mice. Specifically, I hypothesized that dLAN-mediated circadian rhythm disruption heightens pain responsiveness and perturbs the expression of central and peripheral nociception-related peptides and receptors. Thus, I predicted that dLAN would induce thermal hyperalgesia and mechanical allodynia through increased expression of inflammatory factors.

Experimental Procedures

Mice

Forty adult male CFW mice (~8 weeks old) were ordered from Charles River Laboratories. Upon arrival at the WVU vivarium, mice were given one week to acclimate to light-dark (LD) (14:10 h, ~125:0 lux *or* ~33.2:0.0 $\mu\text{W}/\text{cm}^2$ @ 550 nm) housing conditions. Lights went on/off in the vivarium at 05:00 h and 19:00 h EST, respectively. Throughout the study, mice were individually housed in polypropylene cages (30 X 18 X 14 cm) on corn cob bedding (Envigo 7092; Wisconsin, USA) at a temperature of 22 ± 2 °C and a relative humidity of $45 \pm 5\%$. Following acclimation, mice were singly housed and pseudorandomly assigned to either LD or dLAN (14:10 h; ~125:5 lux *or* ~33.2:1.8 $\mu\text{W}/\text{cm}^2$ @ 550 nm) housing conditions. dLAN was produced by Luma5 Standard LED light strips (1.5 W/ft, 5000 K “cool white”, 1200 lumens; Hitlights Inc.; Louisiana, USA). Light measurements were taken by placing both a Mavolux 5032C illuminance meter (Nürnberg, Germany) and an Ophir Starbright irradiance meter (Jerusalem, Israel) in the center of an empty cage with the light sensor facing toward the ceiling. For the entire experiment, mice had access to food (Envigo Teklad 2018; Wisconsin, USA) and reverse osmosis water *ad libitum*.

All experiments were approved by the West Virginia University Institutional Animal Care and Use Committee, and animals were maintained in accordance with NIH Animal Welfare guidelines.

Behavioral Testing

Behavioral testing in this experiment occurred at the following three time points: baseline (1 and 2 days prior to experimental housing), acute (days 3 and 4), and chronic (days 27 and 28). Specifically, electric von Frey assessment was performed on the first day of each timepoint; cold and then hot plate tests were performed on the second day with a 1-hour interstimulus interval between tests. All behavioral testing occurred between *zeitgeber* time (ZT) 06-09. One day prior to baseline testing, mice were habituated to the von Frey and Cold/Hot plate chambers for 30 minutes each.

Following the baseline tests, mice were pseudorandomly assigned to either the LD or the dLAN group; 20 mice were assigned to each group. For the acute and chronic behavioral tests, the researcher performing the von Frey test and determining withdrawal latencies for the hot and cold plate tests was blind to the experimental condition of the mice. Mice were tested in random order. Before testing, mice were allowed 30 minutes to acclimate to the behavioral room to reduce exploratory behavior on testing days.

Von Frey

Mice were given 15 minutes to acclimate to opaque chambers (80 x 115 x 145 mm; Bioseb; Florida, USA) on top of a wire mesh table prior to the onset of testing. Four mechanical sensitivity measurements were then taken by using an electric von Frey device (Bioseb). The first measurement was excluded, and the final three data were averaged as previously described (Ferrier et al., 2016). A minimum of five minutes passed between each measurement. For each measurement, the probe's flexible wire tip was pressed gradually upward against the plantar surface of a weight-bearing hind paw until a nocifensive response was elicited. Nocifensive responses were defined as paw lifts, paw shakes, or jumping. The maximum mechanical withdrawal threshold was recorded for each mouse. A decrease in the maximum withdrawal threshold in this test was correlated with mechanical allodynia (Martinov et al., 2013).

Cold and Hot Plates

Cold plate testing (IITC Life Science Inc.; California, USA) was performed at $0.0^{\circ}\text{C} \pm 1.0^{\circ}\text{C}$, and hot plate testing (IITC Life Science Inc.) was performed at $52.5^{\circ}\text{C} \pm 0.2^{\circ}\text{C}$. The interstimulus interval for cold/hot plate testing was set at a minimum of one hour, with the cold plate test strictly occurring first. As soon as mice were placed onto the plates, stopwatches were started and latency to nocifensive behavior was observed and recorded. Mice were immediately removed from the plates as soon as nocifensive behaviors were exhibited, and withdrawal latencies were recorded. Nocifensive behaviors that were considered sufficient for the termination of either test included hind-paw withdrawal, licking, shaking, or jumping. Hind-paw shaking was the most commonly

observed behavior in both tests. A maximum cutoff time was set as 30s for each test. In these tests, a decrease in latency to nocifensive behavior was correlated with hyperalgesia (Bannon & Malmberg, 2007).

Tissue Collection, RNA Extraction, and qRT-PCR

Tissue was collected on day 30 to avoid observing potential stress-related physiological effects or acute inflammatory responses that may have been induced by behavioral testing. Thus, from ZT 06-08 on day 30, mice were euthanized with intraperitoneal injections of Euthasol (Virbac; Texas, USA). Following unresponsive toe-pinch tests, transcardiac perfusions were subsequently performed with approximately 20 mL of cold 0.01M PBS (Fisher Scientific; Pennsylvania, USA). All collected tissue samples were immediately submerged into RNALater (Qiagen; Maryland, USA), stored overnight at 4 °C, and then stored at -80 °C for up to 3 weeks before dissection. RNA extractions and qRT-PCR were performed as described previously (Walker et al., 2020). RNA was extracted with Trizol Reagent (Invitrogen; California, USA) according to the manufacturer's instructions and was resuspended in RNase-free water. RNA quality and quantity were determined using a Nanodrop spectrophotometer (Thermo Fisher; Wisconsin, USA), and cDNA was then synthesized using SuperScript IV VILO reverse transcriptase (Invitrogen) following the manufacturer's protocol. For subsequent PCR, 4 µL (80 ng) of cDNA were combined with 16 µL of a master-mix solution containing: Taqman Fast Advanced Master Mix (Life Technologies; California, USA), an inventoried probe from Applied Biosystems (Life Technologies), a primer-limited probe for the endogenous control 18S, and nuclease-free water (Table 1). All samples were run in duplicate with the following 2-step real-time PCR cycling conditions: 95 °C for 20 s, followed by 40 cycles of 95 °C for 3 s, and then 60 °C for 30 s. Gene expression was quantified using the relative standard curve method as previously described (Walker et al., 2020).

Statistical Analyses

Individual data points having a within-group Z-score > 2 were defined as outliers and were removed prior to analysis. Prior to analysis, data were tested for normality of distribution using the Shapiro-Wilk test. Data that were not normally distributed were log₂ transformed. Food consumption and behavioral testing data were analyzed using a repeated measures linear mixed-effects model (LMM); post hoc comparisons were made using Sidak's multiple comparisons test. Normally distributed gene expression data were compared using an unpaired Student's t-test. The Mann-Whitney test was used for group comparison in instances where data were not normally distributed upon log₂ transformation. For ease of data visualization, normally distributed data were normalized to the control group (LD) mean, and log₂ transformed data were standardized to the control (LD) mean. All data were analyzed using Prism 8 (GraphPad Software; California, USA). Differences between group means were considered statistically significant when $p \leq 0.05$.

Table 1. Gene names and assay IDs of the Taqman primers used for this experiment.	
Gene Name	Assay ID
<i>Il-6</i>	Mm00446190_m1
<i>Il-1β</i>	Mm00434228_m1
<i>Tnf-α</i>	Mm00443258_m1
<i>Ngf</i>	Mm00443039_m1
<i>Bdnf</i>	Mm00432069_m1
<i>Mor</i>	Mm01188089_m1
<i>Tac1</i>	Mm01166996_m1
<i>Trpa1</i>	Mm01227437_m1
<i>Trpm8</i>	Mm01299593_m1
<i>18s</i>	Hs99999901_s1

Results

dLAN Alters Body Mass and Timing of Food Consumption

dLAN exposure increased the percent change in body mass relative to baseline ($t_{37} = 2.686$, $p < 0.05$; Figure 1A). dLAN altered the timing of food consumption, driving decreased dLAN group food consumption during the active phase (Figure 1B) and increased consumption during the inactive phase (Figure 1C). A main effect of lighting condition was present in active phase consumption ($F_{1,38} = 58.66$, $p < 0.0001$; Figure 1B) and inactive phase consumption ($F_{1,38} = 65.16$, $p < 0.0001$; Figure 1C). Food consumption was not altered by one night of dLAN exposure but was continuously altered in each of the following weeks of measurement ($p < 0.05$; Sidak's multiple comparisons; Figure 1B, C). These data are consistent with previous reports demonstrating that dLAN induces increased body mass via altered timing of food consumption (Fonken et al., 2010).

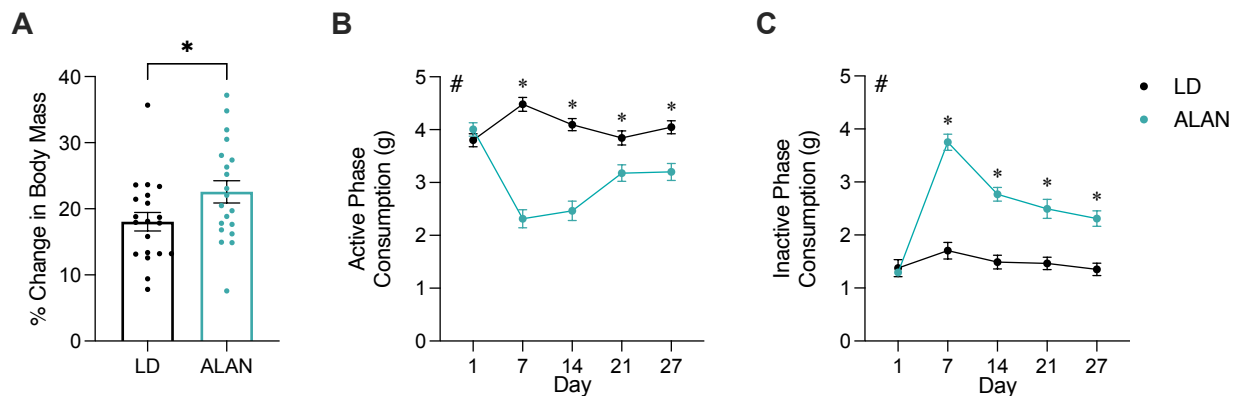


Figure 1. dLAN increases body mass and disrupts timing of food consumption in male mice. Mice housed in dLAN for four weeks had a greater percentage increase in body mass compared to baseline measurements (A). dLAN altered food consumption, resulting in decreased active phase food consumption (B) and increased inactive phase food consumption (C). Error bars represent ± 1 SEM; * $p < 0.05$; # $p < 0.05$, Main effect of lighting condition, LMM.

dLAN Induces Cold Hyperalgesia and Mechanical Allodynia

To assess the effects of dLAN on pain responsiveness, three nociceptive tests designed to assess thermal hyperalgesia and mechanical allodynia were performed. A main effect of lighting was present in the cold plate test ($F_{1,38} = 16.46$, $p < 0.001$; Figure 2A), with reduced response latencies observed in the dLAN group at both the acute and chronic time points ($p < 0.01$ in both cases; Sidak's multiple comparisons). Similarly, there was a main effect of lighting in the electric von Frey test ($F_{1,108} = 10.50$, $p < 0.01$; Figure 2C). Acute exposure to dLAN did not affect mechanical allodynia ($p > 0.05$), but chronic exposure reduced withdrawal thresholds ($p < 0.001$; Sidak's multiple comparisons). Exposure to dLAN did not affect responses to the hot plate at either time point tested ($p > 0.05$ in all comparisons; Figure 2B).

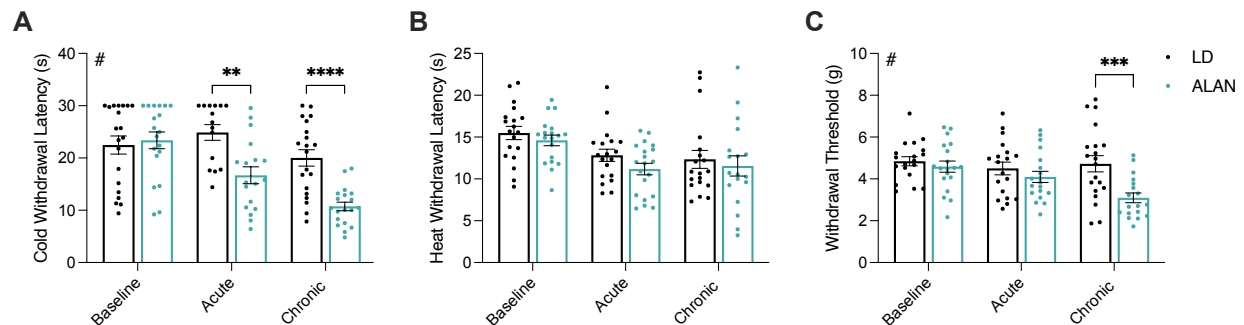


Figure 2. dLAN exposure induces cold hyperalgesia and mechanical allodynia. Mice exposed to dLAN displayed reduced cold plate withdrawal latencies after 3-4 nights (acute) and after 27-28 nights (chronic) of dLAN exposure (A). dLAN housing did not alter hot plate withdrawal latencies (B). At the chronic time point, dLAN mice displayed reduced mechanical withdrawal thresholds in the electric von Frey test (C). Error bars represent ± 1 SEM; * $p < 0.05$; # $p < 0.05$, Main effect of lighting condition, LMM.

dLAN Upregulates Il-6 and Ngf Expression in the Medulla

To investigate the link between dLAN exposure and heightened pain responsiveness, levels of the following pronociceptive transcripts were measured: the pro-inflammatory cytokines *Il-6*, *Il-1 β* , and *Tnf- α* ; the pronociceptive protein substance P's precursor protein, *Tac1*; nerve growth factor (*Ngf*) and brain-derived neurotrophic factor (*Bdnf*), two neurotrophins that have been implicated in pain states. *Il-6* expression was upregulated in the dLAN group ($t_{34} = 3.526$, $p < 0.01$; Figure 3A). Further, *Ngf* expression was also increased in this region ($t_{33} = 2.089$, $p < 0.05$; Figure 3D). There were no differences between *Il-1 β* , *Tnf- α* , *Bdnf*, or *Tac1* expression ($p > 0.05$; Figure 3B, C, E, F).

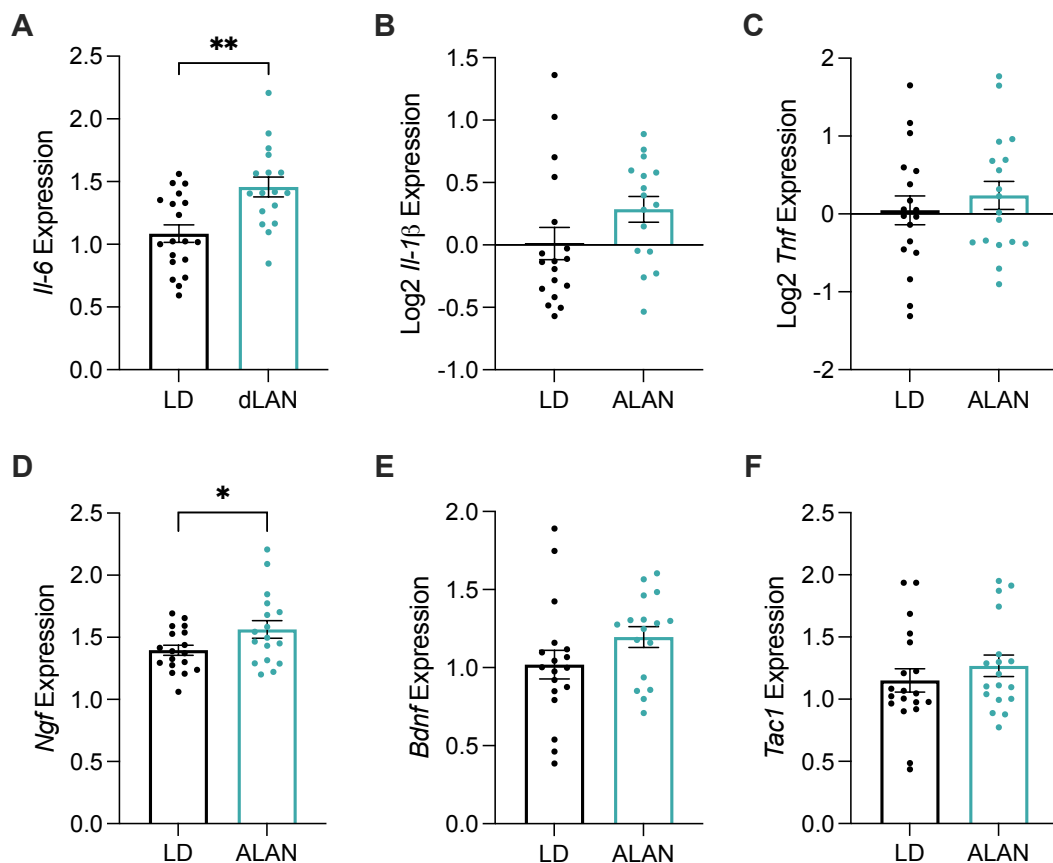


Figure 3. dLAN upregulates *Il-6* and *Ngf* relative expression in the medulla. Mice housed in dLAN for four weeks had upregulated levels of *Il-6* (A) and *Ngf* (D) within the medulla. dLAN housing did not alter *Tnf- α* , *Il-1 β* , *Bdnf*, or *Tac1* relative expression (B, C, E, F). Error bars represent ± 1 SEM; * $p < 0.05$.

Inflammatory and Nociceptive Transcript Expression in Lumbar Spinal Cord and the L3-5 DRG.

To determine the role of the peripheral nervous system in dLAN-induced hyperalgesia, the Lumbar 3-5 DRG were dissected, as these DRG project to the sciatic nerve (Rigaud et al., 2008). No differences in *Tnf- α* , *Il-1 β* , *Il-6*, *Bdnf*, *Ngf*, *Tac1*, *Mor*, *Trpa1*, or *Trpm8* were present in the L3-L5 DRG ($p > 0.05$ in all instances; Figure 4A-H). Similarly, there were no differences in *Tnf- α* , *Il-1 β* , *Il-6*, *Ngf*, *Tac1*, or *Mor* expression in the lumbar region of the spinal cord ($p > 0.05$ in all instances; Figure 5A-E).

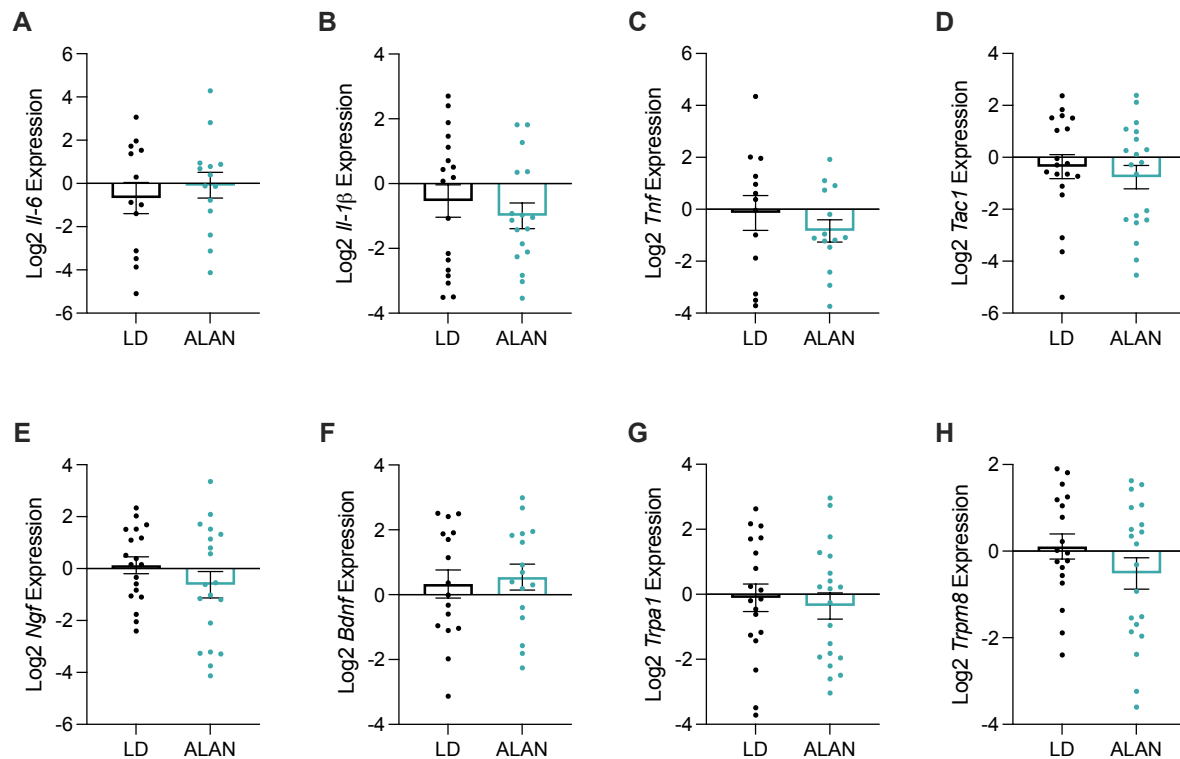


Figure 4. Cytokine, neurotrophin, and peptide transcripts examined in the L3-5 DRG were not affected by dLAN. *Il-6*, *Il-1 β* , *Tnf- α* , *Tac1*, *Ngf*, and *Bdnf* relative expression levels were unaffected (D-F). Gene expression of the ion channel receptors *Trpa1* and *Trpm8* was unaltered at the time of tissue collection (G, H). Error bars represent ± 1 SEM; * $p < 0.05$.

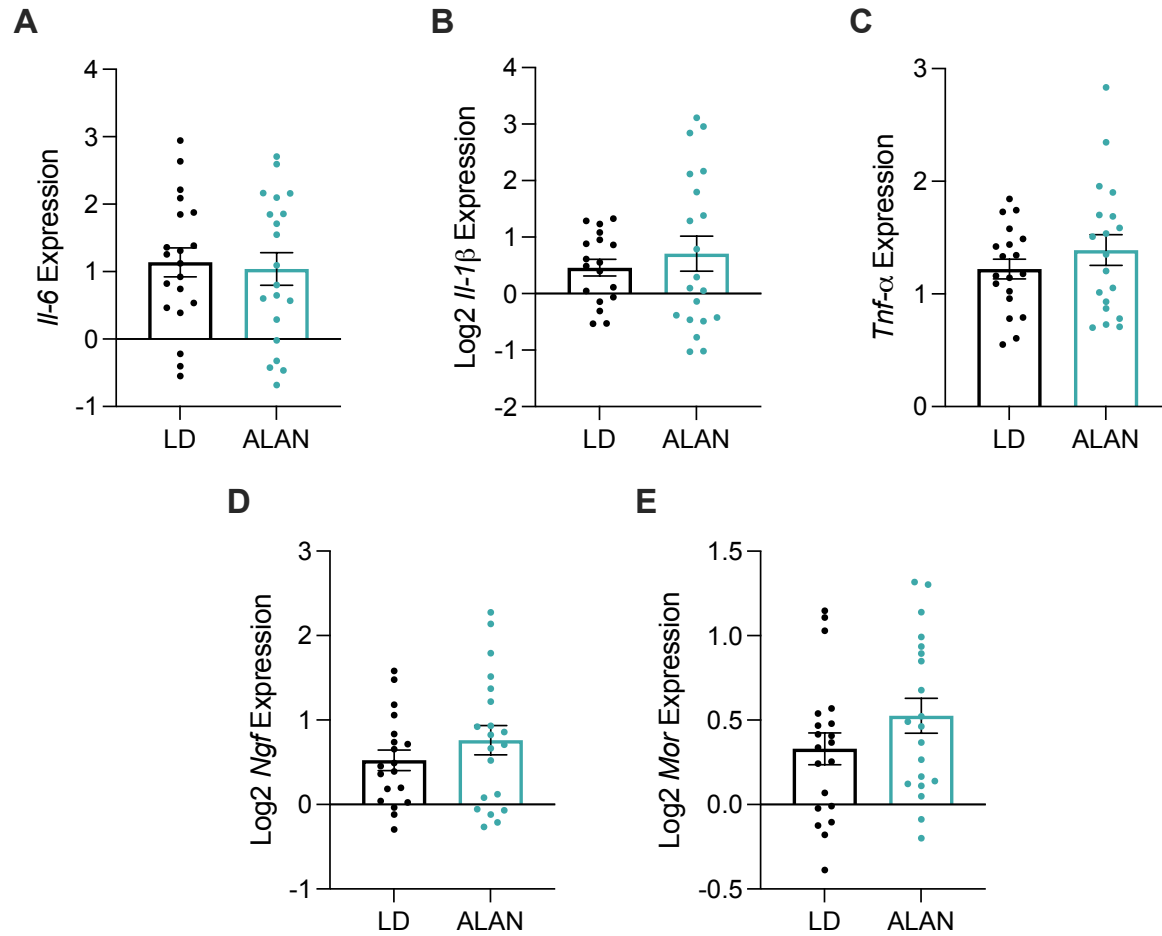


Figure 5. Cytokine, neurotrophin, and peptide transcripts in the lumbar region of the spinal cord were not affected by dLAN. *Il-6*, *Il-1 β* , *Tnf- α* , *Ngf*, and *Bdnf* levels were not different between groups at the time of tissue collection (A-E). Error bars represent ± 1 SEM; * $p < 0.05$.

dLAN Upregulates *Mor* Expression in the PAG

No differences were detected in PAG expression of *Tnf- α* , *Il-1 β* , *Il-6*, *Bdnf*, *Ngf*, or *Tac1* ($p > 0.05$; Figure 6B-F). To further investigate the presence of cold but not heat hyperalgesia in dLAN mice, I examined the potential effect of dLAN on the endogenous opioid system by measuring μ -opioid receptor (*Mor*) expression. Expression of *Mor* was increased in the dLAN group ($t_{33} = 2.704$, $p < 0.05$; Figure 6F).

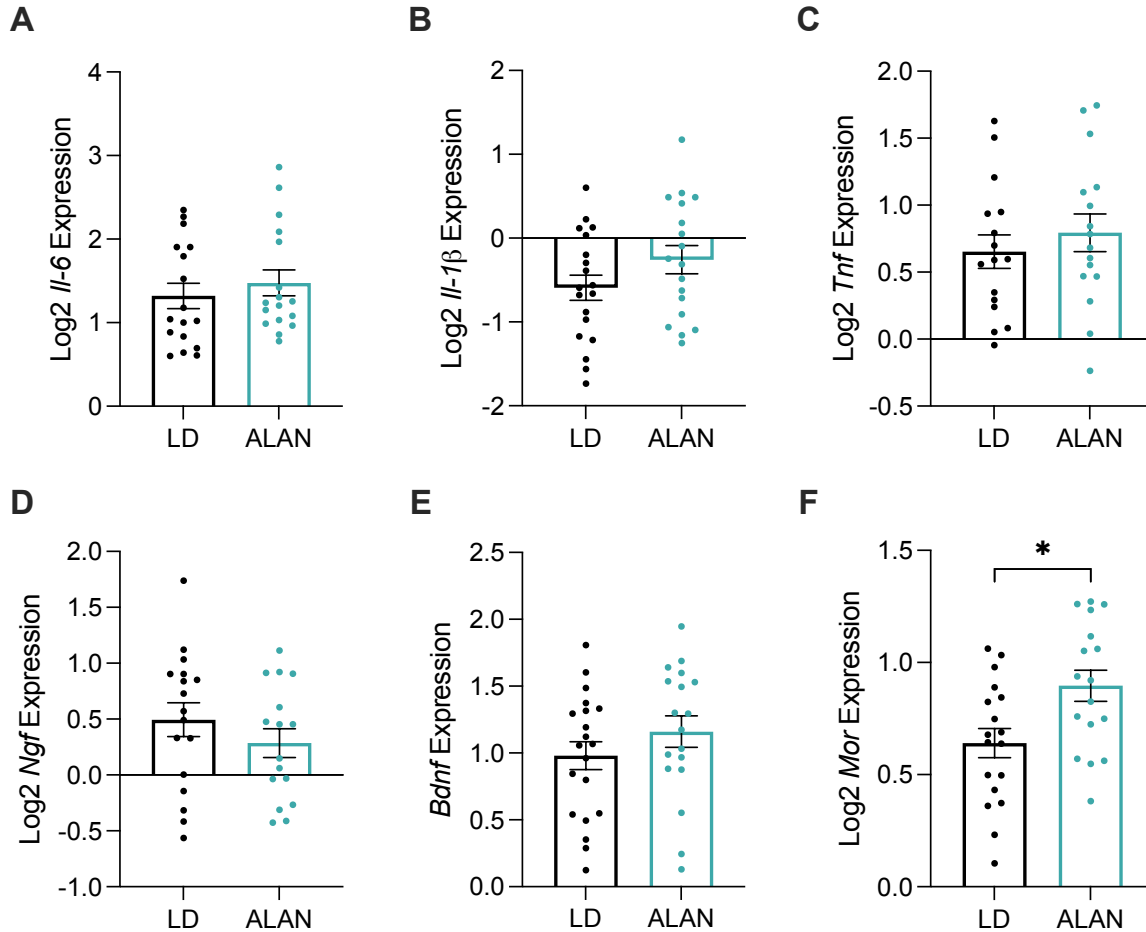


Figure 6. dLAN increases *Mor* relative expression in the PAG. *Il-6*, *Il-1 β* , and *Tnf- α* levels were not different in the PAG of dLAN mice (A-C). Expression of *Ngf* and *Bdnf* was unaffected in the PAG (D, E). *Mor* expression was upregulated in dLAN mice (F). Error bars represent ± 1 SEM; * $p < 0.05$.

Discussion

In this experiment, I examined the effects of acute (3-4 nights) and chronic (28-29 nights) dLAN exposure on both pain responsiveness and the gene expression of several pronociceptive peptides. I observed that male mice exposed to dLAN experienced cold hyperalgesia and mechanical allodynia at acute and chronic time points. In contrast, mice did not exhibit heat hyperalgesia at either assessed time point. Further, dLAN exposure upregulated levels of *Il-6* and *Ngf* in the medulla and increased Mor expression in the PAG.

A common theme of many maladaptive pain states is the presence of central and/or peripheral inflammation. Central inflammation leads to sensitization and hyperalgesia via glial activation and modulation of synaptic activity in pain circuitry (Ji et al., 2018). Specifically, many chronic pain states are correlated with increased central and peripheral levels of *Il-6* and other pro-inflammatory cytokines (Kawasaki et al., 2008). *Il-6* is a pleiotropic cytokine that is suspected to play a major role in the development and maintenance of several chronic and neuropathic pain states (Zhou et al., 2016). For example, a study using a model of cancer-induced bone pain demonstrated that descending facilitatory signaling from the RVM can be activated by the accumulation of pro-inflammatory cytokines, such as *Il-6*, in supra-spinal regions of the CNS (Liu et al., 2012). Additionally, *Il-6* inhibitors delivered intrathecally can alleviate mechanical allodynia associated with peripheral nerve injury (Arruda et al., 2000). As such, the upregulated supra-spinal expression of *Il-6* in dLAN mice (Figure 3A) likely is associated with their heightened pain responsiveness. Notably, a potential source for these increased levels may be activated microglia (Ji & Suter, 2007).

Another mechanism underlying dLAN-induced hyperalgesia may be peripheral inflammation. Previous data demonstrate that LAN disrupts metabolic function and increases peripheral inflammation (Fonken et al., 2013a). LAN exposure is also positively correlated with obesity, a condition associated with chronic pro-inflammatory states (McFadden et al., 2014). Obesity-induced peripheral inflammation can drive peripheral sensitization and heightened pain sensitivity (Hitt et al., 2007; Iannitti et al., 2012; Ray et al., 2011). This peripheral sensitization can induce central sensitization, which leads to

the activation of descending facilitatory signaling from the RVM (Schaible et al., 2011; Urban & Gebhart, 1999). Though no correlations were found between these factors in this study ($p > 0.05$; correlations not shown), I did not specifically examine the effects of dLAN on peripheral inflammation. Accordingly, peripheral inflammation should still be considered as a candidate link between dLAN and altered pain responsiveness. More investigation is needed to elucidate the potential relationship among these variables.

In addition to pro-inflammatory cytokines, several other neurotrophins and peptides, including BDNF, NGF, and substance P, also play a role in the modulation of nociceptive signaling in the central and peripheral nervous systems (Basbaum et al., 2009). Although the role of NGF in peripheral sensitization is well-defined, its modulation of nociception in the central nervous system is less clear (McMahon, 1996). Several experiments have reported on the nociceptive effects of spinal NGF, but the evidence is conflicting as to whether or not upregulated NGF in the spinal cord induces pro- or anti-nociception (Malcangio et al., 2000; Cirillo et al., 2010; Khan & Smith, 2015). To our knowledge, no previous reports have characterized the effects of supra-spinal NGF on nociception. Here, I noted upregulated levels of *Ngf* in the medulla (Figure 3D), which may indicate that NGF modulates nociceptive synaptic plasticity in the brainstem as it does in the spinal cord. Alternatively, the increased levels of *Ngf* may not be biologically relevant in this context. Additional studies are needed to confirm the role of supra-spinal NGF in hyperalgesia.

It is understood that cold and heat hyperalgesia are regulated by different classes of neuronal receptors (Julius, 2013; Lippoldt et al., 2016; Zimmermann et al., 2007). Accordingly, I analyzed transcript levels of the cold-sensing ion channel receptors *Trpm8* and *Trpa1* in the L3-L5 DRG (McKemy, 2005). No differences were seen between groups, suggesting that these receptors may not play a role in dLAN-mediated cold hyperalgesia (Figure 4G, H). However, differences in the expression or sensitization of TRPA1 or TRPM8 may occur at earlier time points of dLAN exposure and then persist in a chronic manner.

Few disease states or pain conditions have been characterized where thermal hyperalgesia is differentially affected, i.e., the presence of cold but not heat hyperalgesia.

Evidence suggests that night-shift work and sleep deprivation may affect cold and heat hyperalgesia differently, but no mechanism has been proposed (Ødegård et al., 2015; Matre et al., 2017; Pieh et al., 2018). Differential thermal hyperalgesia is also reported in the context of opioid-induced hyperalgesia (OIH). In OIH, reduced cold pain thresholds and tolerances are coincident for both opioid-treated and withdrawal patients; this effect is likely mediated by the MOR and TRPM8 receptors (Gong & Jasmin, 2017). For example, exogenous opioid treatment can produce cold, but not heat, hyperalgesia (Chu et al., 2006) and can increase cold sensitivity in the absence of other forms of nociception (Doverty et al., 2001a; Doverty et al., 2001b). It should be noted that OIH can also produce heat hyperalgesia and other forms of hyperalgesia and allodynia in a range of contexts, yet there is currently a limited understanding as to why pain is inconsistently affected by OIH (Angst & Clark, 2006; Roeckel et al., 2017).

To investigate the differential thermal hyperalgesia phenomenon in the context of the endogenous opioid system, *Mor* expression was examined in the PAG and was found to be upregulated in dLAN mice (Figure 6F). The presence of thermal hyperalgesia despite upregulated levels of MOR in the spinal cord has been noted previously (Zaringhalam et al., 2008). Additionally, MOR antagonists attenuate the effects of stress-induced hyperalgesia, indicating that MORs may play a role in the induction of hyperalgesia (Suarez-Roca et al., 2006). Finally, as MOR expression in both the PAG and the brain stem fluctuates in a circadian manner, heightened *Mor* expression after exposure to dLAN suggests that circadian rhythm disruption may affect *Mor* expression (Takada et al., 2013; Yoshida et al., 2005). Although the endogenous opioid system canonically functions to inhibit pain signaling (Glaum et al., 1994), the present data indicate that dLAN exposure alters MOR expression and function.

In this study, I have demonstrated that dLAN exposure augments pain responsiveness in mice. I report that dLAN-induced hyperalgesia can occur in as few as four nights of dLAN exposure. Three molecular candidates that may play a role in heightened pain responsiveness after chronic dLAN exposure are IL-6, NGF, and MOR. Taken together, these findings indicate that dLAN may be an important factor for physicians and patients alike to consider when treating and managing pain symptoms.

Reducing pain levels, and potentially prescribed opioids, may require the consideration of night-time lighting as a mitigating factor.

References

- Angst, M. S., & Clark, J. D. (2006). Opioid-induced hyperalgesia: a qualitative systematic review. *Anesthesiology*, 104(3), 570-587.
- Arruda, J. L., Sweitzer, S., Rutkowski, M. D., & DeLeo, J. A. (2000). Intrathecal anti-IL-6 antibody and IgG attenuates peripheral nerve injury-induced mechanical allodynia in the rat: possible immune modulation in neuropathic pain. *Brain Research*, 879(1-2), 216-225.
- Bannon, A. W., & Malmberg, A. B. (2007). Models of nociception: hot-plate, tail-flick, and formalin tests in rodents. *Current Protocols in Neuroscience, Chapter 8*, Unit 8.9.
- Basbaum, A. I., Bautista, D. M., Scherrer, G., & Julius, D. (2009). Cellular and Molecular Mechanisms of Pain. *Cell*, 139(2), 267-284.
- Bedrosian, T. A., Fonken, L. K., Walton, J. C., Haim, A., & Nelson, R. J. (2011a). Dim light at night provokes depression-like behaviors and reduces CA1 dendritic spine density in female hamsters. *Psychoneuroendocrinology*, 36(7), 1062-1069.
- Bedrosian, T. A., Fonken, L. K., Walton, J. C., & Nelson, R. J. (2011b). Chronic exposure to dim light at night suppresses immune responses in Siberian hamsters. *Biology Letters*, 7(3), 468-471.
- Bodnar, R., & Heinricher, M. M. (2013). Central Mechanisms of Pain Suppression. In *Neuroscience in the 21st Century* (pp. 2595-2619). Springer New York.
- Borniger, J. C., Maurya, S. K., Periasamy, M., & Nelson, R. J. (2014). Acute dim light at night increases body mass, alters metabolism, and shifts core body temperature circadian rhythms. *Chronobiology International*, 31(8), 917-925.
- Cho, Y., Ryu, S.-H., Lee, B. R., Kim, K. H., Lee, E., & Choi, J. (2015). Effects of artificial light at night on human health: A literature review of observational and experimental studies applied to exposure assessment. *Chronobiology International*, 32(9), 1294-1310.

- Chu, L. F., Clark, D. J., & Angst, M. S. (2006). Opioid tolerance and hyperalgesia in chronic pain patients after one month of oral morphine therapy: a preliminary prospective study. *The Journal of Pain*, 7(1), 43-48.
- Cirillo, G., Cavaliere, C., Bianco, M. R., De Simone, A., Colangelo, A. M., Sellitti, S., Alberghina, L., & Papa, M. (2010). Intrathecal NGF administration reduces reactive astrogliosis and changes neurotrophin receptors expression pattern in a rat model of neuropathic pain. *Cellular and Molecular Neurobiology*, 30(1), 51-62.
- Davis, S., Mirick, D. K., & Stevens, R. G. (2001). Night shift work, light at night, and risk of breast cancer. *Journal of the National Cancer Institute*, 93(20), 1557-1562.
- Doverly, M., Somogyi, A. A., White, J. M., Bochner, F., Beare, C. H., Menelaou, A., & Ling, W. (2001a). Methadone maintenance patients are cross-tolerant to the antinociceptive effects of morphine. *Pain*, 93(2), 155-163.
- Doverly, M., White, J. M., Somogyi, A. A., Bochner, F., Ali, R., & Ling, W. (2001b). Hyperalgesic responses in methadone maintenance patients. *Anesthesiology*, 90(1-2), 91-96.
- Ferrier, J., Marchand, F., & Balayssac, D. (2016). Assessment of Mechanical Allodynia in Rats Using the Electronic Von Frey Test. *Bio-Protocol*, 6(18), e1933.
- Fonken, L. K., Workman, J. L., Walton, J. C., Weil, Z. M., Morris, J. S., Haim, A., & Nelson, R. J. (2010). Light at night increases body mass by shifting the time of food intake. *Proceedings of the National Academy of Sciences*, 107(43), 18664-18669.
- Fonken, L. K., Lieberman, R. A., Weil, Z. M., & Nelson, R. J. (2013a). Dim Light at Night Exaggerates Weight Gain and Inflammation Associated With a High-Fat Diet in Male Mice. *Endocrinology*, 154(10), 3817-3825.
- Fonken, L. K., Aubrecht, T. G., Meléndez-Fernández, O. H., Weil, Z. M., & Nelson, R. J. (2013b). Dim light at night disrupts molecular circadian rhythms and increases body weight. *Journal of Biological Rhythms*, 28(4), 262-271.
- Glaum, S. R., Miller, R. J., & Hammond, D. L. (1994). Inhibitory actions of delta 1-, delta 2-, and mu-opioid receptor agonists on excitatory transmission in lamina II neurons of adult rat spinal cord. *The Journal of Neuroscience*, 14(8), 4965-4971.

- Gong, K., & Jasmin, L. (2017). Sustained Morphine Administration Induces TRPM8-Dependent Cold Hyperalgesia. *The Journal of Pain*, 18(2), 212-221.
- Hitt, H. C., McMillen, R. C., Thornton-Neaves, T., Koch, K., & Cosby, A. G. (2007). Comorbidity of obesity and pain in a general population: results from the Southern Pain Prevalence Study. *The Journal of Pain*, 8(5), 430-436.
- Hogan, M. K., Kovalycsik, T., Sun, Q., Rajagopalan, S., & Nelson, R. J. (2015). Combined effects of exposure to dim light at night and fine particulate matter on C3H/HeNHsd mice. *Behavioural Brain Research*, 294, 81-88.
- Iannitti, T., Graham, A., & Dolan, S. (2012). Increased central and peripheral inflammation and inflammatory hyperalgesia in Zucker rat model of leptin receptor deficiency and genetic obesity. *Experimental Physiology*, 97(11), 1236-1245.
- Ji, R. R., Nackley, A., Huh, Y., Terrando, N., & Maixner, W. (2018). Neuroinflammation and Central Sensitization in Chronic and Widespread Pain. *Anesthesiology*, 129(2), 343-366.
- Ji, R. R., & Suter, M. R. (2007). p38 MAPK, microglial signaling, and neuropathic pain. *Molecular Pain*, 3, 33.
- Julius, D. (2013). TRP channels and pain. *Annual Review of Cell and Developmental Biology*, 29, 355-384.
- Kavaliers, M., & Hirst, M. (1983). Daily rhythms of analgesia in mice: effects of age and photoperiod. *Brain Research*, 279(1-2), 387-393.
- Kawasaki, Y., Zhang, L., Cheng, J.-K., & Ji, R.-R. (2008). Cytokine Mechanisms of Central Sensitization: Distinct and Overlapping Role of Interleukin-1, Interleukin-6, and Tumor Necrosis Factor- in Regulating Synaptic and Neuronal Activity in the Superficial Spinal Cord. *Journal of Neuroscience*, 28(20), 5189-5194.
- Khan, N., & Smith, M. T. (2015). Neurotrophins and Neuropathic Pain: Role in Pathobiology. *Molecules*, 20(6), 10657-10688.
- Kloog, I., Haim, A., Stevens, R. G., & Portnov, B. A. (2009). Global co-distribution of light at night (LAN) and cancers of prostate, colon, and lung in men. *Chronobiology International*, 26(1), 108-125.

- Lippoldt, E. K., Ongun, S., Kusaka, G. K., & McKemy, D. D. (2016). Inflammatory and neuropathic cold allodynia are selectively mediated by the neurotrophic factor receptor GFR α 3. *Proceedings of the National Academy of Sciences*, 113(16), 4506-4511.
- Liu, X., Bu, H., Liu, C., Gao, F., Yang, H., Tian, X., Xu, A., Chen, Z., Cao, F., & Tian, Y. (2012). Inhibition of glial activation in rostral ventromedial medulla attenuates mechanical allodynia in a rat model of cancer-induced bone pain. *Journal of Huazhong University of Science and Technology*, 32(2), 291-298.
- Lucas, R. J., Lall, G. S., Allen, A. E., & Brown, T. M. (2012). How rod, cone, and melanopsin photoreceptors come together to enlighten the mammalian circadian clock. *Progress in Brain Research*, 199, 1-18.
- Malcangio, M., Ramer, M. S., Boucher, T. J., & McMahon, S. B. (2000). Intrathecally injected neurotrophins and the release of substance P from the rat isolated spinal cord. *European Journal of Neuroscience*, 12(1), 139-144.
- Martin, S. L., Reid, A. J., Verkhatsky, A., Magnaghi, V., & Faroni, A. (2019). Gene expression changes in dorsal root ganglia following peripheral nerve injury: roles in inflammation, cell death and nociception. *Neural Regeneration Research*, 14(6), 939.
- Martinov, T., Mack, M., Sykes, A., & Chatterjea, D. (2013). Measuring changes in tactile sensitivity in the hind paw of mice using an electronic von Frey apparatus. *Journal of Visualized Experiments*, 82, e51212.
- Matre, D., Knardahl, S., & Nilsen, K. B. (2017). Night-shift work is associated with increased pain perception. *Scandinavian Journal of Work, Environment & Health*, 43(3), 260-268.
- McFadden, E., Jones, M. E., Schoemaker, M. J., Ashworth, A., & Swerdlow, A. J. (2014). The relationship between obesity and exposure to light at night: cross-sectional analyses of over 100,000 women in the Breakthrough Generations Study. *American Journal of Epidemiology*, 180(3), 245-250.
- McKemy, D. D. (2005). How cold is it? TRPM8 and TRPA1 in the molecular logic of cold sensation. *Molecular Pain*, 1, 16.

- McMahon, S. B. (1996). NGF as a mediator of inflammatory pain. *Philosophical Transactions of the Royal Society of London. Series B: Biological Sciences*, 351(1338), 431-440.
- Obayashi, K., Saeki, K., Iwamoto, J., Ikada, Y., & Kurumatani, N. (2013). Exposure to light at night and risk of depression in the elderly. *Journal of Affective Disorders*, 151(1), 331-336.
- Ødegård, S. S., Omland, P. M., Nilsen, K. B., Stjern, M., Gravdahl, G. B., & Sand, T. (2015). The effect of sleep restriction on laser evoked potentials, thermal sensory and pain thresholds and suprathreshold pain in healthy subjects. *Clinical Neurophysiology*, 126(10), 1979-1987.
- Onen, S. H., Alloui, A., Gross, A., Eschallier, A., & Dubray, C. (2001). The effects of total sleep deprivation, selective sleep interruption and sleep recovery on pain tolerance thresholds in healthy subjects. *Journal of Sleep Research*, 10(1), 35-42.
- Pieh, C., Jank, R., Waiß, C., Pfeifer, C., Probst, T., Lahmann, C., & Oberndorfer, S. (2018). Night-shift work increases cold pain perception. *Sleep Medicine*, 45, 74-79.
- Ray, L., Lipton, R. B., Zimmerman, M. E., Katz, M. J., & Derby, C. A. (2011). Mechanisms of association between obesity and chronic pain in the elderly. *Pain*, 152(1), 53-59.
- Reppert, S. M., & Weaver, D. R. (2002). Coordination of circadian timing in mammals. *Nature*, 418(6901), 935-941.
- Rigaud, M., Gemes, G., Barabas, M. E., Chernoff, D. I., Abram, S. E., Stucky, C. L., & Hogan, Q. H. (2008). Species and strain differences in rodent sciatic nerve anatomy: implications for studies of neuropathic pain. *Pain*, 136(1-2), 188-201.
- Roeckel, L. A., Utard, V., Reiss, D., Mouheiche, J., Maurin, H., Robé, A., Audouard, E., Wood, J. N., Goumon, Y., Simonin, F., & Gaveriaux-Ruff, C. (2017). Morphine-induced hyperalgesia involves mu opioid receptors and the metabolite morphine-3-glucuronide. *Scientific Reports*, 7(1), 10406.
- Russart, K. L. G., & Nelson, R. J. (2018). Light at night as an environmental endocrine disruptor. *Physiology & Behavior*, 190, 82-89.

- Schaible, H.-G., Ebersberger, A., & Natura, G. (2011). Update on peripheral mechanisms of pain: beyond prostaglandins and cytokines. *Arthritis Research & Therapy*, 13(2), 210.
- Suarez-Roca, H., Silva, J. A., Arcaya, J. L., Quintero, L., Maixner, W., & Pinerua-Shuhaibar, L. (2006). Role of mu-opioid and NMDA receptors in the development and maintenance of repeated swim stress-induced thermal hyperalgesia. *Behavioural Brain Research*, 167(2), 205-211.
- Takada, T., Yamashita, A., Date, A., Yanase, M., Suhara, Y., Hamada, A., Sakai, H., Ikegami, D., Iseki, M., Inada, E., & Narita, M. (2013). Changes in the circadian rhythm of mRNA expression for μ -opioid receptors in the periaqueductal gray under a neuropathic pain-like state. *Synapse*, 67(5), 216-223.
- Urban, M. O., & Gebhart, G. F. (1999). Supraspinal contributions to hyperalgesia. *Proceedings of the National Academy of Sciences*, 96(14), 7687-7692.
- Walker, W. H., Borniger, J. C., Gaudier-Diaz, M. M., Hecmarie Meléndez-Fernández, O., Pascoe, J. L., Courtney DeVries, A., & Nelson, R. J. (2020). Acute exposure to low-level light at night is sufficient to induce neurological changes and depressive-like behavior. *Molecular Psychiatry*, 25(5), 1080-1093.
- Wei, F., Guo, W., Zou, S., Ren, K., & Dubner, R. (2008). Supraspinal glial-neuronal interactions contribute to descending pain facilitation. *Journal of Neuroscience*, 28(42), 10482-10495.
- Xu, D., Zhao, H., Gao, H., Zhao, H., Liu, D., & Li, J. (2018). Participation of pro-inflammatory cytokines in neuropathic pain evoked by chemotherapeutic oxaliplatin via central GABAergic pathway. *Molecular Pain*, 14, 1744806918783535.
- Yoshida, M., Koyanagi, S., Matsuo, A., Fujioka, T., To, H., Higuchi, S., & Ohdo, S. (2005). Glucocorticoid hormone regulates the circadian coordination of micro-opioid receptor expression in mouse brainstem. *Journal of Pharmacology and Experimental Therapeutics*, 315(3), 1119-1124.
- Zaringhalam, J., Manaheji, H., Mghsoodi, N., Farokhi, B., & Mirzaiee, V. (2008). Spinal mu-opioid receptor expression and hyperalgesia with dexamethasone in chronic

- adjuvant-induced arthritis in rats. *Clinical and Experimental Pharmacology and Physiology*, 35(11), 1309-1315.
- Zhang, J., Li, H., Teng, H., Zhang, T., Luo, Y., Zhao, M., Li, Y. Q., & Sun, Z. S. (2012). Regulation of peripheral clock to oscillation of substance P contributes to circadian inflammatory pain. *Anesthesiology*, 117(1), 149-160.
- Zhou, Y. Q., Liu, Z., Liu, Z. H., Chen, S. P., Li, M., Shahveranov, A., Ye, D. W., & Tian, Y. K. (2016). Interleukin-6: an emerging regulator of pathological pain. *J Neuroinflammation*, 13(1), 141.
- Zimmermann, K., Leffler, A., Babes, A., Cendan, C. M., Carr, R. W., Kobayashi, J., Nau, C., Wood, J. N., & Reeh, P. W. (2007). Sensory neuron sodium channel Nav1.8 is essential for pain at low temperatures. *Nature*, 447(7146), 855-858.

Chapter 3

Artificial Light at Night Exacerbates Cold Neuropathy in a Mouse Model of Type II Diabetes Mellitus

Submitted As:

Bumgarner, J. R., White, R. C., Brown, J. A., & Nelson, R. J. (2023). Artificial Light at Night Exacerbates Cold Neuropathy in a Mouse Model of Type II Diabetes Mellitus. *Frontiers in Neuroscience*, (*Under Review*).

Introduction

Circadian rhythm disruption is a pervasive and nearly ubiquitous aspect of modern human life. Circadian rhythms are intrinsic biological processes that rhythmically fluctuate with a period of about 24 hours; they are set to precisely 24 hours each day by exposure to light during the circadian day (Vitaterna et al., 2001). These rhythms govern many aspects of behavior and physiology, including pain behavior (Bumgarner et al., 2021; Segal et al., 2018; Palada et al., 2020) and metabolic function. Circadian rhythms are aligned to the external environment primarily via solar light-dark cycle cues, and the synchronization of these rhythms with the external rhythmic environment of the Earth is crucial for health (Vitaterna et al., 2001; Patke et al., 2020).

Artificial light at night (ALAN) is one of the most pervasive disruptors of circadian rhythms (Falchi et al., 2016). ALAN exposure is directly associated with several detrimental health, physiological, and behavioral effects in humans and other animals, including elevated inflammation and obesity (Bumgarner & Nelson, 2021; Muscogiuri et al., 2022; Walker et al., 2021). Importantly, our recent work demonstrated that exposure to ALAN can exacerbate pain behavior in male mice after as few as four nights of exposure (Bumgarner et al., 2020). Other forms of circadian rhythm disruption are also associated with exacerbated pain behavior, including night shift work and sleep deprivation (Mun et al., 2022). Because of the intertwined relationship between circadian rhythms and pain, it is important to understand the effects of ALAN on pain beyond the context of typical states of health.

Type II diabetes (T2DM) is estimated to affect over 500 million adults worldwide, representing 10.5% of the adult human population (Robertson et al., 2022). Moreover, T2DM is estimated to represent ~98% of global diabetes diagnoses. A large-scale epidemiological study recently reported that ALAN exposure is positively correlated with T2DM risk (Xu et al., 2023). ALAN can impair metabolic function, for example, by reducing insulin and glucose tolerance and elevating circulating free fatty acids and triglycerides (Fleury et al., 2020; Russart & Nelson, 2018; Mason et al., 2020). Work from our lab recently demonstrated that exposure to ALAN can exacerbate the progression of diabetes in a polygenic mouse model of T2DM (TALLYHO mice) (Russart et al., 2019). Beyond the metabolic consequences of this disease, it is currently estimated that around 50% of individuals with T2DM will develop diabetic neuropathy at some point in their lives (Feldman, 2018; Feldman et al., 2019). This extends the risk potential for the effects of ALAN beyond metabolism.

In this study, I hypothesized that ALAN exposure exacerbates the progression of diabetic neuropathy in female and male mice in a mouse model of T2DM. Diabetes was induced per the protocol previously reported (Nath et al., 2016); then, mice were exposed to dim ALAN (5 lux) for four weeks. I predicted that ALAN exposure would exacerbate the progression of diabetes and diabetic neuropathy.

Materials and Methods

Animals

Adult female and male Swiss Webster (CFW) mice (Charles River Laboratories) were obtained at 7-8 weeks of age and given 1 week to acclimate to standard vivarium conditions (14:10 h light: dark, lights off at ZT12; 150±25:0 lux, 22±2 °C; 12.0 x 6.5 x 5.5" polycarbonate cages). Following arrival, mice were housed in groups of five per cage. After the acclimation period, mice were singly housed, and the experiment began. Reverse osmosis water and food were provided *ad libitum* throughout the duration of the experiment. All studies were approved by the West Virginia University Institutional Animal Care and Use Committee, and animals were maintained in accordance with NIH Animal Welfare guidelines.

T2DM Induction

To induce diabetes, I followed a previously published protocol (Nath et al., 2017). For five weeks starting at the onset of the experiment, mice were given *ad libitum* access to a high-fat diet (21.0% protein, 24.6% carbohydrate, 54.4% fat per kilocalorie; TD.07011, Envigo). The high-fat diet was replaced every two days between ZT03-05. At the beginning of the fourth week of the experiment, mice were given a series of five i.p. injections of 40 mg/kg of streptozotocin (STZ; ICN10055701, Fisher). STZ was prepared daily immediately before injections by dissolving STZ in 0.1M citrate buffer pH 4.5 at a concentration of 10 mg/mL. Injections were administered during the light phase between ZT03-05. Following glucose measurements, animals were pseudorandomly assigned to either LD or ALAN conditions to ensure an even distribution of animals with glucose levels above/below 200 mg/dL between groups. At the conclusion of the experiment, all animals were diabetic based on the 200 mg/dL cutoff. Glucose measurements were measured from tail vein blood using a Contour Next 7377 glucometer and Contour Next 7278 glucose strips.

ALAN Conditions

After the five weeks of T2Dm induction, animals were separated into either LD or ALAN housing conditions. ALAN (5 ± 1 lux) sources were Luma5 Standard LED light strips (1.5 W/ft, 5000K “cool white”, 1200 lumens; Hitlights Inc.). Lux calibrations were conducted by placing a Mavolux 5023C illuminance meter (Gossen) in the center of an empty cage with the light sensor facing toward the ceiling. Animals remained in either LD or ALAN conditions for a total of four weeks.

Behavioral Testing

Pain behavioral testing consisted of a cold plate and electric von Frey testing. Baseline pain behavioral measurements were taken one day before the onset of ALAN/LD experimental housing conditions after the T2DM induction. Pain behavior was then assessed after 2 and 4 weeks of experimental housing conditions. All behavioral

testing was conducted during the light phase between ZT03-06. Animals were given a minimum of 30 minutes to acclimate to the behavioral suite prior to testing.

Cold plate testing (IITC Life Science Inc) was performed at $0.5 \pm 1.0\text{ }^{\circ}\text{C}$. Mice were gently placed onto the cold plate, and a stopwatch was started as soon as their hind paws touched the plate. Two observers watched for any sign of nocifensive response, which included hind paw shakes/extended withdrawals/licking, jumping, or squeaking. As soon as the first nocifensive response was observed, the latency to response was recorded and the animal was promptly removed from the plate. Animals were removed from the place after a cutoff of 90 seconds if no responses were observed.

Electric von Frey testing (Bioseb) was conducted using opaque chambers ($80 \times 115 \times 145\text{ mm}$; Bioseb) on top of a wire mesh table (Bioseb). Mice were given 15 minutes to acclimate to the chambers before the onset of testing. Testing was conducted in a series of four rounds, where the wire tip of the electric von Frey was slowly pressed upwards on the plantar surface of a consistent hind paw of each mouse. The maximum force needed to elicit a response was recorded as the mechanical withdrawal threshold. Responses to the von Frey were defined as paw lifts, paw shakes, or jumping. The withdrawal thresholds from the four rounds were averaged to produce a final threshold score for each animal at each time point.

Statistical Analyses

All data were analyzed using two-way repeated measures ANOVAs. *A priori* planned multiple comparisons were conducted using Fisher's LSD. All analyses were conducted using Prism 9.5.1. Mean differences with an alpha of 0.05 were considered statistically significant.

Results

ALAN Elevates Glucose in Male, but Not Female T2DM Mice

After four weeks of exposure to ALAN, male mice exhibited elevated blood glucose levels (Figure 1A; $p < 0.05$) with a significant interaction between lighting condition exposure and time ($p < 0.05$; $F_{2,56} = 4.615$). There was no significant effect of ALAN exposure on female blood glucose at any time point. At the final time point, there was no difference in the distribution of animals that were considered diabetic per the defined cutoff level. There was a main effect of time on blood glucose levels in both male (Figure 1A; $p < 0.05$; $F_{2,56} = 98.03$) and female mice (Figure 1C; $p < 0.05$; $F_{2,56} = 114.1$) from the conclusion of the T2DM induction and the onset of the experimental lighting condition housing.

ALAN Alters Body Mass Loss in T2DM

A main effect of lighting condition ($p < 0.05$; $F_{1,28} = 5.165$) and an interaction between lighting condition and time ($p < 0.05$; $F_{4,112} = 3.325$) on body mass were observed in male mice (Figure 1B). When examining individual time point differences, ALAN and LD body masses only differed at weeks one and three in male mice (Figure 1B; $p < 0.05$). An interaction between lighting condition and time on body mass was observed in female mice (Figure 1D; $p < 0.05$; $F_{4,112} = 2.741$), but no individual time points were significantly different ($p < 0.05$). A main effect of time was observed in both male ($p < 0.05$; $F_{2,56} = 124.9$) and female mice ($p < 0.05$; $F_{2,56} = 156.3$), indicating a loss in body mass following the conclusion of the T2DM induction protocol. Lastly, there was a significant effect of the T2DM induction protocol on body mass in both male (Supplementary Figure 1A; $p < 0.05$; $F_{5,140} = 406.8$) and female mice (Supplementary Figure 1B; $p < 0.05$; $F_{5,140} = 229.7$).

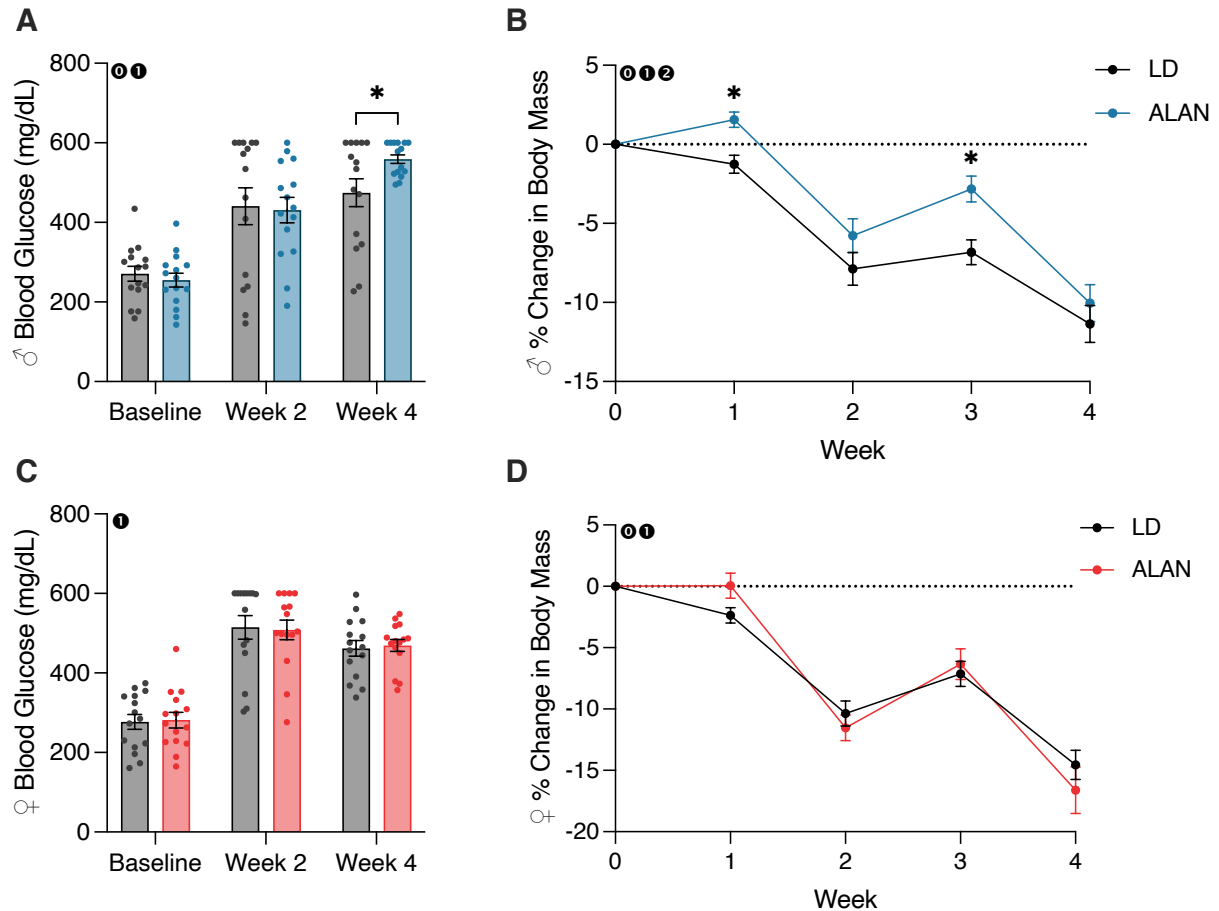


Figure 1. ALAN elevates blood glucose and alters body mass loss. Blood glucose levels following the onset of experimental housing in either ALAN or LD conditions (A, C). The percent change in body mass following the onset of experimental housing (B, D). All data are represented as mean \pm SEM. 0 – Interaction between Lighting Condition and Time; 1 – Main effect of Time; 2 – Main effect of Lighting Condition. * $p < 0.05$.

ALAN Exacerbates Cold Neuropathy in Male, but Not Female T2DM Mice

Male mice exposed to ALAN for four weeks exhibited reduced cold plate withdrawal latencies relative to the LD diabetic male mice (Figure 2A; $p < 0.05$). This difference coincided with a significant interaction between lighting condition and time ($p < 0.05$; $F_{2,56} = 4.109$). When considering within-group changes in cold plate withdrawal latencies, the male ALAN mice had no significant changes in cold plate withdrawal thresholds relative to baseline (Figure 2A; $p > 0.05$). In contrast, male LD mice exhibited elevated withdrawal thresholds relative to their baseline measurements (Figure 2A; $p < 0.05$). There was a main effect of time on cold plate withdrawal latencies in male mice (Figure 2A; $p < 0.05$; $F_{2,56} = 6.358$). No effect of ALAN was observed on cold plate withdrawal thresholds in female mice, but both LD and ALAN female mice had elevated cold plate withdrawal latencies relative to their baseline measurements (Figure 2C; $p < 0.05$) with a main effect of time ($p < 0.05$; $F_{2,56} = 6.767$).

A weak effect of ALAN exposure on mechanical withdrawal thresholds was observed in male mice at the four-week time point, but this effect was not significant (Figure 2B; $p = 0.099$). ALAN did not affect female mechanical withdrawal latencies in female mice (Figure 2D; $p > 0.05$). There was a main effect of time on mechanical withdrawal thresholds in male mice (Figure 2B; $p < 0.05$; $F_{2,56} = 3.713$), indicating a progression of hypoesthesia following the conclusion of the T2DM induction. This effect was not present in females.

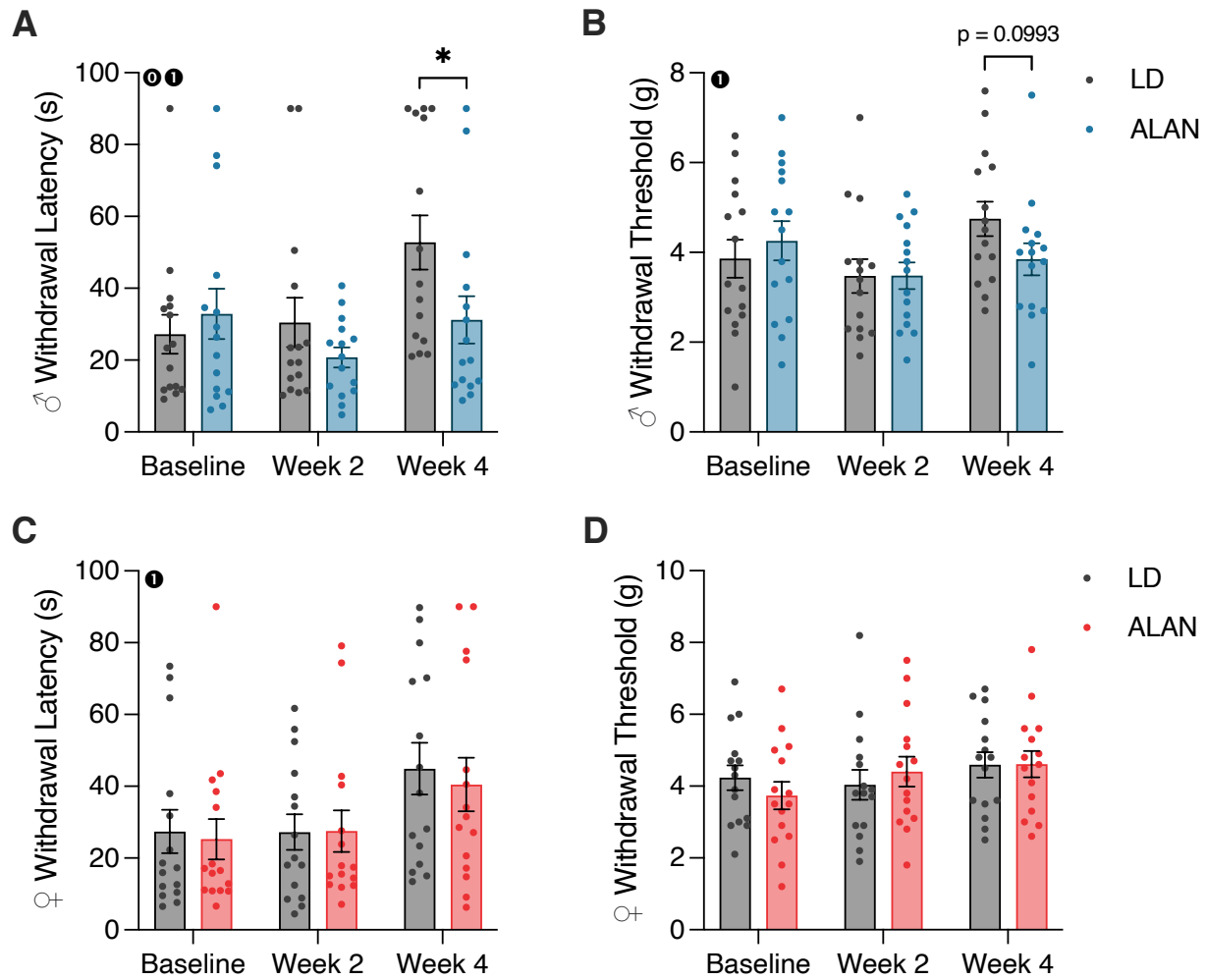
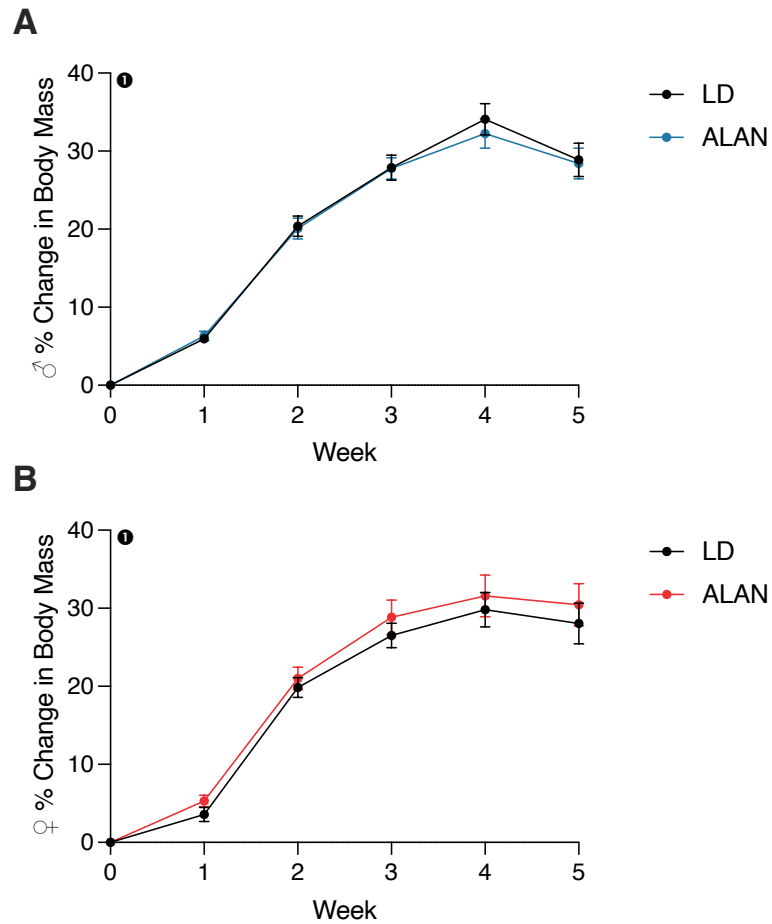


Figure 2. ALAN delays cold plate hypoalgesia in male T2DM mice. Cold plate withdrawal latencies (A, C), and von Frey mechanical withdrawal thresholds (B, D) of female and male mice following the onset of experimental housing. All data are represented as mean \pm SEM. 0 – Interaction between Lighting Condition and Time; 1 – Main effect of Time; 2 – Main effect of Lighting Condition. * $p < 0.05$.



Supplemental Figure 1. Induction of a T2DM-like phenotype increases body mass in female and male mice. The percent change in body mass from the onset of the T2DM protocol to the onset of experimental housing in male (A) and female (B) mice. All data are represented as mean \pm SEM. 1 – Main effect of Time.

Discussion

This study sought to understand the effects of ALAN exposure on the progression of diabetic neuropathy in a mouse model of T2DM. Mice first were exposed to a multi-week high-fat diet and low-dose series of streptozotocin to induce a T2DM phenotype based on a previously validated protocol (Nath et al., 2017). Male mice exposed to ALAN exhibited reduced responsiveness to noxious cold stimuli relative to male control counterparts. Male mice also exhibited elevated blood glucose at the conclusion of the study, and ALAN blunted the loss of body mass in male mice at various time points throughout the study. In contrast, a stark sex difference was observed for each examined metric. ALAN had no observable effects on pain behavior or blood glucose in female mice, but it did alter female body mass loss following T2DM induction.

In humans, diabetic peripheral neuropathy progression can vary, but generally, nociceptive large-diameter thinly myelinated A δ fibers and small-diameter unmyelinated C fibers are first affected, leading to a period of hyperalgesia and allodynia. As the neuropathy progresses and the nociceptive A δ and C fibers continue to degenerate, larger diameter myelinated A β fibers also begin to degenerate, ultimately leading to numbness, hypoalgesia, and loss of sensation (O'Brien et al., 2014). The characterization of the progression of diabetic neuropathy in mice is less clear, but several studies have reported a progression of hypoesthesia (reduced sensitivity to innocuous touch) and hypoalgesia following T2DM induction (De Gregorio et al., 2018; Sasajima et al., 2022). It is possible that the initial phase of hypersensitivity wasn't replicated in these studies due to the acute period of T2DM induction. In contrast to the noted differences in progression of hypoesthesia in male mice in this study, another study reported long-term allodynia using the same T2DM induction protocol as this study, although their study examined female C57BL/6 mice (Castañeda-Corral et al., 2021).

The difference in cold plate withdrawal latencies in male mice exposed to ALAN could be interpreted in two separate ways. One may consider that ALAN led to the development of cold hyperalgesia in male mice relative to the LD counterparts. In contrast, one might consider that ALAN didn't induce a state of hyperalgesia, but instead delayed the onset of hypoalgesia that was noted in male LD mice. Distinguishing between

these two perspectives would require a follow-up study that tested pain behavior more frequently and for longer periods of time to examine the progression of pain behavior. Further insight into the underlying mechanisms behind this effect would require additional examinations, including the assessment of peripheral inflammation and nerve conduction velocity.

The sex differences observed in pain behavior and metabolic phenotypes in this experiment may be explained by underlying sex differences in circadian rhythm biology or the effects of circadian rhythm disruption. Indeed, there are numerous sex differences in circadian rhythms, including the function of the immune, metabolic, and endocrine systems (Walton et al., 2022; Munyoki et al., 2022). Moreover, there are sex differences in the metabolic consequences of circadian rhythm disruption, including the effects of ALAN (Rumanova et al., 2020; Masís-Vargas et al., 2019), simulated shift work (Qian et al., 2019), and jet lag (Feliciano et al., 2019), demonstrating precedence for the observed sex differences in this study. However, further research will be needed to identify the underlying mechanisms of sex differences in circadian rhythm disruption that were observed in this study.

The observed sex differences in pain behavior and metabolic phenotypes in this study may be further explained by underlying sex differences in diabetes or diabetic neuropathy (Kautzky-Willer et al., 2023; Abraham et al., 2018). Numerous metabolic risk factors for T2DM present differently between men and women, including glucose and insulin sensitivity, hormonal regulation of metabolism, and hypertension (Kautzky-Willer et al., 2023; Kautzky-Willer et al., 2016). There are few reports on sex differences in diabetic neuropathy, but some sex differences have been reported. Neuropathy appears to present earlier in men than women (Aaberg et al., 2008; Kamenov et al., 2010), whereas one study reported that women with diabetic polyneuropathy report higher pain intensities (Abraham et al., 2018). There is minimal preclinical research on sex differences in diabetic neuropathy. One study using a diet-induced ‘pre-diabetes’ state reported no sex differences in pain behavior (Elzinga et al., 2021). In all, there is minimal documented evidence of the underlying mechanisms that lead to sex differences in diabetic neuropathy. I propose that the sex differences observed in this study likely are a

result of underlying differences in either the progression of neuropathy following the diabetes induction protocol or the underlying sex differences in the effects of ALAN exposure.

In conclusion, exposure to ALAN exacerbates cold pain behavior and blood glucose levels in male mice, but not female mice, and ALAN altered the loss of body mass following T2DM induction. Further experimentation will be required to understand the underlying mechanisms behind the pain-related consequences of ALAN and the observed sex differences. These results highlight the continuing need to consider circadian rhythms and the mitigation of circadian rhythm disruption in the treatment and management of pain, and the need to consider sex as a biological variable.

References

- Aaberg, M. L., Burch, D. M., Hud, Z. R., & Zacharias, M. P. (2008). Gender differences in the onset of diabetic neuropathy. *Journal of Diabetes and its Complications*, 22(2), 83-87.
- Abraham, A., Barnett, C., Katzberg, H. D., Lovblom, L. E., Perkins, B. A., & Bril, V. (2018). Sex differences in neuropathic pain intensity in diabetes. *Journal of the Neurological Sciences*, 388, 103-106.
- Bumgarner, J. R., & Nelson, R. J. (2021). Light at Night and Disrupted Circadian Rhythms Alter Physiology and Behavior. *Integrative and Comparative Biology*, icab017.
- Bumgarner, J. R., Walker II, W. H., & Nelson, R. J. (2021). Circadian rhythms and pain. *Neuroscience & Biobehavioral Reviews*, 129, 296-306.
- Bumgarner, J. R., Walker, W. H., Liu, J. A., Walton, J. C., & Nelson, R. J. (2020). Dim Light at Night Exposure Induces Cold Hyperalgesia and Mechanical Allodynia in Male Mice. *Neuroscience*, 434, 111-119.
- Castañeda-Corral, G., Velázquez-Salazar, N. B., Martínez-Martínez, A., Taboada-Serrano, J. N., Núñez-Aragón, P. N., González-Palomares, L., Acosta-González, R. I., Petricevich, V. L., Acevedo-Fernández, J. J., & Montes, S. (2021). Characterization of mechanical allodynia and skin innervation in a mouse model of

- Type-2 diabetes induced by cafeteria-style diet and low-doses of Streptozotocin. *Frontiers in Pharmacology*, 11, 628438.
- De Gregorio, C., Contador, D., Campero, M., Ezquer, M., & Ezquer, F. (2018). Characterization of diabetic neuropathy progression in a mouse model of type 2 diabetes mellitus. *Biology Open*, 7(9), bio036830.
- Elzinga, S. E., Savelieff, M. G., O'Brien, P. D., Mendelson, F. E., Hayes, J. M., & Feldman, E. L. (2021). Sex differences in insulin resistance, but not peripheral neuropathy, in a diet-induced prediabetes mouse model. *Disease models & mechanisms*, 14(4), dmm048909.
- Falchi, F., Cinzano, P., Duriscoe, D., Kyba, C. C., Elvidge, C. D., Baugh, K., Portnov, B. A., Rybnikova, N. A., & Furgoni, R. (2016). The new world atlas of artificial night sky brightness. *Science Advances*, 2(6), e1600377.
- Feldman, E. L. (2018). Epidemiology and classification of diabetic neuropathy. *UpToDate®*. Available from www.uptodate.com/contents/epidemiology-and-classification-of-diabetic-neuropathy (accessed 17 February 2016).
- Feldman, E. L., Callaghan, B. C., Pop-Busui, R., Zochodne, D. W., Wright, D. E., Bennett, D. L., Bril, V., Russell, J. W., & Viswanathan, V. (2019). Diabetic neuropathy. *Nature reviews Disease primers*, 5(1), 41.
- Feliciano, E. M. C., Rifas-Shiman, S. L., Quante, M., Redline, S., Oken, E., & Taveras, E. M. (2019). Chronotype, social jet lag, and cardiometabolic risk factors in early adolescence. *JAMA pediatrics*, 173(11), 1049-1057.
- Fleury, G., Masís-Vargas, A., & Kalsbeek, A. (2020). Metabolic implications of exposure to light at night: lessons from animal and human studies. *Obesity*, 28, S18-S28.
- Kamenov, Z. A., Parapunova, R. A., & Georgieva, R. T. (2010). Earlier development of diabetic neuropathy in men than in women with type 2 diabetes mellitus. *Gender medicine*, 7(6), 600-615.
- Kautzky-Willer, A., Harreiter, J., & Pacini, G. (2016). Sex and gender differences in risk, pathophysiology and complications of type 2 diabetes mellitus. *Endocrine Reviews*, 37(3), 278-316.

- Kautzky-Willer, A., Leutner, M., & Harreiter, J. (2023). Sex differences in type 2 diabetes. *Diabetologia*, 66(6), 986-1002.
- Masís-Vargas, A., Hicks, D., Kalsbeek, A., & Mendoza, J. (2019). Blue light at night acutely impairs glucose tolerance and increases sugar intake in the diurnal rodent *Arvicanthis ansorgei* in a sex-dependent manner. *Physiological reports*, 7(20), e14257.
- Mason, I. C., Qian, J., Adler, G. K., & Scheer, F. A. J. L. (2020). Impact of circadian disruption on glucose metabolism: implications for type 2 diabetes. *Diabetologia*, 63(3), 462-472.
- Mun, C. J., Burgess, H. J., Sears, D. D., Parthasarathy, S., James, D., Altamirano, U., Sajith, S., Lakhotia, A., Fillingim, R. B., & Youngstedt, S. D. (2022). Circadian Rhythm and Pain: a Review of Current Research and Future Implications. *Current Sleep Medicine Reports*, 1-10.
- Munyoki, S. K., Goff, J. P., Kolobaric, A., Long, A., Mullett, S. J., Burns, J. K., Jenkins, A. K., DePoy, L., Wendell, S. G., & McClung, C. A. (2022). Circadian rhythms in the gut microbiota shape sex differences in host gene expression and metabolism. *bioRxiv*, 2022.09. 15.508006.
- Muscogiuri, G., Poggiogalle, E., Barrea, L., Tarsitano, M. G., Garifalos, F., Liccardi, A., Pugliese, G., Savastano, S., Colao, A., & Alviggi, C. (2022). Exposure to artificial light at night: A common link for obesity and cancer. *European Journal of Cancer*, 173, 263-275.
- Nath, S., Ghosh, S. K., & Choudhury, Y. (2017). A murine model of type 2 diabetes mellitus developed using a combination of high fat diet and multiple low doses of streptozotocin treatment mimics the metabolic characteristics of type 2 diabetes mellitus in humans. *Journal of Pharmacological and Toxicological Methods*, 84, 20-30.
- O'Brien, P. D., Sakowski, S. A., & Feldman, E. L. (2014). Mouse models of diabetic neuropathy. *ILAR journal*, 54(3), 259-272.
- Palada, V., Gilron, I., Canlon, B., Svensson, C. I., & Kalso, E. (2020). The circadian clock at the intercept of sleep and pain. *Pain*, 161(5), 894-900.

- Patke, A., Young, M. W., & Axelrod, S. (2020). Molecular mechanisms and physiological importance of circadian rhythms. *Nature Reviews Molecular Cell Biology*, 21(2), 67-84.
- Qian, J., Morris, C. J., Caputo, R., Wang, W., Garaulet, M., & Scheer, F. A. J. L. (2019). Sex differences in the circadian misalignment effects on energy regulation. *Proceedings of the National Academy of Sciences*, 116(47), 23806-23812.
- Robertson, R. P., Nathan, D. M., & Mulder, J. E. (2022). Type 2 diabetes mellitus: Prevalence and risk factors. *UpToDate*. Jan, 25.
- Rumanova, V. S., Okuliarova, M., & Zeman, M. (2020). Differential effects of constant light and dim light at night on the circadian control of metabolism and behavior. *International Journal of Molecular Sciences*, 21(15), 5478.
- Russart, K. L. G., Chbeir, S. A., Nelson, R. J., & Magalang, U. J. (2019). Light at night exacerbates metabolic dysfunction in a polygenic mouse model of type 2 diabetes mellitus. *Life Sciences*, 231, 116574.
- Russart, K. L. G., & Nelson, R. J. (2018). Light at night as an environmental endocrine disruptor. *Physiology & Behavior*, 190, 82-89.
- Sasajima, S., Kondo, M., Ohno, N., Ujisawa, T., Motegi, M., Hayami, T., Asano, S., Asano-Hayami, E., Nakai-Shimoda, H., & Inoue, R. (2022). Thermal gradient ring reveals thermosensory changes in diabetic peripheral neuropathy in mice. *Scientific Reports*, 12(1), 1-13.
- Segal, J. P., Tresidder, K. A., Bhatt, C., Gilron, I., & Ghasemlou, N. (2018). Circadian control of pain and neuroinflammation. *Journal of Neuroscience Research*, 96(6), 1002-1020.
- Vitaterna, M. H., Takahashi, J. S., & Turek, F. W. (2001). Overview of circadian rhythms. *Alcohol research & health*, 25(2), 85.
- Walker, W. H., Bumgarner, J. R., Becker-Krail, D. D., May, L. E., Liu, J. A., & Nelson, R. J. (2021). Light at night disrupts biological clocks, calendars, and immune function. *Seminars in Immunopathology*, 1-9.
- Walton, J. C., Bumgarner, J. R., & Nelson, R. J. (2022). Sex Differences in Circadian Rhythms. *Cold Spring Harbor Perspectives in Biology*, a039107.

Xu, Z., Jin, J., Yang, T., Wang, Y., Huang, J., Pan, X., Frank, K., & Li, G. (2023). Outdoor light at night, genetic predisposition and type 2 diabetes mellitus: A prospective cohort study. *Environmental Research*, 219, 115157.

Chapter 4

Artificial Light at Night Exposure Exacerbates Paclitaxel-Induced Mechanical Allodynia in Female Mice

Introduction

Chemotherapy-induced peripheral neuropathy (CIPN) is a common side-effect for cancer patients treated with platinum-based and taxane chemotherapeutics. CIPN prevalence rates vary based on the class of drug, dose density, and the method of pain assessment (Molassiotis et al., 2019; Osmani et al., 2012; Seretny et al., 2014). The presence of preexisting conditions, such as diabetes mellitus, age, and history of neuropathy, can further increase the likelihood of a patient developing CIPN (Windebank & Grisold, 2008). CIPN can negatively impact the quality of life for cancer patients and can lead to limited or halted treatment regimens (Mols et al., 2014).

Management and prevention options for CIPN are limited, as there are currently no approved preventative agents and few treatments available (Hershman et al., 2014). Accordingly, it is crucial to identify preventative interventions that can reduce the severity of CIPN and therefore improve patient outcomes by limiting the disruption of treatment regimens. As the process of developing novel pharmaceuticals to manage CIPN is expensive and lengthy, one readily implementable potential intervention for the management of CIPN may be the reduction or elimination of circadian rhythm disruption in cancer patients.

Circadian rhythms are endogenous cycles that fluctuate over a period of approximately 24 hours. These rhythms include behavioral processes (such as sleep-wake cycles) and physiological processes (such as metabolic, immune, and endocrine functions) (Golombek & Rosenstein, 2010). The nociceptive system is also regulated directly and indirectly by the circadian system (Bumgarner et al., 2021). In healthy mammals, responsiveness follows an activity-dependent circadian pattern, as responsiveness is highest in both diurnal humans and nocturnal mice during the inactive phase (Hagenauer et al., 2017; Kavaliers & Hirst, 1983). This pattern is significantly altered in states of disease (Bumgarner et al., 2023). The current leading hypothesis

explaining the circadian alterations in pain responsiveness is the phase-dependent activity of “On”, “Off”, and serotonergic raphe magnus (RM) neurons located in the rostral ventral medulla (Foo & Mason, 2003). The RM, located in the rostral ventral medulla (RVM), forms an axis with the periaqueductal gray (PAG) that together form a descending regulatory system that either can facilitate or inhibit pain signaling in the dorsal horn of the spinal cord. “On” RM neurons facilitate pain signaling, “Off” RM neurons inhibit pain signaling in the spinal cord, and serotonergic neurons suppress spinal motor withdrawals in response to pain. Additionally, there are circadian variations in the expression of μ -opioid receptors in the PAG, suggesting that the circadian regulation of nociception exists outside of the RVM (Takada et al., 2013).

Disruption of the circadian system can detrimentally affect the processes that it regulates, including pain responsiveness. Altered pain thresholds in the context of circadian disruption can be seen in the context of sleep disruption or night-shift work (Matre et al., 2017; Schuh-Hofer et al., 2013). In the known contexts of disrupted circadian rhythms, pain responsiveness is generally elevated after or during the period of circadian rhythm disruption.

A ubiquitous form of circadian rhythm disruption is exposure to artificial light at night (ALAN; 5 lux). Further, I recently demonstrated that exposure to dim light at night (ALAN; ~5 lux) heightens pain responsiveness in mice (Bumgarner et al., 2020). Accordingly, ALAN exposure may play a role in exacerbating the effects of CIPN. Eliminating exposure to ALAN during chemotherapy treatment may be a preventative method for reducing the severity of CIPN.

In this experiment, I studied the effects of ALAN exposure on the severity of CIPN. I hypothesized that ALAN exposure exacerbates the symptoms associated with CIPN via the upregulation of peripheral and central inflammation. Specifically, I predicted that ALAN would worsen the hyperalgesia and allodynia associated with CIPN. Likely, I predicted that exacerbation of pain responsiveness would result via brain stem inflammation and altered opioid sensitivity in the periaqueductal gray.

Methods

Animals and Experimental Design

Female Swiss Webster mice at ~8 weeks of age were ordered from Charles River Laboratories. Upon arrival, mice were given 1-week to acclimate to vivarium conditions (14:10 LD; lights off at 12 ZT). After the acclimation period (mid-March 2020), a global pandemic broke out, halting all non-critical research at WVU. Three months later, research was provisionally resumed at the institution. Female mice were then ovariectomized, treated subcutaneously with a single dose of meloxicam (5 mg/kg), and were given two weeks to recover before the onset of the experiment. Following gonadectomy surgeries, baseline behavioral testing was conducted. Animals were then pseudo-randomly assigned to LD/ALAN and Vehicle/Paclitaxel groups. Animals had access to food and standard chow (2018 Teklad) *ad libitum* throughout the duration of the experiment. All studies were approved by the West Virginia University Institutional Animal Care and Use Committee, and animals were maintained in accordance with NIH Animal Welfare guidelines.

Paclitaxel Injections

Based on a previously published protocol, animals were treated with 2 mg/kg daily for 5 days beginning concurrently with the onset of ALAN to induce CIPN (Costa et al., 2011). On each day of injections, paclitaxel was diluted to 0.2 mg / mL in saline. Vehicle injections comprised a combination of 0.502 mL of Kolliphor, 0.497 mL of anhydrous ethanol, and 2 mg of citric acid. The vehicle stock was also diluted in saline each day of injections. Injections were conducted between 10 – 12 *Zeitgeber Time* (ZT).

Behavior

Pain responses were tested using the electric von Frey, the cold plate, and the hot plate. Pain behavior was assessed at baseline (3 days before injection/onset of experimental housing) and for 3 additional weeks following the beginning of experimental housing. Behavioral testing at each time point occurred over two days in the following order: electric von Frey on the first day, cold- and hot-plate tests on the

second day. All behavioral testing was conducted between 04 – 08 ZT. Animals were given 30 minutes to acclimate in an adjacent room before experimental testing.

For hot and cold plate testing, animals were placed onto the plates (30-second hot plate cutoff; 60-second cold plate cutoff) while two experimenters examined the mice for nocifensive responses. Nocifensive responses included hind paw shakes/extended withdrawals, hind paw licking, jumping, or squeaking. At the first sign of nocifensive response or the cutoff limit, the animals were promptly removed from the plate and the time was recorded and noted as the withdrawal latency.

For the electric von Frey, the animals were placed in opaque plexiglass chambers on top of a wire mesh grid and were given 15 minutes to acclimate. The electric von Frey was then pressed on a repeated hind paw for each animal for a total of four times, with at least 5 minutes between individual hind paw pokes. The force required to elicit a hind paw withdrawal or nocifensive response was recorded, and the four measurements were averaged to produce a single withdrawal threshold for each animal at each time point.

qRT-PCR

At the time of tissue collection, mice were euthanized via rapid cervical dislocation and decapitation for the collection of blood and tissue for subsequent qRT-PCR experiments. The following tissue was collected: Hind paw epidermis, spinal column, and brain (RVM, PAG dissections). *Tnf*, *Il-1 β* , and *Il-6* transcript expression were examined in the RVM and PAG. *Mor* expression was also examined in the PAG.

Gene Name	Assay ID
<i>Il-6</i>	Mm00446190_m1
<i>Il-1β</i>	Mm00434228_m1
<i>Tnf</i>	Mm00443258_m1
<i>Mor</i>	Mm01188089_m1
<i>18s</i>	Hs99999901_s1

Statistics

Body mass and behavior data were analyzed using three-way ANOVA tests (time, lighting condition, and paclitaxel treatment as factors). Gene expression and IHC

data were analyzed using one-way ANOVA tests. *A priori* planned multiple comparisons were performed using Fisher's LSD test. Outliers were removed from the gene expression data using Grubb's test; no more than one outlier was removed per group. All statistical comparisons were performed using Prism 9.5.1. P-values equal to or less than 0.05 were defined as statistically significant.

Results

ALAN and Paclitaxel Repressively Exacerbate Pain Responsiveness in Mice

Main effects of lighting condition, paclitaxel treatment, time, and interactions among all factors were observed for the electric von Frey test ($p < 0.05$). Paclitaxel injections alone led to allodynic responses as early as week one in comparison to the LD-Vehicle group. A repressive combined effect of ALAN and paclitaxel treatment was observed starting at week 2 and onwards in comparison to the LD-Paclitaxel group ($p < 0.05$). ALAN exposure alone in the presence of vehicle treatment led to reduced withdrawal thresholds in comparison to the LD-Vehicle group at all time points ($p < 0.05$).

No main effects of lighting condition, treatment, or time were observed on the hot or cold plate ($p > 0.05$). *A priori* planned comparisons between individual groups led to the observation that ALAN-Vehicle mice exhibited reduced cold plate withdrawal latencies from week 2 and onwards in comparison to the LD-Vehicle group.

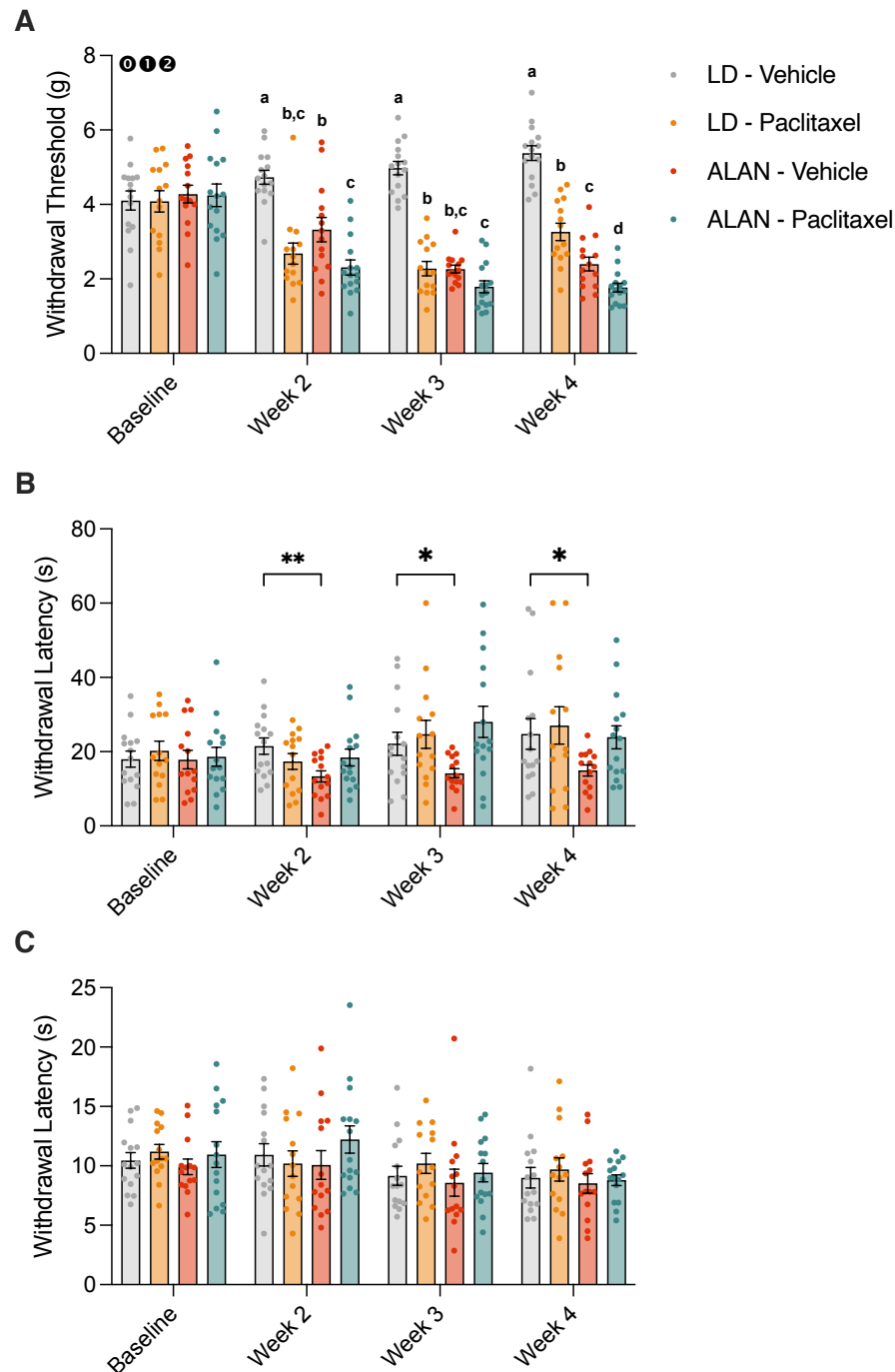


Figure 1. ALAN exposure and paclitaxel treatment have repressive effects on mechanical allodynia in female mice. Mechanical withdrawal thresholds (A), cold plate withdrawal thresholds (B), and hot plate withdrawal thresholds (C) between baseline and week 4 of the experiment. 0 – Interaction between Lighting Condition and Time; 1 – Main effect of Time; 2 – Main effect of Lighting Condition. * $p < 0.05$, ** $p < 0.01$. Bars that do not share letters are significantly different from one another. Data are represented as mean \pm 1 SEM.

ALAN and Paclitaxel Alter Inflammatory Transcript Expression in the RVM and PAG

A main effect of ALAN was observed on *Il-6* expression in the rostral ventromedial medulla (RVM) of female mice ($p > 0.05$). Planned multiple comparisons indicated that ALAN exposure and paclitaxel treatment had a synergistic effect on *Il-6* expression in ALAN-Paclitaxel mice in comparison to all other groups. No differences or main effects were observed in the RVM.

No main effects of lighting condition or treatment were observed on inflammatory or opioid transcript expression in the PAG. There was an observed reduction in PAG *Tnf* expression in all groups in comparison to the LD-Vehicle group ($p < 0.05$ in all instances).

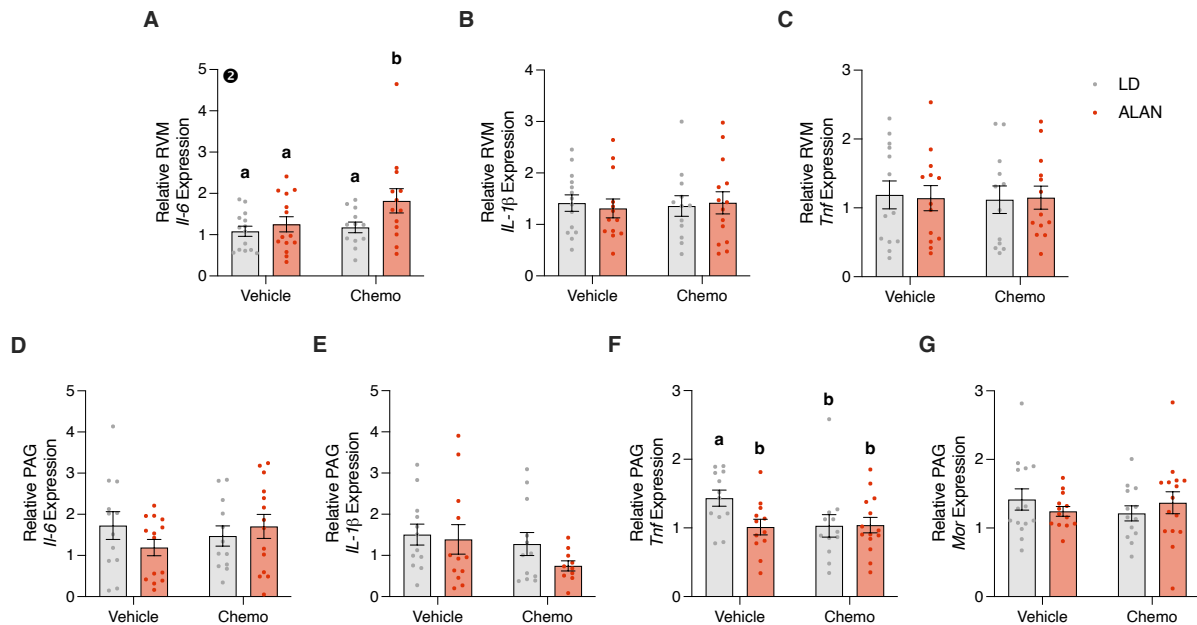


Figure 2. ALAN exposure and paclitaxel treatment alter RVM *Il-6* and PAG *Tnf* expression. RVM expression of *Il-6* (A), *Il-1β* (B), and *Tnf* (C). PAG expression of *Il-6* (D), *Il-1β* (E), and *Tnf* (F), and μ -opioid receptor (*Mor*; G). 2 – Main effect of Lighting Condition. * $p < 0.05$, ** $p < 0.01$. Bars that do not share letters are significantly different from one another. Data are represented as mean \pm 1 SEM.

ALAN and Paclitaxel Treatment Did Not Differentially Alter Body Mass

There was no effect of lighting condition or paclitaxel treatment on body mass changes throughout the experiment ($p > 0.05$). A numeric mean reduction was observed following the paclitaxel injections, but this loss in body mass rebounded following week 1 of the experiment.

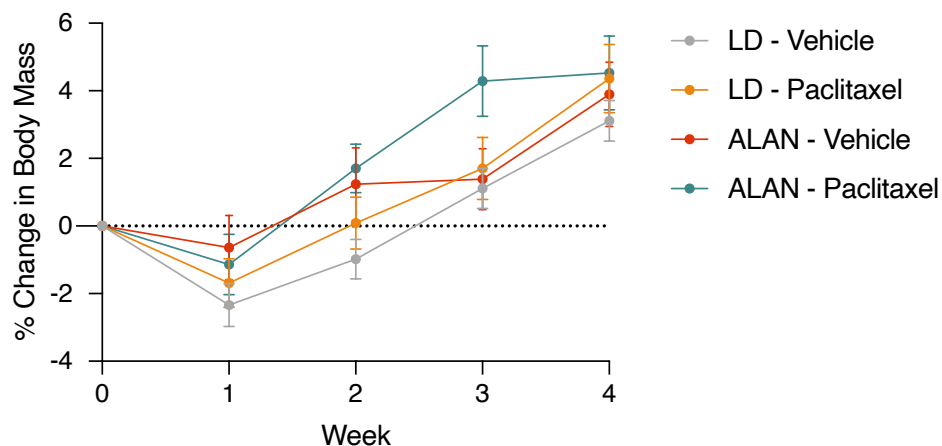


Figure 3. Body mass changes throughout the experiment. The percent change in body mass for all four groups from baseline measurements through the end of the experiment. Data are represented as mean \pm 1 SEM.

Discussion

In this experiment, I examined the combined effects of ALAN exposure and paclitaxel treatment on pain behavior and inflammatory transcript expression in the descending pain modulatory system. I observed a combined repressive effect of ALAN and paclitaxel treatment on allodynia in mice, and ALAN exposure alone was observed to reduce cold plate withdrawal thresholds. Next, a main effect of ALAN was observed on *Il-6* expression in the RVM, with the effect being driven by elevated expression in the ALAN-Paclitaxel group. Lastly, an unexpected reduction in *Tnf* expression was observed in the PAG of all groups relative to the LD-Vehicle control group.

No repressive or synergistic effects were observed on cold pain behavior, which stands in contrast to previously reported effects of ALAN on cold pain hyperalgesia. This was a surprising and uneasily explained result, given that previous reports of paclitaxel on thermal hyperalgesia report both elevations and reductions of withdrawal latencies (i.e., hyperalgesia and hypoalgesia, respectively) (Authier et al., 2000; Höke & Ray, 2014; Klein & Lehmann, 2021). It is possible that an underlying and unrecognized interaction between ALAN and paclitaxel had a specific interaction that mitigated the underlying differences in thermal responsiveness typically observed in CIPN. However, the lack of thermal hyperalgesia in the positive control (i.e., LD – Paclitaxel group) indicated that there may have been an underlying construct validity issue with the model that was implemented. This validity issue is plausible given that others have reported failures to model human hyperalgesia in rodent models of paclitaxel-induced peripheral neuropathy (Hashimoto et al., 2003).

In contrast to the unexpected thermal behavioral observations, the observed effects of ALAN and paclitaxel and their repressive interaction were consistent with previously reported effects of CIPN related to mechanical allodynia (Fumagalli et al., 2021; Bumgarner et al., 2020). These effects were aligned with the original predictions and warrant further exploratory research into this topic, either with the same or similar chemotherapeutics.

IL-6 is a widely recognized inflammatory cytokine in the context of CIPN, both with paclitaxel and other chemotherapeutic treatments (Zhou et al., 2016). Although no

identified studies explicitly examined IL-6 in the RVM following paclitaxel treatment, paclitaxel is reported to elevate serum IL-6 in humans (Pusztai et al., 2004). In contrast, peripheral IL-6 administration has been observed to abolish the thermal hyperalgesic effects of paclitaxel and other chemotherapies in rats in mice (Callizot et al., 2008). The reduction in *Tnf* among all groups relative to LD-Vehicle animals was also unexpected, but given the lack of main effects, this may be a biologically irrelevant difference. Nonetheless, IL-6 elevation may point to an underlying mechanism for our unexpected cold plate effects, but this interpretation is severely limited by a lack of mechanistic examination. As such, the observed synergistic effect of ALAN and paclitaxel in the RVM highlights a potential underlying point of interest for follow-up studies.

Follow-up studies seeking to re-examine the combined effects of ALAN and CIPN should seek to test other chemotherapies at extended time points and should strive to identify underlying mechanisms behind the effects. These results and future results contribute to the growing body of evidence that ALAN and other circadian rhythm disruptors must be considered as mitigating factors in the treatment of pain.

References

- Authier, N., Gillet, J.-P., Fialip, J., Eschalier, A., & Coudore, F. (2000). Description of a short-term Taxol®-induced nociceptive neuropathy in rats. *Brain Research*, 887(2), 239-249.
- Bumgarner, J. R., McCray, E. W., & Nelson, R. J. (2023). The disruptive relationship among circadian rhythms, pain, and opioids. *Frontiers in Neuroscience*, 17, 1109480.
- Bumgarner, J. R., Walker II, W. H., & Nelson, R. J. (2021). Circadian rhythms and pain. *Neuroscience & Biobehavioral Reviews*, 129, 296-306.
- Bumgarner, J. R., Walker, W. H., Liu, J. A., Walton, J. C., & Nelson, R. J. (2020). Dim Light at Night Exposure Induces Cold Hyperalgesia and Mechanical Allodynia in Male Mice. *Neuroscience*, 434, 111-119.
- Callizot, N., Andriambeloson, E., Glass, J., Revel, M., Ferro, P., Cirillo, R., Vitte, P.-A., & Dreano, M. (2008). Interleukin-6 protects against paclitaxel, cisplatin and

- vincristine-induced neuropathies without impairing chemotherapeutic activity. *Cancer chemotherapy and pharmacology*, 62, 995-1007.
- Costa, R., Motta, E. M., Dutra, R. C., Manjavachi, M. N., Bento, A. F., Malinsky, F. R., Pesquero, J. B., & Calixto, J. B. (2011). Anti-nociceptive effect of kinin B1 and B2 receptor antagonists on peripheral neuropathy induced by paclitaxel in mice. *British Journal of Pharmacology*, 164(2b), 681-693.
- Foo, H., & Mason, P. (2003). Brainstem modulation of pain during sleep and waking. *Sleep Medicine Reviews*, 7(2), 145-154.
- Fumagalli, G., Monza, L., Cavaletti, G., Rigolio, R., & Meregalli, C. (2021). Neuroinflammatory process involved in different preclinical models of chemotherapy-induced peripheral neuropathy. *Frontiers in Immunology*, 11, 626687.
- Golombek, D. A., & Rosenstein, R. E. (2010). Physiology of circadian entrainment. *Physiological Reviews*, 90(3), 1063-1102.
- Hagenauer, M. H., Crodelle, J. A., Piltz, S. H., Toporikova, N., Ferguson, P., & Booth, V. (2017). The modulation of pain by circadian and sleep-dependent processes: A review of the experimental evidence. In A. Layton & L. Miller (Eds.), *Women in Mathematical Biology* (pp. 1-21). Springer, Cham.
- Hashimoto, K., Sakuma, Y., Kato, Y., & Kotani, J. (2003). A rat paclitaxel model does not develop thermal hyperalgesia. *Journal of Osaka Dental University*, 37(2), 115-117.
- Hershman, D. L., Lacchetti, C., Dworkin, R. H., Lavoie Smith, E. M., Bleeker, J., Cavaletti, G., Chauhan, C., Gavin, P., Lavino, A., Lustberg, M. B., Paice, J., Schneider, B., Smith, M. L., Smith, T., Terstriep, S., Wagner-Johnston, N., Bak, K., Loprinzi, C. L., & American, S. O. C. O. (2014). Prevention and management of chemotherapy-induced peripheral neuropathy in survivors of adult cancers: American Society of Clinical Oncology clinical practice guideline. *Journal of Clinical Oncology*, 32(18), 1941-1967.
- Höke, A., & Ray, M. (2014). Rodent models of chemotherapy-induced peripheral neuropathy. *ILAR journal*, 54(3), 273-281.

- Kavaliers, M., & Hirst, M. (1983). Daily rhythms of analgesia in mice: effects of age and photoperiod. *Brain Research*, 279(1-2), 387-393.
- Klein, I., & Lehmann, H. C. (2021). Pathomechanisms of paclitaxel-induced peripheral neuropathy. *Toxics*, 9(10), 229.
- Matre, D., Knardahl, S., & Nilsen, K. B. (2017). Night-shift work is associated with increased pain perception. *Scandinavian Journal of Work, Environment & Health*, 43(3), 260-268.
- Molassiotis, A., Cheng, H. L., Lopez, V., Au, J. S. K., Chan, A., Bandla, A., Leung, K. T., Li, Y. C., Wong, K. H., Suen, L. K. P., Chan, C. W., Yorke, J., Farrell, C., & Sundar, R. (2019). Are I mis-estimating chemotherapy-induced peripheral neuropathy? Analysis of assessment methodologies from a prospective, multinational, longitudinal cohort study of patients receiving neurotoxic chemotherapy. *BMC Cancer*, 19(1), 132.
- Mols, F., Beijers, T., Vreugdenhil, G., & van de Poll-Franse, L. (2014). Chemotherapy-induced peripheral neuropathy and its association with quality of life: a systematic review. *Support Care Cancer*, 22(8), 2261-2269.
- Osmani, K., Vignes, S., Aissi, M., Wade, F., Milani, P., Lévy, B. I., & Kubis, N. (2012). Taxane-induced peripheral neuropathy has good long-term prognosis: a 1- to 13-year evaluation. *Journal of Neurology*, 259(9), 1936-1943.
- Pusztai, L., Mendoza, T. R., Reuben, J. M., Martinez, M. M., Willey, J. S., Lara, J., Syed, A., Fritsche, H. A., Bruera, E., & Booser, D. (2004). Changes in plasma levels of inflammatory cytokines in response to paclitaxel chemotherapy. *Cytokine*, 25(3), 94-102.
- Schuh-Hofer, S., Wodarski, R., Pfau, D. B., Caspani, O., Magerl, W., Kennedy, J. D., & Treede, R. D. (2013). One night of total sleep deprivation promotes a state of generalized hyperalgesia: a surrogate pain model to study the relationship of insomnia and pain. *Pain*, 154(9), 1613-1621.
- Seretny, M., Currie, G. L., Sena, E. S., Ramnarine, S., Grant, R., MacLeod, M. R., Colvin, L. A., & Fallon, M. (2014). Incidence, prevalence, and predictors of

chemotherapy-induced peripheral neuropathy: a systematic review and meta-analysis. *PAIN®*, 155(12), 2461-2470.

Takada, T., Yamashita, A., Date, A., Yanase, M., Suhara, Y., Hamada, A., Sakai, H., Ikegami, D., Iseki, M., Inada, E., & Narita, M. (2013). Changes in the circadian rhythm of mRNA expression for μ -opioid receptors in the periaqueductal gray under a neuropathic pain-like state. *Synapse*, 67(5), 216-223.

Windebank, A. J., & Grisold, W. (2008). Chemotherapy-induced neuropathy. *Journal of the Peripheral Nervous System*, 13(1), 27-46.

Zhou, Y.-Q., Liu, Z., Liu, Z.-H., Chen, S.-P., Li, M., Shahveranov, A., Ye, D.-W., & Tian, Y.-K. (2016). Interleukin-6: an emerging regulator of pathological pain. *Journal of Neuroinflammation*, 13(1), 1-9.

Chapter 5

Investigating the Mechanisms of Disrupted Pain Behavior Induced by Exposure to Artificial Light at Night

Introduction

The three previous chapters demonstrated the detrimental effects of artificial light at night (ALAN) exposure on rodent pain behavior in both typical and atypical health contexts. ALAN exposure reduced cold plate withdrawal latencies, i.e., *cold hyperalgesia* in healthy and diabetic male mice (Chapters 1 and 2)(Bumgarner et al., 2020; Bumgarner et al., 2023b). ALAN exposure also exacerbated mechanical allodynia in female mice treated with paclitaxel as well as exacerbated cold plate withdrawal latencies in female mice treated with control vehicle injections (Chapter 3).

Additional preliminary transcript analysis from these chapters also provided insight into the potential underlying mechanisms responsible for the effects of ALAN on pain behavior. First, ALAN exposure led to *Il-6* transcript upregulation in both the rostral ventromedial medulla (RVM) of female mice and the whole medulla of male mice (Chapters 1 and 3)(Bumgarner et al., 2020), implicating neuroinflammation and immune activation as possible underlying modes of pain behavior alteration. Next, ALAN exposure led to upregulated μ -opioid receptor (*Mor*) expression in the periaqueductal gray of male mice (Chapter 1)(Bumgarner et al., 2020), indicating an underlying disrupted function of the endogenous opioid system. These data and additional insights gained from concurrent studies in our lab at the time generated three hypotheses to address the underlying mechanisms of the observed effects.

Beyond the preliminary evidence generated in this body of work, ample evidence points to the central and peripheral inflammatory effects of ALAN exposure (Walker et al., 2021). Central and peripheral immune cells exhibit circadian rhythms both via intrinsic clock gene feedback loops and peripheral synchronizing rhythms, such as humoral cues (Scheiermann et al., 2013). These rhythms regulate the expression of cytokine transcription across the 24-hour day (Sato et al., 2014; Sugimoto et al., 2014). Disruption of clock gene loops by circadian rhythm disruption can heighten immune activation and

stimulate the production of pro-inflammatory cytokines (Vieira et al., 2020). This evidence and the supporting evidence from the previous chapters lead to **Hypothesis One** of this chapter: Exposure to artificial light at night alters pain behavior in mice by inducing immune cell activation in the rostral ventromedial medulla of mice.

The function of the endogenous opioid system is also regulated by circadian rhythms (Bumgarner et al., 2023a; Bumgarner et al., 2021; Knezevic et al., 2022). Endogenous opioids and their ligands exhibit rhythmic expression in the nervous system and periphery across the day. For example, *Mor* expression levels vary across the day in the periaqueductal gray of male mice (Takada et al., 2013). Opioid binding efficacy also varies across the day (Knezevic et al., 2022). This variation can be associated with daily variations in opioid efficacy and patient requests for opioid administration in the clinic (Junker & Wirz, 2010). Beyond this, the circadian system and opioid system form a feedback loop, where disruption of one system can disrupt the function of the other. The observed altered *Mor* expression in the PAG and the intertwined relationship between the circadian and opioid systems lead to **Hypothesis Two** of this chapter: Exposure to artificial light at night alters pain behavior in mice by impairing the function of the endogenous opioid system.

Finally, given the translational implications of the effects of ALAN on pain behavior, there is a need to understand minimally invasive solutions to the effects of ALAN. The central clock of the circadian system in mammals is the suprachiasmatic nucleus of the hypothalamus (SCN). The SCN aligns and coordinates the internal circadian rhythms of the body as well as synchronizes internal circadian rhythms with the external environment. The primary cells responsible for relaying environmental photic cues to the SCN are known as intrinsically photosensitive retinal ganglion cells (ipRGCs) of the retina. These cells express melanopsin, a photosensitive pigment with peak sensitivity to short-wavelength light (~480 nm, blue). Activation of ipRGCs by blue light leads to direct stimulation and entrainment of the SCN via ipRGC projections along the retinohypothalamic tract.

The importance of blue light for SCN and circadian entrainment is a natural cause to investigate the contribution of short-wavelength light to the detrimental effects of ALAN

on pain behavior. Previously published work demonstrated that filtering the blue light from ALAN sources can ameliorate the otherwise detrimental effects of ALAN on metabolic dysfunction in mice (Nagai et al., 2019). Unpublished work from our lab also demonstrated that ‘blue cut’ ALAN has blunted effects on cerebral infarct volume in a mouse model of stroke in comparison to a wider spectrum of white ALAN (Liu et al., 2022, Unpublished). It is worth highlighting the distinction between blue-cut ALAN vs. long-wavelength ALAN in these experiments. A human-based approach to mitigating the effects of ALAN might be only using long-wavelength red light for nighttime lighting. However, mice lack cones with peak sensitivity to long-wavelength (red) light. Red light can stimulate photoreception in the mouse but at 12 times less sensitivity in comparison to humans (Peirson et al., 2018). Exposing mice to red light to model human ALAN exposure presents a fundamental issue of construct validity. Hence, filtering short-wavelength light from ALAN sources provides a translational model with improved construct validity. The importance of blue light to circadian rhythm entrainment and previous evidence supporting the ameliorative effects of filtering blue light from ALAN sources lead to **Hypothesis Three** of this chapter: The effects of ALAN on pain behavior in mice are dependent on short wavelength light.

Three separate experiments were conducted to address the three outlined hypotheses. These experiments were designed to provide collective insight into the potential underlying mechanisms by which ALAN exposure alters pain behavior in mice. Each presented hypothesis was tested separately using both female and male mice exposed to ALAN for up to four weeks.

Methods

Animals and Lighting

Adult female and male Swiss Webster mice (strain code 024; Charles River Laboratories) were obtained at 7-8 weeks of age and given 1 week to acclimate to standard vivarium conditions (14:10 h light: dark, lights off at ZT12; 150±25:0 lux, 22±2 °C). Following arrival, mice were housed in groups of five per cage. After the acclimation period, mice were singly housed, and the experiment began. Reverse osmosis water and

food were provided *ad libitum* throughout the duration of the experiment. Mice in Experiments 1 and 2 were housed in the university vivarium in static cages (30 X 18 X 14 cm polycarbonate cages). Mice in Experiment 3 were housed in our lab satellite facility in light-controlled, ventilated racks (30.5 x 16.5 x 14.0 cm polycarbonate cages; Lab Products). ALAN sources were Luma5 Standard LED light strips (1.5 W/ft, 5000K “cool white”, 1200 lumens; Hitlights Inc.); lux calibrations were conducted by placing a Mavolux 5023C illuminance meter (Gossen) in the center of an empty cage with the light sensor facing towards the ceiling. All studies were approved by the West Virginia University Institutional Animal Care and Use Committee, and animals were maintained in accordance with NIH Animal Welfare guidelines.

Experiment 1 - Examining Microglial Activation in the RVM and PAG Following ALAN Exposure

Mice were exposed to either control light-dark (LD) or ALAN conditions for one week ($n = 15$). Body mass and daily food consumption (active and inactive phases) were recorded weekly. Food consumption was measured between ZT 11 – 12 for the inactive phase and ZT 02 – 03 for the active phase. A subset of animals ($n = 6$) was selected to examine microglial morphology via IBA1 staining in the RVM and PAG at the end of the experiment.

Experiment 2 – Examining the Effects of ALAN Exposure on Morphine Analgesia in Mice

Female and male mice ($n = 11 - 15$) were exposed to ALAN for either four or 28 nights. Baseline cold plate withdrawal thresholds were determined for all mice, and animals were pseudo-randomly assigned to LD or ALAN conditions and morphine or saline injections. Starting at ZT 06 on the day of behavioral testing (either 4 or 28 nights after the onset of experimental housing), animals were injected i.p. with either 6 mg/kg morphine sulfate diluted in saline (07-892-4699; Patterson Vet) (Ruiz-Medina et al., 2011) or 0.1 mL/kg of saline. 30 minutes following the injections, animals were placed on the cold plate, and cold plate withdrawal latencies and the total number of nocifensive

responses were recorded (see *Behavioral Testing* methods). Behavioral testing was concluded by ZT 08 on each day.

Experiment 3 – Examining the Contribution of Short Wavelength Light to the Effects of ALAN on Pain Behavior in Mice

Female and male mice ($n = 15$) were exposed to either LD or ALAN conditions for four weeks in our satellite SunCalc chambers (see *Animals and Lighting* methods). Custom light strips were constructed and used to hold either Luma5 Standard LED strips or Luma5 Standard LED enclosed in short wavelength filter sheets (821 Zircon UV Blue Blocker; Lee Filters), and sub 505nm filtering was confirmed using an Ophir Starbright irradiance meter (Jerusalem, Israel). Body mass measurements and von Frey testing were conducted weekly between ZT 05-08. Cold plate testing was only conducted at baseline and week 4 to avoid sensitization. Von Frey testing was conducted before cold plate testing at the baseline and 4-week time points.

Immunohistochemistry

Animals were euthanized via lethal overdose of sodium pentobarbital between ZT 06 – 08 in the light phase. Six animals per group were pseudo-randomly selected for microglial morphology examination in the PAG and RVM. Following pentobarbital euthanasia, the selected animals were perfused transcardially with 0.1 M PBS and 4% paraformaldehyde (PFA) in 0.1 M PBS. Brains were then dissected and post-fixed overnight in 4% PFA solution at 4 °C. Brains were then cryoprotected in (cryoprotectant solution: 30% sucrose in 0.2 M phosphate buffer) for 48 hours before being sectioned at 40 μ m at -20 °C (Thermo Scientific). RVM sections were collected between Bregma -6.45 through -4.83. PAG sections were collected following the RVM sections through Bregma -2.91. Sections containing the RVM and PAG were placed into cryoprotectant solution and frozen at -20 °C before further image processing.

Free-floating sections were rinsed 3x in 1X TBS for five minutes, incubated in 0.05 M sodium citrate in 1X TBS for 30 min for antigen retrieval, and rinsed 3x in 1X TBS for five minutes. Sections were then incubated in 0.1 M glycine in 1X TBS for 30 minutes

followed by another 3 x 5-minute series of 1X TBS washes. Sections were incubated in a concentrated blocking solution (1X TBS with 20% normal goat serum (NGS), 0.3% Triton-X, and 1% Hydrogen Peroxide) for 30 minutes before being incubated overnight in primary antibody (goat anti-rabbit IgG, 1:5000; Vector Laboratories).

On the following morning, sections were rinsed in a dilute blocking solution (1X TBS with 1% NGS and 0.02% Triton-X) for 3 x 10-minute washes. Sections were then incubated in the biotinylated secondary antibody (goat anti-rabbit IgG, 1:500; Vector Laboratories) for 1 hour at room temperature. Tissue was rinsed in 1X TBS with 0.2% Triton-X for 3 x 10-minute washes. Immunostaining was then amplified using the streptavidin/HRP technique (Vectastain ABC kit; Vector Laboratories), rinsed for 3 x 15-minute 1X TBS washes, and then incubated in diaminobenzidine (DAB; Vector Laboratories). Sections were mounted on slides and coverslipped with Permount (Fisher Scientific).

Imaging and Image Quantification

Slides were scanned in brightfield using MIF Olympus VS120 Slide Scanner at 10X (3.45 μm x 3.45 μm pixel size). The RVM and PAG were then manually segmented with region guidance from the Allen Institute p56 Mouse Brain Atlas. Segmented regions were using a custom script implemented with the Napari viewer (0.4.17). Images were first converted to 8-bit grayscale, masked, and cropped using the manual segmentation polygon. Two features were extracted from the data. First, nuclei were segmented by filtering thresholding the masked image with the Yen filter, applying with a median filter (radius 4 px) followed by a background removal with a top-hat filter (radius 30 px), and counting the objects with an area greater than 35 pixels. The density of nuclei per mm^2 of tissue was calculated by dividing the number of segmented nuclei from the Next, the percent area fraction of the microglia was determined by applying a triangle threshold, re-connecting processes (via binary opening, dilation, and then erosion), and then summing the area of all objects with an area greater than 20 pixels. The percent area fraction of microglia was then calculated by dividing the summed area by the area of the manual

segmentation mask. All image processing operations were applied using scikit-image (0.19.3). Python 3.8.8 was used for the image analyses.

Behavioral Testing

Cold plate testing (IITC Life Science Inc) was performed at 0.5 ± 1.0 C°. Mice were gently placed onto the cold plate, and a stopwatch was started as soon as their hind paws touched the plate. Two observers watched for any sign of nocifensive response, which included hind paw shakes/extended withdrawals/licking, jumping, or squeaking. Behavioral testing was recorded in both experiments. In Experiment 2, as soon as the first nocifensive response was observed, the latency to response was recorded; the total number of nocifensive responses was counted and recorded across the testing session. In Experiment 3, as soon as the first nocifensive response was observed, the latency to response was recorded and the animal was promptly removed from the plate. Animals were removed from the place after a cutoff of either 60 seconds (Experiment 3) or 90 seconds (Experiment 2).

Electric von Frey testing was performed on a wire mesh grid in opaque plexiglass chambers (Bioseb). Animals were given 15 minutes to acclimate to the chambers, and then four mechanical withdrawal threshold measurements were taken by pressing the electric von Frey on the plantar surface of a consistent hind paw until a response was observed. Responses included withdrawal or licking of the hind paw, jumping, or squeaking. An inter-stimulus interval of at least 2 minutes was applied to avoid sensitization. The four measurements per animal were averaged to produce a single withdrawal threshold per animal at each time point.

Animals were given at least 30 minutes to acclimate to the adjacent behavioral testing suite before the onset of testing.

Statistics

In Experiment 1 body mass data were analyzed using unpaired t-tests, and IBA1 results were analyzed with 2-way ANOVAs. In Experiment 2, body mass changes were analyzed with repeated measures 2-way ANOVAs (4 nights) and repeated measures 3-

way ANOVAs (28 nights). A maximum of one outlier per group was removed from the behavioral data of Experiment 2 using Grubb's test. Behavioral data in Experiment 1 were analyzed with repeated measures 3-way ANOVAs (withdrawal latencies) and 2-way ANOVAs (total responses). In Experiment 3, body mass and behavioral data were analyzed using repeated measures 2-way ANOVAs. *A priori* planned multiple comparisons were conducted using t-tests (food consumption, Experiment 1) or Fisher's LSD. Data were analyzed using Prism 9.5.1. P-values less than 0.05 were defined as statistically significant.

Results

Experiment 1 – ALAN Does Not Alter Microglia Morphology or Density in the RVM or PAG of Mice

ALAN exposure for one week led to a significant percent change in body mass in both male and female mice ($p < 0.05$; Figure 1B, D; unpaired *t*-test). The effect of ALAN on body mass directly coincided with an alteration in the timing of food consumption. Female and male mice exposed to ALAN for one week ate more food during their inactive phase in comparison to LD animals and their baseline measurements ($p < 0.05$; Figure 1A, C). There were main effects of both time and lighting condition as well as an interaction of main effects on food consumption in both male and female mice ($p < 0.05$; 2-way ANOVA). There was no difference in the total food consumed between lighting conditions in either sex ($p > 0.05$ in both cases).

Following one week of ALAN exposure, animals were euthanized, and brains were collected to analyze microglial morphology in the RVM and PAG based on the supporting evidence indicating disrupted immune and cellular function in the descending pain modulatory system. Microglial activation and density were assessed via IBA1 staining. RVM and PAG regions of interest were manually segmented using the Allen Institute p56 mouse brain atlas. Microglial cell density and percent area fraction of IBA1 were analyzed using two separate and fine-tuned image processing algorithms (Figure 2E). ALAN exposure did not alter microglial cell density (Figure 2A, C) or the percent area fraction of IBA1 staining (Figure 2B, D) in either the RVM or PAG of female or male mice.

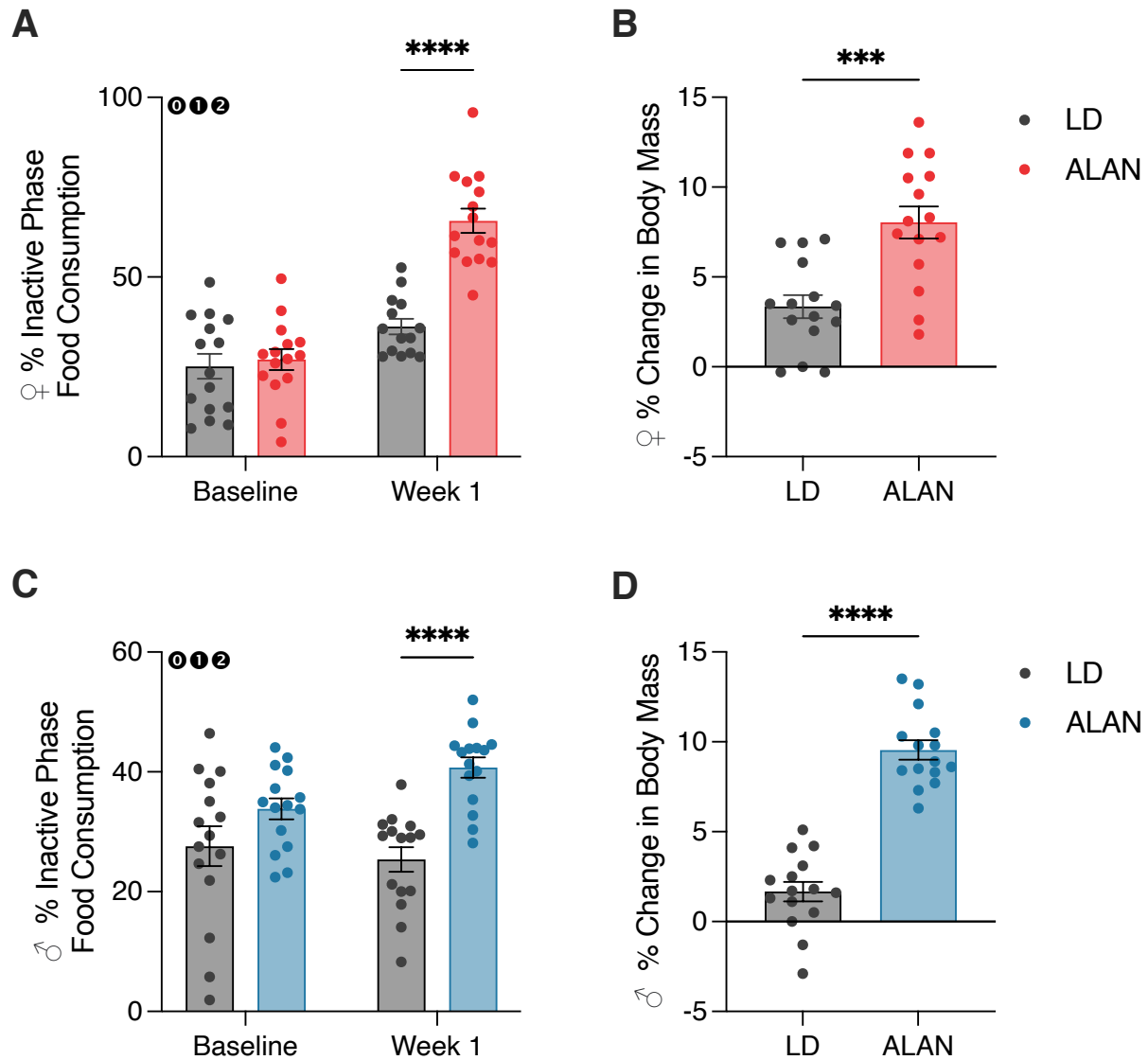


Figure 1. One week of ALAN exposure increases body mass and shifts the timing of food intake to the inactive phase in female and male mice. The percent of inactive phase food consumption in female (A) and male (C) mice. The percent change in body mass after one week of ALAN exposure in female (B) and male (D) mice. All data are represented as mean \pm SEM. 0 – Interaction between Lighting Condition and Time; 1 – Main effect of Time; 2 – Main effect of Lighting Condition. *** $p < 0.001$, **** $p < 0.0001$.

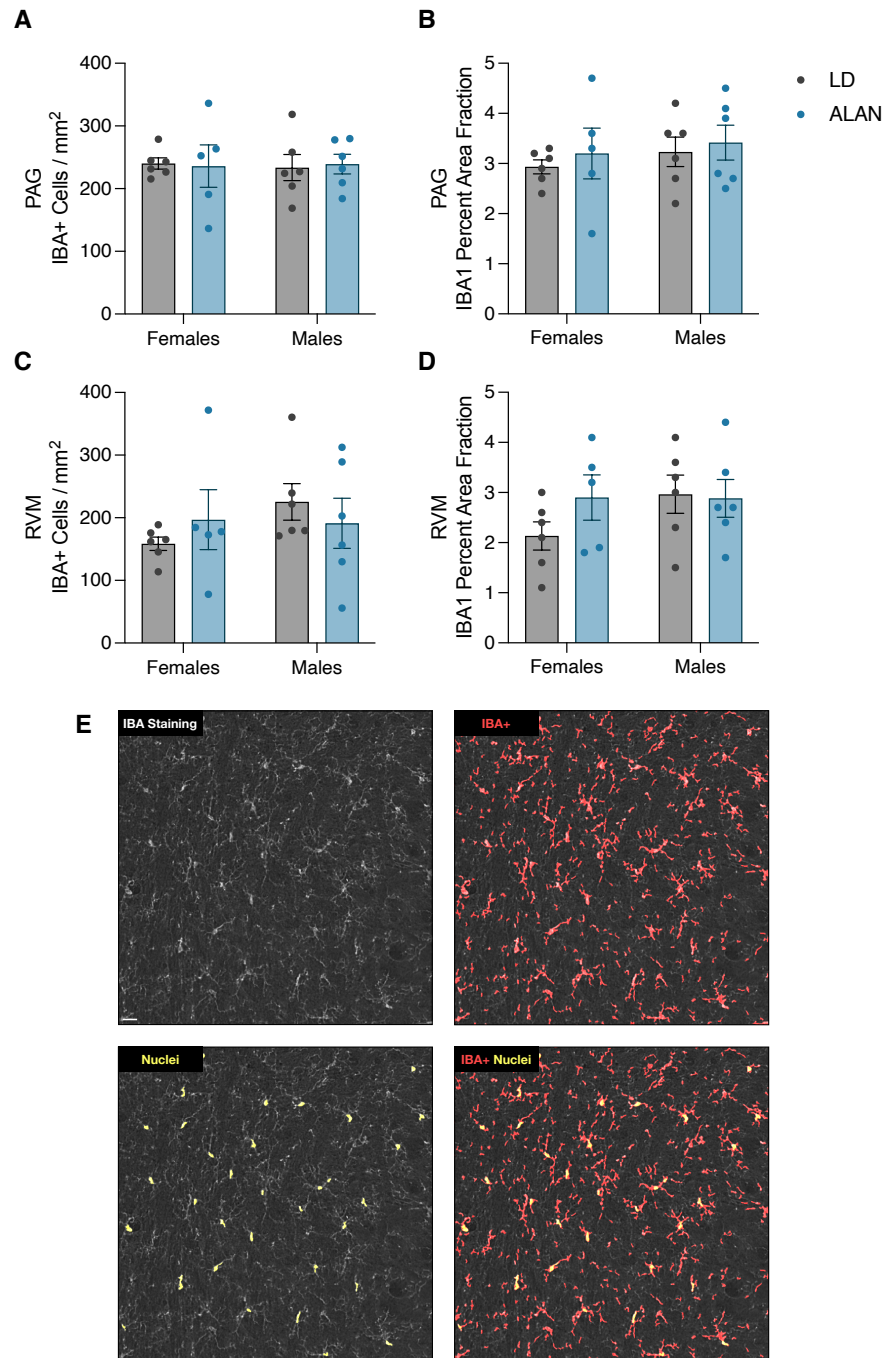


Figure 2. ALAN exposure does not alter microglial cell density or IBA1 percent area fraction in the PAG or RVM of mice. The density of microglia in the PAG (A) and the RVM (C), as determined by nucleus segmentation. The percent area fraction of IBA1 staining in the PAG (B) and the RVM (D). An example visualization of microglia nucleus and IBA1+ segmentation in the PAG of a male LD animal (E). The scale bar in the first panel of E represents 99.33 μm . All data are represented as mean \pm SEM.

Experiment 2 – ALAN Exposure Does Not Alter Morphine-Induced Analgesia in Mice

To test the hypothesis that ALAN alters the function of the endogenous opioid system, female and male mice were exposed to ALAN for both 4 and 28 nights, time points that corresponded to the original ALAN and pain behavior experiment (Chapter 1) (Bumgarner et al., 2020). At the end of each time point, the animals were treated with either saline or morphine injections.

There was a main effect of lighting condition on body mass in both sexes in the 4-night experiment ($p < 0.05$ in both instances; Figure 3A, B). In the 4-night experiment, both the saline and morphine ALAN male groups gained significantly more mass compared to the male LD counterparts ($p < 0.05$; Figure 3B). Only the saline ALAN female mice were significantly different from the LD saline group in the 4-night experiment ($p < 0.05$; Figure 3A).

There were main effects of lighting condition and treatment as well as an interaction of the effects for both sexes on body mass in the 28-night experiment ($p < 0.05$ in all instances; Figure 4A, B). In the 4-night experiment, morphine injections significantly increased withdrawal latencies and the total number of nocifensive responses across the 90-second cold plate testing window in both female and male mice, regardless of lighting condition (main effect of treatment, $p < 0.05$ in all instances; Figure 5A – D). No main effect of lighting condition was observed on withdrawal latencies in either sex ($p > 0.05$), but there was a significant reduction in cold plate withdrawal latencies between the LD and ALAN saline-treated male mice ($p < 0.05$; Figure 5B). Further, there was a main effect of lighting condition on the total number of nocifensive responses in male mice ($p < 0.05$). Male ALAN – Saline mice also exhibited elevated total nocifensive responses across the 90-second behavioral test in comparison to the Male LD – Saline mice ($p < 0.01$; Figure 5D).

In the 28-night experiment, there was a main effect of treatment on total nocifensive responses in both sexes and withdrawal latency in female mice ($p < 0.05$ in all instances; Figure 6A, C, D). There was a main effect of lighting condition on the withdrawal latency in male mice ($p < 0.01$), but there was no effect of treatment on withdrawal latency in male mice ($p > 0.05$; Figure 6B). No effects of lighting condition

were observed on total nocifensive responses in female or male mice ($p > 0.05$ in both instances; Figure 6C, D).

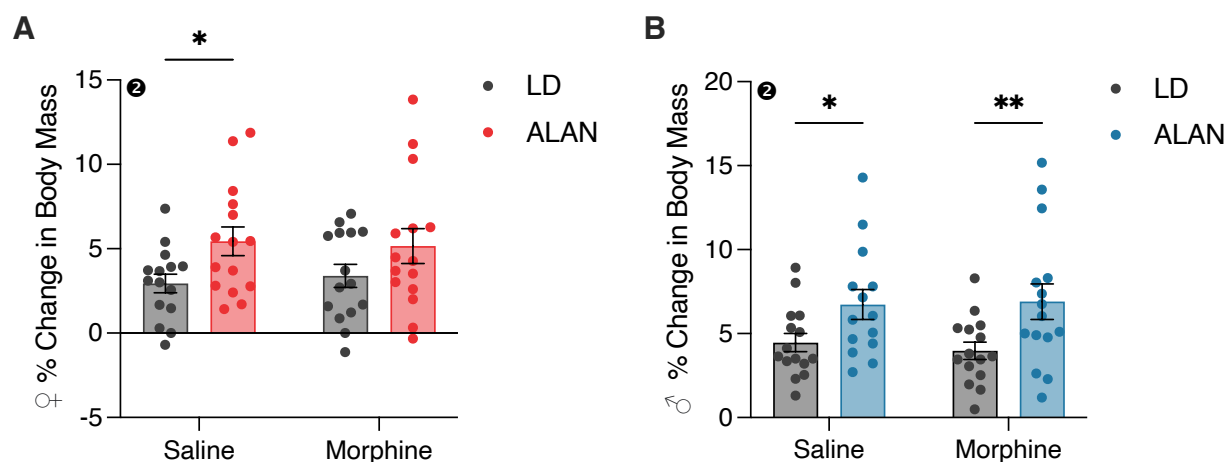


Figure 3. Four nights of ALAN exposure increases body mass in mice. The percent change in body mass after four nights of ALAN exposure in female (A) and male (B) mice. All data are represented as mean \pm SEM. 2 – Main effect of Lighting Condition. * $p < 0.05$, ** $p < 0.01$.

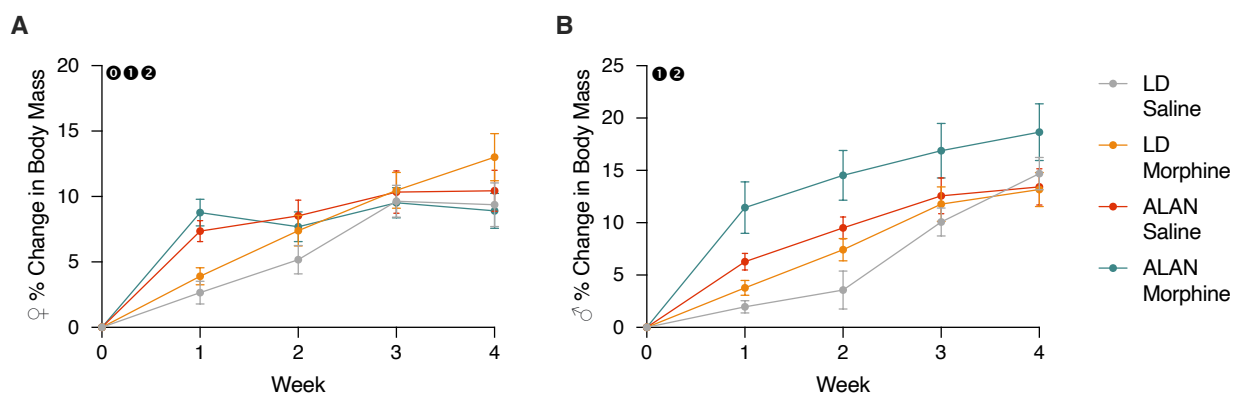


Figure 4. 28 nights of ALAN exposure increases body mass in mice. The percent change in body mass after 28 nights of ALAN exposure in female (A) and male (B) mice. All data are represented as mean \pm SEM. 0 – Interaction between Lighting Condition and Time; 1 – Main effect of Time; 2 – Main effect of Lighting Condition.

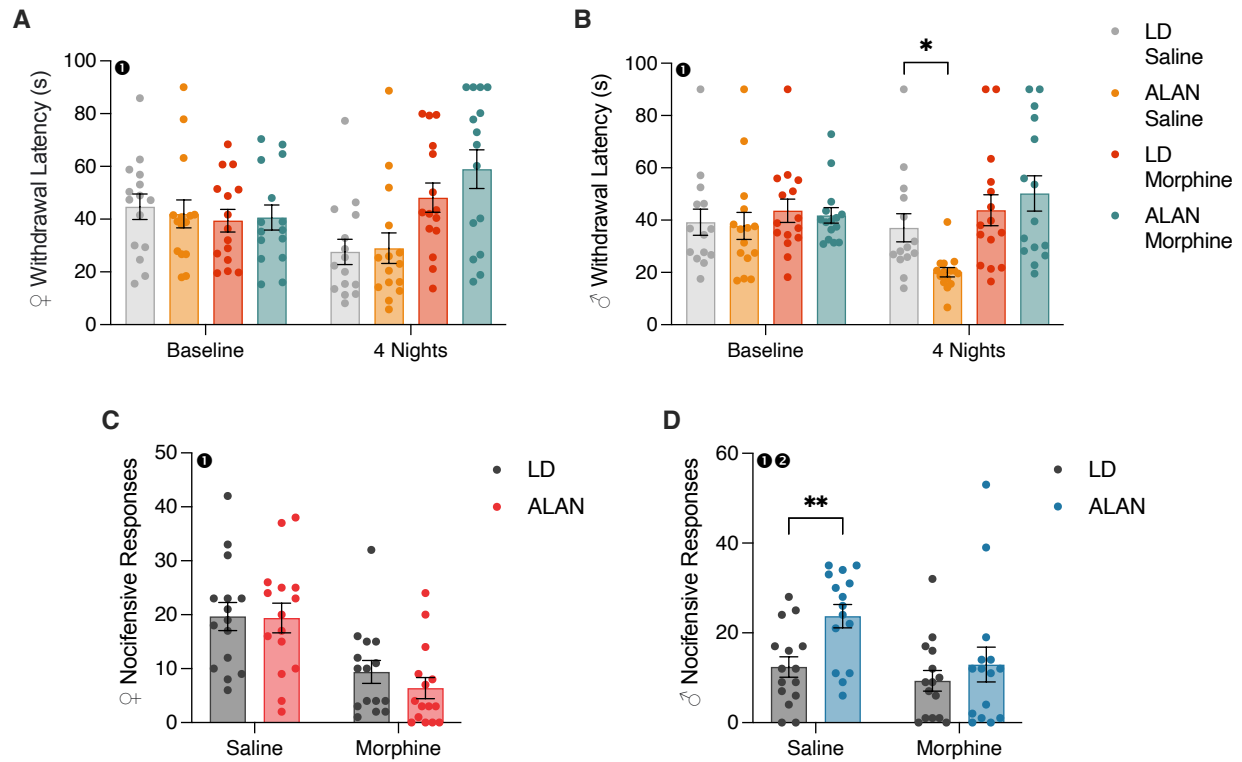


Figure 5. Four nights of ALAN exposure does not alter morphine-induced analgesia in mice. Cold plate withdrawal latencies in female (A) and male (B) mice. The total number of nocifensive responses across the 90-second testing window in female (C) and male (D) mice. All data are represented as mean \pm SEM. Cold plate withdrawal latencies 1 – Main effect of Treatment; 2 – Main effect of Lighting Condition. * $p < 0.05$, ** $p < 0.01$.

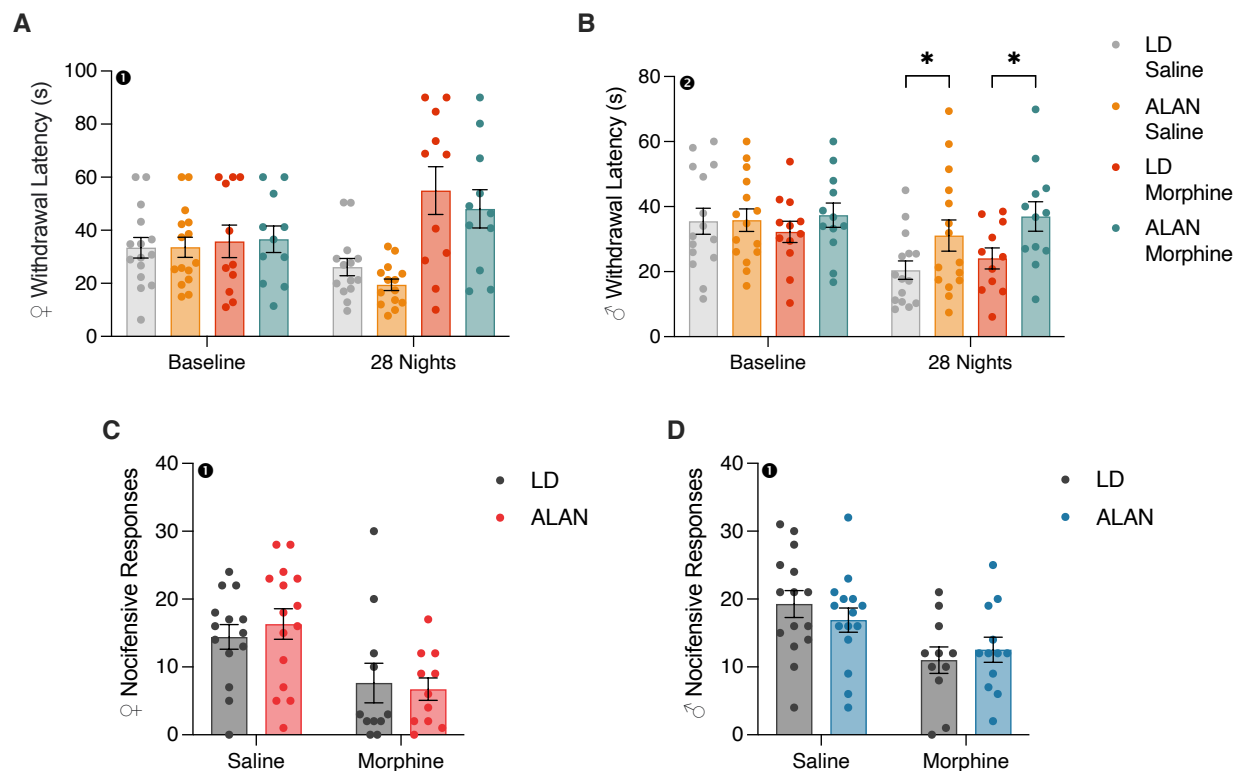


Figure 6. 28 nights of ALAN exposure does not alter morphine-induced analgesia in mice. Cold plate withdrawal latencies in female (A) and male (B) mice. The total number of nocifensive responses across the 90-second testing window in female (C) and male (D) mice. All data are represented as mean \pm SEM. Cold plate withdrawal latencies 1 – Main effect of Treatment; 2 – Main effect of Lighting Condition. * $p < 0.05$.

Experiment 3– ALAN and bcLAN Did Not Alter Body Mass or Pain Behavior in Mice Housed in SunCalc Chambers

To test the hypothesis that short-wavelength light is essential for the detrimental effects of ALAN on pain behavior in mice, mice were exposed to LD, ALAN, or blue cut ALAN (bcLAN) conditions for four weeks. There was a main effect of time on body mass in both sexes ($p < 0.0001$ in both instances); there was no main effect of lighting condition on body mass in either sex ($p > 0.05$ in both instances; Figure 7A, B).

There was no effect of lighting condition on mechanical withdrawal thresholds in either sex ($p > 0.05$ in both instances), but withdrawal thresholds did decrease over the experiment in both sexes with main effects of time ($p < 0.001$ in both instances; Figure 7C, D). There was no effect of time or lighting condition on cold plate withdrawal latencies in either sex ($p > 0.05$ in all instances; Figure 7E, F).

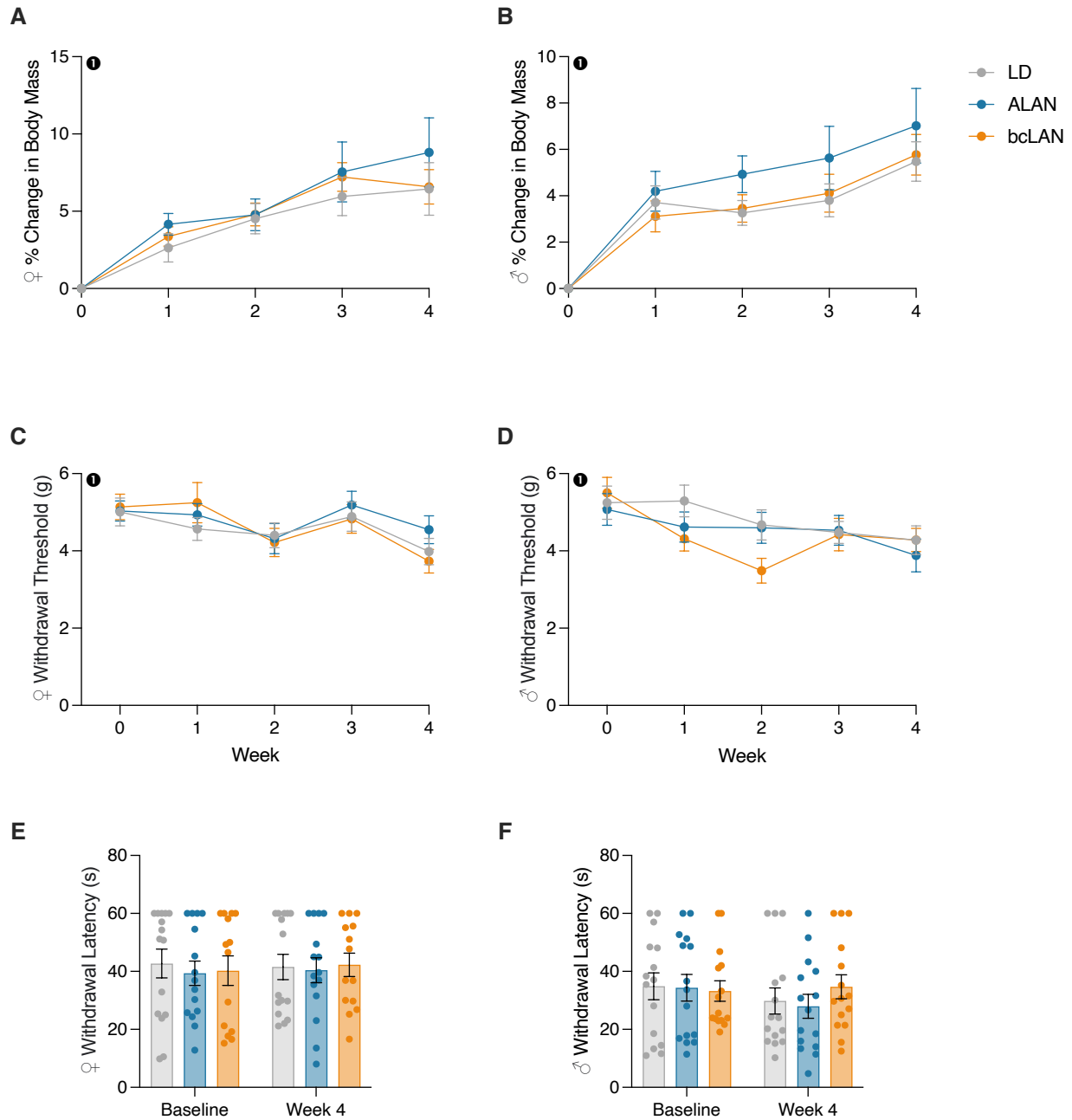


Figure 6. Blue-cut ALAN (bcLAN) and ALAN did not alter body mass or pain behavior in SunCalc chambers. The percent change in body mass in female (A) and male (B) mice. Mechanical withdrawal thresholds in female (C) and male (D) mice. Cold plate withdrawal latencies in female (E) and male (F) mice. All data are represented as mean \pm SEM. 1 – Main effect of Time.

Discussion

Three hypotheses on the mechanisms underlying the effects of ALAN on pain behavior in mice were proposed. These hypotheses stated that: 1. Microglial activation in the descending pain modulatory system facilitates the disrupted pain behavior induced by ALAN exposure; 2. ALAN impairs the function of the endogenous opioid system; and 3. The short wavelength spectrum of ALAN is necessary to disrupt pain behavior. None of these hypotheses could be rejected based on the data presented in this chapter.

ALAN exposure in Experiments 1 and 2 increased body mass in both female and male mice, which is consistent with over a decade of previously reported effects in both humans and non-human species (Rybnikova et al., 2016). In contrast, in Experiment 3, exposure to ALAN or bcLAN did not alter body mass in either female or male mice housed in SunCalc ventilated chambers located in our satellite vivarium. This lack of effect indicates that there was a serious issue with the underlying validity of Experiment 3. A natural hypothesis for the cause of this issue is that the effects of ALAN on pain behavior were masked by some consequence of the SunCalc housing chambers. Differences in behavioral tests have been reported within the same species of mice when housed on static racks vs. ventilated racks (Åhlgren & Voikar, 2019). This may be due to the stressful nature of high airflow turnover for rodents or hypothermia from ventilated chambers if they are not regulated appropriately (Davidson et al., 2005; Baumans et al., 2002; Neigh et al., 2005). A unique and alternative hypothesis can also be proposed: exposure to canine scent masked the behavioral consequences ALAN in this experiment. This hypothesis may be elaborated upon further by contacting the author of this dissertation.

The underlying rationale for the failure to reject the first and second hypotheses of this chapter is less intriguing. Indeed, both experiments appeared to have face validity, given the replication of previously observed effects of ALAN on body mass in mice (Bumgarner & Nelson, 2021). It is possible that the previously observed inflammation in the RVM (Chapters 1 and 3) led to acute microglial, but not persistent microglial activation. Instead, the neuroinflammation may be directly altering the function of neurons in these regions (Mottahedin et al., 2017), with the inflammatory cytokines originating from the periphery. This is plausible, given that ALAN can induce peripheral inflammation (Walker

et al., 2021). Lastly, it is possible that the two-dimensional IBA1 analysis in this experiment did not provide the granularity needed to observe microglial activation or morphological alterations following ALAN.

The failure to reject the hypothesis of Experiment 3 may be related to the route of morphine administration (Turner et al., 2011), the dose used, or the timing of behavioral testing following administration. It is possible that one or multiple of these effects masked potential underlying differences in disrupted endogenous opioid signaling induced by ALAN.

There are numerous insights to be gained from the data presented in this chapter. Despite the unglamorous nature of null results, a cascading set of alternative hypotheses and experiments can now be generated to further elucidate the underlying mechanisms by which ALAN induces pain behavior in mice (Platt, 1964). These hypotheses may indeed be null, indicating that future efforts should be directed along different lines of reasoning. Alternatively, there are nuanced aspects of the experiments that can be manipulated to re-test these hypotheses (i.e., dosage, timing, housing environment). I propose that future work should continue to examine the contributions of central and peripheral inflammation, opioid signaling, and light spectrums to the effects of ALAN on pain. These mechanisms may provide greater insight into how to mitigate the detrimental effects of ALAN on human and environmental health.

References

- Åhlgren, J., & Voikar, V. (2019). Housing mice in the individually ventilated or open cages—Does it matter for behavioral phenotype. *Genes, Brain and Behavior*, 18(7), e12564.
- Baumans, V., Schlingmann, F., Vonck, M., & van Lith, H. A. (2002). Individually ventilated cages: beneficial for mice and men. *Journal of the American Association for Laboratory Animal Science*, 41(1), 13-19.
- Bumgarner, J. R., McCray, E. W., & Nelson, R. J. (2023a). The disruptive relationship among circadian rhythms, pain, and opioids. *Frontiers in Neuroscience*, 17, 1109480.
- Bumgarner, J. R., & Nelson, R. J. (2021). Light at Night and Disrupted Circadian Rhythms Alter Physiology and Behavior. *Integrative and Comparative Biology*, icab017.
- Bumgarner, J. R., Walker II, W. H., & Nelson, R. J. (2021). Circadian rhythms and pain. *Neuroscience & Biobehavioral Reviews*, 129, 296-306.
- Bumgarner, J. R., White, R. C., Brown, J. A., & Nelson, R. J. (2023b). Artificial Light at Night Exacerbates Cold Neuropathy in a Mouse Model of Type II Diabetes Mellitus. *Frontiers in Neuroscience*, (Under Review).
- Bumgarner, J. R., Walker, W. H., Liu, J. A., Walton, J. C., & Nelson, R. J. (2020). Dim Light at Night Exposure Induces Cold Hyperalgesia and Mechanical Allodynia in Male Mice. *Neuroscience*, 434, 111-119.
- Davidson, A. J., London, B., Block, G. D., & Menaker, M. (2005). Cardiovascular tissues contain independent circadian clocks. *Clinical and Experimental Hypertension*, 27(2-3), 307-311.
- Junker, U., & Wirz, S. (2010). Chronobiology: influence of circadian rhythms on the therapy of severe pain. *Journal of Oncology Pharmacy Practice*, 16(2), 81-87.
- Knezevic, N. N., Nader, A., Pirvulescu, I., Pynadath, A., Rahavard, B. B., & Candido, K. D. (2022). Circadian pain patterns in human pain conditions—A systematic review. *Pain Practice*, 23(1), 94-109.
- Mottahedin, A., Ardalan, M., Chumak, T., Riebe, I., Ek, J., & Mallard, C. (2017). Effect of neuroinflammation on synaptic organization and function in the developing brain:

- implications for neurodevelopmental and neurodegenerative disorders. *Frontiers in Cellular Neuroscience*, 11, 190.
- Nagai, N., Ayaki, M., Yanagawa, T., Hattori, A., Negishi, K., Mori, T., Nakamura, T. J., & Tsubota, K. (2019). Suppression of Blue Light at Night Ameliorates Metabolic Abnormalities by Controlling Circadian Rhythms. *Investigative Ophthalmology & Visual Science*, 60(12), 3786-3793.
- Neigh, G. N., Bowers, S. L., Korman, B., & Nelson, R. J. (2005). Housing environment alters delayed-type hypersensitivity and corticosterone concentrations of individually housed male C57BL/6 mice. *Animal Welfare*, 14(3), 249-257.
- Peirson, S. N., Brown, L. A., Pothecary, C. A., Benson, L. A., & Fisk, A. S. (2018). Light and the laboratory mouse. *Journal of Neuroscience Methods*, 300, 26-36.
- Platt, J. R. (1964). Strong Inference: Certain systematic methods of scientific thinking may produce much more rapid progress than others. *Science*, 146(3642), 347-353.
- Ruiz-Medina, J., Ledent, C., & Valverde, O. (2011). GPR3 orphan receptor is involved in neuropathic pain after peripheral nerve injury and regulates morphine-induced antinociception. *Neuropharmacology*, 61(1-2), 43-50.
- Rybnikova, N. A., Haim, A., & Portnov, B. A. (2016). Does artificial light-at-night exposure contribute to the worldwide obesity pandemic. *International Journal of Obesity*, 40(5), 815-823.
- Sato, S., Sakurai, T., Ogasawara, J., Takahashi, M., Izawa, T., Imaizumi, K., Taniguchi, N., Ohno, H., & Kizaki, T. (2014). A circadian clock gene, Rev-erba, modulates the inflammatory function of macrophages through the negative regulation of Ccl2 expression. *Journal of Immunology*, 192(1), 407-417.
- Scheiermann, C., Kunisaki, Y., & Frenette, P. S. (2013). Circadian control of the immune system. *Nature Reviews Immunology*, 13(3), 190-198.
- Sugimoto, T., Morioka, N., Zhang, F. F., Sato, K., Abe, H., Hisaoka-Nakashima, K., & Nakata, Y. (2014). Clock gene Per1 regulates the production of CCL2 and interleukin-6 through p38, JNK1 and NF- κ B activation in spinal astrocytes. *Molecular and Cellular Neurosciences*, 59, 37-46.

- Takada, T., Yamashita, A., Date, A., Yanase, M., Suhara, Y., Hamada, A., Sakai, H., Ikegami, D., Iseki, M., Inada, E., & Narita, M. (2013). Changes in the circadian rhythm of mRNA expression for μ -opioid receptors in the periaqueductal gray under a neuropathic pain-like state. *Synapse*, 67(5), 216-223.
- Turner, P. V., Brabb, T., Pekow, C., & Vasbinder, M. A. (2011). Administration of substances to laboratory animals: routes of administration and factors to consider. *Journal of the American Association for Laboratory Animal Science*, 50(5), 600-613.
- Vieira, E., Mirizio, G. G., Barin, G. R., de Andrade, R. V., Nimer, N. F. S., & La Sala, L. (2020). Clock Genes, Inflammation and the Immune System-Implications for Diabetes, Obesity and Neurodegenerative Diseases. *International Journal of Molecular Sciences*, 21(24).
- Walker, W. H., Bumgarner, J. R., Becker-Krail, D. D., May, L. E., Liu, J. A., & Nelson, R. J. (2021). Light at night disrupts biological clocks, calendars, and immune function. *Seminars in Immunopathology*, 44(2), 165-173.

Part 2

Artificial Light at Night Alters Cerebrovascular Structure in Mice

Chapter 6

Circadian Regulation of the Blood-Brain Barrier and Angiogenesis

1. Introduction

1.1 Circadian Rhythms

Circadian rhythms are fundamental biological features of nearly every organism on Earth (Reppert & Weaver, 2002). These rhythms are endogenous biological rhythms that fluctuate over periods of around 24 hours, hence *circa* (about) *diem* (day). As a result of the Earth's axial orbital rotation, the state of the environment changes over the day as the sun rises and sets. This axial rotation also leads to cyclical changes in the availability of energetic and environmental resources. Circadian rhythms ultimately serve to enable the optimal physiological and behavioral function of organisms in the Earth's cyclical environment (Bumgarner & Nelson, 2021).

Biological clocks are the evolutionary solution to the Earth's cyclical environment (Partch et al., 2014). These clocks are the foundational components of circadian rhythms and are present in all organisms that exhibit circadian rhythms (with mild genetic variations). Biological clocks produce circadian rhythms via the so-called clock gene transcription-translation feedback loop (TTFL) (Partch et al., 2014). The clock gene TTFL cycles over periods of around 24 hours via the activation and repression of two branches of genes. In the positive (activation) loop of the TTFL, CLOCK, and BMAL1 are expressed and then heterodimerize in the nucleus of the cell. This heterodimer then is translocated into the nucleus of the cell where it engages the negative (repressive) loop of the TTFL by promoting the expression of PER and CRY proteins and repressing further expression of CLOCK/BMAL. PER and CRY proteins heterodimerize in the cytoplasm, translocate to the nucleus, and disengage CLOCK/BMAL from promoter/repressor sequences, thereby preventing their own expression, and restarting the loop. Other peripheral loops are also present, including the ROR, REV-ERB α , and CKII loops (Partch et al., 2014).

Importantly, the clock genes of the TTFL activate and repress the expression of other genes throughout the genome. Endogenous circadian rhythms are then produced because of the 24-hour expression patterns of the core clock genes (Takahashi, 2017).

The TTFL is present in nearly every cell of rhythmic organisms. In humans, the TTFL is estimated to regulate around 43% of the genome (Zhang et al., 2014); anywhere between 5 and 20% of any individual cell's genome is expressed rhythmically (Takahashi, 2017). These percentages indicate the wide control of circadian rhythms over almost all aspects of behavior and physiology. Importantly to the context of this review, circadian rhythms also regulate the function of the blood-brain barrier and angiogenesis. Disruption of these rhythms has critical implications for the function and integrity of the cardiovascular system, including the blood-brain barrier.

1.2 Blood-Brain Barrier

The blood-brain barrier (BBB) is a strictly regulated and highly restrictive vascular barrier that separates the parenchyma of the central nervous system from the periphery of the body (Daneman, 2012). The restrictive barrier properties of the BBB are essential for typical homeostatic function within the nervous system for several reasons (Daneman & Prat, 2015). First, neurons require finely tuned and highly regulated extracellular environments to generate action potentials and regenerate membrane potentials during periods of rest and activity (Blanchette & Daneman, 2015). The free flow of extracellular fluid of the parenchyma to the circulatory system would disrupt this balance. Next, the BBB serves to prevent circulating toxins from entering the CNS and causing unnecessary harm to neurons and glia (Daneman & Prat, 2015). Finally, because organisms may encounter toxins or pathogens through the air they breathe or through skin damage, the BBB prevents unnecessary immune challenges from entering the brain (Obermeier et al., 2013). Of note, this does not mean that the central nervous system is unaffected by peripheral immune challenges, as peripherally circulating cytokines are known to cross the BBB, and peripheral immune challenges can change peripheral immune trafficking behavior across the BBB (Obermeier et al., 2013).

The BBB comprises a collection of cells that fall into two primary classes: endothelial cells and mural cells (Obermeier et al., 2013). Endothelial cells are the cells that form the walls of blood vessels either by connecting or folding onto other endothelial cells or their own processes. Mural cells of the BBB primarily include astrocytes and

pericytes, but microglia and other immune cells can interact with and regulate BBB function and integrity (Daneman, 2012).

In contrast to peripheral vasculature, the BBB is not fenestrated, and BBB endothelial cells are connected via tight junctions that strictly limit the flow of circulating solutes into the CNS. These tight junctions are made up of various transmembrane protein classes, including occludins, claudins, and junction adhesion molecules. Although all endothelial cells of the body express some forms of these tight junction proteins, CNS endothelial cells have transcription profiles that are enriched and regulated because of 1. direct cellular contact with and 2. exposure to extracellular signaling molecules produced by astrocytic end feet and pericyte mural cells. Although numerous other BBB regulatory pathways exist, the PDGFBB-PDGFR- β pericyte-endothelial (Daneman et al., 2010) and Hh-PTCH1 astrocyte-endothelial signaling pathways (Daneman & Prat, 2015) are two of the primary pathways that promote CNS endothelial cell phenotypes.

Exogenous and endogenous molecular transport across the BBB is strictly regulated due to the molecular and physiological properties of CNS endothelial cells (Wong et al., 2013). Small ions and water pass across the BBB in and out of the CNS via passive and active diffusion through membrane channels. Oxygen, CO₂, and other lipophilic molecules, such as ethanol and caffeine are passively transported across the endothelial cell membranes into and out of the CNS. Beyond this, larger molecular transport across the BBB depends on solute carriers, receptors, or adsorption-mediated transportation. Many molecules that may pass the BBB passively are even actively effluxed back into the vascular luminal space from endothelial cells (Wong et al., 2013). For example, paclitaxel, a common chemotherapeutic used to treat a variety of cancers, is actively effluxed out of the CNS and endothelial cells via the PGP transporter (Löscher & Potschka, 2005).

1.3 Angiogenesis

Angiogenesis is a critical aspect of development and vascular maintenance in health and disease (Eelen et al., 2020). In stages of development, blood vessels in and out of the CNS are formed through the process of vasculogenesis, where angioblasts

differentiate into endothelial cells and blood vessels are formed via cell-cell and cell-extracellular matrix interactions coordinated by growth signaling factors. After development, blood vessels remain in a relatively quiescent state, as most of the necessary vasculature has already been created. However, in adulthood, the formation of blood vessels via angiogenesis does occur in a variety of contexts, including both states of health and disease (Senger & Davis, 2011). The hallmark signaling pathways responsible for angiogenesis are the VEGF/VEGFR and Delta-Notch signaling pathways; importantly, the two primary VEGF receptors play different roles in the positive and negative regulation of angiogenesis (Shibuya, 2011).

Moreover, vascular remodeling is another important aspect of vascular health and maintenance, where the size and shape of vessels are modulated in response to changing tissue states. However, an important distinction of vascular remodeling is that no new vessels are formed; only the size and shape of existing vessels are altered (Siafakas et al., 2007).

2. The Circadian Regulation of the BBB and Angiogenesis

Circadian rhythms coordinate the function of nearly all biological processes. In this section, I will highlight several articles that directly and correlatively demonstrate the regulation of circadian of the BBB and angiogenesis.

2.1 Circadian Regulation of the Blood-Brain Barrier

Circadian rhythms of the BBB are regulated both by the peripheral clocks of the cells that constitute it and by other peripheral signaling cues that are coordinated by the master clock of the body. (Paschos & FitzGerald, 2010). First, every cell of the BBB exhibits the clock gene TTFL, including endothelial cells (Nakai et al., 2022), pericytes (Mastrullo et al., 2022), and astrocytes (Brancaccio et al., 2019). Additionally, in addition to the cells of the BBB, the cells that make up the neurovascular unit also exhibit clock gene TTFL, including smooth muscle cells, (Nonaka et al., 2001) and neurons (Xiao et al., 2021).

Circadian clock gene TTFLs in individual cell types of the BBB and NVU are also capable of modulating rhythms of neighboring cell types. For example, pericytes are demonstrated to induce rhythmicity in endothelial cells in *in vitro* co-cultures, although the exact signaling mechanisms outside of the TTFL are not yet known (Mastrullo et al., 2022). The mentioned study proposed that pericyte production and release of lactate may be a critical signaling factor in this context (Mastrullo et al., 2022). Further, astrocytes can directly and indirectly modulate the rhythmicity of neurons (Brancaccio et al., 2017). Finally, the cells of the NVU exhibit synchronized rhythmicity of the TTFL across the brain, as demonstrated by rat whole-brain vascular isolations (Durgan et al., 2017).

Although the presence of the clock gene TTFL in these cells alone is not enough to explicitly say that these cells exhibit circadian rhythmicity in function, explicit circadian variations in vascular and BBB function have been observed. First, vascular tone, blood flow, and vasodilatory responses are all observed to be directly modulated by circadian rhythms (Paschos & FitzGerald, 2010). One study examined vascular tone dynamics of cortical penetrating arteries in mice as they transitioned through sleep-wake phases (Bojarskaite et al., 2022). Artery diameters increased during periods of sleep, and frequencies of diameter changes also increased during periods of sleep (Bojarskaite et al., 2022). The effects in this study were only examined in the context of sleep, so it is not possible to state that the tone alterations are circadian in nature. Instead, they may be modulated only by homeostatic sleep pressure variations. However, the data presented are still directly relevant to diurnal variations in BBB structure and function (Bojarskaite et al., 2022).

There is correlative evidence to indicate that there may be circadian variations in the expression of tight junction molecules in endothelial cells of the BBB. It has been demonstrated that Occludin and Claudin-1 exhibit diurnal concentration variations in the epithelium of the mouse large intestine (Kyoko et al., 2014). Additionally, unpublished results from Ramanath and Campbell demonstrated rhythmic expression of ZO-1, Occludin, and Claudin-5 in mouse endothelial cell cultures. Further work needs to be conducted to improve our understanding of the circadian regulation of tight junction molecules in the BBB and the signaling factors that promote their expression.

BBB permeability to endogenous and exogenous molecules varies across the day (Cuddapah et al., 2019). A variety of endogenous molecules are demonstrated to have varying uptake into the CNS across the day. Two cytokines, IL-6 and TNF are demonstrated to have greater uptake into the CNS in the late stages of the active phase. In humans, IL-6 CNS accumulation peaks at 19:00h (Agorastos et al., 2014), and in mice, TNF CNS accumulation peaks between 20-23h (Pan et al., 2002). Hormone transportation across the BBB into the CNS also varies across the day, including the accumulation of leptin (Pan & Kastin, 2001), norepinephrine (Ziegler et al., 1976), and prostaglandin D2 (Pandey et al., 1995). Lastly, other endogenous peptides exhibit diurnal rhythmicity in BBB transcytosis, including β -amyloid (Kress et al., 2018) and DSIP, a sleep-promoting peptide (Banks et al., 1985).

The BBB also exhibits diurnal variations in permeability to exogenous molecules. One group demonstrated that the function of the ATP-binding cassette sub-family B member 1 transporter channel (also known as p-glycoprotein1 (Löscher & Potschka, 2005)) has rhythmic function across the day (Savolainen et al., 2016). The first group to determine this used an exogenous substrate for Pgp and determined that the efflux of this substrate out of the CNS varied across the day in rats, with reduced efflux function occurring at the beginning of the active phase (Savolainen et al., 2016). Next, the Segal group examined exogenous molecule transportation across the BBB in *Drosophila melanogaster*. In their seminal article, Zhang et al. examined the permeability of the BBB to rhodamine B and phenytoin (an anti-epileptic) across the day (Zhang et al., 2018). They observed reduced efflux of rhodamine B and phenytoin during the inactive phase and specifically identified gap-junction regulation of intracellular Mg^{2+} to be the primary circadian coupling mechanism that drove this effect (Zhang et al., 2018).

In a subsequent study, the same group identified rhythmic efflux variations *in vivo* in mice and *in vitro* in mice and human endothelial cells (Zhang et al., 2021). In this article, they proposed that a similar mechanism was responsible for the variations in Pgp efflux function, but this conclusion might be considered somewhat problematic. The group used bulk-sequencing transcriptomics to identify rhythmic gene expression variations in mouse brain endothelial cells. The issue with their conclusion comes from the fact that a minute

percentage of their extracted endothelial genomes exhibited rhythmic variations (< 0.5%). Moreover, clock genes in the isolated endothelial cells were not rhythmically expressed, indicating a potential issue with the construct validity of this experiment (Zhang et al., 2021). Regardless, the functional observations were consistent with previous and current functional observations, demonstrating the value of this study.

An additional study from our group expanded upon functional variations in BBB permeability properties. Because several of the previous studies demonstrated variations in Pgp function across the day, Walker hypothesized that these variations could be leveraged to improve the delivery of paclitaxel, a chemotherapeutic agent, into the brain to treat brain metastases of breast cancer (Walker 2nd et al., 2021). Indeed, a diurnal rhythm in the permeability of paclitaxel across the blood-tumor barrier was observed, and this variation was harnessed to demonstrate differences in treatment efficacy. Treatment during the peak permeability window increased cellular death in the brain metastases and increased the median survival outcome (Walker 2nd et al., 2021).

2.2 Circadian Regulation of Angiogenesis

Emerging evidence indicates that angiogenesis is regulated by circadian rhythms. First, several studies have indicated the direct role of the circadian clock on angiogenesis *in vivo* and *in vitro*. Indeed, circadian transcription factor binding sites, including E-boxes, D-boxes, F-boxes, and ROREs are present in the promoter regions of numerous angiogenic proteins (Jensen et al., 2014). To date, two studies have examined the modulation of angiogenesis by circadian rhythms in zebrafish. The first study demonstrated that VEGF production was elevated at night in developing zebrafish (Jensen et al., 2012). Eliminating the light-dark cycle from the environment by exposing the animals to constant light led to blunted levels of angiogenesis (Jensen et al., 2012). This effect was recapitulated via Bmal1 knockouts (Jensen et al., 2012). In contrast, Per2 knockouts rescued angiogenesis in fish housed in constant lighting conditions (Jensen et al., 2012). The second zebrafish study corroborated these effects, demonstrating that Bmal1 knockout reduced angiogenesis, whereas Per2 knockouts increased angiogenesis (Jensen & Cao, 2013).

In mice, there has been little direct examination of clock gene regulation of angiogenic genes in healthy mice. One study examined clock gene regulation of VEGF in rodent tumor cells. Their work demonstrated that Clock and Bmal1 positively regulate VEGF, whereas Per2 and Cry1 negatively regulate VEGF in tumor cells (Koyanagi et al., 2003). Other work has demonstrated that Per2 is necessary for the proper function of endothelial progenitor cells following myocardial infarction in mice, although cell function was examined *in vitro* (Sun et al., 2014). Finally, one study examined angiogenesis *in vitro* and demonstrated that clock synchronization of pericytes and endothelial cells increased tube formation and endothelial cell counts relative to desynchronized cells (Mastrullo et al., 2022).

Angiogenesis is also indirectly modulated by the circadian clock via cyclically secreted humoral and local signaling factors. For example, cortisol is secreted cyclically across the day, with the greatest serum concentrations occurring at the beginning of the active phase. Cortisol is known to inhibit VEGF-A expression in a variety of cell types and tissues, including smooth muscle cells (Nauck et al., 1998), chondrocytes (Koedam et al., 2002), and tumors (Yano et al., 2006). Two other cyclically secreted factors, Prokineticin1 and -2 also play roles in angiogenesis. Prokineticin1 can induce the expression of VEGF (Kisliouk et al., 2005), and Prokineticin2-receptor can destabilize endothelial walls, potentially promoting the integration of proliferating endothelial cells (Monnier & Samson, 2010). Finally, endothelial nitric oxide synthase (eNOS) concentrations are rhythmic (Shang et al., 2016). Angiogenic and vascular stabilization responses resulting from VEGF are directly correlated with NO production levels, which in the endothelium are dependent on eNOS (Fukumura et al., 2001). Although the relationship between circadian rhythms and the VEGF-eNOS-NO angiogenic signaling pathway has not been directly examined, the rhythmic expression of eNOS indicates that a relationship exists.

3. Circadian Rhythm Disruption Impairs Cardiovascular Function

Disruption of circadian rhythms has negative effects on cardiovascular function and health (Crnko et al., 2018; Morris et al., 2016; Meléndez-Fernández et al., 2021). For

example, blood pressure was elevated in humans exposed to a simulated shift work paradigm (Morris et al., 2017). Similarly, a jet lag model increased blood pressure in Wistar-Kyoto rats (Kishi & Sunagawa, 2011). Rats exposed to artificial light at night for 5 weeks exhibited reduced nocturnal systolic blood pressure alongside disrupted daily heart rate rhythms (Molcan et al., 2019).

Circadian rhythm disruption can also impair outcomes in the context of cardiovascular disease. Mice exposed to five days of 20-hour light cycles following experimental myocardial infarction exhibited abnormal vascular remodeling, infarct expansion, and increased immune infiltration into the infarcted myocardium (Alibhai et al., 2014). Mice exposed to one week of artificial light at night following cerebral ischemia had increased mortality, neuroinflammation, and IBA1 immunoreactivity (Fonken et al., 2019). Even a single night of exposure to artificial light at night can increase the penumbral volume following experimental stroke in mice (Weil et al., 2020).

Lastly, circadian rhythm disruption can directly alter vascular modeling and remodeling. For example, clock gene disruption alters vascular development in zebrafish (Jensen et al., 2012; Jensen & Cao, 2013). BMAL1 knockdown can impair vascular smooth muscle cell proliferation induced by PDGF-BB (Takaguri et al., 2020). Acute exposure to artificial light at night can alter angiogenic transcript and protein levels in the hippocampus of mice (Walker et al., 2020).

Together, these studies summarize the direct consequences of circadian rhythm disruption on cardiovascular function in both health and disease. These effects can be prolonged, but they can also be rapid, as evident from impaired cardiovascular function from even a single night of disrupted circadian rhythms as a single night of disrupted circadian rhythms.

4. Conclusion

Circadian rhythms coordinate almost every aspect of biology, including the BBB and angiogenesis. The relationship between the circadian and cardiovascular systems is important to consider and understand in both health and disease. Understanding this relationship can enable improved cardiovascular health and may even enable an

improved ability to target and deliver therapeutics. In all, the regulation of the cardiovascular system by circadian rhythms highlights the importance of circadian rhythm hygiene to cardiovascular health.

5. References

- Agorastos, A., Hauger, R. L., Barkauskas, D. A., Moeller-Bertram, T., Clopton, P. L., Haji, U., Lohr, J. B., Geraciotti, T. D., Patel, P. M., Chrousos, G. P., & Baker, D. G. (2014). Circadian rhythmicity, variability and correlation of interleukin-6 levels in plasma and cerebrospinal fluid of healthy men. *Psychoneuroendocrinology*, *44*, 71-82.
- Alibhai, F. J., Tsimakouridze, E. V., Chinnappareddy, N., Wright, D. C., Billia, F., O'Sullivan, M. L., Pyle, W. G., Sole, M. J., & Martino, T. A. (2014). Short-term disruption of diurnal rhythms after murine myocardial infarction adversely affects long-term myocardial structure and function. *Circulation Research*, *114*(11), 1713-1722.
- Banks, W. A., Kastin, A. J., & Selznick, J. K. (1985). Modulation of immunoactive levels of DSIP and blood-brain permeability by lighting and diurnal rhythm. *Journal of Neuroscience Research*, *14*(3), 347-355.
- Blanchette, M., & Daneman, R. (2015). Formation and maintenance of the BBB. *Mechanisms of Development*, *138 Pt 1*, 8-16.
- Bojarskaite, L., Bjørnstad, D. M., Vallet, A., Binder, K. M. G., Cunen, C., Heuser, K., Kuchta, M., Mardal, K.-A., & Enger, R. (2022). Sleep cycle-dependent vascular dynamics enhance perivascular cerebrospinal fluid flow and solute transport. *bioRxiv*, 2022.07.14.500017.
- Brancaccio, M., Edwards, M. D., Patton, A. P., Smyllie, N. J., Chesham, J. E., Maywood, E. S., & Hastings, M. H. (2019). Cell-autonomous clock of astrocytes drives circadian behavior in mammals. *Science*, *363*(6423), 187-192.

- Brancaccio, M., Patton, A. P., Chesham, J. E., Maywood, E. S., & Hastings, M. H. (2017). Astrocytes control circadian timekeeping in the suprachiasmatic nucleus via glutamatergic signaling. *Neuron*, 93(6), 1420-1435. e5.
- Bumgarner, J. R., & Nelson, R. J. (2021). Light at Night and Disrupted Circadian Rhythms Alter Physiology and Behavior. *Integrative and Comparative Biology*, *icab017*.
- Crnko, S., Cour, M., Van Laake, L. W., & Lecour, S. (2018). Vasculature on the clock: Circadian rhythm and vascular dysfunction. *Vascular Pharmacology*, 108, 1-7.
- Cuddapah, V. A., Zhang, S. L., & Sehgal, A. (2019). Regulation of the blood–brain barrier by circadian rhythms and sleep. *Trends in Neurosciences*, 42(7), 500-510.
- Daneman, R. (2012). The blood-brain barrier in health and disease. *Annals of Neurology*, 72(5), 648-672.
- Daneman, R., & Prat, A. (2015). The blood-brain barrier. *Cold Spring Harb Perspect Biol*, 7(1), a020412.
- Daneman, R., Zhou, L., Kebede, A. A., & Barres, B. A. (2010). Pericytes are required for blood-brain barrier integrity during embryogenesis. *Nature*, 468(7323), 562-566.
- Durgan, D. J., Crossland, R. F., & Bryan, R. M. (2017). The rat cerebral vasculature exhibits time-of-day-dependent oscillations in circadian clock genes and vascular function that are attenuated following obstructive sleep apnea. *Journal of Cerebral Blood Flow & Metabolism*, 37(8), 2806-2819.
- Eelen, G., Treppe, L., Li, X., & Carmeliet, P. (2020). Basic and therapeutic aspects of angiogenesis updated. *Circulation Research*, 127(2), 310-329.
- Fonken, L. K., Bedrosian, T. A., Zhang, N., Weil, Z. M., DeVries, A. C., & Nelson, R. J. (2019). Dim light at night impairs recovery from global cerebral ischemia. *Experimental Neurology*, 317, 100-109.
- Fukumura, D., Gohongi, T., Kadambi, A., Izumi, Y., Ang, J., Yun, C. O., Buerk, D. G., Huang, P. L., & Jain, R. K. (2001). Predominant role of endothelial nitric oxide synthase in vascular endothelial growth factor-induced angiogenesis and vascular permeability. *Proceedings of the National Academy of Sciences*, 98(5), 2604-2609.

- Jensen, L. D., & Cao, Y. (2013). Clock controls angiogenesis. *Cell Cycle*, 12(3), 405-408.
- Jensen, L. D., Cao, Z., Nakamura, M., Yang, Y., Bräutigam, L., Andersson, P., Zhang, Y., Wahlberg, E., Länne, T., Hosaka, K., & Cao, Y. (2012). Opposing effects of circadian clock genes *bmal1* and *period2* in regulation of VEGF-dependent angiogenesis in developing zebrafish. *Cell Reports*, 2, 231-241.
- Jensen, L. D., Gyllenhaal, C., & Block, K. (2014). Circadian angiogenesis. *Biomolecular Concepts*, 5(3), 245-256.
- Kishi, T., & Sunagawa, K. (2011). *Experimental 'jet lag' causes sympathoexcitation via oxidative stress through AT 1 receptor in the brainstem*. In *2011 Annual International Conference of the IEEE Engineering in Medicine and Biology Society* (pp. 1969-1972). IEEE.
- Kisliouk, T., Podlovni, H., & Meidan, R. (2005). Unique expression and regulatory mechanisms of EG-VEGF/prokineticin-1 and its receptors in the corpus luteum. *Annals of Anatomy*, 187(5-6), 529-537.
- Koedam, J. A., Smink, J. J., & van Buul-Offers, S. C. (2002). Glucocorticoids inhibit vascular endothelial growth factor expression in growth plate chondrocytes. *Molecular and Cellular Endocrinology*, 197(1-2), 35-44.
- Koyanagi, S., Kuramoto, Y., Nakagawa, H., Aramaki, H., Ohdo, S., Soeda, S., & Shimeno, H. (2003). A molecular mechanism regulating circadian expression of vascular endothelial growth factor in tumor cells. *Cancer Research*, 63(21), 7277-7283.
- Kress, G. J., Liao, F., Dimitry, J., Cedeno, M. R., FitzGerald, G. A., Holtzman, D. M., & Musiek, E. S. (2018). Regulation of amyloid- β dynamics and pathology by the circadian clock. *Journal of Experimental Medicine*, 215(4), 1059-1068.
- Kyoko, O. O., Kono, H., Ishimaru, K., Miyake, K., Kubota, T., Ogawa, H., Okumura, K., Shibata, S., & Nakao, A. (2014). Expressions of tight junction proteins Occludin and Claudin-1 are under the circadian control in the mouse large intestine: implications in intestinal permeability and susceptibility to colitis. *PLoS One*, 9(5), e98016.

- Löscher, W., & Potschka, H. (2005). Blood-brain barrier active efflux transporters: ATP-binding cassette gene family. *NeuroRx*, 2(1), 86-98.
- Mastrullo, V., Van Der Veen, D. R., Gupta, P., Matos, R. S., Johnston, J. D., McVey, J. H., Madeddu, P., Velliou, E. G., & Campagnolo, P. (2022). Pericytes' circadian clock affect endothelial cells' synchronization and angiogenesis in a 3D tissue engineered scaffold. *Frontiers in Pharmacology*, 13, 867070.
- Meléndez-Fernández, O. H., Walton, J. C., DeVries, A. C., & Nelson, R. J. (2021). Clocks, Rhythms, Sex, and Hearts: How Disrupted Circadian Rhythms, Time-of-Day, and Sex Influence Cardiovascular Health. *Biomolecules*, 11(6), 883.
- Molcan, L., Sutovska, H., Okuliarova, M., Senko, T., Krskova, L., & Zeman, M. (2019). Dim light at night attenuates circadian rhythms in the cardiovascular system and suppresses melatonin in rats. *Life Sciences*, 231, 116568.
- Monnier, J., & Samson, M. (2010). Prokineticins in angiogenesis and cancer. *Cancer Letters*, 296(2), 144-149.
- Morris, C. J., Purvis, T. E., Mistretta, J., Hu, K., & Scheer, F. A. J. L. (2017). Circadian misalignment increases C-reactive protein and blood pressure in chronic shift workers. *Journal of Biological Rhythms*, 32(2), 154-164.
- Morris, C. J., Purvis, T. E., Hu, K., & Scheer, F. A. (2016). Circadian misalignment increases cardiovascular disease risk factors in humans. *Proceedings of the National Academy of Sciences*, 113(10), E1402-11.
- Nakai, H., Tsuchiya, Y., Koike, N., & Asano..., T. (2022). Comprehensive Analysis Identified the Circadian Clock and Global Circadian Gene Expression in Human Corneal Endothelial Cells. *Investigative Ophthalmology & Visual Science*, 63, 16.
- Nauck, M., Karakiulakis, G., Perruchoud, A. P., Papakonstantinou, E., & Roth, M. (1998). Corticosteroids inhibit the expression of the vascular endothelial growth factor gene in human vascular smooth muscle cells. *European Journal of Pharmacology*, 341(2-3), 309-315.
- Nonaka, H., Emoto, N., Ikeda, K., Fukuya, H., Rohman, M. S., Raharjo, S. B., Yagita, K., Okamura, H., & Yokoyama, M. (2001). Angiotensin II induces circadian gene

- expression of clock genes in cultured vascular smooth muscle cells. *Circulation*, 104(15), 1746-1748.
- Obermeier, B., Daneman, R., & Ransohoff, R. M. (2013). Development, maintenance and disruption of the blood-brain barrier. *Nature Medicine*, 19(12), 1584-1596.
- Pan, W., Cornélissen, G., Halberg, F., & Kastin, A. J. (2002). Selected contribution: circadian rhythm of tumor necrosis factor-alpha uptake into mouse spinal cord. *Journal of Applied Physiology*, 92(3), 1357-1362.
- Pan, W., & Kastin, A. J. (2001). Diurnal variation of leptin entry from blood to brain involving partial saturation of the transport system. *Life Sciences*, 68(24), 2705-2714.
- Pandey, H. P., Ram, A., Matsumura, H., & Hayaishi, O. (1995). Concentration of prostaglandin D2 in cerebrospinal fluid exhibits a circadian alteration in conscious rats. *Biochemistry and Molecular Biology Education*, 37(3), 431-437.
- Partch, C. L., Green, C. B., & Takahashi, J. S. (2014). Molecular architecture of the mammalian circadian clock. *Trends in Cell Biology*, 24(2), 90-99.
- Paschos, G. K., & FitzGerald, G. A. (2010). Circadian clocks and vascular function. *Circulation Research*, 106(5), 833-841.
- Reppert, S. M., & Weaver, D. R. (2002). Coordination of circadian timing in mammals. *Nature*, 418(6901), 935-941.
- Savolainen, H., Meerlo, P., Elsinga, P. H., Windhorst, A. D., Dierckx, R. A., Colabufo, N. A., van Waarde, A., & Luurtsema, G. (2016). P-glycoprotein Function in the Rodent Brain Displays a Daily Rhythm, a Quantitative In Vivo PET Study. *AAPS J*, 18(6), 1524-1531.
- Senger, D. R., & Davis, G. E. (2011). Angiogenesis. *Cold Spring Harbor Perspectives in Biology*, 3(8), a005090.
- Shang, X., Pati, P., Anea, C. B., Fulton, D. J., & Rudic, R. D. (2016). Differential Regulation of BMAL1, CLOCK, and Endothelial Signaling in the Aortic Arch and Ligated Common Carotid Artery. *Journal of Vascular Research*, 53(5-6), 269-278.

- Shibuya, M. (2011). Vascular endothelial growth factor (VEGF) and its receptor (VEGFR) signaling in angiogenesis: a crucial target for anti-and pro-angiogenic therapies. *Genes & Cancer*, 2(12), 1097-1105.
- Siafakas, N. M., Antoniou, K. M., & Tzortzaki, E. G. (2007). Role of angiogenesis and vascular remodeling in chronic obstructive pulmonary disease. *International Journal of Chronic Obstructive Pulmonary Disease*, 2(4), 453.
- Sun, Y. Y., Bai, W. W., Wang, B., Lu, X. T., Xing, Y. F., Cheng, W., Liu, X. Q., & Zhao, Y. X. (2014). Period 2 is essential to maintain early endothelial progenitor cell function in vitro and angiogenesis after myocardial infarction in mice. *Journal of Cellular and Molecular Medicine*, 18(5), 907-918.
- Takaguri, A., Sasano, J., Akihiro, O., & Satoh, K. (2020). The role of circadian clock gene BMAL1 in vascular proliferation. *European Journal of Pharmacology*, 872, 172924.
- Takahashi, J. S. (2017). Transcriptional architecture of the mammalian circadian clock. *Nature Reviews. Genetics*, 18(3), 164-179.
- Walker 2nd, W. H., Sprowls, S. A., Bumgarner, J. R., Liu, J. A., Meléndez-Fernández, O. H., Walton, J. C., Lockman, P. R., DeVries, A. C., & Nelson, R. J. (2021). Circadian Influences on Chemotherapy Efficacy in a Mouse Model of Brain Metastases of Breast Cancer. *Frontiers in Oncology*, 11, 752331-752331.
- Walker, W. H., Borniger, J. C., Gaudier-Diaz, M. M., Hecmarie Meléndez-Fernández, O., Pascoe, J. L., Courtney DeVries, A., & Nelson, R. J. (2020). Acute exposure to low-level light at night is sufficient to induce neurological changes and depressive-like behavior. *Molecular Psychiatry*, 25(5), 1080-1093.
- Weil, Z. M., Fonken, L. K., Walker, W. H., Bumgarner, J. R., Liu, J. A., Melendez-Fernandez, O. H., Zhang, N., DeVries, A. C., & Nelson, R. J. (2020). Dim light at night exacerbates stroke outcome. *European Journal of Neuroscience*, 52(9), 4139-4146.
- Wong, A. D., Ye, M., Levy, A. F., Rothstein, J. D., Bergles, D. E., & Searson, P. C. (2013). The blood-brain barrier: an engineering perspective. *Frontiers in Neuroengineering*, 6, 7.

- Xiao, Y., Yuan, Y., Jimenez, M., Soni, N., & Yadlapalli, S. (2021). Clock proteins regulate spatiotemporal organization of clock genes to control circadian rhythms. *Proceedings of the National Academy of Sciences*, 118(28), e2019756118.
- Yano, A., Fujii, Y., Iwai, A., Kageyama, Y., & Kihara, K. (2006). Glucocorticoids suppress tumor angiogenesis and in vivo growth of prostate cancer cells. *Clinical Cancer Research*, 12(10), 3003-3009.
- Zhang, R., Lahens, N. F., Ballance, H. I., Hughes, M. E., & Hogenesch, J. B. (2014). A circadian gene expression atlas in mammals: implications for biology and medicine. *Proceedings of the National Academy of Sciences*, 111(45), 16219-16224.
- Zhang, S. L., Lahens, N. F., Yue, Z., Arnold, D. M., Pakstis, P. P., Schwarz, J. E., & Sehgal, A. (2021). A circadian clock regulates efflux by the blood-brain barrier in mice and human cells. *Nature Communications*, 12(1), 617.
- Zhang, S. L., Yue, Z., Arnold, D. M., Artiushin, G., & Sehgal, A. (2018). A Circadian Clock in the Blood-Brain Barrier Regulates Xenobiotic Efflux. *Cell*, 173(1), 130-139.e10.
- Ziegler, M. C., Lake, C. R., Wood, J. H., & Ebert, M. H. (1976). Circadian rhythm in cerebrospinal fluid noradrenaline of man and monkey. *Nature*, 264(5587), 656-658.

Chapter 7

Open-source analysis and visualization of segmented vasculature datasets with VesselVio

Published As:

Bumgarner, J. R., & Nelson, R. J. (2022). Open-source analysis and visualization of segmented vasculature datasets with VesselVio. *Cell Reports Methods*, 2(4), 100189.

Introduction

The acquisition of high-resolution and large-scale 3D vasculature datasets has been facilitated by recent and continual developments of powerful imaging technologies, including light sheet fluorescence microscopy (LSM) (Di Giovanna et al., 2018; Kirst et al., 2020; Todorov et al., 2020) and micro-computed tomography (μ CT) (Quintana et al., 2019; Schaad et al., 2017). Simultaneously, constant improvements in computational power and the widespread availability of powerful programming languages provide great means to process and extract detailed features from the resulting datasets. The use of micron-scaled imaging technologies and powerful computational tools to characterize the intricate details of microvascular networks will improve understanding of microvascular structure, function, and remodeling in health and disease.

Despite ongoing advancements in imaging technologies and open-source image segmentation software for 3D vasculature datasets (Kirst et al., 2020; Todorov et al., 2020; Haft-Javaherian et al., 2019), the publication of open-source and stand-alone analysis software applications that do not require prior programming experience is scarce. Existing standalone analysis tools that are accessible and freely available are unable to extract features from 3D datasets (Zudaire et al., 2011; Niemisto et al., 2005). Other current open-access, terminal-based analysis packages have similar 2D limitations (Mazzaferri et al., 2018; Montoya-Zegarra et al., 2019; Rust et al., 2020). Open-source analysis tools and software packages capable of analyzing 3D datasets are limited. Several of these tools depend on uncorrected centerline analyses, provide limited feature

output, and markedly over-label branch points (Arganda-Carreras et al., 2010; Todorov et al., 2020). Other modern analysis packages that extract more accurate (Kirst et al., 2020; Tetteh et al., 2020) and detailed features (Hahn et al., 2019; Chapman et al., 2015) from 3D vascular networks require considerable programming skills or heavy interaction with terminals, potentially leading to unwelcome usage barriers and steep learning curves for researchers. Many publications also make use of private code or proprietary software for feature extractions (Jafarnejad et al., 2019; Epah et al., 2018; Kelch et al., 2015). In these instances, limited code availability and high software prices can hinder widespread analysis access. Thus, there is an apparent need for an easily accessible tool for 3D vasculature dataset analysis.

Here I present *VesselVio*, an open-source application for the analysis and visualization of vasculature datasets and vascular graphs. The backend pipelines leverage custom feature extraction techniques, high-level Python libraries, just-in-time compilation, and parallel processing for rapid, detailed feature extraction and visualization of vasculature datasets. To make these analysis pipelines easily accessible, I also developed a downloadable (or single-line executable) front-end application. To test the performance and utility of *VesselVio*, I analyzed ground-truth synthetic vascular datasets, annotated mouse whole-brain datasets imaged using LSM, mouse inferior colliculus segmentations imaged using μ CT, 2D retinography images, and preconstructed mouse whole-brain vascular graphs.

Methods

Animals

All experiments were approved by the West Virginia University Institutional Animal Care and Use Committee, and animals were maintained in accordance with NIH Animal Welfare guidelines. Adult female and male CFW mice (7 to 8 weeks of age; strain #024; Charles River Laboratories, USA) were obtained and maintained under 14:10 light-dark cycles ($150 \pm 25:0$ lux light: dark; lights on from 0500-1900 h). Following arrival, animals were given 1 week to acclimate to vivarium conditions before tissue collection. Food

(2018 Teklad; Envigo, USA) and reverse osmosis water were provided *ad libitum* throughout the entire duration of the experiment.

Vascular Corrosion Casting and μ CT Imaging

Vascular casts of mouse brains were created using a resin corrosion casting method described previously (Quintana et al., 2019). Perfusions occurred in the light phase between 1200-1600 h. Prior to perfusion, mice were injected i.p. with 25 U of heparin (63739-931-28; McKesson Corporation, USA) in 250 μ L of saline and then deeply anesthetized with isoflurane (4% induction, 1.5% maintenance) and 0.4 L/min oxygen flow mixture. Following confirmation of complete anesthetization with a pedal withdrawal reflex test, mice were transcardially perfused at a flow rate of 4 mL/min first with 15 mL of 25 U/mL heparin in saline, followed by 15 mL of 4% paraformaldehyde (#416780030; Acros Organics, Belgium) in saline with a pH of 7.4, followed lastly with PU4ii resin (VasQTEC, Switzerland) formulated exactly as directed by the manufacturer with methyl ethyl ketone dilution (M209, Fisher Chemical, USA). Five days after perfusion, the craniums were decalcified with a 12-h wash of 5% formic acid (BDH4554; VWR International, USA), the brains were dissected, and the remaining tissue was removed from the casts with two 12-h washes of 7.5% KOH (BDH7622; VWR International, USA) at 50 °C. Casts were then rinsed with three 1-hour Milli-Q water washes, and the cleaned casts were osmicated in a 1% solution of osmium tetroxide (#75632; Sigma Aldrich, USA) for 12 hours to allow for optimal x-ray diffraction during μ CT scans. Casts were imaged on a SkyScan 1272 (Bruker, USA) at 50 kV/ 200 μ A with 360° rotations in step sizes of 0.17°, no filter, 900 ms frame exposures, and 4 frame averages/step to produce an isotropic voxel resolution of 2.7 μ m³. Scan parameters were determined based on the manufacturer's guidance to achieve optimal X-ray transmission through the sample. Scans were then reconstructed using NRecon (Bruker) with beam hardening corrections at 15%, ring artifacts reduction at 3, smoothing at 0, custom alignment compensations set for each sample, and 0.02-0.40 dynamic image ranges. Following reconstruction, the volumes were resliced coronally for inferior colliculi segmentations. Using interpolated polygonal tracing with CTAn (Bruker), inferior colliculi were manually segmented from

bregma -4.9 to -5.4 using the lobule 2 of the cerebellar vermis as a landmark for bregma -4.9 (Supplemental Video 1) (Paxinos & Franklin, 2019). Scans, reconstructions, reslicing, and inferior colliculi segmentations were all conducted using the Bruker SkyScan analysis software suite. The resulting segmentations were analyzed at a $2.7 \mu\text{m}^3$ isotropic resolution with a $10 \mu\text{m}$ isolated segment filter length and a $5 \mu\text{m}$ endpoint segment prune length (Supplemental Table 1B).

Dataset details

BalbC Mouse Brain Vasculature Datasets

The BalbC whole-brain vasculature datasets were sourced from the VesSAP repository (Todorov et al., 2020). To analyze the whole brain datasets, 483 regions were selected using the Annotation Processing page. The downloaded brains were loaded directly into the program without alteration and were analyzed at a $3 \mu\text{m}^3$ isotropic resolution with a $10 \mu\text{m}$ isolated segment filter length and a $5 \mu\text{m}$ endpoint segment prune length (Supplemental Table 1A).

HRF Dataset

The HRF image dataset was downloaded directly from the HRF Image Database (Budai et al., 2013). The images were loaded directly into the program and analyzed with a 10 px isolated segment filter length and a 5 px endpoint segment prune length (Supplemental Table 1C).

Synthetic Dataset

Twenty synthetic vasculature datasets with corresponding branch point label datasets were downloaded and holes in the vasculature were manually filled (Tetteh et al., 2020). The datasets were then loaded into the program and analyzed with a 10-voxel isolated segment filter length and a 5.5-voxel endpoint segment prune length. Branch point labels from the labeled datasets were quantified by skeletonizing the spheres around the branch points, labeling the components, and counting the components (Supplemental Table 1E).

VesselVio Pipeline

Dataset Input and Processing Preparation

Images are loaded into VesselVio using the Simple-ITK image reader or nibabel, depending on the file type (Lowekamp et al., 2013; Brett et al., 2020). It is important to note that VesselVio is only compatible with vascular datasets that have been pre-segmented. To ensure that datasets loaded into the program are prepared appropriately for subsequent analysis, all loaded volumes are binarized and prepared as n-dimensional contiguous arrays of 0-value background and 1-value foreground elements. All array processing in VesselVio is conducted using NumPy and Numba (Harris et al., 2020; Lam et al., 2015).

Volume Skeletonization and Centerline Extraction

VesselVio employs a custom implementation of a widely used medial axis parallel thinning algorithm to locate vessel centerlines from 2D and 3D datasets (Lee et al., 1994), with speed optimizations and parallel processing enabled by Numba. This algorithm was selected because it produces comparatively few erroneous branch point extensions, particularly when used with high-resolution datasets. This algorithm is also capable of thinning 2D and 3D datasets, making it optimal for this pipeline. Following skeletonization, $(n, 3)$ or $(n, 2)$ arrays are created containing Cartesian coordinate information of the location of all vessel centerlines.

Radii Calculations

Before the creation of the undirected graph, vessel centerline radii measurements are conducted. Previous publications focused on voxel/pixel vasculature analysis have utilized Euclidean distance transforms (EDT) on segmented vasculature images to find centerline radii (Tsai et al., 2009; Todorov et al., 2020). These blanketed EDT methods find the Euclidean distance (ED) from the centerline point to the center of the nearest non-vessel neighbor point. However, an apparent unconsidered flaw in this traditional method is that finding the ED to the nearest non-vessel neighbor can overestimate the radius of the vessel if its nearest non-vessel neighbors are 6-connected in 3D space

($N_6(v)$) or 4-connected in 2D space ($N_4(p)$) (Supplemental Table 1D). For example, given an isotropic voxel resolution of $1 \mu\text{m}^3$, a straight vessel along the X-axis that is 1 voxel thick should have a putative radius of $0.5 \mu\text{m}$ (Figure S1D). However, the traditional EDT method will record this vessel as having a radius of $1 \mu\text{m}^3$, doubling the apparent diameter. This is because ED measurements are calculated between the coordinates of the center of the centerline voxel and the *center* of its nearest non-vessel neighbor. Radii inflations in traditional EDT measurements are less pronounced as vessels become larger, but small-diameter vessels can be binned incorrectly using this blanketed technique.

To avoid this overestimation of vessel size, distance calculations can be made to the *face* of $N_6(v)$ or the *edge* of $N_4(p)$ non-vessel neighbors. To achieve this, a modified EDT (mEDT) calculation was implemented with 0.5-unit corrections for all $N_6(v)$ or $N_4(p)$ non-vessel neighbors (Figure S1D-F). When the nearest non-vessel neighbors are located beyond the immediate $N_{26}(v)$ or $N_8(p)$ space, the mEDT is applied to points that are connected to the centerline point only via face-to-face steps in 3D space or edge-to-edge steps in 2D space (i.e., not to diagonally connected points). In other words, given the phenotypical tubular shape of vessels, the mEDT approach is not applied to non-vessel neighbors of the sets $N_{26}(v) - N_6(v)$ and $N_8(p) - N_4(p)$ or non-vessel points beyond $N_{26}(v)$ or $N_8(p)$ neighborhoods that are situated diagonally to the centerline point (Figure S1D-F).

In previous publications, EDTs are applied to the entire image, and the centerline values are then extracted. However, this process is computationally expensive and leads to difficulty in making the intended 1D corrections. As such, the mEDT method is only applied to centerline points, rather than the entire image. Points in the previously constructed centerline coordinate arrays are used as seeds for the placement of expanding boxes that search centerline point neighborhoods for non-vessel neighbors. This box expands around a centerline point until at least four non-vessel neighbors in the binarized volume are identified, rather than a single neighbor as with previous

$$(1) d_{radius}(c, b) = \sqrt{\sum_{i=1}^n (c_i - b_i)^2} \quad (2) d_{radius} = mEDT_{LUT}[|c_x - b_x|, |c_y - b_y|, |c_z - b_z|]$$

implementations. Then, rather than directly computing the ED (square root of the sum of squared deltas) between the centerline point and neighbor (1), the absolute deltas of the centerline and neighbor coordinates are computed and loaded into a lookup table with precomputed mEDT values (2). This lookup table is constructed based on the input resolution to provide the half-unit corrections along the described orientations (e.g., an XYZ delta array of (0,0,5) returns a 4.5 voxel distance).

After the distance for each non-vessel neighbor is calculated, the four lowest values are averaged, and this average is defined as the radius for the centerline point. Four values are averaged to improve the accuracy of radii measurements and account for potential small vessel surface divots, bubbles, or imaging artifacts common in various vascular preparation techniques, such as corrosion casting. This process is parallelly repeated for all centerline points.

Graph Construction

Following radii measurements, undirected graphs are constructed to represent the vasculature skeleton. Graph creation and processing in VesselVio uses the Python igraph package (Csardi & Nepusz, 2006). To construct the vascular graphs, the number of centerline points is identified, and an equal number of isolated vertices are added to the graph. At this point, 2D images are padded as 3D arrays. Centerline points are assigned an index based on their order of appearance in the point coordinate array. Each vertex is given a coordinate and radius attribute based on its corresponding point values. Next, the (xmax, ymax, zmax) oriented 13-connectivity neighborhood of all centerline points is scanned to identify $N_{26}(v)$ neighbors. Upon neighbor identification, an edge is created between the vertices. Unidirectional scanning in the edge identification process prevents parallel edges from being created (Kirst et al., 2020).

Clique Cluster Processing

Branch points in the constructed graphs are identified based on degrees of connectivity; if a vertex has a degree greater than two, it is defined as a branch point (Todorov et al., 2020; Arganda-Carreras et al., 2010). Because the graphs are

constructed based on 26 connectivity, this identification method leads to artificial inflation of identified branch points. This is because, at individual branch point junctions, multiple vertices can have > 2 neighbors (Figure 2A). In graphical space, these falsely identified branch points form small all-to-all connected loops (*cliques*); clusters of these cliques are also common occurrences.

To correct spuriously labeled branch points, a two-pass filtering algorithm was developed that led to a correction accuracy of 97.4% (Figure 2B). This approach resolves clique clusters that are categorized into three classes. In the first pass, class 1 clusters are eliminated; these clusters were observed to be the most common type of cluster present in the examined datasets (Supplemental Table 1F). Class 1 clusters are identified by isolating maximal cliques with three/four vertices from the main graph. Vertices in these cliques are then weighted based on their radius and the radius of their neighbors in the main graph (Figure S1G). The connection between the lowest weighted candidates in the clique is then removed, thereby eliminating three-vertex cliques and simplifying four-vertex cliques.

In the second pass, class 2 and 3 clique clusters are corrected. These classes are large clusters of cliques that arise due to binarization, vessel filling, or skeletonization errors. Class 2 clique clusters contain < 50 vertices, whereas class 3 clusters contain ≥ 50 vertices. Class 2 clusters are eliminated by finding the mean radius of the vertices, identifying external projections, and creating a new vertex with this mean radius that connects to the identified projection targets (Figure S1H). The class 2 filter also resolves the previously simplified four-vertex cliques. Class 3 clusters are eliminated using a sliding window approach that scans over the cluster along the longest axis. During each window, the same algorithm for class 2 is applied, where a new single vertex is created with the mean radii of the original window vertices and preserved external projections. The new vertices created along the sliding window are then connected (Figure S1I).

Isolated and Endpoint Segment Processing

Following graph creation, $n \neq 2$ -degree vertices are filtered from the graph. The remaining components are then scanned, and isolated segments and endpoint segments

shorter than user-defined lengths are pruned (Supplemental Video 6). Following the removal of isolated segments from the graph, voxels/pixels are also removed from the corresponding segment in the volume for visualization purposes.

Feature Extraction

All individual segment characteristics and whole-network features are extracted from the constructed graph. Branch point and endpoint counts are determined by the number of $n > 3$ and $n = 1$ -degree vertices in the graph, respectively. Segments are identified in the graph by filtering $n > 2$ -degree vertices and then sorting through the remaining individual components. After each segment is identified, the mean, minimum, maximum, and standard deviation of the segment radius is calculated. Because calculating segment length based on vertex-vertex edges produces paths that are irregular to the vessel surface, a smoother path is constructed by creating a B-spline of varying degrees from the coordinates of the original segment vertices using the *geomdl* package (Bingol & Krishnamurthy, 2019). The length along the spline is then approximated using ED calculations between a defined number of points along the spline identified using the *Cox-De Boor* algorithm (Bingol & Krishnamurthy, 2019). Then, tortuosity measurements are created by finding the arc-cord ratio of the segment (segment length divided by the ED between the start and end points). Finally, the lateral surface area and volume of the segment are found using the mean radius and segment length. Averages of segments are then identified and automatically binned for ease of analysis. Segment partitioning is also calculated by dividing the number of segments by the total network length (Corliss et al., 2019).

Annotated Volume Processing

Datasets can be loaded alongside annotated volumes for subregion analysis. First, a JSON annotation processing file is created on the Annotation Processing page. Users can select specific regions of interest from several pre-loaded Allen Brain Atlas annotation trees, including the CCFv3 p56 mouse brain tree (Wang et al., 2020), can load their own annotation trees, or can create individual ROI identifiers for custom annotations, such as

those created with ITK-Snap. Then, this annotation file is loaded alongside the binarized vascular volume and the annotated volume dataset for analysis/visualization. Volumes with integer/float id-based annotations must be loaded as NIfTI files for annotation analysis. Separately, RGB-based annotations (e.g., .png series of RGB annotations) can be loaded. RGB annotation testing was conducted using QuickNII (Puchades et al., 2019).

The backend pipeline analyzes annotation regions (ROIs) in bins of 254 annotations. During each bin iteration, the selected ROIs are assigned values from 1-255, and the IDs from the identified ROI regions are cast onto the correlating voxels in the vasculature dataset to create a labeled vasculature dataset. This labeled dataset is then temporarily cached on the disk as a NumPy file for memory-mapping dataset access to prevent excessive working memory requirements. During the ROI segmentation process, the volume of each ROI is calculated and stored. At the stage of analyzing each ROI, the individual ROI-associated vasculature is segmented from the temporary labeled dataset for subsequent skeletonization and analysis. Following the analysis of each ROI, the constructed graph is added to a single main graph with preserved spatial and connectivity information. This main graph can then be exported for custom analyses. However, because most graph formats do not allow list/array attributes, the coordinates of the path of segments are eliminated during the process of reducing the centerline-based graph (vertices represent centerlines, edges represent centerline connections) to a branch-point graph (vertices represent branch points, edges represent segments). Instead, this geometric segment path information can be retrieved through custom modifications, as the segment coordinates are stored as an edge attribute that can be extracted or modified before saving the graph.

Mesh Visualization and Application Interface

To construct meshes for visualization, I leverage the high-level Python package PyVista (Sullivan & Kaszynski, 2019) that wraps The Visualization Toolkit. I create individual polydata datasets from our segment splines, apply tube filters to create centerline and scaled network meshes, and assign each tube a radius, length, tortuosity,

surface area, and scalar for visualization. All scalars and scaled segment sizes are based on the mean of segment features. These segments are combined into an undirected grid for surface extraction and subsequent rendering. Additional branch point and endpoint meshes are created. Then, original (voxel/pixel-based) and smoothed surface meshes (marching cubes based-based) are created from the filtered input volume so researchers can visually validate the output features from the program by comparing simple/scaled networks to the original/smoothed meshes. Lastly, the construction of the front-end application for VesselVio was accomplished with PyQt5 under GNU GPLv3 licensing (Figure S1A-C).

Computational resources

VesselVio was developed with Python 3.8 and was tested locally on a 2019 16” MacBook Pro (2.6 GHz 6-Core Intel Core i7, Intel UHD Graphics 630 16GB) and a Windows 10 computer with dual 3.39 GHz Intel Xeon Gold 6128 processors, 128 GB of Sk Hynix Ddr4 Sdram Memory Module RAM, and dual 8GB NVIDIA Quadro P4000 graphics cards.

Data and code availability

- The synthetic vasculature and inferior colliculus vasculature datasets have been deposited at the Harvard DataVerse Repository and are publicly available as of the date of publication. DOIs are listed in the key resources table. The BalbC whole-brain vascular datasets can be found via the VesSAP repository (<https://github.com/vessap/vessap>). The HRF dataset can be downloaded from the HRF Image Database (<https://www5.cs.fau.de/research/data/fundus-images/>).
- All original code has been deposited at <https://zenodo.org> and is publicly available as of the date of publication. DOIs are listed in the key resources table. Downloads for Windows and MacOS as well as the source code can be found on the VesselVio GitHub repository (<https://github.com/JacobBumgarner/VesselVio>).

Quantification and statistical analysis

All statistical analyses were conducted using Prism 9 (GraphPad; USA). Synthetic vasculature results were analyzed using one-way ANOVA tests and repeated-measures two-way ANOVA tests. HRF datasets were analyzed using one-way ANOVA tests. Mice IC data were analyzed using two-tailed student's t-tests. Distributions of segment counts per radii bin, average segment length per radii bin, and segment tortuosity per radii bin were all analyzed using two-way ANOVA tests. Following main effects observations in one- or two-way ANOVA tests, multiple comparisons were made using Sidak's test. P-values below 0.05 were considered statistically significant.

Results

Graphical User Interface Enables Dataset Loading, Analysis, and Visualization

I sought to build an open-source application that allows users to extract and visualize numerous quantitative features from vascular networks (Figure S1A-C). VesselVio was developed for vascular datasets that have already been binarized, making it compatible with datasets of any imaging origin (Figure 1A). The application is also compatible with preconstructed graphs from other programs. Further, binarized volumes can be loaded alongside annotations, such as the p56 mouse brain atlas from the Allen Brain Institute, to analyze region-specific features (Figure 1C).

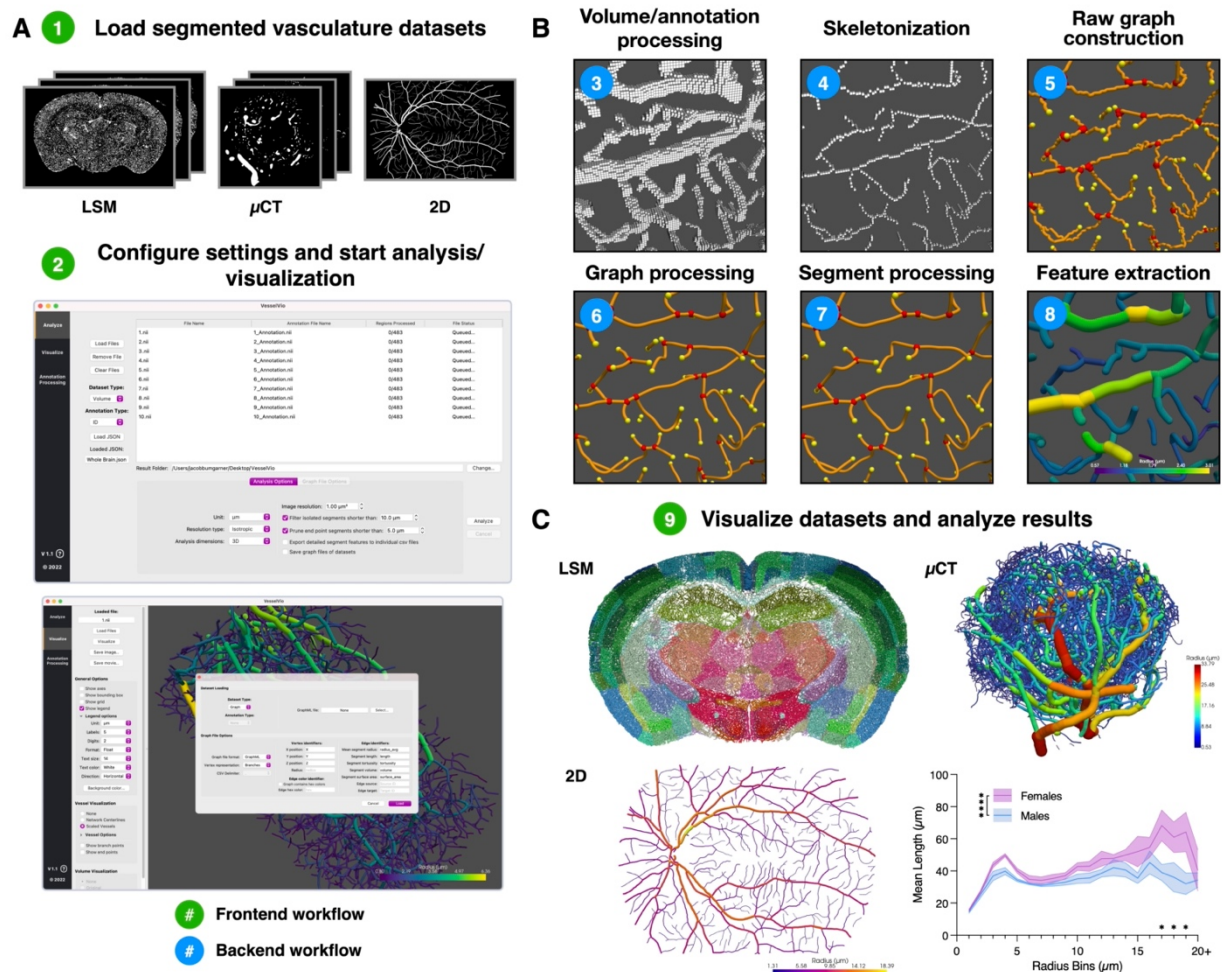


Figure 1. Overview of the VesselVio pipeline for vascular network processing. (A) Pre-binarized datasets, annotated volumes, and graphs are loaded into the program with custom analysis and feature export parameters. (B) Centerlines are extracted from the loaded datasets to create undirected graphs. Centerlines are smoothed, spurious branch points are filtered, and segments are processed before feature extraction. (C) The resulting datasets can be visualized for inspection of result accuracy with subsequent result export for analysis.

Centerline Extraction and Graph Construction Enable Detailed Network Feature Extraction

The features of a vascular network can be extracted by identifying the centerlines of the network and creating undirected graphs from the centerline points (Selle et al., 2002; Czech et al., 2011; Lee et al., 1994). Local neighborhood connectivity of the skeleton points is identified and used to create an undirected graph, $G = (V, E)$. Graphs are constructed using the Python package *igraph*, which was selected because of its efficiency with graph loading and shortest path finding, as well as its native compatibility with Windows and MacOS. Following initial graph construction, the datasets undergo a series of correction processes that eliminate spurious branch points, smooth centerlines, and remove isolated/endpoint segments at user-defined lengths (Figure 1B). These initial processing stages enable downstream quantifications of network and segment features (Figure 1C).

Spurious Branch Point Clique Filtering Improves Branch Point Quantification

After graph construction, network endpoints and branch points are identified by examining the degree of connectivity of the centerline vertices (Figure 2A), a commonly used approach (Arganda-Carreras et al., 2010; Hahn et al., 2019; Todorov et al., 2020). Although centerline neighbor 26-connectivity can be used to accurately detect endpoints, this approach spuriously over-labels branch points, leading to artificially inflated counts (Figure 2B). Some programs allow for interactive user input to correct mislabeled segments, inaccurate centerlines, or spurious branch points (e.g., *Imaris* (Quintana et al., 2019)). However, manually correcting branch points in 3D datasets can become tedious and time-intensive, particularly when datasets are many gigabytes large. Presented here is an automated approach to correct these spuriously labeled branch points.

Spuriously labeled branch points form small, all-to-all connected subgraphs in the constructed graphs, otherwise known as *cliques*. Previous techniques used to eliminate spurious branch point cliques rely on parent vessel orientations (Palágyi et al., 2006) or generate candidate weights based on 26-neighborhood connectivity (Staff et al., 2009). *VesselVio* implements a two-pass filter that eliminates spurious branch point cliques

through weighting based on the candidate vertex radius and the radii of neighboring vertices. Weighting candidates based on radius in addition to connectivity also mimics parent vessel hierarchy and improves segment radii calculations (Figure 2A).

To test our approach, a set of synthetically generated vasculature datasets with ground truth branch point labels were acquired and analyzed (Tetteh et al., 2020), and results were compared to previous programs (Arganda-Carreras et al., 2010; Todorov et al., 2020). VesselVio clique filtering resulted in a mean 97.4% accuracy of branch point labeling ($N = 20$). Further, the hierarchical branch point filtering of VesselVio results in a mean 2.6 % error that outperforms the mean 122.3 % error of previous techniques (Figure 2B).

Modified Euclidean Distance Calculations for Segment Radius Estimation

Several techniques exist for identifying vessel radii. One technique involves recording the largest maximally inscribed spheres that can rest within mesh vessel centerline points (Antiga et al., 2003; Antiga & Steinman, 2004), but this technique often depends on the creation of directed graphs (i.e., manually directed vessel hierarchy) and thus was not suitable for an automated pipeline. A similar method identifies the Euclidian distance between a vessel centerline and the center of the nearest non-vessel neighbor (Kirst et al., 2020; Mouches & Forkert, 2019). However, one pitfall to this approach is that vessels with near-resolution or at-resolution radii are incorrectly sized when their closest non-vessel neighbor is connected by a voxel face or a pixel edge (Figure 2C), leading to oversized single-voxel/-pixel vessels (Figure 2D). This issue is not as apparent for non-vessel neighbors connected to voxel edges/corners or pixel corners (Figure S1D-F). As such, a simple half-unit correction is implemented along specific orientations to preserve small-segment radii measurements for non-vessel neighbors connected to voxel faces and pixel edges (Figure 2C-F).

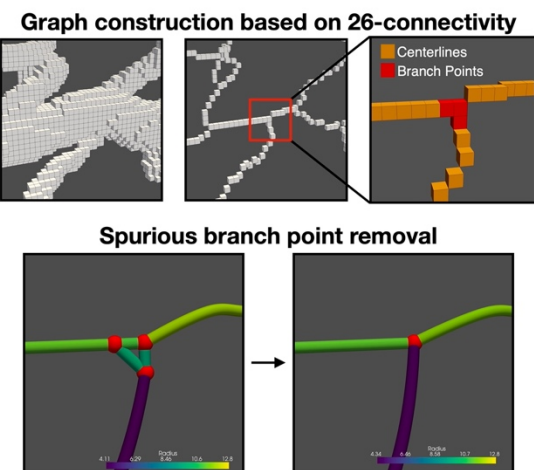
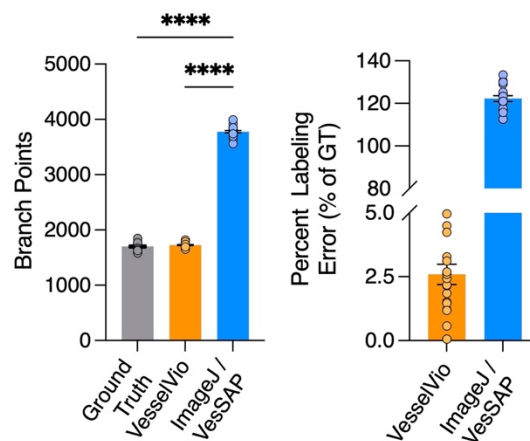
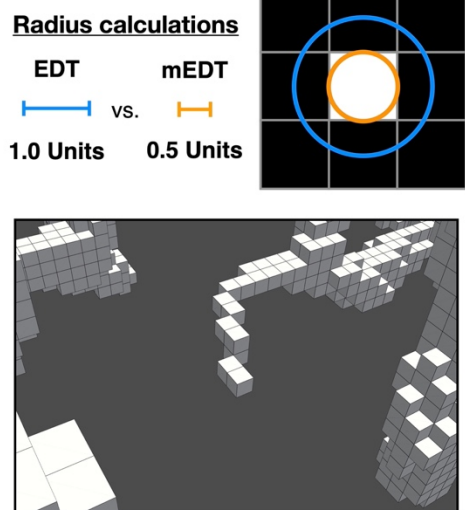
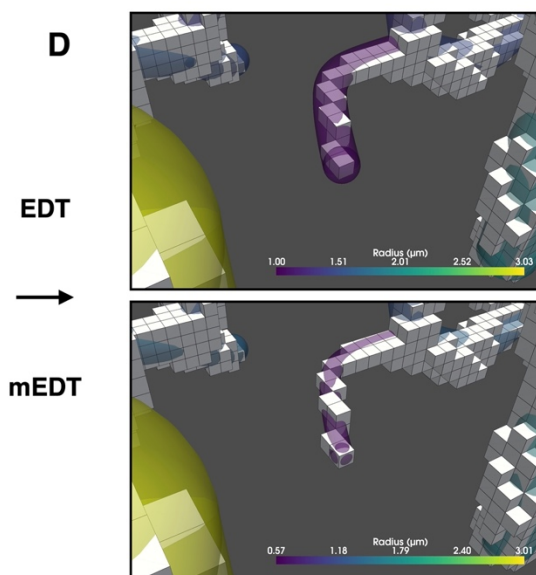
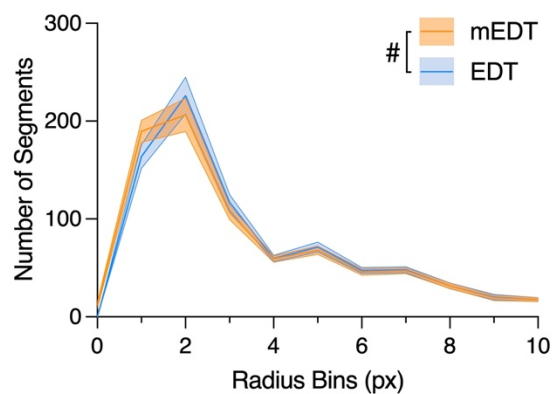
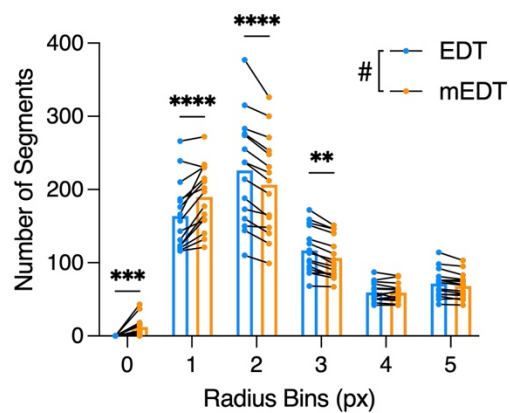
A**B****C****D****E****F**

Figure 2. Spurious branch point filtering and modified radius calculations improve feature quantification. (A) Clique clusters formed by spuriously labeled branch points are eliminated by weighting the radius of the candidate points and their neighbors. (B) Branch point filtering compared to ground-truth labeled synthetic vasculature datasets and an existing analysis pipeline ($n = 20$). (C) Modified Euclidean distance transform (mEDT) radius calculations for non-vessel neighbors connected to voxel faces or pixel edges. (D) Comparisons between EDT and mEDT radius calculations for an edge-vessel with single-voxel width at numerous points. (E) Comparison of the distribution of segments along 0-10 px radius bins from the glaucomatous HRF images ($n = 15$). (F) Repeated measures analysis of the change of radii in 0-5 px radius bins using EDT and mEDT. Data are represented as mean \pm SEM. (B) Data analyzed using a one-way ANOVA. (E and F) Data analyzed using a repeated measures two-way ANOVA. Multiple comparisons were conducted using Sidak's test. # - Interaction of Measurement method x Segment size. ** - $p < 0.01$, *** - $p < 0.001$, **** - $p < 0.0001$.

VesselVio Provides Detailed Feature Reporting

Following the identification of branch points, endpoints, and centerline radii, individual vessel segments, and their features can be isolated from vascular networks. Segment features extracted in the analysis pipeline include average length, radius, tortuosity, surface area, and volume. Next, this information is used to identify network features, including network volume and skeleton length, vessel segment partitioning, segment counts, and averages of segment features. Graph file exports from VesselVio enable users to independently identify relevant network characterization metrics, such as cohesion, network diameter, or clustering coefficient measurements (Hahn et al., 2019). Additionally, the centerline coordinate information extracted from the network is stored in the graph under a coordinates attribute, which can be accessed for custom geometric analyses. Lastly, by leveraging the same back-end analysis pipeline with an additional mesh-construction stage, VesselVio can render vascular datasets for visualization and inspection of results (Figure 1C).

3D Dataset Compatibility and Utility Testing

Analysis of Annotated Mouse Cerebrovasculature Imaged with LSM

To demonstrate compatibility with 3D volumes, multiple datasets were analyzed. First, publicly available BalbC mouse whole-brain vasculature datasets were acquired; these datasets were imaged with LSM (Todorov et al., 2020). To examine inter-regional network characteristics, 483 structures representative of the whole brain were selected using the Annotation Processing page (Figure S1C). The brains were subsequently loaded and analyzed ($n = 3$; Figure S2A-F). Branch point and segment density observations revealed connectivity variations among the major regions (Figure 3A, B). An average of 95.1 cm² of vascular surface area (Figure 3C) and an average 190.0 meters of vasculature were observed in the brains (Figure 3D). Further, an average of 3.5 million branch points were identified across the brain (Supplemental Table 1A). Network surface area and length were observed to be largely proportioned within the isocortex and fiber tracts (Figure 3C, D).

Analysis of Male and Female Mouse Inferior Colliculus Segmentations Imaged with μ CT

Next, cerebrovascular resin casts of female and male CFW mice ($n = 5$) were created as described previously (Quintana et al., 2019). Following cast creation, imaging, and volume reconstruction, the inferior colliculi (IC) were segmented and analyzed (Supplemental Video 2). Network feature analysis revealed two primary sex differences in these datasets: female mice had greater average segment length and segment surface area compared to males (Figure 3G, J), with peak differences occurring in the 17-19 μ m vessel ranges (Figure 3H, K). Numerous other features were analyzed, but no sex differences were observed (Figure 3M-R). Analysis runtimes of these datasets were compared to the VesSAP pipeline (Todorov et al., 2020). VesselVio analysis runtimes (32.2 ± 21.5 s) outperformed VesSAP runtimes (341.5 ± 78.9 s; Figure S2G). Further, the runtime scaling of the pipeline was tested; processing speed was observed to scale linearly with voxel counts (Figure S2H).

Compatibility Testing with Additional 3D Datasets

Several other 3D vasculature datasets were also examined. First, an isotropic rodent lymph node microvascular network imaged with synchrotron μ CT was visualized to reveal complex capillary networks (Supplemental Video 3) (Jafarnejad et al., 2019). Next, the arterial and venous cerebrovasculature of an individual human brain from a public dataset was composited and visualized (Supplemental Video 4) (Bernier et al., 2018). Finally, an anisotropic extraction of cerebrovasculature from C57 mice was examined (Supplemental Video 5) (Di Giovanna et al., 2018).

Together, the analysis and visualization of rodent cerebrovasculature, rodent lymph node, and human cerebrovasculature datasets demonstrate VesselVio's compatibility with 3D datasets generated with various imaging techniques.

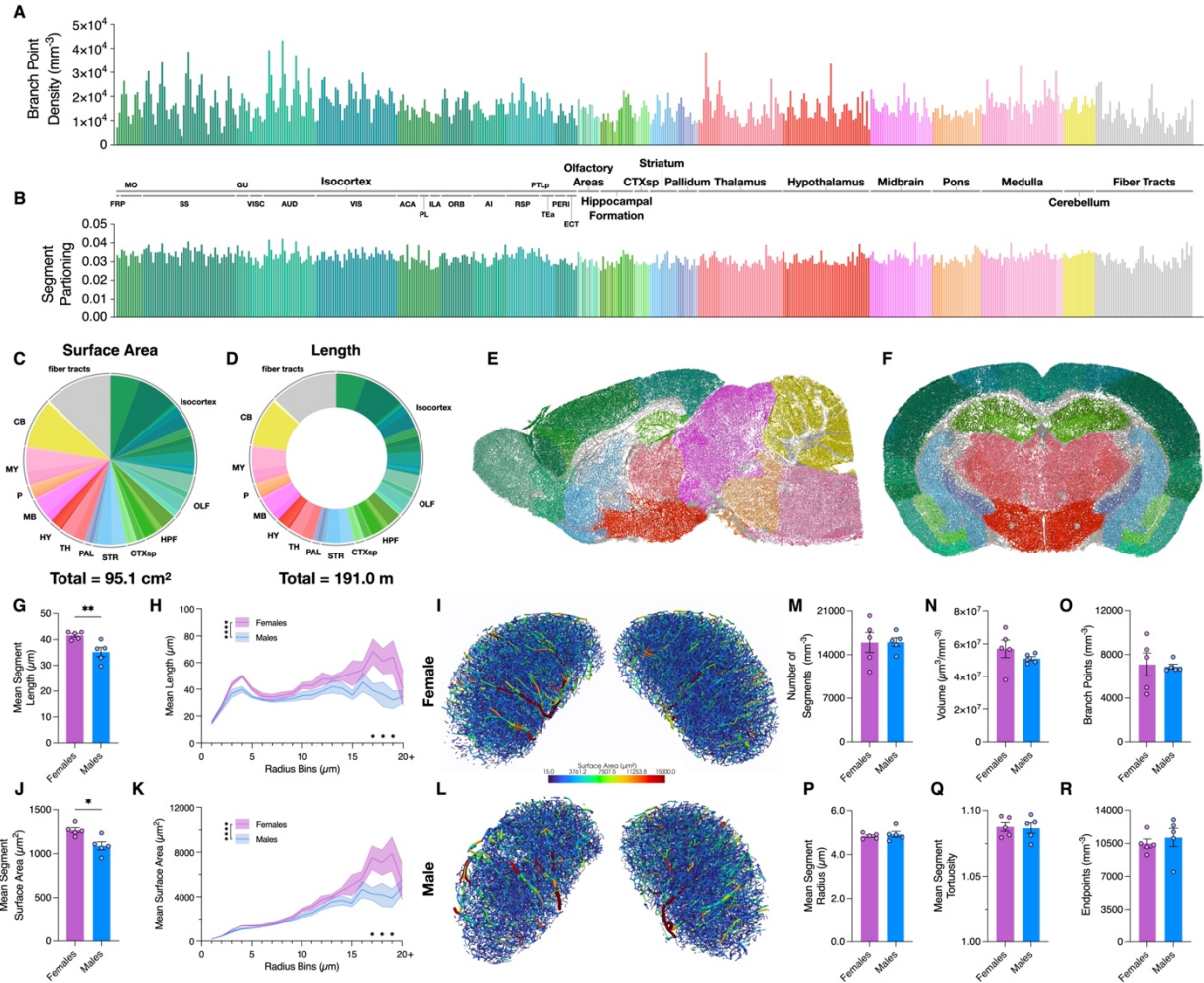


Figure 3. Analysis of BalbC whole-brain vasculature datasets and CFW inferior colliculus (IC) vasculature segmentations highlight 3D analysis capabilities. (A) Branch point and (B) vessel segment partitioning across 483 subregions ($n = 3$). (C) The mean total vascular volume and (D) network length of the BalbC datasets. (E) Sagittal and (F) coronal views of BalbC cerebrovasculature colored with the corresponding Allen Brain Atlas CCFv3 annotations. (G) Sex difference in the mean segment length and (H) the mean length of large diameter vessels in the IC ($n = 5$). (J) Sex difference in the mean segment surface area and (K) the mean surface area of large diameter vessels in the IC. (I and L) visualizations of the mean vessel surface area in the female and male IC. (M through R) Comparisons in the (M) number of segments, (N) network volume, (O) branch point density, (P) mean segment radius, (Q) mean segment tortuosity, and (R) endpoint density. Data are represented as mean \pm SEM. (G, J, M through R) Data were analyzed using a two-tailed student's t-test. (H and K) data analyzed using 2-way ANOVA. Multiple comparisons were conducted using Sidak's test. * - $p < 0.05$, ** - $p < 0.01$, **** - $p < 0.0001$.

Analysis of Human 2D Retinography Datasets Highlights Disease-Specific Vascular Phenotypes

To demonstrate the utility of VesselVio with 2D datasets, retinographs sourced from the HRF Image Database were analyzed and compared (Budai et al., 2013). This database contains high-resolution images of healthy control patients, patients with diabetic retinopathy, and patients with glaucomatous eyes. Analyses revealed several topological and segment-based differences among the groups. Relative to healthy controls, diabetic patients present with reductions in vessel percentage area fraction and surface area (Figure 4A, C), reduced average segment radius (Figure 4K), and increased vessel tortuosity (Figure 4L, O). Next, relative to healthy controls, glaucomatous retinas had reduced vascular surface area (Figure 4A, C), increased branch point counts (Figure 4D), increased segment counts (Figure 4F), and reduced average segment length (Figure 4J). Finally, the mean radius of segments was reduced in both groups compared to healthy controls, as well as the distribution of segments across small and medium radius bins (Figure 4K, M).

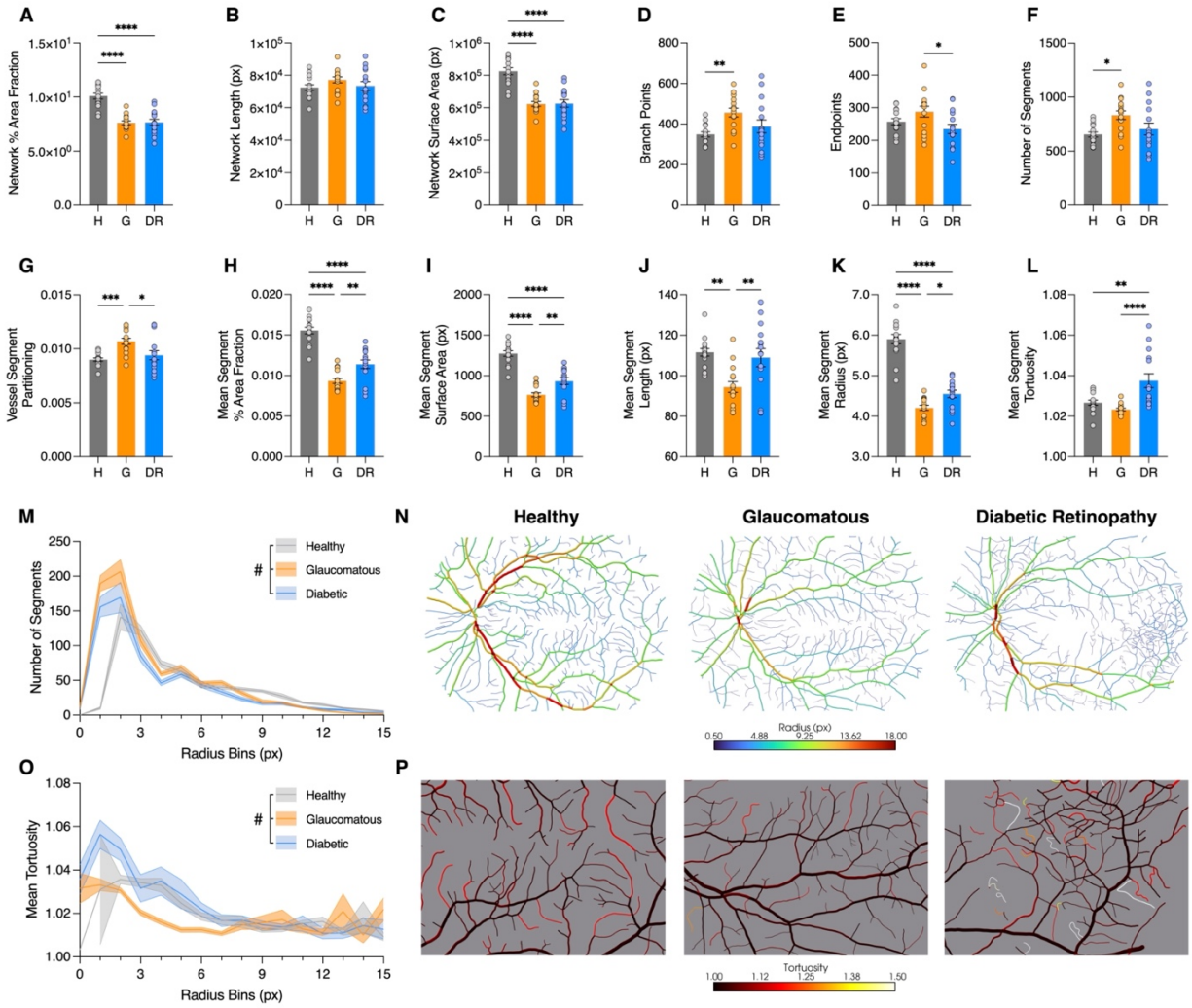


Figure 4. Analysis of images from the HRF database demonstrates compatibility with 2D datasets. (A through G) Comparisons of network features for health – H, diabetic – D, glaucomatous patients – G ($n = 15$), including (A) vascular percent area fraction, (B) length, (C) surface area, (D) branch points, (E) endpoints, (F) segment counts, and (G) segment partitioning. (H through L), Averaged segment features, including (H) segment percent area fraction (PAF), (I) surface area, (J) length, (K) radius, and (L) tortuosity. (M) Distribution of segments across 0-15 px radius segment bins. (O) Mean tortuosity of segments in 0-15 px radius segment bins. Data are represented as mean \pm SEM. (A through L) Data analyzed using a one-way ANOVA. (M and O) Data were analyzed using a two-way ANOVA. Multiple comparisons were conducted using Sidak's test. # - Main effect of health condition, * - $p < 0.05$, ** - $p < 0.01$, *** - $p < 0.001$, **** - $p < 0.0001$.

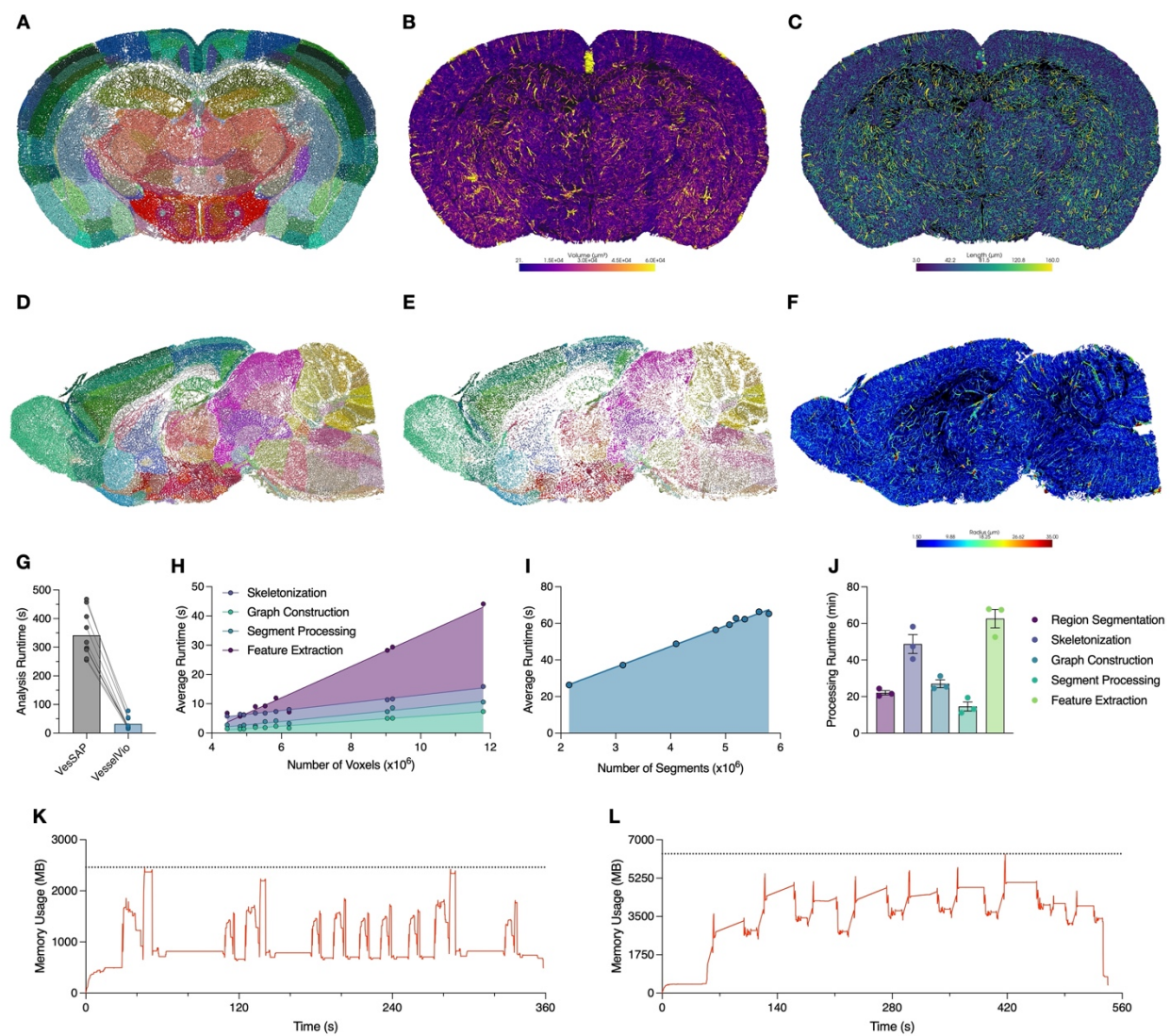


Figure S2.

Figure S1. VesselVio application interface; Euclidean distance transform (EDT) vs. modified EDT (mEDT) radius calculations; and Clique cluster filtering examples, related to Figures 1 and 2. (A) The analysis page, where binarized volumes and preconstructed graphs can be loaded and analyzed alongside dataset annotations. (B) The visualization page for observation of vascular networks. Meshes can be colored by segment radius, length, tortuosity, surface area, volume, or percent area fraction features with various color themes, depending on analysis parameters. Networks can also be visualized alongside original voxel/pixels or smoothed volume meshes. (C) The annotation processing page, where several default brain annotation trees from the Allen Brain Institute can be loaded for region-specific vascular analysis. Custom trees can also be loaded for other species or structures in addition to custom individual regions of interest. (D) mEDT distance calculations from the centerline point [V] to the nearest non-vessel neighbors connected by voxel faces or pixel edges [X] have 0.5-unit corrections. (E and F) mEDT distances to pixel corner-connected/voxel edge-connected [Y] as well as voxel corner-connected [Z] non-vessel neighbors are calculated in the same manner. (G, H, I) Example filtering results for class 1-3 clique clusters.

Figure S2. Coronal and sagittal slice views of a BalbC cerebrovasculature dataset; VesselVio processing speeds and memory usage profiles, related to Figure 3. (A-C) A coronal slice of cerebrovasculature showing (A) colorized annotations, (B) segment volume scalars, and (C) segment length scalars. (D-F) a sagittal slice of cerebrovasculature showing (D) colorized annotations, (E) vessel branch point density colorized with region annotations, and (F) segment radius scalars. (G) VesselVio vs. VesSAP analysis speeds of the ten inferior colliculus datasets ($n=10$; 3 speed trials per point). (H) Runtime scaling of the individual steps of the analysis pipeline for the ten inferior colliculus datasets (3 speed trials per point). (I) Linear runtime scaling ($n=9$; 3 speed trials per point) of the analysis of nine whole-brain pre-constructed graphs generated by Paetzold *et al.* 2021, *arXiv*. (J) Analysis runtimes for individual components of the analysis pipeline during the analysis of the three BalbC whole-brain datasets generated by Todorov *et al.* 2020, *Nature Methods*. (K) Memory usage profile of the analysis of the ten inferior colliculus datasets. (L) Memory usage profile of the analysis of the nine whole-brain pre-constructed graphs.

Discussion

I developed an open-source application, VesselVio, for the analysis and visualization of segmented 2D and 3D vasculature datasets. Focus was centered on constructing an analysis pipeline capable of producing quantitative characterizations of numerous whole-network and small-scale segment features. Ground-truth result comparisons and three sets of analyses were conducted to demonstrate the accuracy of VesselVio for vasculature analysis.

The first two sets of analyses examined whole-brain vascular characteristics of BalbC mice and sex differences in the cerebrovasculature of female and male CFW mice. There are many sex differences in the cardiovascular system, including vascular tone (Boese et al., 2017), microcirculation (Huxley & Kemp, 2018), and blood-brain barrier function (Robison et al., 2019; Humphries et al., 2017). In the latter analysis, I sought to examine how the cerebrovascular network in a specific nucleus, the inferior colliculus (IC), may differ by sex. IC analyses revealed differences in the average length and surface area of segments, particularly large segments. The resulting whole-brain analyses provided continued insight into inter-regional differences in vascular density (Kirst et al., 2020; Ji et al., 2021). These results serve to demonstrate 3D network analysis utility of VesselVio.

The third set of analyses examined retinal vascular networks of healthy controls, DR patients, and patients with glaucoma. Alterations in retinal microvascular networks are associated with vision loss (Carmeliet, 2005), and structural changes associated with excessive or reduced angiogenesis can also serve as indicators for underlying disease states (Lee et al., 2015; Selvam et al., 2018). Our analyses recapitulated previously reported reduced vessel area and diameter in glaucomatous eyes (Chan et al., 2017), as well as increased segment tortuosity of DR eyes (Sasongko et al., 2011). Contrasting results in DR eyes were noted compared to previous studies that reported increased vessel diameters (Bek, 2017; Klein et al., 2012), whereas I and others observed decreased diameters (Adhi et al., 2013; Fryczkowski et al., 1988). However, these differences may be due to the vessel type (the HRF vessels are not separated by arterial/venous hierarchy), or vascular region analyzed. Although VesselVio is not

intended to be used in any clinical diagnostic contexts, this analysis demonstrates the ability of this application to identify and characterize vascular network alterations in pathological conditions.

Future studies seeking to pinpoint detailed microvasculature alterations or broadly characterize regional vascular network features can employ the analytical and visualization components of VesselVio to obtain and enhance understanding of their results. In sum, VesselVio bridges the gap between modern vasculature imaging and analysis techniques by providing an optimized, open-source analysis pipeline and user-friendly application free for use.

Limitations of Study

In common with most analytical programs, the functionality of VesselVio is limited by the quality or resolution of the images that are loaded into the program. For example, if anisotropic datasets are loaded without pre-smoothing filters, then the skeletonization of these datasets can produce erroneous segments. To adjust for these errors, the option to prune small, connected end segments is included (Supplemental Video 6), but this pruning is unbiased and could hinder some types of analyses, such as angiogenesis assessments.

Rather than analyzing whole-brain datasets at once without subregion selection (e.g., brain stem analysis), in this pipeline, it is optimal to segment the brain into smaller regions prior to analysis (e.g., interbrain, midbrain, & hindbrain analysis). This is because region-based analysis occurs after region segmentation, rather. A limitation of this approach is that region annotation prior to skeletonization can lead to boundary effects, where vessels that cross annotation boundaries become disconnected during graph construction. The most notable effect of this disconnection would be altered endpoint counts. This approach was selected because of the offered speed optimizations and drastic memory usage reductions, as specific research questions often analyze subregional vasculature rather than whole-brain vasculature. In contrast, because of these boundary effects, it may be argued that VesselVio is most suitable for the analysis of small-to-medium-sized datasets where subregion analysis is not necessary. Future

approaches may seek to find a balance between this pipeline and other headless open-source pipelines, such as TubeMap (Kirst et al., 2020), that avoid boundary effects by requiring greater memory availability.

The presence of spurious branch points is unavoidable in the process of the implemented skeletonization algorithm and 26-connectivity graph construction. When holes or imaging artifacts are present in datasets, the skeletonization algorithm can also produce erroneous centerlines. VesselVio takes an automated approach to correct these spurious branch points and erroneous centerlines. A limitation of the automated branch point filtering algorithms may mean that in some instances, the automated correction of spurious branch points or erroneous centerlines may be less optimal than manual corrections. However, given that there can be hundreds to hundreds of thousands of spurious branch points in skeletonized datasets, manual corrections are not feasible. Future contributions may seek to implement user-guided graph construction that can match the efficiency of our automated approach.

Because VesselVio requires that binarized datasets be loaded for analysis, our radius calculations are based on the binary volume and its centerline. Though our mEDT radius calculations enable more detailed radius assessments than the traditional EDT calculations, this radius calculation method is likely not as effective as recent approaches that use vessel-filled datasets, which are created with corrosion casting or fluorescent gel perfusion techniques. This approach adjusts uncentered centerlines and calculates the radius of centerline voxels based on an iterative assessment of vessel fluorescence intensity and angle (Ji et al., 2021). As such, future contributions to this application may seek to support radius calculations for vessel-filled datasets that are based on this described approach (Ji et al., 2021).

Finally, because VesselVio is a GUI-based application primarily intended for standalone downloads, bundling the application for distribution acts as a limitation to speed. Bundling leads to slower performance in comparison to the non-bundled terminal-based version of our application or other headless analysis pipelines. Although functionality is equivalent between the bundled application and the application built from

terminals at runtime, terminal builds offer more efficiency on startup and analysis. Because of this, single-line executable usage of the app is detailed in our documentation.

References

- Adhi, M., Brewer, E., Waheed, N. K., & Duker, J. S. (2013). Analysis of morphological features and vascular layers of choroid in diabetic retinopathy using spectral-domain optical coherence tomography. *JAMA Ophthalmology*, 131(10), 1267-1274.
- Antiga, L., Ene-lordache, B., & Remuzzi, A. (2003). Computational geometry for patient-specific reconstruction and meshing of blood vessels from MR and CT angiography. *IEEE Transactions on Medical Imaging*, 22(5), 674-684.
- Antiga, L., & Steinman, D. A. (2004). Robust and objective decomposition and mapping of bifurcating vessels. *IEEE Transactions on Medical Imaging*, 23(6), 704-713.
- Arganda-Carreras, I., Fernández-González, R., Muñoz-Barrutia, A., & Ortiz-De-Solorzano, C. (2010). 3D reconstruction of histological sections: Application to mammary gland tissue. *Microscopy Research and Technique*, 73(11), 1019-1029.
- Bek, T. (2017). Diameter changes of retinal vessels in diabetic retinopathy. *Current Diabetes Reports*, 17(10), 1-7.
- Bernier, M., Cunnane, S. C., & Whittingstall, K. (2018). The morphology of the human cerebrovascular system. *Human Brain Mapping*, 39(12), 4962-4975.
- Bingol, O. R., & Krishnamurthy, A. (2019). NURBS-Python: An open-source object-oriented NURBS modeling framework in Python. *SoftwareX*, 9, 85-94.
- Boese, A. C., Kim, S. C., Yin, K.-J., Lee, J.-P., & Hamblin, M. H. (2017). Sex differences in vascular physiology and pathophysiology: estrogen and androgen signaling in health and disease. *American Journal of Physiology-Heart and Circulatory Physiology*, 313(3), H524-H545.
- Brett, M., Markiewicz, C. J., Hanke, M., Côté, M.-A., Cipollini, B., McCarthy, P., Jarecka, D., Cheng, C. P., Halchenko, Y. O., Cottaar, M., Larson, E., Ghosh, S., Wassermann, D., Gerhard, S., Lee, G. R., Wang, H.-T., Kastman, E., Kaczmarzyk, J., Guidotti, R., . . . freec84. (2020). nipy/nibabel: 3.2.1.
- Budai, A., Bock, R., Maier, A., Hornegger, J., & Michelson, G. (2013). Robust vessel segmentation in fundus images. *International Journal of Biomedical Imaging*, 2013.
- Carmeliet, P. (2005). Angiogenesis in life, disease and medicine. *Nature*, 438(7070), 932-936.

- Chan, K. K. W., Tang, F., Tham, C. C. Y., Young, A. L., & Cheung, C. Y. (2017). Retinal vasculature in glaucoma: a review. *BMJ Open Ophthalmology*, 1, e000032.
- Chapman, B. E., Berty, H. P., & Schulthies, S. L. (2015). Automated generation of directed graphs from vascular segmentations. *Journal of Biomedical Informatics*, 56, 395-405.
- Corliss, B. A., Mathews, C., Doty, R., Rohde, G., & Peirce, S. M. (2019). Methods to label, image, and analyze the complex structural architectures of microvascular networks. *Microcirculation*, 26(5), e12520.
- Csardi, G., & Nepusz, T. (2006). The igraph software package for complex network research. *InterJournal, Complex Systems*, 1695(5), 1-9.
- Czech, W., Dzwinel, W., Arodz, T., & Dudek, A. Z. (2011). Exploring complex networks with graph investigator research application. *Computing and Informatics*, 30(2), 381-410.
- Di Giovanna, A. P., Tibo, A., Silvestri, L., Müllenbroich, M. C., Costantini, I., Mascaro, A. L. A., Sacconi, L., Frasconi, P., & Pavone, F. S. (2018). Whole-brain vasculature reconstruction at the single capillary level. *Scientific Reports*, 8(1), 1-11.
- Epah, J., Pálfi, K., Dienst, F. L., Malacarne, P. F., Bremer, R., Salamon, M., Kumar, S., Jo, H., Schürmann, C., & Brandes, R. P. (2018). 3D imaging and quantitative analysis of vascular networks: a comparison of ultramicroscopy and micro-computed tomography. *Theranostics*, 8, 2117.
- Fryczkowski, A. W., Sato, S. E., & Hodes, B. L. (1988). Changes in the diabetic choroidal vasculature: scanning electron microscopy findings. *Annals of Ophthalmology*, 20(8), 299-305.
- Haft-Javaherian, M., Fang, L., Muse, V., Schaffer, C. B., Nishimura, N., & Sabuncu, M. R. (2019). Deep convolutional neural networks for segmenting 3D in vivo multiphoton images of vasculature in Alzheimer disease mouse models. *PLoS One*, 14(3), e0213539.
- Hahn, A., Bode, J., Krüwel, T., Solecki, G., Heiland, S., Bendszus, M., Tews, B., Winkler, F., Breckwoldt, M. O., & Kurz, F. T. (2019). Glioblastoma multiforme restructures the topological connectivity of cerebrovascular networks. *Scientific Reports*, 9(1), 1-17.

- Harris, C. R., Millman, K. J., van der Walt, S. J., Gommers, R., Virtanen, P., Cournapeau, D., Wieser, E., Taylor, J., Berg, S., & Smith, N. J. (2020). Array programming with NumPy. *Nature*, *585*(7825), 357-362.
- Humphries, K. H., Izadnegadar, M., Sedlak, T., Saw, J., Johnston, N., Schenck-Gustafsson, K., Shah, R. U., Regitz-Zagrosek, V., Grewal, J., & Vaccarino, V. (2017). Sex differences in cardiovascular disease—impact on care and outcomes. *Frontiers in Neuroendocrinology*, *46*, 46.
- Huxley, V. H., & Kemp, S. S. (2018). Sex-specific characteristics of the microcirculation. In P. L. M. Kerkhof & V. M. Miller (Eds.), *Sex-Specific Analysis Of Cardiovascular Function* (pp. 307-328). Springer.
- Jafarnejad, M., Ismail, A. Z., Duarte, D., Vyas, C., Ghahramani, A., Zawieja, D. C., Celso, C. L., Poologasundarampillai, G., & Moore, J. E. (2019). Quantification of the whole lymph node vasculature based on tomography of the vessel corrosion casts. *Scientific Reports*, *9*(1), 1-11.
- Ji, X., Ferreira, T., Friedman, B., Liu, R., Liechty, H., Bas, E., Chandrashekar, J., & Kleinfeld, D. (2021). Brain microvasculature has a common topology with local differences in geometry that match metabolic load. *Neuron*, *109*(7), 1168-1187. e13.
- Kelch, I. D., Bogle, G., Sands, G. B., Phillips, A. R. J., LeGrice, I. J., & Dunbar, P. R. (2015). Organ-wide 3D-imaging and topological analysis of the continuous microvascular network in a murine lymph node. *Scientific Reports*, *5*(1), 1-19.
- Kirst, C., Skriabine, S., Vieites-Prado, A., Topilko, T., Bertin, P., Gerschenfeld, G., Verny, F., Topilko, P., Michalski, N., & Tessier-Lavigne, M. (2020). Mapping the fine-scale organization and plasticity of the brain vasculature. *Cell*, *180*(4), 780-795. e25.
- Klein, R., Myers, C. E., Lee, K. E., Gangnon, R., & Klein, B. E. K. (2012). Changes in retinal vessel diameter and incidence and progression of diabetic retinopathy. *Archives of Ophthalmology*, *130*(6), 749-755.
- Lam, S. K., Pitrou, A., & Seibert, S. (2015). *Numba: A llvm-based python jit compiler*. In 7 (pp. 1-6).
- Lee, R., Wong, T. Y., & Sabanayagam, C. (2015). Epidemiology of diabetic retinopathy, diabetic macular edema and related vision loss. *Eye and Vision*, *2*(1), 1-25.

- Lee, T.-C., Kashyap, R. L., & Chu, C.-N. (1994). Building skeleton models via 3-D medial surface axis thinning algorithms. *CVGIP: Graphical Models and Image Processing*, 56(6), 462-478.
- LoweKamp, B. C., Chen, D. T., Ibáñez, L., & Blezek, D. (2013). The design of SimpleITK. *Frontiers in Neuroinformatics*, 7, 45.
- Mazzaferri, J., Larrivée, B., Cakir, B., Sapieha, P., & Costantino, S. (2018). A machine learning approach for automated assessment of retinal vasculature in the oxygen induced retinopathy model. *Scientific Reports*, 8(1), 1-11.
- Montoya-Zegarra, J. A., Russo, E., Runge, P., Jadhav, M., Willrodt, A.-H., Stoma, S., Nørrelykke, S. F., Detmar, M., & Halin, C. (2019). AutoTube: a novel software for the automated morphometric analysis of vascular networks in tissues. *Angiogenesis*, 22(2), 223-236.
- Mouches, P., & Forkert, N. D. (2019). A statistical atlas of cerebral arteries generated using multi-center MRA datasets from healthy subjects. *Scientific Data*, 6(1), 1-8.
- Niemisto, A., Dunmire, V., Yli-Harja, O., Zhang, W., & Shmulevich, I. (2005). Robust quantification of in vitro angiogenesis through image analysis. *IEEE Transactions on Medical Imaging*, 24(4), 549-553.
- Palágyi, K., Tschirren, J., Hoffman, E. A., & Sonka, M. (2006). Quantitative analysis of pulmonary airway tree structures. *Computers in Biology and Medicine*, 36(9), 974-996.
- Paxinos, G., & Franklin, K. B. J. (2019). *Paxinos and Franklin's the Mouse Brain in Stereotaxic Coordinates*. Academic Press.
https://play.google.com/store/books/details?id=x3aQDwAAQBAJ&source=gbs_api
- Puchades, M. A., Csucs, G., Ledergerber, D., Leergaard, T. B., & Bjaalie, J. G. (2019). Spatial registration of serial microscopic brain images to three-dimensional reference atlases with the QuickNII tool. *PLoS One*, 14(5), e0216796.
- Quintana, D. D., Lewis, S. E., Anantula, Y., Garcia, J. A., Sarkar, S. N., Cavendish, J. Z., Brown, C. M., & Simpkins, J. W. (2019). The cerebral angiome: High resolution MicroCT imaging of the whole brain cerebrovasculature in female and male mice. *NeuroImage*, 202, 116109.

- Robison, L. S., Gannon, O. J., Salinero, A. E., & Zuloaga, K. L. (2019). Contributions of sex to cerebrovascular function and pathology. *Brain Research*, 1710, 43-60.
- Rust, R., Kirabali, T., Grönnert, L., Dogancay, B., Limasale, Y. D. P., Meinhardt, A., Werner, C., Laviña, B., Kulic, L., & Nitsch, R. M. (2020). A practical guide to the automated analysis of vascular growth, maturation and injury in the brain. *Frontiers in Neuroscience*, 14, 244.
- Sasongko, M. B., Wong, T. Y., Nguyen, T. T., Cheung, C. Y., Shaw, J. E., & Wang, J. J. (2011). Retinal vascular tortuosity in persons with diabetes and diabetic retinopathy. *Diabetologia*, 54(9), 2409-2416.
- Schaad, L., Hlushchuk, R., Barré, S., Gianni-Barrera, R., Haberthür, D., Banfi, A., & Djonov, V. (2017). Correlative imaging of the murine hind limb vasculature and muscle tissue by MicroCT and light microscopy. *Scientific Reports*, 7(1), 1-12.
- Selle, D., Preim, B., Schenk, A., & Peitgen, H.-O. (2002). Analysis of vasculature for liver surgical planning. *IEEE Transactions on Medical Imaging*, 21(11), 1344-1357.
- Selvam, S., Kumar, T., & Fruttiger, M. (2018). Retinal vasculature development in health and disease. *Progress in Retinal and Eye Research*, 63, 1-19.
- Staff, I. E. E. E., Shi, R., Society, I. E. E. E. E. I. M. A. B., xue, T. L. G. D., & Engineers, I. O. E. A. E. (2009). *2009 2nd International Conference on Biomedical Engineering and Informatics*. IEEE. http://books.google.com/books?id=vmcGRQAACAAJ&hl=&source=gbp_api
- Sullivan, C. B., & Kaszynski, A. A. (2019). PyVista: 3D plotting and mesh analysis through a streamlined interface for the Visualization Toolkit (VTK). *Journal of Open Source Software*, 4(37), 1450.
- Tetteh, G., Efremov, V., Forkert, N. D., Schneider, M., Kirschke, J., Weber, B., Zimmer, C., Piraud, M., & Menze, B. H. (2020). Deepvesselnet: Vessel segmentation, centerline prediction, and bifurcation detection in 3-d angiographic volumes. *Frontiers in Neuroscience*, 14, 592352.
- Todorov, M. I., Paetzold, J. C., Schoppe, O., Tetteh, G., Shit, S., Efremov, V., Todorov-Völgyi, K., Düring, M., Dichgans, M., & Piraud, M. (2020). Machine learning analysis of whole mouse brain vasculature. *Nature Methods*, 17(4), 442-449.

- Tsai, P. S., Kaufhold, J. P., Blinder, P., Friedman, B., Drew, P. J., Karten, H. J., Lyden, P. D., & Kleinfeld, D. (2009). Correlations of neuronal and microvascular densities in murine cortex revealed by direct counting and colocalization of nuclei and vessels. *Journal of Neuroscience*, 29(46), 14553-14570.
- Wang, Q., Ding, S.-L., Li, Y., Royall, J., Feng, D., Lesnar, P., Graddis, N., Naeemi, M., Facer, B., & Ho, A. (2020). The Allen mouse brain common coordinate framework: a 3D reference atlas. *Cell*, 181(4), 936-953. e20.
- Zudaire, E., Gambardella, L., Kurcz, C., & Vermeren, S. (2011). A computational tool for quantitative analysis of vascular networks. *PLoS One*, 6(11), e27385.

Supplemental Video Titles (See Original Publication)

Supplemental Video 1. Mouse inferior colliculus vasculature manual segmentation, Related to Figure 3

Supplemental Video 2. Female mouse inferior colliculus vasculature visualization, Related to Figure 3

Supplemental Video 3. Mouse lymph node vasculature visualization, Related to STAR Methods

Supplemental Video 4. Human left-hemisphere cerebrovasculature visualization, Related to STAR Methods

Supplemental Video 5. Mouse cerebrovasculature visualization and application demonstration, Related to STAR Methods

Supplemental Video 6. Segment processing demonstration, Related to STAR Methods

Supplemental Table Title (See Original Publication)

Supplemental Table 1. Data from the analysis of mouse whole-brain, mouse inferior colliculus, human retinography, and synthetic vasculature datasets. Related to Figures 2-4.

Chapter 8

Acute Exposure to Artificial Light at Night Alters Hippocampal Vascular Structure in Mice

Published As:

Bumgarner, J. R., Walker II, W. H., Quintana, D. D., White, R. C., Richmond, A. A., Meléndez-Fernández, O. H., Liu, J. A., Becker-Krail, D. D., Walton, J. C., & Simpkins, J. W. (2023). Acute Exposure to Artificial Light at Night Alters Hippocampal Vascular Structure in Mice. *iScience*, 106996.

Introduction

The function of the cardiovascular system is coordinated across the day by circadian rhythms (Thosar et al., 2018). Circadian rhythms are endogenously driven cyclical processes with periods of about 24 hours (hence *circa*: about, *diem*: a day). These rhythms regulate and optimize the timing of various behavioral, physiological, and cellular processes in response to fluctuating energetic resource availability and the need for periods of rest (Rana et al., 2020). Proper alignment and integrity of circadian rhythms are vital for cardiovascular health (Thosar et al., 2018).

Cardiovascular circadian rhythms are generated and modulated across the day by both rhythms within the cardiovascular system and by rhythmic humoral and neuronal signaling cues that act on the cardiovascular system (Rana et al., 2020). For example, in mice, myocardial oxidative metabolism varies across the day in response to varying systemic energetic demands during sleep/wake activity (Young et al., 2001). Aortic tight-junction and extracellular matrix transcriptomic profiles also vary across the day, including rhythmic variation in genes such as claudin-5, junctional adhesion molecule-1, and elastin (Rudic et al., 2005). Circadian rhythms regulate several other cardiovascular processes, including vascular tone (Panza et al., 1991), blood pressure (Douma & Gumz, 2018), heart rate (Black et al., 2019), and angiogenesis (Jensen et al., 2014). The coordination of many of these processes is necessary for responding to and recovering from varying energetic needs across the day (Rana et al., 2020).

Alignment of internal circadian rhythms to the external environment is vital for health (Walker et al., 2020b). This alignment primarily occurs by solar light-dark signaling cues. Disruption of circadian rhythms leads to many negative physiological and behavioral consequences. Of the many circadian rhythm disruptors present in our modern environments, artificial light at night (ALAN) is the most pervasive (Bumgarner & Nelson, 2021). ALAN affects a growing 80% of the global human population; this metric exceeds 99% in the US and Europe (Falchi et al., 2016). Circadian rhythm disruption caused by ALAN exposure has detrimental effects on the cardiovascular system (Meléndez-Fernández et al., 2021).

Previous evidence has demonstrated the rapid consequences of short-term exposure to ALAN (Walker et al., 2020a). Mice exposed to just four nights of ALAN exhibited increased neuroinflammation, increased depressive-like behavior, and importantly, altered angiogenic transcript profiles in the hippocampus (Walker et al., 2020a). Female and male mice exposed to as few as four nights of 5 lux of ALAN exhibited reduced hippocampal VEGF-A expression and elevated *Vegfr-1* expression, indicating disrupted angiogenic signaling (Walker et al., 2020a). VEGF-A is a potent angiogenic signaling factor (Duffy et al., 2004); reduction of VEGF-A signaling can reduce vascular density and alter vascular function (Olfert et al., 2009; Gharakhanian et al., 2019). Moreover, VEGFR-1 is capable of potentiating angiogenesis (Park et al., 2016), but also can sequester VEGF-A and inhibit angiogenesis (Kikuchi et al., 2019).

Based on this evidence, I hypothesized that four nights of exposure to 5 lux of ALAN alters vascular structure in the hippocampus of CFW mice. I tested this hypothesis by examining 2D sections of lectin-labeled hippocampal vasculature, large-scale 3D reconstructions of hippocampal vasculature generated with corrosion casting, and hippocampal bulk-sequencing transcriptome profiling.

Methods

Animals

Adult female and male Swiss Webster (CFW) mice (7-8 weeks old; Charles River Laboratories) were obtained and given 1 week to acclimate to standard vivarium

conditions (14:10 h light: dark; 150 ± 25.0 lux, 22 ± 2 °C; 12.0 x 6.5 x 5.5” polycarbonate cages). Upon arrival, mice were housed in groups of five per cage. Following the acclimation period, mice were singly housed and randomly assigned to either the vivarium light-dark (LD) cycle or dim artificial light at night (ALAN; 14:10 h; $150 \pm 25.5 \pm 1$ lux) housing conditions with lights on at 05:00 h and off at 19:00 h. ALAN sources were Luma5 Standard LED light strips (1.5 W/ft, 5000K “cool white”, 1200 lumens; Hitlights Inc.); lux calibrations were conducted by placing a Mavolux 5023C illuminance meter (Gossen) in the center of an empty cage with the light sensor facing towards the ceiling. After group assignment, the animals were placed in their respective lighting conditions for a total of four nights prior to lectin perfusion, corrosion casting, or tissue collection. Food (2018 Teklad; Envigo) and reverse osmosis water were provided *ad libitum* throughout the entire duration of the experiment. All studies were approved by the West Virginia University Institutional Animal Care and Use Committee, and animals were maintained in accordance with NIH Animal Welfare guidelines.

Resin Perfusions

Between 12:00-16:00 h on the day following the 4th experimental night of LD or ALAN conditions, resin casting perfusions were conducted as described previously (Quintana et al., 2019). Prior to perfusion, animals were deeply anesthetized with isoflurane and injected intraperitoneally (i.p.) with 25 U of heparin (63739-931-28; McKesson Corporation) in 250 μ L of saline. Following the absence of a response to the pedal reflex tests (confirming deep anesthetization), mice were transcardially perfused at a flow rate of 4 mL/min first with 15 mL of 25U/mL heparin in saline and then with 15 mL of 4% paraformaldehyde dissolved in 1x PBS (#416780030; Acros Organics). Next, animals were perfused with PU4ii resin that was formulated as described by the manufacturer’s guidelines (VasQTec). Experimental groups were stratified across multiple days of perfusions.

Five days following the resin perfusions, the craniums were dissected and decalcified with a 12 h wash of 5% formic acid (BDH4554; VWR International). The brains were then dissected, and the remaining tissue was removed from the casts with two 12 h

washes of 7.5% KOH (BDH7622; VWR International) at 50°C. Casts were rinsed with Milli-Q water and subsequently osmicated in 1% osmium tetroxide (#75632; Sigma Aldrich) for 12 h. Casts were then washed, frozen, and lyophilized prior to being mounted for μ CT scanning.

μ CT Scanning

The resulting cerebrovascular casts were imaged on a SkyScan 1272 (Bruker) with the following parameters: 50 kV/ 200 μ A with no filter; 360° rotation in step sizes of 0.17°; 900 ms exposures; 4 frame averages/step to produce an isotropic voxel resolution of 2.7 μ m³. Scans were reconstructed using NRecon (Bruker) with the following parameters: beam hardening corrections at 15%, ring artifact reduction at 3, smoothing at 0, custom alignment compensations set for each sample, and 0.02-0.40 dynamic image ranges. Scan and reconstruction parameters were determined based on the manufacturer's guidelines. Following reconstructions, the volumes were resliced coronally. Volumes were then loaded into CTAn (Bruker), and the dorsal hippocampal CA1, CA2/3, and dentate gyrus volumes between the approximate bregma -1.6 and -2.6 coordinates were manually segmented using the transverse hippocampal vessels and main vessels of the hippocampus (Zhang et al., 2019) as intra- and inter-regional boundary guides alongside the p56 Allen Institute mouse brain atlas. Manual segmentations were interpolated at distances of 0.1 mm. Segmented vasculature volumes from the casting data were analyzed using VesselVio 1.1.1 (Bumgarner & Nelson, 2022), with a 10 μ m filter for isolated segments and a 5 μ m filter for endpoint segment pruning to account for skeletonization errors.

RNA-Sequencing

Between 1200-1400 h on the day following the fourth night of experimental housing conditions, brains were collected from a separate cohort of mice. Following rapid cervical dislocation and decapitation, brains were dissected and stored in RNAlater at -80 °C (Thermo Fisher) until subsequent hippocampal dissections. RNA was extracted from hippocampal tissue using TRIzol (Invitrogen), and the quantity and purity of RNA

were examined using a NanoDrop One (Thermo Fisher). All samples had 260/280 nm absorption ratios above 1.8. Short-read paired-end 150 bp sequencing was conducted by Genewiz using Illumina HiSeq X machines, with a sufficiently high RNI integrity number (RIN) confirmed by Genewiz prior to sequencing. Sequence reads were trimmed using Trimmomatic v.0.36 (Bolger et al., 2014), and trimmed reads were mapped to the GRCm38 reference genome using STAR v.2.5.2b (Bolger et al., 2014; Dobin et al., 2013). ENSEMBL gene ids were converted to gene symbols using biotools.fr. RNA-Seq data were analyzed using DESeq2 (Love et al., 2014). Prior to analysis, lncRNA, miRNA, and pseudogenes were removed from the results list. Gene ontology and pathway analyses were conducted with Metascape.

Tomato Lectin Perfusion and Lectin Analysis

Mice were intravenously (tail vein) injected with 200 μ L of DyLight-594 tagged tomato (*Lycopersicon esculentum*) lectin in 0.1 M PBS (0.5 mg/ml; Vector Laboratories). The lectin solution was allowed to circulate for 5 minutes, and then mice were given a lethal overdose of sodium pentobarbital followed by transcardial perfusion with ~50 ml 4% paraformaldehyde (PFA) in 0.1 M PBS. The brain was dissected and post-fixed overnight in fresh 4% PFA solution. Tissues were cryoprotected in 30% sucrose in 0.2 M phosphate buffer until sunk. Tissues were frozen on dry ice and then maintained at -80 °C until sectioning. Tomato lectin injections and tissue collection occurred between 14:00 and 16:00 h.

Tissue was subsequently sectioned at 40 μ m, and hippocampal regions between bregma -1.23 and -3.63 were imaged using a BZ-X710 microscope (Keyence). The images were loaded into ImageJ, and the RGB channels were split. The three hippocampal regions of interest – the CA1, CA2/3, and dentate gyrus (DG) – were then manually outlined on the DAPI channel (blue) while referencing the adult mouse Allen Brain Reference Atlas. Outlines were then applied to the lectin channel (red), which was thresholded using the default algorithm to measure the percent area fraction of lectin staining. Percent area fractions were then weighted across the area of all sections for

individual animals. Lectin image processing was conducted with FIJI v2.3.0 (Schneider et al., 2012).

Quantification and Statistical Analysis

The CA1 & DG region lectin data were analyzed using unpaired *t*-tests and the CA2/3 region lectin data were analyzed with a Mann-Whitney test based on a non-normal distribution of data. The specific test used for the analysis of each region was determined by examining the normality of residuals as determined by the Shapiro-Wilk test and the similarity between variances as determined by F-test for variance. Outliers were detected in the lectin data using Grubb's test; no more than one outlier was removed per group. All lectin perfusion tests were one-tailed based on our *a priori* hypothesis supported by previous evidence (Walker et al., 2020a). The vascular corrosion cast data were analyzed using 2-way ANOVAs; *a priori* planned comparisons between LD and ALAN conditions within sexes were made using Fisher's LSD. Outlier detection in the lectin vascular data was conducted using Grubb's test; outliers were not examined in the casting data due to reduced sample sizes. Mean differences with P-values < 0.05 were considered statistically significant. All analyses were conducted using Prism 9 (GraphPad). All statistical results and analyses are available in the Summary Table uploaded to Harvard Dataverse; the DOI can be found in the Key Resources Table.

Results

ALAN Alters Hippocampal Vascular Density

To assess the effects of ALAN exposure on hippocampal vascularity, I first perfused fluorescently labeled lectin, a carbohydrate-binding protein used to label vasculature. Following imaging, the CA1, CA2/3, and dentate gyrus of the hippocampus were manually segmented to examine the percent area fraction (PAF) of lectin staining (Figure 1A-H). There were no sex differences in lectin PAF (see Summary Table), so the results between sexes were combined for subsequent lectin analyses. Reduced vascular density was observed in both the CA1 (Figure 1I) and DG (Figure 1K) of mice exposed to ALAN, supporting the hypothesis that ALAN disrupts cerebrovascular structure.

Segmented lectin percent area fraction was not significantly different in the CA2/3 of mice exposed to ALAN (Figure 1J).

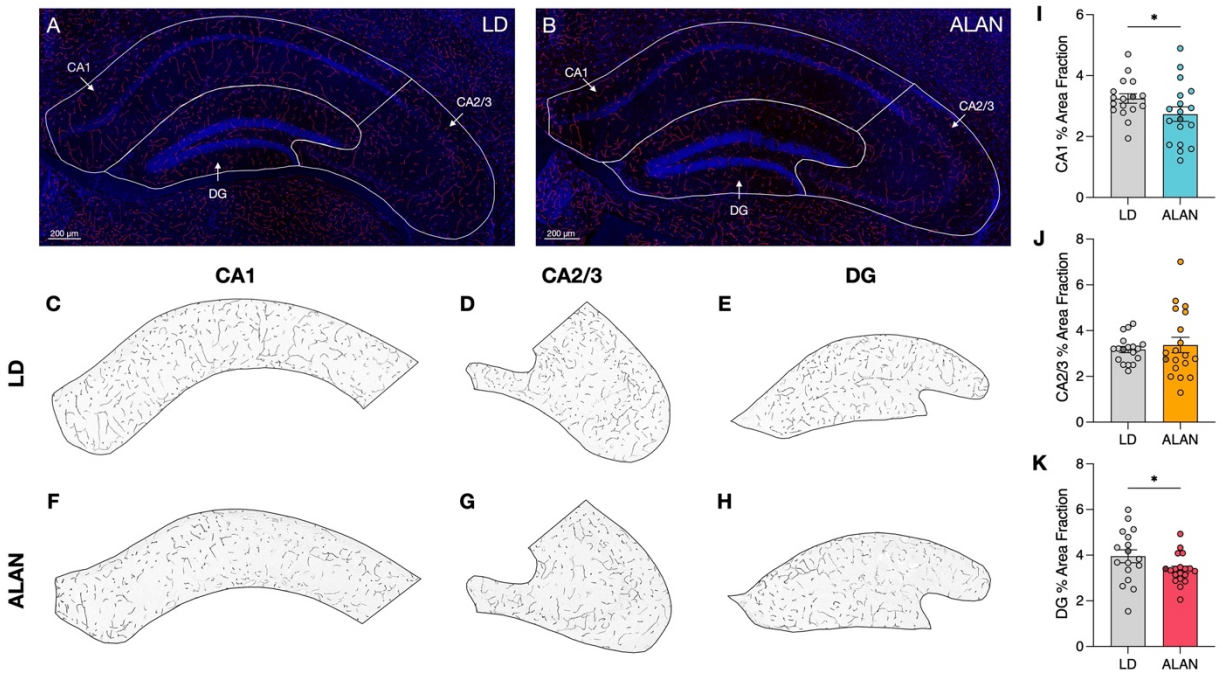


Figure 1. ALAN Exposure Reduces Lectin Percent Area Fraction in Hippocampal CA1 and DG. **A, B.** Lectin perfusion enabled the visualization and segmentation of the CA1, CA2/3, and dentate gyrus (DG) of the hippocampus of male and female mice exposed to either LD (**C-E**) or artificial light at night (**F-H**). Percent area fraction was calculated and compared in the CA1 (**I**), CA2/3 (**J**), and the DG (**K**) ($n = 9$ females/group, $n = 9-10$ males/group). Data were analyzed with a one-tailed t -test, as supported by an *a priori* hypothesis generated from evidence by Walker et al., 2020. Scale bars represent $200 \mu\text{m}$. Data are represented as mean \pm SEM. * $p < 0.05$.

ALAN Exposure Alters the Density of Small-to-Medium Vessels in the Hippocampus

Following the observation of reduced lectin-labeled vascular density, I sought to comprehensively examine the effects of ALAN on region-wide hippocampal vascular networks. To do this, cerebrovasculature casts were created using a corrosion casting procedure and were imaged using μ CT (Quintana et al., 2019). This enabled the 3D segmentation of the CA1, CA2/3, and DG for subsequent quantification of numerous vascular characteristics.

Vascular networks can be characterized by examining the whole-network topology as well as the mean features of individual segments (Kirst et al., 2020). First, the density of hippocampal vascularization by varying radii of vessels per mm^3 of tissue was examined in all three segmented regions. Female and male groups were separated in the subsequent analyses due to sex differences in several vascular features across the examined regions (e.g., Fig 3A-C, Supplemental Figure 2). In both the CA1 (Figure 2A; $n_{\text{females}} = 7-8$, $n_{\text{males}} = 5-7$) and the CA2/3 (Figure 2B) of female mice exposed to ALAN, the density of vessels with radii of 4-7 μm was reduced. Similarly, ALAN exposure reduced the density of 3-6 μm radius vessels in the DG of male mice (Figure 2F; Supplemental Video 1). In the female CA1 and CA2/3 as well as the DG of male mice exposed to ALAN, there was an interaction between exposure to ALAN and the size of vessels that were reduced. There were no reductions in the vascular density in the DG of female mice (Figure 2C) or the CA1 or CA2/3 of male mice exposed to ALAN (Figure 2D, F).

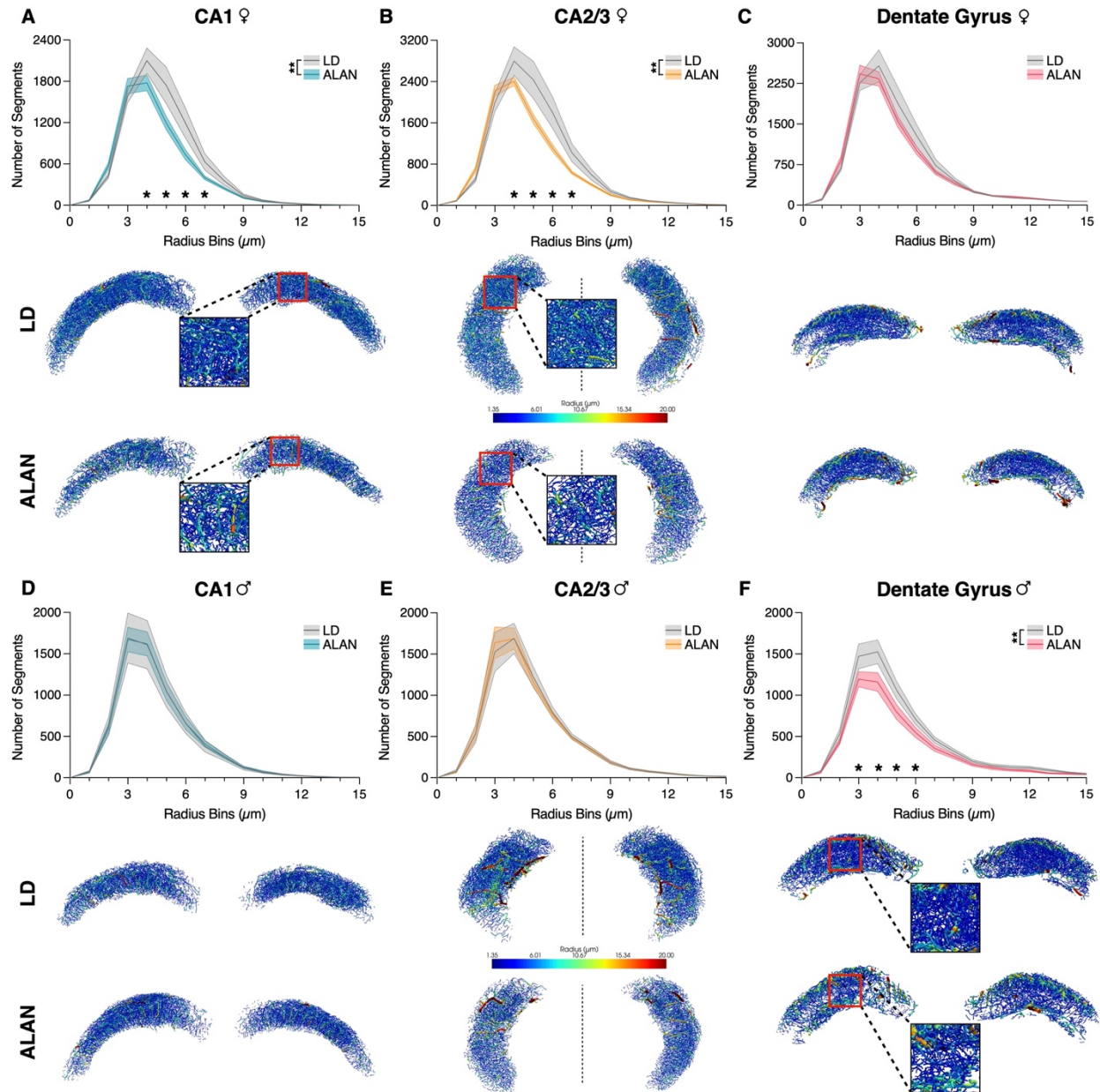


Figure 2. ALAN alters the density of small-to-medium-sized vessels in the hippocampus of female and male mice. Vessel density by radius bins was assessed in female hippocampal CA1 (**A**), CA2/3 (**B**), and dentate gyrus (**C**) and in male hippocampal CA1 (**D**), CA2/3 (**E**), and dentate gyrus (**F**) ($n = 7-8$ females/group, $n = 5-7$ males/group). Data were analyzed using a two-way ANOVA with ALAN and radius size as the main effects. Sexes were analyzed separately. The dentate gyri in **F** have a scale bar from 1.35 – 25.0 μm . Data are represented as mean \pm SEM. * $p < 0.05$, ** $p < 0.01$.

ALAN Alters Network Structure and Topology in the CA2/3 of Female Mice

To further understand the effects of ALAN on whole-network vascular characteristics, I examined network volume and surface area in the corrosion casting μ CT datasets. To do this, dorsal hippocampal vasculature was manually segmented, as described in the methods. In the CA2/3 of female mice, ALAN reduced the total network volume (Figure 3A) as well as the total network surface (Figure 3B) area per mm^3 of segmentation volume. Volume and surface area differences were not observed in the CA1 or DG of either sex exposed to ALAN (Supplemental Figure 1). Next, the effects of ALAN on the mean characteristics of individual segments were examined. ALAN increased the mean tortuosity (Supplemental Figure 2F) and reduced the mean radius (Supplemental Figure 2H) of vessels in the CA2/3 of female mice. No other alterations in individual segment characteristics were observed (Supplemental Figure 2). Lastly, to examine the effects of ALAN on vascular network topology, I examined branch point and endpoint density as metrics of connectivity. ALAN exposure reduced network branch point density (Figure 3C) and increased endpoint density (Figure 3D) in the CA2/3 of female mice. These effects were not observed in any male hippocampal regions or the CA1 or DG of female mice (Supplemental Figure 1).

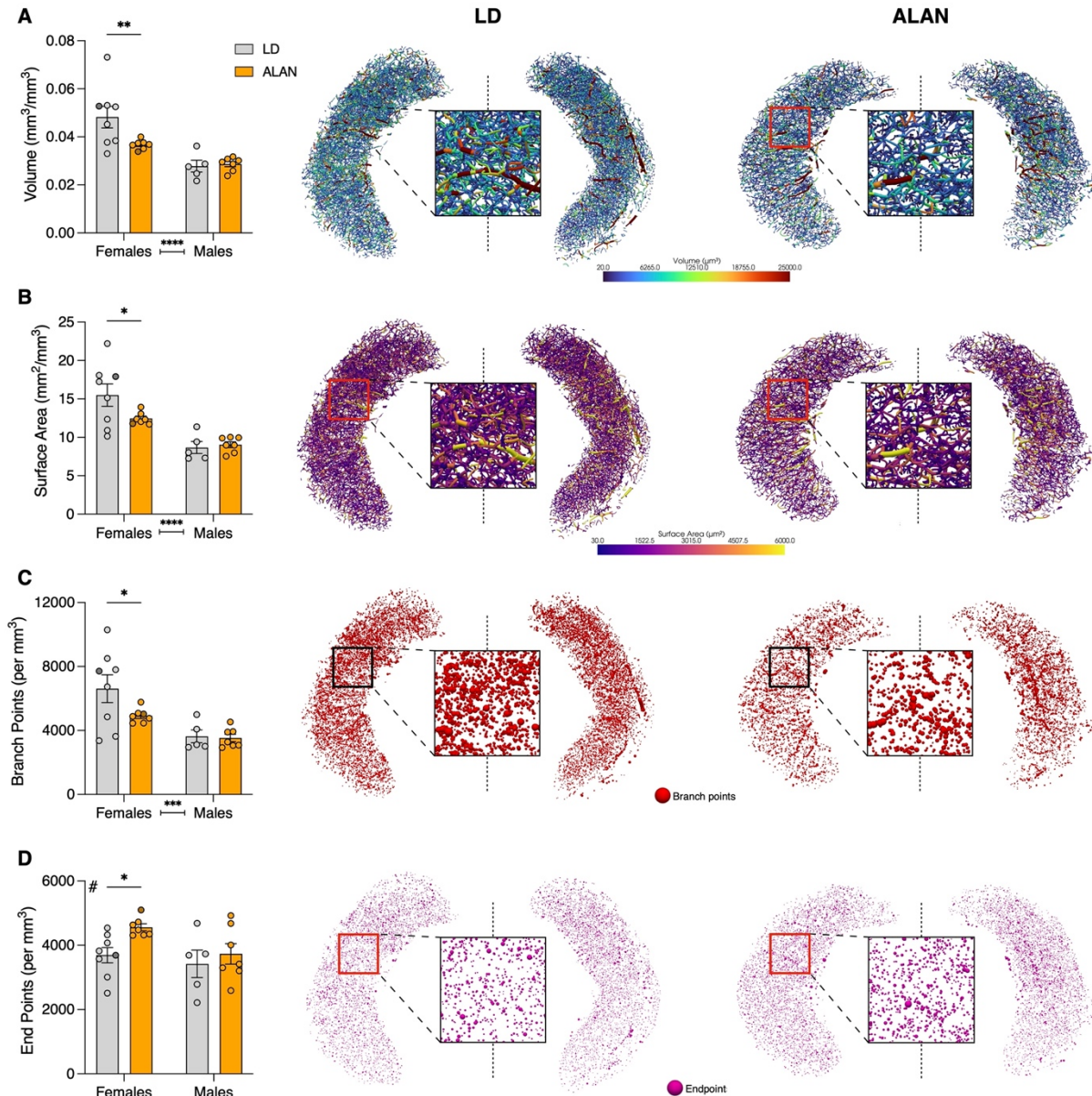


Figure 3. ALAN alters the structure and topological features of the CA2/3 in female mice. The effects of ALAN on network volume (**A**) and surface area (**B**) were examined. Network connectivity was also assessed by examining branch point (**C**) and endpoint density (**D**) ($n = 7-8$ females/group, $n = 5-7$ males/group). Data were analyzed using a two-way ANOVA and planned multiple comparisons within sex were made using Fisher's LSD. # - Main effect of lighting condition. Data are represented as mean \pm SEM. * $p < 0.05$, ** $p < 0.01$, *** $p < 0.001$, **** $p < 0.0001$.

ALAN Alters Hippocampal Vascular Transcriptomic Profiles

Finally, to gain initial insight into the mechanisms by which ALAN exposure leads to altered hippocampal vasculature, I performed bulk-tissue RNA-sequencing on hippocampal dissections of mice exposed to four nights of ALAN. Several hundred differentially expressed genes were observed (Figure 4A, B), with minor overlap between sexes (Figure 4C). In females, I observed alterations in gene ontologies associated with extracellular matrix maintenance and organization, which included upregulated *Bmp7* and downregulated, *Col4a4*, *Col20a1*, and *Lamc2*, *Lama2*, among others (Figure 4D, F). Additional alterations in genes associated with angiogenesis were also observed in females exposed to ALAN, including downregulated *Nid1* and *Ctsg*. In male mice exposed to ALAN, I observed alterations of gene ontologies associated with blood vessel morphogenesis, angiogenesis, and blood-brain barrier maintenance, including upregulated *Fgfr2*, *Anxa2*, and *Mcam* and downregulated *Notch4*, *Coro1c*, and *Klf4* (Figure 4G).

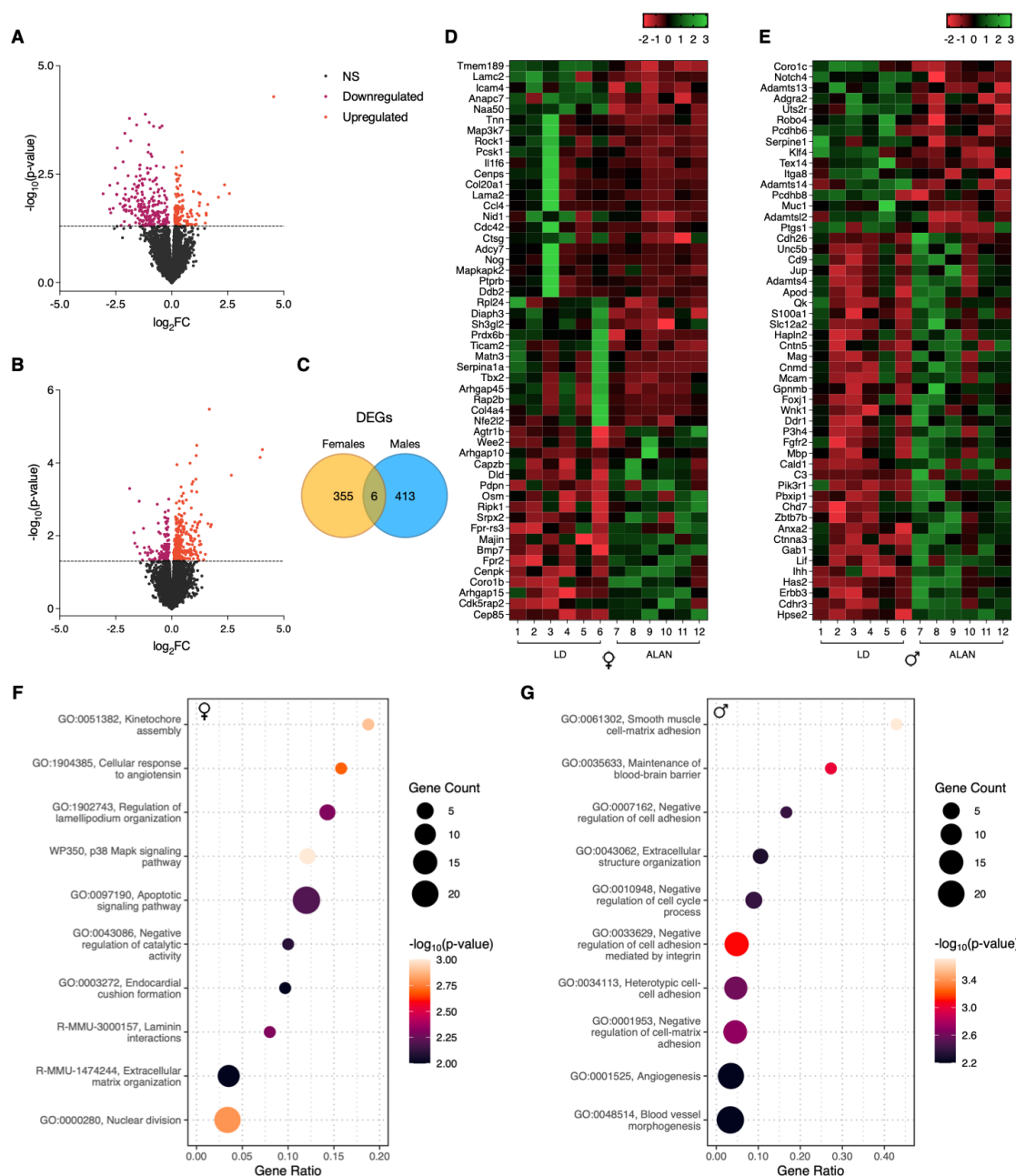
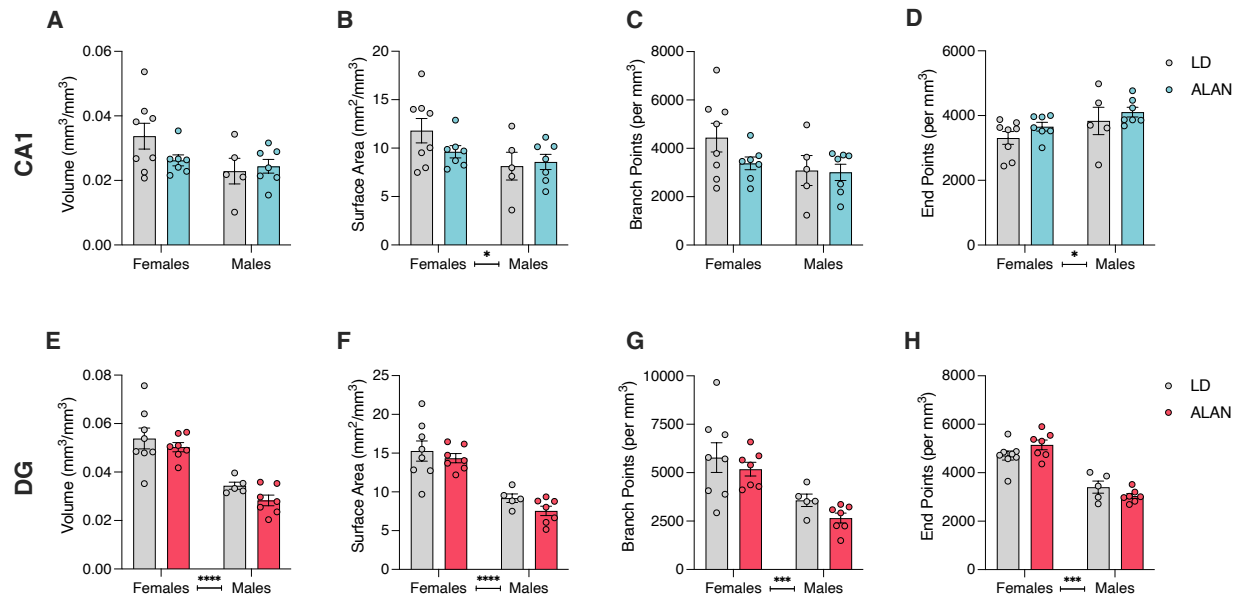
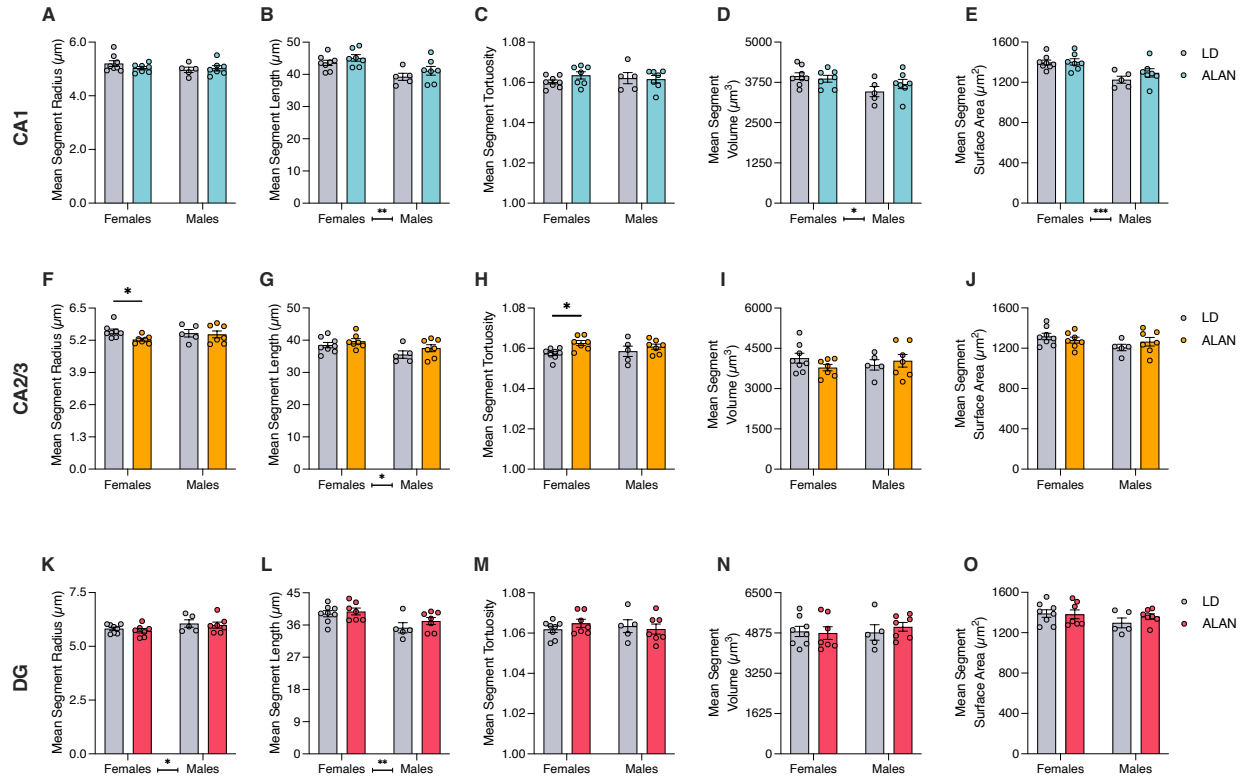


Figure 4. ALAN exposure alters gene expression related to angiogenesis, extracellular matrix composition, and blood-brain-barrier integrity. **A, B.** Volcano plots visualizing differentially the results of the sequencing analyses. **C.** Venn diagram showing overlap of differentially expressed genes between sexes. **D, E.** Heatmaps visualizing differentially expressed genes tied to relevant extracellular matrix organization, blood vessel morphogenesis, or angiogenesis pathways. **F, G.** Gene ontology bubble plots demonstrating significantly altered biological pathways (n = 6 animals/group).



Supplemental Figure 1 – Network structure and connectivity features of the CA1 and DG following ALAN exposure, related to Figure 3. **A, E.** Vascular volume, **B, C.** Surface area. **C, G.** Branch point density, **D, H.** Endpoint density is not modulated in the CA1 (**A-D**, blue) or dentate gyrus (**E-H**, red) of mice exposed to ALAN. Data were analyzed using a two-way ANOVA. Data are represented as mean \pm SEM. * $p < 0.05$, *** $p < 0.001$, **** $p < 0.0001$.



Supplemental Figure 2 – ALAN alters various mean segment features in the CA1, CA2/3, and DG of mice, related to Figure 3. No mean segment features were altered in the CA1 (**A-E**, blue) or dentate gyrus (**K-O**, red) of mice exposed to ALAN. ALAN exposure reduced the mean segment radius (**F**) and increased vessel segment tortuosity (**H**) in the CA2/3 (orange) of female mice. Mean segment length, volume, and surface area were not modulated in the CA2/3 of mice exposed to ALAN (**G**, **I**, **J**). Data are represented as mean \pm SEM. * $p < 0.05$, ** $p < 0.01$, *** $p < 0.001$.

Discussion

The present study demonstrates that exposure to ALAN on a short time scale can rapidly alter the structure and density of vasculature in the hippocampus of male and female mice. Our preliminary analysis of vascular density using lectin perfusion indicates reduced vascularity in both the CA1 and the DG of the hippocampus. Following this preliminary analysis, 3D hippocampal vascular network alterations following exposure to ALAN were examined using corrosion casting. 3D structural analysis revealed that ALAN reduces the density of small-to-medium-sized vessels in the CA1 and CA2/3 of female mice and the DG of male mice. Moreover, in the CA2/3 of female mice, ALAN reduces vascular volume and surface area, increases vessel tortuosity, and alters network topology as indicated by decreased branch point and increased endpoint density. Follow-up examination of hippocampal transcriptome profiles indicates altered gene patterns associated with vascular morphogenesis and extracellular matrix organization.

The evidence presented in this study is consistent with several lines of work that demonstrate that circadian rhythm disruption can directly impair vascular structure and function (Chellappa et al., 2019). For example, rats exposed to dim ALAN at levels of 1-2 lux for 5 weeks exhibited reduced nocturnal systolic blood pressure, altered heart rate rhythms, and altered cardiovascular responses to norepinephrine (Molcan et al., 2019). In the same study, exposure to ALAN for 2 weeks elevated aortic expression of endothelial nitric oxide synthase (Molcan et al., 2019). Similar cardiovascular disruption is observed in spontaneously hypertensive rats exposed to dim ALAN (Rumanova et al., 2019). ALAN exposure increased systolic blood pressure and reduced systolic blood pressure variability (Rumanova et al., 2019). Humans exposed to a 3-day simulated shift work paradigm exhibited elevated both systolic and diastolic blood pressure as well as reduced nocturnal systolic blood pressure dipping (Morris et al., 2016).

In the context of cardiovascular pathology, a week of exposure to ALAN in a rodent model of cerebral ischemia led to increased mortality, neuroinflammation, and IBA1 immunoreactivity, a marker for activated microglia/macrophages (Fonken et al., 2019). Moreover, a single night of ALAN exposure increases infarct penumbral volume following experimental stroke in mice (Weil et al., 2020). Other work has demonstrated that Per2

is necessary for the proper function of endothelial progenitor cells following myocardial infarction in mice, although cell function was examined *in vitro* (Sun et al., 2014).

ALAN exposure may also have indirectly induced the vascular structural alterations observed in this study via inflammation. ALAN exposure induces states of neuroinflammation in humans and other species (Walker et al., 2021), and inflammation is associated with vascular remodeling (Intengan & Schiffrin, 2001; Muramatsu et al., 2012; Pearson-Leary et al., 2017). Siberian hamsters exposed to ALAN exhibit elevated hippocampal *Tnf* (Bedrosian et al., 2013). Male mice exposed to ALAN exhibit elevated hippocampal *Tnf* and *Il-6* (Hogan et al., 2015) as well as medullar *Il-6* (Bumgarner et al., 2020). Moreover, in the context of the short-term scale of ALAN exposure demonstrated in this study, our previous work demonstrated that only 3 nights of exposure to 5 lux of ALAN increased hippocampal *Il-1 β* in female mice (Walker et al., 2020a). Elevated neuroinflammation may be a determining factor for the presence of altered cerebral vascular structure in this study, as adult angiogenesis is thought to primarily be driven by inflammation (Pearson-Leary et al., 2017). Future work may seek to examine inflammatory alterations and their relation to vascular structure and remodeling.

Angiogenesis and vascular remodeling are regulated by clock genes, directly implicating the ability of circadian rhythm disruption to alter vascular structure (Paschos & FitzGerald, 2010). Indeed, circadian transcription factor binding sites, including E-boxes, D-boxes, F-boxes, and ROREs are present in the promoter regions of numerous angiogenic proteins (Jensen et al., 2014). Disruption of the clock gene expression loop can alter vascular development in zebrafish (Jensen et al., 2012; Jensen & Cao, 2013). An *in vitro* assessment of angiogenesis demonstrated that clock synchronization of pericytes and endothelial cells increased tube formation and endothelial cell counts relative to desynchronized cells, further implicating the circadian clock in vascular remodeling (Mastrullo et al., 2022). Further, *Bmal1* knockout mice exhibit pathological carotid artery vascular remodeling (Anea et al., 2009). Lastly, as previously noted and as supported by our transcriptomic results, ALAN can alter angiogenic signaling in mice (Walker et al., 2020a).

The observed regional sex differences in vascular network alterations may be a result of underlying sex differences in cardiovascular circadian rhythms (Walton et al., 2022) or sex differences in the effects of circadian rhythm disruption (Bailey & Silver, 2014). For example, there are sex differences in basal cardiovascular tone (Merz & Cheng, 2016) and heart rate variability (Koenig & Thayer, 2016), and these differences persist when examined across the day (O'Connor et al., 2007; Hermida et al., 2002; Hermida et al., 2007; Hermida et al., 2013). Sex differences in inflammatory responses and immune function following ALAN exposure have also been previously noted (Cissé et al., 2017; Cissé et al., 2020; Walker et al., 2020a). Sex differences in angiogenic transcript alterations in the hippocampus following ALAN exposure have also been reported (Walker et al., 2020a). As noted, VEGF-A was decreased in both sexes, but *Vegfr-1* was only increased in female hippocampal tissue (Walker et al., 2020a). Of note, the observed sex differences were only detected in the 3D casting data. This is likely because, in contrast to 2D lectin staining, network analysis with 3D can detect fine-grained differences in vasculature (Quintana et al., 2019). Lastly, the observed sex differences may also be an effect of circulating estrogen, as estrogen does play a role in vascular reactivity (Miller & Duckles, 2008) and vascular remodeling (Gros et al., 2016).

Previous research examining the effects of ALAN on zebra finch physiology has demonstrated hippocampal-specific and sex-differential effects. One study noted that female zebra finch exposed to 5 lux of ALAN for 7 weeks exhibited increased neuronal recruitment to the medial striatum, hippocampus, and the nidopallium caudale. However, ALAN only increased total neuronal density in the hippocampus, highlighting a hippocampal-specific effect of ALAN (Moaraf et al., 2020). A follow-up study examining ALAN exposure on male zebra finches observed that ALAN increased neuronal recruitment in several other structures, but not the hippocampus. In contrast to the observed results in females, ALAN did not increase neuronal density or neuronal recruitment in the hippocampus of male zebra finches after six weeks of 5 lux of ALAN exposure (Moaraf et al., 2021). Notably, ALAN exposure did alter neuronal recruitment and density in other brain regions (Moaraf et al., 2021). These region- and sex-specific

effects of ALAN on hippocampal neuronal characteristics are tangential but complementary to the effects observed in the present study.

Future work may seek to directly examine the effects of restoring hippocampal vascularization on hippocampal function, for example via intraventricular infusion of VEGF. To assess the contribution of female sex hormones to the observed sex differences in ALAN-induced hippocampal vascular alterations, future experiments may examine effects in ovariectomized mice or stratify female mice by estrus phase for vascular structure comparisons.

The present study provides further insight into a growing body of work relating disrupted circadian rhythms and impaired cardiovascular function. The effects of ALAN exposure on cerebrovascular structure on such a rapid timescale highlight the continuing need to consider it as a dangerous and pervasive circadian rhythm disruptor.

Limitations of Study

There are several limitations present in this study. An important limitation of this study is that the presented evidence is primarily characteristic and correlative in the context of previously published results. Next, the vascular characterizations in this study were conducted *ex vivo*, preventing inferences about blood flow dynamics and real-time insights into vascular remodeling. A further limitation was our narrowed examination of dorsal hippocampal vascular alterations due to the limitations of our manual structure segmentation from the 3D reconstructions. Future work may seek to examine vascular alterations using 3D LSM approaches that allow for automatic region registration and segmentation. Moreover, I did not directly examine the concentration of circulating sex hormones to determine their potential role in the underlying observed sex differences. A final limitation of this study was the single timepoint examination of the effects of ALAN on hippocampal vascular structure. Future multi-timepoint examinations may elucidate whether there are underlying circadian differences in structural alterations that are disrupted by ALAN exposure.

Author Contributions

J.R.B., W.H.W. II, A.C.D., and R.J.N. conceived the idea and aims of the manuscript. J.R.B., D.D.Q., R.C.W, A.A.R., and J.A.L., acquired and analyzed the 3D corrosion casting data. J.R.B., W.H.W. II, and O.H.M.F acquired and analyzed the lectin data. J.R.B., D.D.B.K., and J.C.W. acquired and analyzed the RNA-seq data. J.R.B. and R.J.N. wrote the manuscript. All authors discussed the results and consulted on the manuscript.

References

- Anea, C. B., Zhang, M., Stepp, D. W., Simkins, G. B., Reed, G., Fulton, D. J., & Rudic, R. D. (2009). Vascular disease in mice with a dysfunctional circadian clock. *Circulation*, 119(11), 1510-1517.
- Bailey, M., & Silver, R. (2014). Sex differences in circadian timing systems: implications for disease. *Frontiers in Neuroendocrinology*, 35(1), 111-139.
- Bedrosian, T. A., Weil, Z. M., & Nelson, R. J. (2013). Chronic dim light at night provokes reversible depression-like phenotype: possible role for TNF. *Molecular Psychiatry*, 18(8), 930-936.
- Black, N., D'Souza, A., Wang, Y., Piggins, H., Dobrzynski, H., Morris, G., & Boyett, M. R. (2019). Circadian rhythm of cardiac electrophysiology, arrhythmogenesis, and the underlying mechanisms. *Heart Rhythm*, 16(2), 298-307.
- Bolger, A. M., Lohse, M., & Usadel, B. (2014). Trimmomatic: a flexible trimmer for Illumina sequence data. *Bioinformatics*, 30(15), 2114-2120.
- Bumgarner, J. R., & Nelson, R. J. (2022). Open-source analysis and visualization of segmented vasculature datasets with VesselVio. *Cell Reports Methods*, 2(4), 100189.
- Bumgarner, J. R., & Nelson, R. J. (2021). Light at Night and Disrupted Circadian Rhythms Alter Physiology and Behavior. *Integrative and Comparative Biology*, icab017.
- Bumgarner, J. R., Walker, W. H., Liu, J. A., Walton, J. C., & Nelson, R. J. (2020). Dim Light at Night Exposure Induces Cold Hyperalgesia and Mechanical Allodynia in Male Mice. *Neuroscience*, 434, 111-119.
- Chellappa, S. L., Vujovic, N., Williams, J. S., & Scheer, F. A. J. L. (2019). Impact of circadian disruption on cardiovascular function and disease. *Trends in Endocrinology & Metabolism*, 30(10), 767-779.
- Cissé, Y. M., Russart, K., & Nelson, R. J. (2020). Exposure to dim light at night prior to conception attenuates offspring innate immune responses. *PLoS One*, 15(4), e0231140.

- Cissé, Y. M., Russart, K. L., & Nelson, R. J. (2017). Parental Exposure to Dim Light at Night Prior to Mating Alters Offspring Adaptive Immunity. *Scientific Reports*, 7, 45497.
- Dobin, A., Davis, C. A., Schlesinger, F., Drenkow, J., Zaleski, C., Jha, S., Batut, P., Chaisson, M., & Gingeras, T. R. (2013). STAR: ultrafast universal RNA-seq aligner. *Bioinformatics*, 29(1), 15-21.
- Douma, L. G., & Gumz, M. L. (2018). Circadian clock-mediated regulation of blood pressure. *Free Radical Biology and Medicine*, 119, 108-114.
- Duffy, A. M., Bouchier-Hayes, D. J., & Harmey, J. H. (2004). Vascular endothelial growth factor (VEGF) and its role in non-endothelial cells: autocrine signalling by VEGF. In J. H. Harmey (Ed.), *VEGF and Cancer* (pp. 133-144). Kluwer Academic/Plenum Publishers.
- Falchi, F., Cinzano, P., Duriscoe, D., Kyba, C. C., Elvidge, C. D., Baugh, K., Portnov, B. A., Rybnikova, N. A., & Furgoni, R. (2016). The new world atlas of artificial night sky brightness. *Science Advances*, 2(6), e1600377.
- Fonken, L. K., Bedrosian, T. A., Zhang, N., Weil, Z. M., DeVries, A. C., & Nelson, R. J. (2019). Dim light at night impairs recovery from global cerebral ischemia. *Experimental Neurology*, 317, 100-109.
- Gharakhanian, R., Su, S., & Aprahamian, T. (2019). Vascular Endothelial Growth Factor-A Deficiency in Perivascular Adipose Tissue Impairs Macrovascular Function. *Frontiers in Physiology*, 10, 687.
- Gros, R., Hussain, Y., Chorzyczewski, J., Pickering, J. G., Ding, Q., & Feldman, R. D. (2016). Extent of vascular remodeling is dependent on the balance between estrogen receptor α and G-protein-coupled estrogen receptor. *Hypertension*, 68(5), 1225-1235.
- Hermida, R. C., Ayala, D. E., Fernández, J. R., Mojón, A., Alonso, I., & Calvo, C. (2002). Modeling the circadian variability of ambulatorily monitored blood pressure by multiple-component analysis. *Chronobiology International*, 19(2), 461-481.
- Hermida, R. C., Ayala, D. E., Mojón, A., Fontao, M. J., Chayán, L., & Fernández, J. R. (2013). Differences between men and women in ambulatory blood pressure

- thresholds for diagnosis of hypertension based on cardiovascular outcomes. *Chronobiology International*, 30(1-2), 221-232.
- Hermida, R. C., Ayala, D. E., & Portaluppi, F. (2007). Circadian variation of blood pressure: the basis for the chronotherapy of hypertension. *Advanced Drug Delivery Reviews*, 59(9-10), 904-922.
- Hogan, M. K., Kovalycsik, T., Sun, Q., Rajagopalan, S., & Nelson, R. J. (2015). Combined effects of exposure to dim light at night and fine particulate matter on C3H/HeNHsd mice. *Behavioural Brain Research*, 294, 81-88.
- Intengan, H. D., & Schiffrin, E. L. (2001). Vascular remodeling in hypertension: roles of apoptosis, inflammation, and fibrosis. *Hypertension*, 38(3 Pt 2), 581-587.
- Jensen, L. D., Gyllenhaal, C., & Block, K. (2014). Circadian angiogenesis. *Biomolecular Concepts*, 5(3), 245-256.
- Jensen, L. D., & Cao, Y. (2013). Clock controls angiogenesis. *Cell Cycle*, 12(3), 405-408.
- Jensen, L. D., Cao, Z., Nakamura, M., Yang, Y., Bräutigam, L., Andersson, P., Zhang, Y., Wahlberg, E., Länne, T., Hosaka, K., & Cao, Y. (2012). Opposing effects of circadian clock genes *bmal1* and *period2* in regulation of VEGF-dependent angiogenesis in developing zebrafish. *Cell Reports*, 2, 231-241.
- Kikuchi, R., Stevens, M., Harada, K., Oltean, S., & Murohara, T. (2019). Anti-angiogenic isoform of vascular endothelial growth factor-A in cardiovascular and renal disease. *Advances in Clinical Chemistry*, 88, 1-33.
- Kirst, C., Skriabine, S., Vieites-Prado, A., Topilko, T., Bertin, P., Gerschenfeld, G., Verny, F., Topilko, P., Michalski, N., & Tessier-Lavigne, M. (2020). Mapping the fine-scale organization and plasticity of the brain vasculature. *Cell*, 180(4), 780-795. e25.
- Koenig, J., & Thayer, J. F. (2016). Sex differences in healthy human heart rate variability: A meta-analysis. *Neuroscience & Biobehavioral Reviews*, 64, 288-310.
- Love, M. I., Huber, W., & Anders, S. (2014). Moderated estimation of fold change and dispersion for RNA-seq data with DESeq2. *Genome Biology*, 15(12), 1-21.
- Mastrullo, V., Van Der Veen, D. R., Gupta, P., Matos, R. S., Johnston, J. D., McVey, J. H., Madeddu, P., Velliou, E. G., & Campagnolo, P. (2022). Pericytes' circadian clock

- affect endothelial cells' synchronization and angiogenesis in a 3D tissue engineered scaffold. *Frontiers in Pharmacology*, 13, 867070.
- Meléndez-Fernández, O. H., Walton, J. C., DeVries, A. C., & Nelson, R. J. (2021). Clocks, Rhythms, Sex, and Hearts: How Disrupted Circadian Rhythms, Time-of-Day, and Sex Influence Cardiovascular Health. *Biomolecules*, 11(6), 883.
- Merz, A. A., & Cheng, S. (2016). Sex differences in cardiovascular ageing. *Heart*, 102(11), 825-831.
- Miller, V. M., & Duckles, S. P. (2008). Vascular actions of estrogens: functional implications. *Pharmacological Reviews*, 60(2), 210-241.
- Moaraf, S., Heiblum, R., Okuliarová, M., Hefetz, A., Scharf, I., Zeman, M., & Barnea, A. (2021). Evidence that artificial light at night induces structure-specific changes in brain plasticity in a diurnal bird. *Biomolecules*, 11(8), 1069.
- Moaraf, S., Heiblum, R., Vistoropsky, Y., Okuliarová, M., Zeman, M., & Barnea, A. (2020). Artificial Light at Night Increases Recruitment of New Neurons and Differentially Affects Various Brain Regions in Female Zebra Finches. *International Journal of Molecular Sciences*, 21(17), 6140.
- Molcan, L., Sutovska, H., Okuliarova, M., Senko, T., Krskova, L., & Zeman, M. (2019). Dim light at night attenuates circadian rhythms in the cardiovascular system and suppresses melatonin in rats. *Life Sciences*, 231, 116568.
- Morris, C. J., Purvis, T. E., Hu, K., & Scheer, F. A. (2016). Circadian misalignment increases cardiovascular disease risk factors in humans. *Proceedings of the National Academy of Sciences*, 113(10), E1402-11.
- Muramatsu, R., Takahashi, C., Miyake, S., Fujimura, H., Mochizuki, H., & Yamashita, T. (2012). Angiogenesis induced by CNS inflammation promotes neuronal remodeling through vessel-derived prostacyclin. *Nature Medicine*, 18(11), 1658-1664.
- O'Connor, M. F., Motivala, S. J., Valladares, E. M., Olmstead, R., & Irwin, M. R. (2007). Sex differences in monocyte expression of IL-6: role of autonomic mechanisms. *American Journal of Physiology-Regulatory, Integrative and Comparative Physiology*, 293(1), R145-51.

- Olfert, I. M., Howlett, R. A., Tang, K., Dalton, N. D., Gu, Y., Peterson, K. L., Wagner, P. D., & Breen, E. C. (2009). Muscle-specific VEGF deficiency greatly reduces exercise endurance in mice. *The Journal of Physiology*, 587(8), 1755-1767.
- Panza, J. A., Epstein, S. E., & Quyyumi, A. A. (1991). Circadian variation in vascular tone and its relation to alpha-sympathetic vasoconstrictor activity. *New England Journal of Medicine*, 325(14), 986-990.
- Park, K., Amano, H., Ito, Y., Kashiwagi, S., Yamazaki, Y., Takeda, A., Shibuya, M., Kitasato, H., & Majima, M. (2016). Vascular endothelial growth factor receptor-1 (VEGFR-1) signaling enhances angiogenesis in a surgical sponge model. *Biomedicine & Pharmacotherapy*, 78, 140-149.
- Paschos, G. K., & FitzGerald, G. A. (2010). Circadian clocks and vascular function. *Circulation Research*, 106(5), 833-841.
- Pearson-Leary, J., Eacret, D., Chen, R., Takano, H., Nicholas, B., & Bhatnagar, S. (2017). Inflammation and vascular remodeling in the ventral hippocampus contributes to vulnerability to stress. *Translational Psychiatry*, 7(6), e1160.
- Quintana, D. D., Lewis, S. E., Anantula, Y., Garcia, J. A., Sarkar, S. N., Cavendish, J. Z., Brown, C. M., & Simpkins, J. W. (2019). The cerebral angiome: High resolution MicroCT imaging of the whole brain cerebrovasculature in female and male mice. *NeuroImage*, 202, 116109.
- Rana, S., Prabhu, S. D., & Young, M. E. (2020). Chronobiological Influence Over Cardiovascular Function: The Good, the Bad, and the Ugly. *Circulation Research*, 126(2), 258-279.
- Rudic, R. D., McNamara, P., Reilly, D., Grosser, T., Curtis, A. M., Price, T. S., Panda, S., Hogenesch, J. B., & FitzGerald, G. A. (2005). Bioinformatic analysis of circadian gene oscillation in mouse aorta. *Circulation*, 112(17), 2716-2724.
- Rumanova, V. S., Okuliarova, M., Molcan, L., Sutovska, H., & Zeman, M. (2019). Consequences of low-intensity light at night on cardiovascular and metabolic parameters in spontaneously hypertensive rats. *Canadian Journal of Physiology and Pharmacology*, 97(9), 863-871.

- Schneider, C. A., Rasband, W. S., & Eliceiri, K. W. (2012). NIH Image to ImageJ: 25 years of image analysis. *Nature Methods*, 9(7), 671-675.
- Sun, Y. Y., Bai, W. W., Wang, B., Lu, X. T., Xing, Y. F., Cheng, W., Liu, X. Q., & Zhao, Y. X. (2014). Period 2 is essential to maintain early endothelial progenitor cell function in vitro and angiogenesis after myocardial infarction in mice. *Journal of Cellular and Molecular Medicine*, 18(5), 907-918.
- Thosar, S. S., Butler, M. P., & Shea, S. A. (2018). Role of the circadian system in cardiovascular disease. *Journal of Clinical Investigation*, 128(6), 2157-2167.
- Walker, W. H., Borniger, J. C., Gaudier-Diaz, M. M., Hecmarie Meléndez-Fernández, O., Pascoe, J. L., Courtney DeVries, A., & Nelson, R. J. (2020a). Acute exposure to low-level light at night is sufficient to induce neurological changes and depressive-like behavior. *Molecular Psychiatry*, 25(5), 1080-1093.
- Walker, W. H., Walton, J. C., DeVries, A. C., & Nelson, R. J. (2020b). Circadian rhythm disruption and mental health. *Translational Psychiatry*, 10(1), 28.
- Walker, W. H., Bumgarner, J. R., Becker-Krail, D. D., May, L. E., Liu, J. A., & Nelson, R. J. (2021). Light at night disrupts biological clocks, calendars, and immune function. *Seminars in Immunopathology*, 44(2), 165-173.
- Walton, J. C., Bumgarner, J. R., & Nelson, R. J. (2022). Sex Differences in Circadian Rhythms. *Cold Spring Harbor Perspectives in Biology*, a039107.
- Weil, Z. M., Fonken, L. K., Walker, W. H., Bumgarner, J. R., Liu, J. A., Melendez-Fernandez, O. H., Zhang, N., DeVries, A. C., & Nelson, R. J. (2020). Dim light at night exacerbates stroke outcome. *European Journal of Neuroscience*, 52(9), 4139-4146.
- Young, M. E., Razeghi, P., Cedars, A. M., Guthrie, P. H., & Taegtmeier, H. (2001). Intrinsic diurnal variations in cardiac metabolism and contractile function. *Circulation Research*, 89(12), 1199-1208.
- Zhang, X., Yin, X., Zhang, J., Li, A., Gong, H., Luo, Q., Zhang, H., Gao, Z., & Jiang, H. (2019). High-resolution mapping of brain vasculature and its impairment in the hippocampus of Alzheimer's disease mice. *National Science Review*, 6, 1223-1238.

Supplemental Information Titles (See Original Publication)

Supplemental Video 1 – ALAN reduces vessel segment density in the dentate gyrus of male mice, related to Figure 2.

Chapter 9

Conclusions

Life on Earth is governed around the clock by circadian rhythms. These ever-present and intrinsic rhythms are involved in nearly every aspect of behavior in physiology. Proper synchronization of internal circadian rhythms with the external rhythmic environment of the Earth is essential for health.

Despite the importance of circadian rhythms to health, the modern human environment is inconducive to robust and uncorrupted circadian hygiene. Humans in industrialized societies are exposed to ever-growing 24-hour cycles of work and media alongside numerous circadian rhythm disruptors. The most ubiquitous circadian rhythm disruptor of the modern environment is artificial light at night (ALAN). Decades of ongoing research have revealed numerous detrimental health consequences associated with ALAN exposure.

This dissertation investigated and reported two novel consequences of ALAN exposure on physiology and behavior in mice. The experiments and aims were generated with both clinically translational and basic biological interests in mind. Each experiment and hypothesis was generated using supporting evidence and a set of devised alternative hypotheses. Experiments were methodically and strictly controlled, conducted, and reported.

First, I demonstrated the negative effects of ALAN exposure on pain behavior in mice (Part 1). ALAN consistently heightened responsiveness to painful cold stimuli. Mechanical sensitivity was inconsistently altered in my observations, but in general, ALAN induced states of mechanical hyper-responsiveness. These effects were observed both in the contexts of health and disease, including models of chemotherapy-induced neuropathy and diabetic neuropathy of type II diabetes. Robust underlying mechanisms responsible for these effects were not pinpointed, but my experiments pointed towards nuanced effects of neuroinflammation and alerted endogenous opioid signaling. In all, these data support the body of knowledge surrounding circadian rhythm disruption and

pain. The data point to the need for scientists and clinicians to consider circadian rhythm disruption as a mitigating factor for pain.

Second, I demonstrated the negative effects of ALAN exposure on cerebrovascular structure in mice (Part 2). These observations relied heavily on several computational and analytical advancements that I also concurrently contributed to the field of vasculature research in the form of my published app, VesselVio. Importantly, the effects of ALAN on hippocampal vasculature in mice were observed after only four nights of exposure. In all, this evidence highlights the importance of implementing evidence-based hospital and home lighting for patients recovering from cardiovascular disease.

Beyond the contribution of new insights into the detrimental effects of ALAN, this work also highlighted numerous interesting sex differences in circadian rhythm disruption. These observations emphasize the importance of considering and studying sex as a biological variable. Such efforts will maximize the translational value of preclinical experiments.

This collection of research is a small contribution to the massive body of knowledge generated on the topic of circadian rhythm disruption. It may provide further insight into future experiments hoping to uncover new mechanisms, behavioral, or physiological consequences of ALAN exposure and circadian rhythm disruption. It may be refined, supported, or refuted. It may be lost in the endless sea of public information. Regardless of the external impact, this collection of research has helped to shape me into the young scientist that I am today. I hope that these observations and discoveries may contribute to ongoing public health initiatives aimed at improving the quality of life of humans and other animals.